STRUCTURAL SYSTEMS

RESEARCH PROJECT

Report No.
SSRP–06/15

HYGROTHERMAL EFFECTS ON DURABILITY AND MOISTURE KINETICS OF FIBER-REINFORCED POLYMER COMPOSITES

by

PADMAVATHI SURATHI

VISTASP M. KARBHARI

Interim Report Submitted to the California Department of Transportation Under Contract No. 59A0309.

June 2006

Department of Structural Engineering
University of California, San Diego
La Jolla, California 92093-0085

University of California, San Diego
Department of Structural Engineering
Structural Systems Research Project

Report No. SSRP–06/15

Hygrothermal Effects on Durability and moisture Kinetics of Fiber-Reinforced Polymer Composites

by

Padmavathi Surathi
Graduate Student Researcher

Vistasp M. Karbhari
Professor of Structural Engineering

Interim Report Submitted to the California Department of Transportation
Under Contract No. 59A0309

Department of Structural Engineering
University of California, San Diego
La Jolla, California 92093-0085

June 2006

Technical Report Documentation Page

1. Report No.	2. Government Accession No.	3. Recipient's Catalog No.
FHWA/CA/ES-07/01		

4. Title and Subtitle	5. Report Date
Hygrothermal Effects on Durability and Moisture Kinetics of Fiber-Reinforced Polymer Composites	June 2006
	6. Performing Organization Code

7. Author(s)	8. Performing Organization Report No.
Padmavathi Surathi and Vistasp M. Karbhari	UCSD / SSRP-06/15

9. Performing Organization Name and Address	10. Work Unit No. (TRAIS)
Department of Structural Engineering School of Engineering University of California, San Diego La Jolla, California 92093-0085	11. Contract or Grant No. 59A0309

12. Sponsoring Agency Name and Address	13. Type of Report and Period Covered
California Department of Transportation Division of Engineering Services 1801 30th St., West Building MS-9-2/5I Sacramento, California 95807	Interim Report
	14. Sponsoring Agency Code

15. Supplementary Notes

Prepared in cooperation with the State of California Department of Transportation. This report is one of a series of reports

16. Abstract

Fiber-Reinforced Polymer (FRP) composites offer many advantages over conventional materials for applications in the marine and civil infrastructure areas. Their increasing widespread use emphasizes the need to predict their performance over long periods of time after being subjected to exposure to different environmental conditions. The kinetics of fluid sorption E-glass/vinylester composites is studied widely using the Fickian and Langmuir diffusion models. The time and temperature dependence of the rate of diffusion and maximum moisture content are analyzed and moisture kinetics data is assessed is assessed for use in performance predictions.

It is seen that various processes of degradation, both reversible and irreversible, are induced in the composite materials on exposure to moisture. The durability characteristics of unidirectional E-glass-Vinylester composites under the influence of relative humidity and immersion in water at different temperatures are investigated. The correlation between tensile and flexural strength data is investigated using statistical models. This research attempts to analyze the behavior of FRP composites exposed to the aforementioned environments and theoretically model their effects on the mechanical properties (tensile strength, tensile modulus, flexural strength and short beam shear strength) of the FRP composites, for purposes of long-term prediction. This study attempts to develop an initial correlation between effects due to immersion in deionized water with those due to exposure to humidity to further develop techniques for prediction of durability of these materials under field conditions.

17. Key Words	18. Distribution Statement
Durability; E-Glass; Moisture; Temperature; Humidity; Mechanical Properties; Deterioration	No restrictions. This document is available to the public through the National Technical Information Service, Springfield, Virginia 22161

19. Security Classification (of this report)	20. Security Classification (of this page)	21. No. of Pages	22. Price
Unclassified	Unclassified	291	

Disclaimer

The contents of this report reflect the views of the authors who are responsible for the facts and the accuracy of the data presented herein. The contents do not necessarily reflect the official views or policies of the State of California or the Federal Highway Administration. This report does not constitute a standard, specification, or regulation.

The United States Government does not endorse products or manufacturers. Trade and manufacturers' names appear in this report only because they are considered essential to the object of the document.

Table of Contents

List of Figures

List of Tables

ABSTRACT

Fiber-Reinforced Polymer (FRP) composites offer many advantages over conventional materials for applications in the marine and civil infrastructure areas. Their increasing widespread use emphasizes the need to predict their performance over long periods of time after being subjected to exposure to different environmental conditions. The kinetics of fluid sorption E-glass/vinylester composites is studied widely using the Fickian and Langmuir diffusion models. The time and temperature dependence of the rate of diffusion and maximum moisture content are analyzed and moisture kinetics data is assessed is assessed for use in performance predictions.

It is seen that various processes of degradation, both reversible and irreversible, are induced in the composite materials on exposure to moisture. The durability characteristics of unidirectional E-glass-Vinylester composites under the influence of relative humidity and immersion in water at different temperatures are investigated. The correlation between tensile and flexural strength data is investigated using statistical models. This research attempts to analyze the behavior of FRP composites exposed to the aforementioned environments and theoretically model their effects on the mechanical properties (tensile strength, tensile modulus, flexural strength and short beam shear strength) of the FRP composites, for purposes of long-term

prediction. This study attempts to develop an initial correlation between effects due to immersion in deionized water with those due to exposure to humidity to further develop techniques for prediction of durability of these materials under field conditions.

Chapter 1

Introduction

1.1 Background

Recent years have witnessed a substantial increase in the use of Fiber-Reinforced Polymer (FRP) Composites in place of conventional construction materials. Engineers around the world are leaning towards FRP composites because of their high specific strength and stiffness characteristics, lightweight, tailorability, endurance to fatigue loading and the ease of fabrication.

FRP composites have found a wide variety of applications in both new construction and rehabilitation projects alike. Pre-stressing tendons and reinforcing bars made from FRP [1] are now being used in new construction projects. Repair and rehabilitation of existing structures is also being carried out using FRP composites. FRP is being extensively used in the seismic retrofit [2] of concrete and steel bridge columns and slabs. In addition to these, FRP composites are being utilized for architectural applications like roofing and partition walls.

However, the use of FRP to its fullest potential has been hampered by the fact that there is concern about their reliability and performance over long periods of time. Exposure to humidity, water, alkalis, elevated temperatures and other harsh environments can induce physical and chemical changes in polymer composites. On exposure to water or moisture, FRP composites have been reported to show reduction in strength [3,4], plasticization of the

matrix [5,6,7] and also degradation of the fiber/matrix interface [8,9]. Environmental exposure can induce various chemical and physical processes of degradation in FRP composites. The relative rates of these degradation processes depend on the chemistry of the fiber and matrix, temperature, length of exposure and the stress state [10]. Therefore, a better understanding of the behavior of the FRP composites under these environments is absolutely essential to aid in the optimal design and the prediction of service-life of structural components constructed from these materials.

The most noticeable effect of exposure to moisture is the plasticization of the matrix due to the interruption of Van Der Waals bonds between the polymer chains [11]. This in turn reduces the glass transition temperature of the polymer matrix, and can lead to a decrease in the matrix dominated strength and stiffness properties. In some cases, moisture introduces micro-cracks in the fiber/matrix interface thereby interfering with the transfer of loads from the matrix to the fibers. Some fibers like glass and Kevlar are also susceptible to moisture induced degradation. Polymer composites are invariably exposed in civil infrastructure to moisture or humid air in their applications. By far, moisture in combination with elevated temperatures is one of the most widely studied exposures. The “hot-wet” environment is generally considered to be a very severe exposure condition and is hence used widely for materials screening.

Measurement of moisture uptake is a common method used to characterize the hygrothemal behavior of polymer composites, since deterioration is most often initiated by moisture. Theoretical models based on either classical Fickian diffusion or non-classical diffusion are used to determine the maximum moisture content and the rate of diffusion [12, 13].

Moisture sorption in FRP composites not only affects the dimensional stability but also affects the mechanical properties of the composites. As a result of this, determination of the rate of degradation of mechanical properties and the resulting effect on service life is of utmost importance to engineers. This study attempts to investigate the effects of immersion in water and exposure to humidity at different temperatures on the mechanical properties of unidirectional E-glass Vinylester composites. Durability characteristics of E-glass Vinylester composites in these environments are studied by employing life prediction models.

1.2 Objectives of the Research

The primary objective of the research reported in this report is to develop a fundamental understanding of the effects of hygrothermal exposure (related to both immersion and humidity based conditioning) on durability of E-glass/Vinylester composites. In addition to the goals of developing an understanding of moisture kinetics and deteriorative mechanisms, this study attempts to develop an initial correlation between effects due to immersion in deionized water with those due to exposure to humidity in an attempt to further develop techniques for prediction of longer-term durability of these materials under field conditions. It must be noted that although complete immersion is often used as a means of characterization of durability, and as a method of acceleration, data cannot directly be applied to prediction of service-life under field environments which intrinsically consists not of immersion, but rather varying periods at different levels of temperature and humidity.

1.3 Overview of the Investigation

The Literature Review consists of a brief description of the findings of studies dealing with sorption kinetics and hygrothermal ageing of polymer composites. It also

reviews the effects of moisture sorption on glass fiber-reinforced composites. Results of previous experiments on glass fiber-reinforced composites and the validity of various life predictive models are also discussed.

In the next chapter, material specifications and the test methods employed to measure the moisture uptake and to determine the loss of mechanical properties are discussed. The next chapter presents the results of the moisture sorption tests and tensile strength, flexural strength and short beam shear strength experiments.

In chapter 5, data from the moisture uptake experiments are analyzed using Fickian and Langmuir diffusion models and the kinetics of moisture sorption are studied. The equilibrium moisture contents and diffusion coefficients for different temperatures are determined. The results from the analyses of data using the two diffusion models are compared and the suitability of diffusion models for the data is assessed. The results are also compared with previously published data.

Chapter 6 discusses the correlation between tensile strength and flexural strength and the ability to predict one from the other. A two parameter Weibull distribution model is used to predict values of tensile and flexural strength, which are then compared to the experimental values.

In chapter 7, prediction of mechanical strength characteristics of the E-glass Vinylester composite specimen is discussed. The experimental data is analyzed using two models, namely the Arrhenius Rate Model and the Phani-Bose Model. The results from the analyses of Tensile, Flexural and Short-Beam Shear data are presented and the life prediction models are utilized to determine the remaining life of the polymer composite. The advantages and shortcomings of the two models are discussed and the results from the two models are compared.

Chapter 8 discusses the prediction of service-life of the polymer composite exposed to humidity and the correlation between moisture and humidity is discussed. The last chapter focuses on the conclusions drawn from the research and discusses further research needs.

Since this investigation is concerned with durability of materials it is important that the term, durability, be defined as it relates to this investigation. Durability, in the current context, is defined as the ability of a materil to resist physical, mechanical and/or chemical degradation for a specified period of time under specified environmental conditions and load regimes.

1.4 References

1. Malvar L.J., "Durability of Composites in Reinforced Concrete", Proceedings of the First International Conference on Durability of Composites for Construction, Sherbrooke, Quebec, Canada, August 1998, pp. 361-372.

2. Reay J.T., Pantelides C.P., Reaveley L.D., Ring T.A., "Long Term Durability of Carbon FRP Composites Applied to RC Bridges: State Street Bridge on Interstate 80", *Report No. CVEEN-04/1*, University of Utah, Salt Lake City Utah, 2004.

3. Bank L.C., Gentry T.R., and Barkatt A., "Accelerated Test Methods to Determine the Long-Term Behavior of FRP Composite Structures: Environmental Effects", *Journal of Reinforced Plastics and Composites*, 1995, Vol. 14, pp. 559-587.

4. Williams C.J., "The Effect of Moisture Absorption on Room Temperature Mechanical Properties of Reinforced Polymer Composites", Research and Development Report, Ship Materials Engineering Department, David Taylor Research Center, Report DTRC-SME-91/35, January 1991.

5. Allred R.E., "The Effect of Temperature and Moisture Content on the Flexural Response of Kevlar/Epoxy Laminates I (0/90) Filament Orientation" *Journal of Composite Materials*, 1981, Vol. 15, pp. 100-116.

6. Allred R.E., "The Effect of Temperature and Moisture Content on the Flexural Response of Kevlar/Epoxy Laminates II (+or-45, 0/90) Filament Orientation" *Journal of Composite Materials*, 1981, Vol. 15, pp. 117-132.

7. Chateauminois A., Chabert B., Soulier J.P., Vincent L., "Hygrothermal Ageing Effects on the Static Fatigue of Glass/Epoxy Composites", *Composites*, 1993, Vol. 24, Issue 7, pp. 547-555.

8. Liao Y.T., "A Study of Glass Fiber-Epoxy Composite Interfaces", *Polymer Composites*, December 1989, Vol. 10, Issue 6, pp. 424-428.

9. Gautier L., Mortaigne B., and Bellenger V., "Interface Damage Study of Hydrothermally Aged Glass-Fiber Reinforced Polyester Composites", *Composites Science and Technology*, 1999, Vol. 59, pp. 2329-2337.

10. Schutte C.L., "Environmental Durability of Glass-fiber Composites", *Materials Science and Engineering*, 1994, Vol. R13, pp. 265-324.

11. Wolff E.G., “Moisture Effects on Polymer Matrix Composites”, *SAMPE Journal*, 1993, Vol. 29, Issue 3, pp. 11-19.

12. Shen C. and Springer G.S., “Moisture Absorption and Desorption of Composite Materials”, Environmental effects on Composite Materials, 1988, Ed., Springer G. S., Vol. 3, pp. 15-34.

13. Ghorbel I. and Valentin D., “Hydrothermal Effects on the Physico-Chemical Properties of Pure and Glass Fiber Reinforced Polyester and Vinylester Resins”, *Polymer Composites*, 1993, Vol. 14, Issue 4, pp. 324-334.

Chapter 2

Literature Review

2.1 Moisture Absorption in Polymeric Composites

Polymeric Composites exposed to moisture undergo a wide variety of physico-chemical changes. Experiments have revealed that plasticization and hydrolysis are the two main causes of degradation of polymeric matrices and polymeric composites during the hygrothermal aging process [1]. Before delving into the processes of degradation, it is very important to understand the kinetics of transport and moisture diffusion processes in polymeric composites. Water molecules dissolve on the polymer surface and diffuse through the bulk by a series of activated steps under the driving force of concentration gradients. Both solubility and diffusivity are involved in the process. Diffusion is the process by which matter is transported from one part to another as a result of random molecular motion [2]. Classical Diffusion behavior in polymer matrices can be classified as follows [3]:

(i) Case I or Fickian Diffusion: Rate of the diffusion is much less than that of polymer segment mobility.

(ii) Case II: Rate of diffusion is much greater than the polymer segment mobility and is strongly dependent on swelling kinetics.

(iii) Anomalous or Non-Fickian Diffusion: Rate of diffusion and polymer segment mobility are comparable. Anomalous behavior can be considered as intermediate between the case I and case II types of diffusion.

In this study, the moisture sorption data is analyzed with Fickian and Non-Fickian diffusion (Langmuir) models.

2.1.1 Classical Fickian Diffusion

Fickian diffusion is characterized by the following features (Fig. 2.1) [2]:

(i) Both sorption and desorption curves are functions of the square root of time and are linear in the initial stage and the linear region extends to at least $M_t/M_m = 0.6$, where M_t is the moisture absorbed by the composite specimen at time t and M_m is the maximum moisture content absorbed by the specimen.

(ii) Reflective symmetry between weight gain of initially dry specimens and weight loss data of saturated coupons, when the diffusion coefficient is constant.

(iii) Above the linear portion, the rate of diffusion decreases until an equilibrium moisture content is reached.

(iv) The sorption behavior obeys the film thickness scaling law: the uptake curves obtained by plotting M_t/M_m vs. $\sqrt{t}/h$ (reduced sorption curves) coincide regardless of the thickness of the specimen (t is the time and h is the thickness of the specimen)

(v) The Diffusion coefficient, D, is a function of temperature T (in degrees Kelvin), and can be expressed as

$$D = D_0 \exp\left(\frac{-E_a}{RT}\right)$$

where D_0 is a constant, E_a is the activation energy of the diffusion process and R is the universal gas constant (8.3144 J mol^{-1} K^{-1}).

It must, however be noted that the Fickian model does not hold good for all temperatures and moisture contents. Fickian diffusion theory also assumes that during the process of moisture sorption only reversible physical reactions occur in the polymer matrix [2, 4].

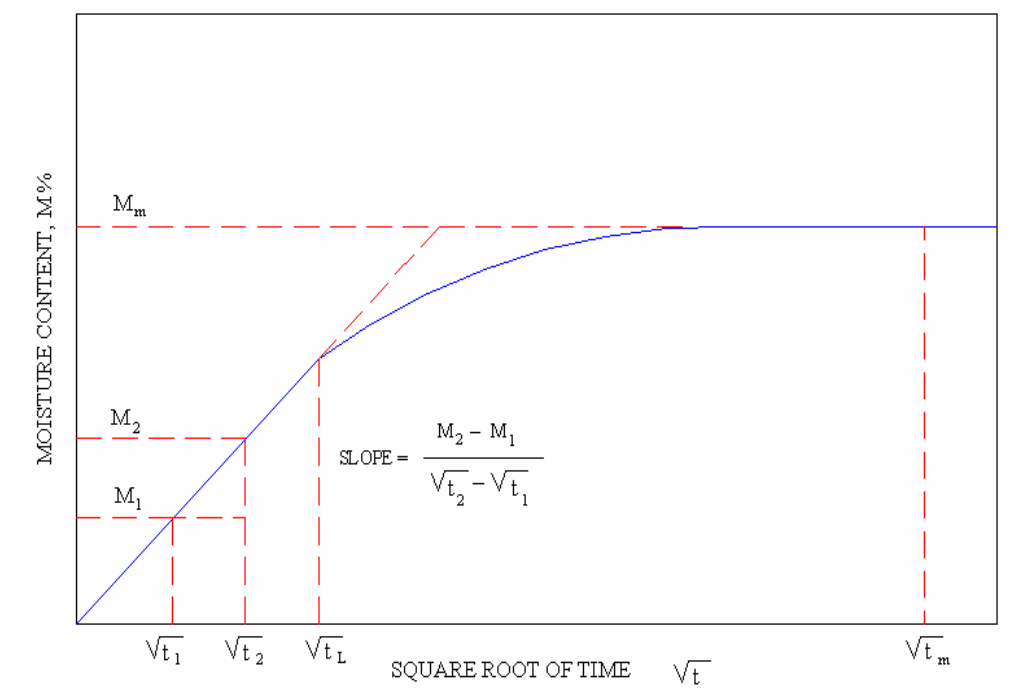

Fig 2.1 Shape of a typical Fickian diffusion curve

2.1.2 Non- Fickian Diffusion

It has been observed that in many cases Fickian diffusion behavior is not observed [5,6]. Figure 2.2 shows the departures from the Fickian diffusion as postulated by Weitsman [6]. Curve A in Figure 2.2, classified as Pseudo-Fickian, depicts a continuous gradual increase in the moisture content, with equilibrium never being attained. Curve B in Figure 2.2 represents Two-Stage sorption behavior, wherein the initial uptake is rapid and a linear

function of the square root of time. The sorption curve then approaches a quasi-equilibrium followed by a slow approach towards a true equilibrium.

Curve S represents a sigmoid behavior – the sorption curves are sigmoid in shape with a single inflection point. Curve C corresponds to rapidly increasing moisture content, usually accompanied by large deformations and mechanical failure. Lastly Curve D in Figure 2.2 represents weight loss that is attributed to irreversible chemical or physical degradation of the material.

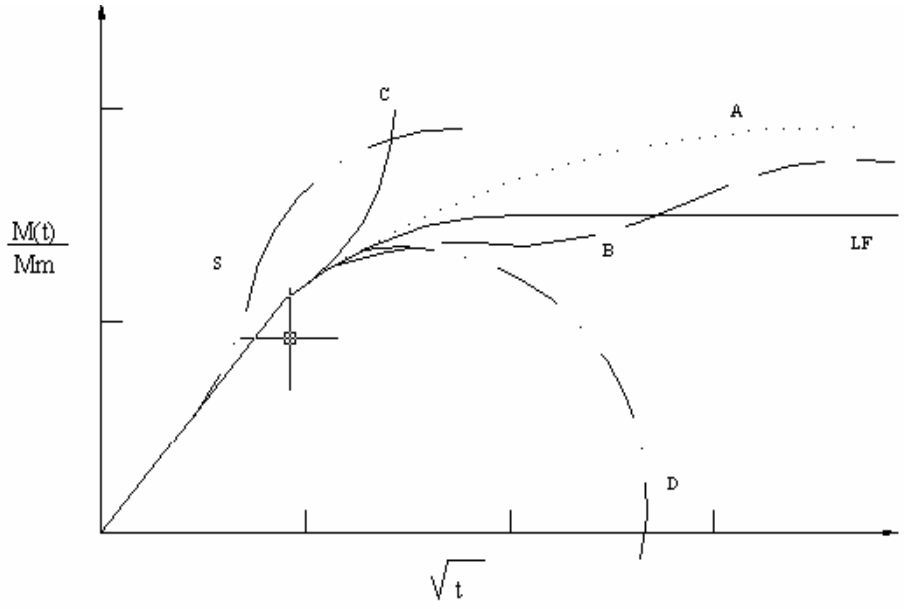

Fig 2.2 Schematic curves representing different types of anomalous diffusion in polymeric composites (After Weitsman [6])

A number of models have been proposed to describe anomalous diffusion in polymeric composites, but there is still lack of a single general theory for anomalous diffusion in polymeric composites. Roy et al. [7] utilized moisture gain data for an epoxy resin immersed in salt solution at different temperatures, to propose a methodology, which enables the characterization of non-Fickian diffusion coefficients. These diffusion coefficients can be used subsequently to predict the moisture concentration profiles through the thickness of the polymer.

The departure from the classical diffusion is attributed to the time-dependent response of the polymer analogous to viscoelastic mechanical response. Cai and Weitsman [8] proposed a model correlating the non-Fickian moisture gain data with a set of time-dependent boundary conditions, as motivated by the viscoelastic mechanical response. This procedure allows the reduction of non-Fickian moisture gain data in a way that enables the evaluation of the diffusion coefficients and through-thickness moisture concentration profiles. More information on non-Fickian diffusion models can be found in [9 – 14].

The Langmuir Diffusion Model, which is often used to describe non-Fickian response, is a dual mode sorption model, which assumes that the penetrant molecules are divided into two populations, one that is dissolved in the polymer and is hence able to diffuse, and another that is absorbed in the micro-voids and is therefore locally immobilized [15].

Bonniau and Bunsell [16] compared the Fickian and Langmuir diffusion theories by applying the diffusion models to water sorption data of Glass Epoxy composites. A review of experimentally observed anomalous diffusion behavior in polymers has been made by Hopfenberg and Stannett [17].

2.1.3 Factors Affecting the Diffusion Coefficient

Diffusion can be defined as the process by which matter is transported from one part of a system to another as a result of random molecular motion [6]. The diffusion coefficient describes the rate of diffusion of particles, depending on the particle size, viscosity and temperature. Diffusion coefficient is a function of absolute temperature and has been shown to increase with increase in temperature. Diffusion coefficient is related to temperature as follows:

$$D = D_0 \exp\left(\frac{-E_a}{RT}\right) \qquad \text{(Equation 2.1)}$$

where D_0 is a constant, E_a is the activation energy of the diffusion process and R is the universal gas constant. This equation was defined by Arrhenius in 1899 and is applicable to determination of any reaction rate based on a temperature driven process. Because the relationship of the rate of diffusion to activation energy and temperature is exponential, a small change in temperature or activation energy causes a large change in the rate of diffusion. Activation energy of the diffusion process is determined by calculating D at different temperatures T, plotting the logarithm of D against $1/T$ on a graph, and determining the slope of the straight line that best fits the points. A linear fit across the entire regime indicates dominance of a single moisture driven deteriorative mechanism, whereas a kink indicates the point of transition between two diffusion regimes.

The diffusion coefficient also depends on the moisture concentration of the environment, chemical structure of polymer matrix and imperfections like micro-cracks in the polymer matrix, and the degree of cross-linking of the polymer. It has been proved that the

rate of degradation of polymers exposed to moisture is directly related to the rate of moisture sorption of the polymer [18].

The process of moisture sorption is primarily influenced by internal factors – fiber volume fraction, orientation of the fibers, and external factors- moisture concentration and temperature [19, 20]. It has been observed that, in general, diffusion coefficients decrease with increase in fiber volume fraction [21].

2.1.4 Factors Affecting Equilibrium Moisture Content

Experimental evidence indicates that the maximum moisture content is insensitive to the temperature but depends on the moisture content of the environment. For a material immersed in liquid, the maximum moisture content, M_m is a constant [2]. Equilibrium moisture content is also affected by the previous thermal history, existing damages in the composite and the chemical stability of the resin.

2.2 Hygrothermal Ageing of Composites

The degradation of the mechanical properties of polymeric composites, after exposure to a combination of moisture and temperature is referred to as hygrothermal ageing. Hygrothermal ageing is the summation of physical and chemical changes in the composite material. Changes in the mechanical properties of the composites due to hygrothermal ageing can be reversible or irreversible or a combination of the two depending on the exposure time and temperature [22]. It should be noted that these changes can be affected through application of sustained load. However, this will not be considered in the current investigation.

The chemical effects of moisture on polymeric composites result from the interaction between the water molecules and one or more of the matrix constituents and/or the fibers. Water molecules hydrolyze the polymer bonds, leading to dissolution and leaching of water-soluble polymer molecules. In addition, the dissolution products react with the polymer molecules, leading to further degradation [3]. Since polymeric composites are made with a combination of various fibers and polymeric matrices, the degree of chemical interactions with moisture depends on the physical and chemical composition of the composite material. Damage caused to fibers, matrix cracking and debonding of fiber/matrix interface due to chemical changes in the composite permanently alters the mechanical properties of the composite [22].

2.2.1 Hygrothermal Effects on Polymer Matrices

Moisture affects polymeric composites physically by plasticizing the matrix and thus lowering its glass transition temperature. Changes caused due to plasticization and swelling can usually be reversed on removal of the sorbed moisture from the material. The plasticization phenomenon is related to the increase in the free volume of the polymer and to the destruction of intra-molecular hydrogen bonds. Glass transition temperature T_g is an important physical property of thermosetting polymers like vinylesters and polyesters. Glass transition temperature is defined the critical temperature at which polymers undergo a change from a glassy/elastic to soft rubbery/viscoelastic state.

At low temperatures, polymers are in a glassy state and are characterized by high values of modulus of relaxation and elastic behavior. The only molecular motion possible is vibration around fixed positions, because there is not enough thermal energy to facilitate rotation and translation. When the temperature is increased, the increase in thermal energy

makes rotation and translation possible. The polymer then becomes like resilient leather characterized by a sharp drop in the relaxation modulus. This region is called the transition region. Following the glass transition, the modulus reaches a plateau [23] (Fig 2.3). Thus above the T_g, the strength and stiffness properties of the polymer decrease relative to its properties below the T_g [24].

Moisture sorption by the polymeric matrix lowers its T_g, thereby causing the polymer to soften at lower temperatures. Allred reported the effect of glass transition temperature on the behavior of Kevlar/Epoxy composites [25, 26]. It has been shown that the moisture sorption decreases the T_g thus lowering the mechanical properties.

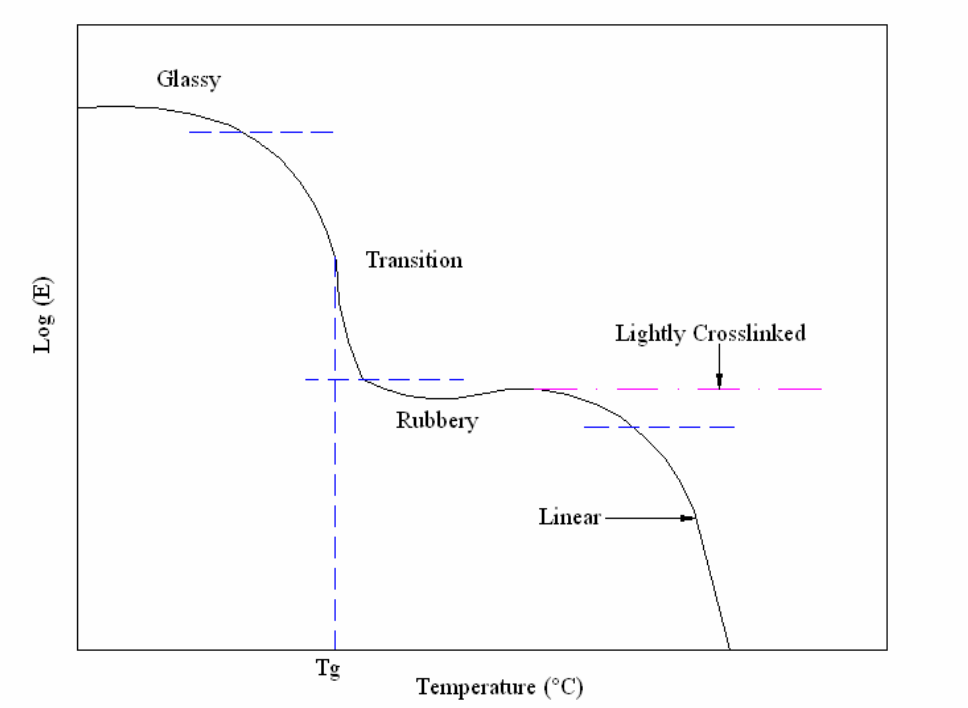

Fig 2.3 Modulus E as a function of temperature for a typical amorphous polymer (After Tissaoui [23])

Chateauminois et al. [27] studied the static fatigue behavior of hygrothermally aged unidirectional Glass/Epoxy composites and the failure mechanisms associated with fatigue damage were investigated under three-point flexural loading. Depending on the ageing temperature, two failure modes were observed: fiber microbuckling on the compression side or progressive cracking on the tensile side. Microbuckling was related to the reversible plasticization of the epoxy matrix and the cracking on the tensile side was attributed to the irreversible weakening of the fibers and the interface at higher ageing temperatures.

Glass transition temperature has been used characterize the physical effects of moisture on polymers by Ghorbel and Valentin [1] and Birger et al [28]. Another physical effect of moisture on polymers is the generation of internal stresses due to the accumulation of water molecules in the micro-cracks and voids of the polymer matrix [3]. These internal stresses cause localized failures in the matrix.

Apicella et al. [29] studied the influence of the chemistry of polyester resins on the retention of their mechanical properties after exposing Glass/Polyester composites to water at different temperatures (25 and 90 ^{o}C). It was found that the relative hydrolytic damage decreased as follows: isophthalic resins > bisphenol-B > bisphenol – A > vinylester. The authors suggested that the susceptibility to hydrolytic attack increased with an increase in the number of ester groups in the polymer repeat unit. Apicella et al. [30] also investigated the influence of water sorption on the mechanical properties of glass fiber-reinforced polyester composites immersed in water at temperatures of 20, 40, 60, 90 and 100 ^{o}C. The mechanical properties of the polymeric matrix showed significant reduction in the glass transition region, due to the progressive softening of the initially glassy system. The degradation mechanisms were associated with both the low chemical resistance and the possible migration of some of

the components initially present in the thermoset, which was evident from the weight losses observed for samples aged at higher temperatures.

2.2.2 Hygrothermal Effects on Fibers

Glass fibers, unlike graphite fibers, which are inert, are prone to attack by moisture and aqueous solutions [24, 31]. It has been observed that the amount of strength reduction in GFRP composites due to long-term load application is more pronounced when the composite is wet than when it is dry [31].

The chemical effects on glass fibers can be demonstrated with the following equations, which present a sequence of reactions leading to cleavage of silicon-oxygen bonds and to their conversion to hydroxysilane [3].

$$Si-ONa + H_2O \rightarrow Si-OH + NaOH$$
$$Si-O-Si + OH^- \rightarrow Si-OH + Si-O^-$$
$$Si-O^- + H_2O \rightarrow Si-OH + OH^-$$

The overall reaction, which is autocatalytic due to the gradual increase in the pH level, results in degradation and flaw formation at the glass fiber surface and in significant strength reduction of the glass-fiber reinforced composite.

Tensile, Compressive and Interlaminar shear strengths are known to decrease in GFRP composites exposed to hygrothermal ageing. Carol Williams [31] provides a comprehensive review of the response of GFRP and CFRP composites to moisture sorption. Wyatt and Ashbee provide a comparison of behavior of GFRP and CFRP composites on exposure to water [32]. The differences in the behavior of glass fibers and graphite fibers have been attributed to their different affinities to water (the surface of a carbon fiber being hydrophobic and that of a glass fiber hydrophilic) and the interface they form with the matrix.

Carbon fibers are almost immune to moisture attack at lower temperatures and any degradation whatsoever is due to the degradation of the polymer matrix. This has been clearly demonstrated by Wyatt and Ashbee [32]. However the CFRP composites showed debonding at the fiber/matrix interface at temperatures higher than 100 ^{o}C. On the other hand GFRP composites showed significant damage due to fiber pitting and debonding at the fiber/matrix interface. Ehrenstein and Spaude subjected different types of individual glass fibers to moisture and various corrosive media and reported axial or spiral cracking in the glass fibers [33].

Water has been found to accelerate the rate of crack growth in glass fibers [34]. This is due to two factors- first, water reduces the surface energy of the glass fiber, resulting in less energy required for crack formation and the second, water reduces the energy required to break the Si-O bond by a considerable amount, thus helping in the propagation of cracks. Pultruded glass-fiber reinforced vinylester matrix composites were subjected to environmental ageing in water and salt solutions at 25 ^{o}C and 75 ^{o}C by Liao et al [35]. Aging in water and salt solutions results in degraded flexural and tensile properties of the pultruded E-glass fiber reinforced vinylester composite. Also, comparison of the sizes of fracture mirrors on the broken ends of the fibers in aged and un-aged samples suggested that environmental ageing degraded the glass fibers. In addition, degradation of the fiber/matrix interface region during the aging process was also reported.

2.2.3 Hygrothermal Effects on the Interfacial Region

The interface is defined as the non-homogenous region that lies between the matrix and the fibers. The adhesion between the fiber and matrix has to be good for the polymer composite to have properties that are advantageous. In order for the composite to maintain its

properties on exposure to moisture, the interface must resist degradation due to moisture sorption [36].

Ishida and Koenig [37] have published reviews addressing the mechanisms of reinforcement of glass-fiber composites under wet conditions. To identify the mechanisms of attack at the interface, it is necessary to understand the chemistry, structure and morphology at the interface. The fibers are treated with coupling agents to enhance their adhesion with the polymer matrix. In glass-fiber reinforced composites, the coupling agents react chemically with glass fibers, through silicon hydroxyl groups and also with the resin through an organic functional group that is compatible with the chemistry of the resin. Experimental studies of the interface formed through the coupling agent revealed complicated multi-layered structure. The deposition of coupling agents from water results in three layers on the glass-fiber surface: a monolayer, a chemi-sorbed layer, a physic-sorbed layer [36].

Plueddemann [38] suggested that water is necessary to aid fiber-matrix bonding. He proposed a theory in which coupling agents provide a bond at the interface that is capable of using the hydrolytic intrusion of water, with self-healing, as a means of stress relaxation without interrupting the bond between polymer matrix and fiber.

Several investigations of the interfacial region and its influences on the strength of the composites have been done. Straub et al. [39] conducted microbond tests on P-Aramid/DGEBA Epoxy composites exposed to temperatures ranging from 21 – 130 ^{o}C. The interfacial shear strength was found to decrease with the increasing testing rate and the effect was more pronounced below the glass transition temperature.

Liao [40] investigated the reaction between the coupling agent and epoxy matrix in E-glass fiber reinforced epoxy composites, using Fourier Transform Infrared Spectroscopy

(FTIR). He found that a greater amount of coupling agent is needed for composites in hydrothermal conditions than is required for dry conditions. His experiments demonstrated that the interface will be more stable when the amount of coupling agent increases at the interface, since the layers of the interface can be leached out when subjected to hydrothermal conditions.

Gautier et al. [41] subjected two types of glass-fiber reinforced polyester composites to immersion in water at different temperatures (30, 50, 70 and 100 ^{o}C). Osmotic cracking in matrix, interface and interfacial bonding were identified. Decrease in inter-laminar shear strength was reported which was attributed to interfacial debonding induced by differential swelling.

The effect of fiber coatings on the mechanical properties of unidirectional glass-reinforced composites was studied by Podgaiz and Williams [42]. It was reported that the coating of fibers with an elastomer leads to a significant improvement in the impact strength together with a slight decrease in the tranverse tensile strength.

2.2.4 Effect of Humidity on Composites

The equilibrium moisture content reaches a constant value when the material is fully submerged in water. But its value varies with the relative humidity when the material is exposed to humid air [43]. The equilibrium moisture content for materials exposed to humid air can be expressed as

$$M_m = a\phi^b \qquad \text{(Equation 2.2)}$$

where a and b are constants and ϕ is the relative humidity.

Bonniau and Bunsell [16] studied the water sorption behavior of glass-fiber reinforced epoxy composites subjected to humid air at relative humidities ranging from 0-100 % and temperatures of 23 ^{0}C, 40 ^{0}C, 60 ^{0}C, 80 ^{0}C, 90 ^{0}C. Damage was reported in the composites subjected to relative humidity levels of 90 –100 % for exposure times exceeding two weeks. Micro cracking of the resin surface was attributed for the damage.

Birger et al. [28] studied the response of graphite-epoxy composite specimens subjected to flexural loading, after exposure to humid air at 95 % relative humidity and at a temperature of 50 ^{0}C. It was reported that the mechanical properties and failure mechanisms of the composites under flexural loading are affected by hygrothermal ageing. Also, ageing in 95 % relative humidity at 50 ^{0}C resulted in a drop in the glass transition temperature.

Collings [44] subjected carbon/epoxy composites to humid environments at various temperatures, which were representative of six different climates at different locations in the world. The effect of these climates on total moisture level and distribution is reported for various thicknesses of the carbon/epoxy laminate. A constant relative humidity environment that will produce a representative moisture level in all parts of the composite is proposed.

The effect of humidity of on glass fiber reinforced polyester and vinylester composites was studied by Springer et al. by subjecting them to humid air [45]. Tests were performed at temperatures of 23 ^{0}C and 93 ^{0}C with the composites exposed to humid air at 50 % and 100 % relative humidities. The weight gain of specimens for the specimens exposed to humid air at 100 % relative humidity followed Non Fickian behavior. A decrease in ultimate tensile strength, short-beam shear strength, tensile modulus and shear modulus was observed with increase of exposure time.

2.2.5 Summary of Previous Research

Table 2.1-2.5 present the summary of some previous research on hygrothermal ageing of polymeric composites.

Table: 2.1 Resin systems subjected to environmental ageing

Author(s)	Fiber	Matrix	Test Environment	Test Temperature (^{o}C)	Test Duration
Chin, Nguyen and Aouadi [56]	- - -	Vinylester, Isopolyester, Epoxy	Distilled water, Salt solution, and artificial concrete pore solution	22, 60	400 hours
Ghorbel and Valentin [1]	- -	Polyester Vinylester	Immersion in water	60	3900 hours
Roy et al. [7]	-	Epoxy Resin	Salt water solution	23, 50, 60, 70	6 months

Table: 2.2 Kevlar fiber-reinforced polymer composites subjected to environmental ageing

Author(s)	Fiber	Matrix	Test Environment	Test Temperature (^{o}C)	Test Duration
Aditya and Sinha [21]	Kevlar Kevlar/ Carbon	Epoxy Epoxy	Relative Humidity 95 %	70	900 hours
Allred [25]	Kevlar 49	Epoxy	Immersion in Distilled Water	21, 90, 150	-

Table: 2.3 Glass fiber-reinforced polymer composites subjected to environmental ageing

Author(s)	Fiber	Matrix	Test Environment	Test Temperature (^{o}C)	Test Duration
Aditya and Sinha [21]	Glass Glass	Epoxy Polyester	Relative Humidity 95 %	70	900 hours
Bonniau and Bunsell [16]	E-glass	Bisphenol A Epoxy	0 –100 % RH	25 to 90	-
Chateauminois et al. [27]	R-Glass	DGEBA – based Epoxy	Distilled water	30, 50, 70 and 90	100 days
Gautier, Mortaigne and Bellenger [41]	Glass	Polyester	Immersion in Water	30 to 100	10000 hours
Ghorbel and Valentin [1]	Glass Glass	Polyester Vinylester	Immersion in water	60	3900 hours
Karbhari [67]	E-glass	Vinylester	Immersion in water Relative Humidity 56%	5, 23, 40, 60 23	225 weeks
Marsh, Lasky, Seraphim and Springer [62]	E-glass	Epoxy	Immersion in Water under pressure	50, 75,85 and 100	145 hours

Table 2.3 contd.

Author(s)	Fiber	Matrix	Test Environment	Test Temperature (^oC)	Test Duration
Phani and Bose [4]	E-glass	Isophthalic Polyester	Immersion in Water	50 80 100	480 hours 72 hours 25 hours
Pritchard and Speake [52]	Glass	Isophthalic Polyester	Immersion in water	30, 45, 60, 70, 80 and 100	30 days
Rao et al. [19]	Jute Glass	Epoxy Epoxy	Immersion in distilled water Relative Humidity, 32 %, 76%, 92%, 98%	25, 40 and 60	2500 hours
Springer, Sanders, Tung [45]	E-glass	Polyester	Saturated Salt water No.2 Diesel Fuel Lubrication oil Antifreeze mixture Indolene Humid air 50 % RH Humid air 100 % RH	23, 93 23, 93 23, 93 23, 93 23, 93 3, 93 23, 93	6 months 6 months 6 months 6 months 6 months 6 months 6 months
Wyatt and Ashbee [32]	E-glass	Polyester	Immersion in water	20 and 100	1500 hours

Table: 2.4 Carbon/Graphite fiber-reinforced polymer composites subjected to environmental ageing

Author(s)	Fiber	Matrix	Test Environment	Test Temperature (^{o}C)	Test Duration
Birger et al. [28]	Graphite	Epoxy	Thermal Ageing	170	626 hours
			Immersion in water	23	960 hours
				50	155 hours
			Relative humidity 95 %	100	115 hours
				50	960 hours
Han and Nairn [71]	Carbon	Polyimide	Immersion in Water	80	1000 hours
			Relative Humidity-62, 50, 76%	80	
Loos and Springer [61]	Graphite	Epoxy	No.2 Diesel Fuel, Jet A fuel, Aviation oil, Saturated Salt water, Distilled water	27 to 49	300 days
			Humid air 100 % RH	50, 70, 92	
			Humid air 40 %, 60% RH	65	
			Humid air 25 % RH	92	

Table 2.4 contd.

Author(s)	Fiber	Matrix	Test Environment	Test Temperature (^{o}C)	Test Duration
Mazor, Broutman and Eckstein [68]	Carbon Graphite	Epoxy Epoxy	Relative Humidity 0% Distilled water Sea water	Room Temperature Room Temperature Room Temperature	
Parvatareddy et al. [66]	Carbon	Cyanate Ester	Ambient air, At reduced air pressure, nitrogen	150	9 months
Shen and Springer [43]	Graphite		Humid air- 0, 50, 75, 100 % Saturated Steam Immersion in water	27, 48, 70, 92 120, 150 70, 92, 150	-
Wyatt and Ashbee [32]	E-glass	Polyester	Immersion in water	20 and 100	1500 hours

2.3 Performance Prediction Models

A number of empirical and theoretical models have been proposed for performance prediction of Fiber Reinforced Polymer Composites. A brief description of some of the models, which are frequently used, is given below.

2.3.1 Arrhenius Prediction Model

The Arrhenius Prediction Model is one of the commonly used life prediction models in accelerated life testing [46]. It is a very convenient model to use in cases where the acceleration variable is temperature. The model is derived from the Arrhenius reaction rate equation proposed by the Swedish Chemist Svandte Arrhenius in 1887. The Arrhenius reaction rate equation is given by,

$$R(T) = A\exp\left[\frac{-E_a}{KT}\right] \qquad \text{(Equation 2.3)}$$

where R is the rate of the reaction,

A is a non-thermal constant,

E_a is the activation energy in Joules,

T is the absolute temperature (Kelvin),

K is the Boltzmann's constant, 1.38 x 10^{-23} J/ K.

The Arrhenius life-stress relationship is formulated by assuming that the life is proportional to the inverse reaction rate of the process.

$$L(T) = C\exp\left[\frac{B}{T}\right] \qquad \text{(Equation 2.4)}$$

where L(T) represents the quantifiable life measure,

T is the temperature,

C is one of the model parameters to be determined,

B is another model parameter to be determined.

The Arrhenius life-stress relationship is linearized by taking natural logarithms on both sides of the equation and the property retention data is fitted through the linearized model. The result is a linear relationship between the percent retention of the property and the natural logarithm of time. This relationship is then utilized for deriving an equation relating the percent retention and the different temperatures to which the composite was subjected. These relationships obtained can be used for prediction of life at temperatures other than those used in the experiment.

2.3.2 Phani and Bose Prediction Model

Phani and Bose investigated the strength characteristics of a E-glass/ Polyester chopped strand mat (CSM laminate) immersed in water, using flexural strength tests. The characterization of hydrothermal ageing of the laminates by means of acousto-ultrasonic technique shows that the flexural strength σ_t after exposure time t is given by the relation [47],

$$\sigma_t = (\sigma_0 - \sigma_\infty)\exp[-t/\tau] + \sigma_\infty \qquad \text{(Equation 2.5)}$$

where σ_0 and σ_∞ are the flexural strength at times 0 and ∞, respectively and τ is a characteristic time dependent on temperature.

It was found that the reduction of the strength of CSM laminates due to hydrothermal effects is a rate process for which the temperature influences only the rate constant. The rate constant follows the Arrhenius equation [48],

$$\frac{1}{\tau} = \frac{1}{\tau_0} \exp\left[\frac{-E_a}{RT}\right] \qquad \text{(Equation 2.6)}$$

where $1/\tau$ is the rate constant,

E_a is the activation energy in Joules,

$1/\tau_0$ is a constant,

R is the universal gas constant (8.314 J/mol),

T is the temperature (Kelvin).

From equations 2.1 and 2.6 it is evident that the rate constant is nothing but the diffusion coefficient. The percent retention data is fitted to the equation 2.5 using regression analysis. This analyses yields relationships between the flexural strength and time at different temperatures. By plotting $1/\tau$ against 1/T, the values of E_a and τ_0 are found. Using the value of the constants calculated, equations 2.5 and 2.6 are combined to give the strength degradation with time and temperature.

Time and Temperature Superposition principle (TTSP) is applied to the degradation process and a master curve for the process is obtained by shifting the data on the logarithmic time scale. This master curve makes determination of strength at any temperature possible, if the activation energy of the process is known. Thus, strength retention experiments need to be conducted only at one temperature to estimate the degradation at different temperatures.

2.3.3 Time and Temperature Superposition Model

Time and Temperature Superposition is a well known principle that works for certain types of viscoelastic materials and relates the effect of time and the effect of

temperature, enabling us to substitute time with elevated temperature [49, 50, 51]. When stiffness or strength properties are plotted against the logarithm of time for different temperatures, they form a set of smooth curves. TTSP is based on the assumption that these curves match each other when shifted horizontally along logarithmic time scale.

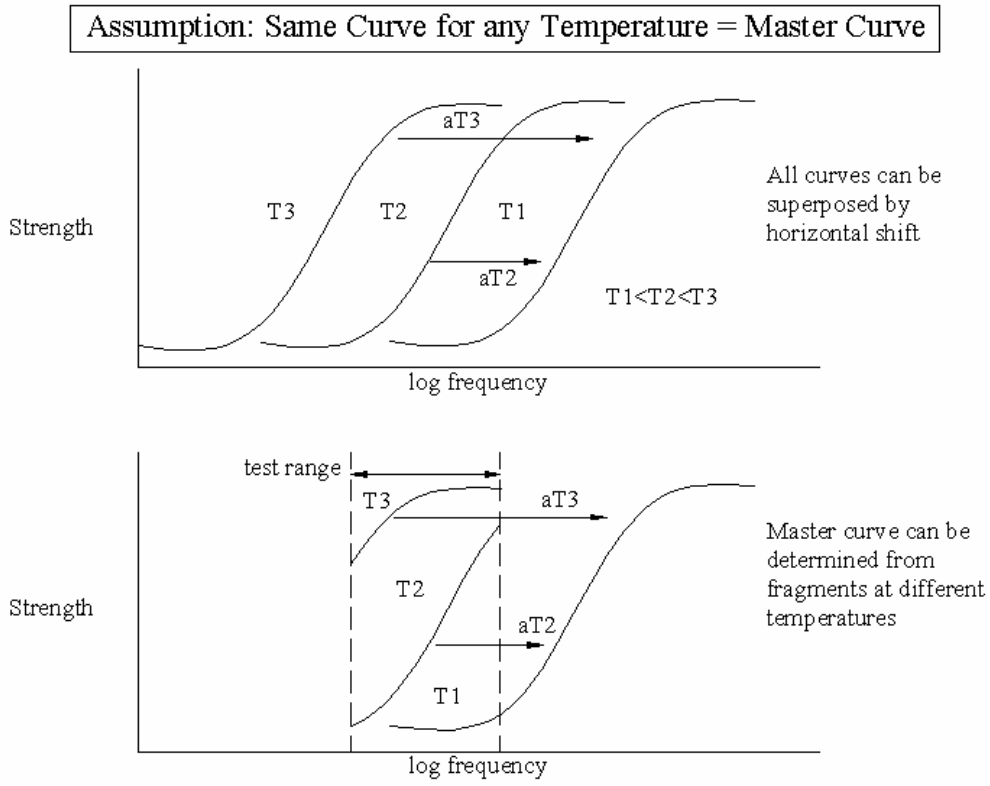

Fig 2.4 Time Temperature Superposition Principle (After Kuraishi [50])

Time dependent data at a particular temperature is selected as reference to determine the shift factor on the time scale. The properties for each test temperature are plotted on a logarithmic time scale, the data for the reference temperature are held fixed, and the other curves are shifted horizontally along the time scale until the points form a single curve. A small vertical shift can be applied to achieve the best superposition. The

resulting curve is called the master curve, which can be used to predict the strength and stiffness properties at temperatures other than those used in the experiments.

It should be noted that superposition is mostly an approximation and therefore extrapolation for long-term exposures, outside temperature ranges used in the experiments is not reliable. The TTSP principle does not work, if there are multiple degradation processes involved. If the data is determined with sufficient accuracy over a large enough time range (three or more decades), superposition will show that the curves actually do not form a single curve. In many cases, data is available only for a limited amount of time, and under these conditions superposition may appear to work, when it does not.

2.3.4 Pritchard and Speake Prediction Model

Pritchard and Speake describe a predictive model for the mechanical property degradation in E-glass/Polyester composites due to immersion in water at different temperatures [52]. The degradation in the properties was found to be a function of the absorbed moisture content, but was shown to be independent of the temperature of sorption even when the sorption temperature exceeded the glass transition temperature of the resin. According to Pritchard and Speake [52], two steps are necessary to predict material properties: 1) the prediction of water sorption kinetics at temperatures outside the experimental range, and 2) the establishment of empirical relationships between moisture content and the properties.

The Fickian absorption model can be extended to find the absorption curve for temperatures outside the experimental range. By plotting maximum moisture content from the Fickian absorption model against temperature, it is possible to estimate the values of moisture uptake at temperatures outside the experimental range. The diffusion coefficients

for the temperatures outside the experimental range can also be found by extrapolation of the Arrhenius plots.

A curve-fitting program was used to obtain an empirical relationship between the mechanical properties and the absorbed moisture contents. The best fits obtained from the program were of the form,

$$p = a\left(1 - e^{-b\exp[-cM_t]}\right) + d \qquad \text{(Equation 2.7)}$$

where p is the residual property,

M_t is the moisture absorption at time t,

a, b, c and d are empirical constants.

This equation can be used to predict the residual mechanical properties at various temperatures. The validity of these predictions depends on all degradation processes being functions of absorbed water content, and on their being accelerated by temperature in the same way and to the same extent as the water absorption process.

2.3.5 Phillips Prediction Model

Phillips [53] investigated the stress rupture in glass-fiber reinforced polyester composites exposed to air and aqueous environments. He assumed that below the level of stress, which causes immediate failure σ_0, there exists a functional relationship between the time to failure, t and the corresponding stress σ_t. The Phillips prediction model relates the stress and the time to failure as follows:

$$\frac{\sigma_t}{\sigma_0} = A - B\log t \qquad \text{(Equation 2.8)}$$

where σ_t is the stress at time t,

σ_0 is the initial stress,

A and B are empirical constants.

The property retention data can be fitted to equation 2.7 using regression analysis. The empirical constants are found from the regression analysis and thus prediction of long-term strength properties is made possible.

2.4 References

1. Ghorbel I. and Valentin D., "Hydrothermal Effects on the Physico-Chemical Properties of Pure and Glass Fiber Reinforced Polyester and Vinylester Resins", *Polymer Composites*, 1993, Vol. 14, Issue 4, pp. 324-334.

2. Crank J. and Park G. S., Diffusion in Polymers, Academic Press, New York, 1968.

3. Marom G., "The Role of Water Transport in Composite Materials", Polymer Permeability, Comyn J, Ed., Elsevier, New York, 1975, pp. 341-374.

4. Crank J., The Mathematics of Diffusion, Clarendon Press, Oxford, UK, 1967.

5. Comyn J., Polymer Permeability, Elsevier, New York, 1975.

6. Weitsman J., "Effect of Fluids on Polymeric Composites-A Review", Report to Office of Naval Research, Mechanical and Aerospace Engineering and Engineering Science, University of Tennessee, Report MAES98-5.0-CM, 1998.

7. Roy S., Xu W.X., Park S.J. and Liechti K.M., "Anomalous Moisture Diffusion in Viscoelastic Polymers: Modeling and Testing", *Journal of Applied Mechanics*, June 2000, Vol. 67, pp. 391-396.

8. Cai L.W., and Weitsman Y., "Non-Fickian Moisture Diffusion in Polymeric Composites", *Journal of Composite Materials*, 1994, Vol. 28, Issue 2, pp. 130-154.

9. Connelly T.M., and Turner J.C.R., "Two-Phase Diffusion- Diffusion through Polymers and Polymer Blends", *Chemical Engineering Science*, 1979, Vol. 34, pp. 319-323.

10. Weitsman Y., "Moisture in Composites: Sorption and Damage", Fatigue in Composite Materials, K L Reifsnider Ed., Elsevier Science Publishers, pp. 385-429.

11. Ruthven D.M., "The Rectangular Isotherm Model for Adsorption Kinetics", *Adsorption*, December 2000, Vol. 6, Issue 4, pp. 287-291.

12. Tsotsis T.K., and Weitsman Y., "A Simple Graphical Method for Determining Diffusion Parameters for Two-Stage Sorption in Composites", *Journal of Materials Science Letters*, 1994, Vol. 13, pp. 1635-1636.

13. Wong T., and Broutman L., "Moisture Diffusion in Epoxy Resins Part I: Non-Fickian Sorption Processes", *Polymer Engineering Science*, 1985, Vol. 25, Issue 9, pp. 521-528.

14. Wong T. and Broutman L., "Water in Epoxy Resins Part II: Diffusion Mechanisms", *Polymer Engineering Science*, 1985, Vol. 25, Issue 9, pp. 529-534.

15. Carter H.G., and Kibler K.G., "Langmuir Type Model for Anomalous Moisture Diffusion in Composite Resins", *Journal of Composite Materials*, 1978, Vol. 12, pp. 118-131.

16. Bonniau P. and Bunsell A.R., "A Comparative Study of Water Absorption Theories Applied to Composites", *Journal of Composite Materials*, 1981, Vol. 15, pp. 272-293.

17. Hopfenberg H.B. and Stannett V.T., "The Diffusion and Sorption of Gases and Vapors in Glassy Polymers", The Physics of Glassy Polymers, Ed., Haward R.N., Applied Science Publishers, London, 1973, pp. 504-518.

18. Stannett V., "Simple Gases", Diffusion in Polymers, Ed., Crank J and Park G S, Academic Press, New York, 1968, pp. 41-73.

19. Rao R.M.V.G.K., Balasubramanian N. and Chanda M., "Factors Affecting Moisture Absorption in Polymer Composites Part I: Influence of Internal Factors", *Journal of Reinforced Plastics and Composites*, 1984, Vol. 3, pp. 232-245.

20. Rao R.M.V.G.K., Balasubramanian N. and, Chanda M., "Factors Affecting Moisture Absorption in Polymer Composites Part II: Influence of External Factors", *Journal of Reinforced Plastics and Composites*, 1984, Vol. 3, pp. 246-253.

21. Aditya P.K., and Sinha P.K., "Diffusion Coefficients of Polymeric Composites Subjected to Periodic Hygrothermal Exposure", *Journal of Reinforced Plastics and Composites*, 1992, Vol. 11, pp. 1035-1047.

22. Antoon M.K., and Koening J.L., "The Structural and Moisture Stability of the Matrix Phase in Glass-Reinforced Epoxy Composites", *Journal of Macromolecular Science- Review Macromolecular Chemistry*, 1980, Vol. C19, Issue 1, pp. 135-173.

23. Tissaoui J., Doctoral Thesis, " Effects of Long-term Creep on the Integrity of Modern Wood Structures", Department of Civil Engineering, Virginia Polytechnic Institute and State University, Blacksburg, Virginia, December 1996, 120 pp.

24. Bank L.C., Gentry T.R. and Barkatt A., "Accelerated Test Methods to Determine the Long-Term Behavior of FRP Composite Structures: Environmental Effects", *Journal of Reinforced Plastics and Composites*, 1995, Vol. 14, pp. 559-587.

25. Allred R.E., "The effect of temperature and moisture content on the flexural response of Kevlar/epoxy laminates I (0/90) filament orientation" *Journal of Composite Materials*, 1981, Vol. 15, pp. 100-116.

26. Allred R.E., "The effect of temperature and moisture content on the flexural response of Kevlar/epoxy laminates II (+or-45, 0/90) Filament orientation" *Journal of Composite Materials*, 1981, Vol. 15, pp. 117-132.

27. Chateauminois A., Chabert B., Soulier J.P. and Vincent L., "Hygrothermal Ageing Effects on the Static Fatigue of Glass/Epoxy Composites", *Composites*, 1993, Vol. 24, Issue 7, pp. 547-555.

28. Birger S., Moshonov A. and Kenig S., "The Effects of Thermal and Hygrothermal Ageing on the Failure Mechanisms of Graphite-Fabric Epoxy Composites subjected to Flexural Loading", *Composites*, 1989, Vol. 20, Issue (4), pp. 341-348.

29. Apicella A., Migliaresi C., Nicolais L., Iaccarino L. and Roccotelli S., "The Water Ageing of Unsaturated Polyester-based Composites: Influence of Resin Chemical Structure", *Composites*, October 1983, Vol. 14, Issue 4, pp. 387-92.

30. Apicella A., Migliaresi C., Nicodemo L., Nicolais L., Iaccarino L. and Roccotelli S., " Water Sorption and Mechanical Properties of a Glass-reinforced Polyester Resin", *Composites*, October 1982, Vol. 13, Issue 4, pp. 406-410.

31. Williams C.J., "The Effect of Moisture Absorption on Room Temperature Mechanical Properties of Reinforced Polymer Composites", Research and Development Report, Ship Materials Engineering Department, David Taylor Research Center, Report DTRC-SME-91/35, January 1991.

32. Wyatt R.C. and Ashbee H.G., "Debonding in Carbon/Fiber Resin Polyester Composites Exposed to Water: Comparison with E-glass Fiber Composites", *Fiber Science and Technology*, July 1969, Vol. 2, Issue 1, pp. 29-40.

33. Ehrenstein G.W. and Spaude R., "A Study of Corrosion Resistance of Glass Fiber Reinforced Polymers", *Composite Structures*, 1984, Vol. 2, pp. 191-200.

34. Michalske T.A. and Bunker B.C., "The fracturing of glass", *Scientific American*, Dec 1987, Vol. 257, Issue 6, pp. 78-85.

35. Liao K., Schultheisz C.R. and Hunston D.L., "Effects of Environmental Ageing on the Properties of Pultruded GFRP", *Composites: Part B*, 1999, Vol. 30, pp. 485-493.

36. Schutte C.L., "Environmental Durability of Glass-fiber Composites", *Materials Science and Engineering*, 1994, Vol. R13, pp. 265-324.

37. Ishida H. and Koenig J., "The Reinforcement Mechanism of Fiber-Glass Reinforced Plastics under Wet Conditions: A Review," *Polymer Engineering and Science*, February 1978, Vol. 18, Issue 2, pp. 128-145.

38. Plueddemann E.P., "Water is the key to new theory on resin-to-fiber bonding", *Modern Plastics*, March 1970, Vol. 47, pp. 92-98.

39. Straub A., Slivka M. and Schwartz P., "A Study of the Effects of Time and Temperature on the Fiber/Matrix Interface Strength Using the Microbond Test", *Composite Science and Technology*, 1997, Vol. 57, pp. 991-994.

40. Liao Y.T., "A Study of Glass Fiber-Epoxy Composite Interfaces", *Polymer Composites*, December 1989, Vol. 10, Issue 6, pp. 424-428.

41. Gautier L., Mortaigne B. and Bellenger V., "Interface Damage Study of Hydrothermally Aged Glass-Fiber Reinforced Polyester Composites", *Composite Science and Technology*, 1999, Vol. 59, pp. 2329-2337.

42. Podgaiz R.H. and Williams R.J., "Effect of Fiber Coatings on Mechanical Properties of Unidirectional Glass-Reinforced Composites", *Composite Science and Technology*, 1997, Vol. 57, pp. 1071-1076.

43. Shen C. and Springer G.S., "Moisture Absorption and Desorption of Composite Materials", Environmental effects on Composite Materials, 1988, Ed., Springer G. S., Vol. 3, pp. 15-34.

44. Collings T.A., "The Effect of Observed Climatic Conditions on the Moisture Equilibrium Level of Fiber-Reinforced Plastics", *Composites*, January 1986, Vol. 17, Issue 1, pp. 33-41.

45. Springer G.S., Sanders B.A. and Tung R.W., "Environmental Effects on Glass Fiber Reinforced Polyester and Vinylester Composites", *Journal of Composite Materials*, July 1980, Vol. 14, pp. 213-232.

46. Reliasoft Corporation Website, www.reliasoft.com

47. Phani K.K. and Bose N.R., "Hydrothermal Ageing of CSM- Laminate During Water Immersion- An Acousto-Ultrasonic Study", *Journal of Materials Science*, October 1986, Vol. 21, Issue 10, pp. 3633-3637.

48. Phani K.K. and Bose N.R., "Temperature Dependence of Hydrothermal Ageing of CSM- Laminate during Water Immersion", *Composites Science and Technology*, 1987, Vol. 29, Issue 2, pp. 79-87.

49. Liao K., Schulthiesz C.R., Hunston D.L. and Brinson L.C., "Long-term Durability of Fiber-Reinforced Polymer Matrix Composite Materials for Infrastructure Applications – A Review", *Journal of Advanced Materials*, 1998, Vol. 30, Issue 4, pp. 3-40.

50. Kuraishi A., "Durability Analysis of Composite Structures Using the Accelerated Testing Methodology", Doctoral Dissertation, Department of Aeronautics and Astronautics, Stanford, California, Stanford University, 2001, 143 pp.

51. Fesko D G, "Time-Temperature Superposition for Block Copolymers", Doctoral Dissertation, Department of Materials Science, Pasadena, California, California Institute of Technology**,** 1971**,** 202 pp.

52. Pritchard G. and Speake S.D., "The Use of Water Absorption Kinetic Data to Predict Laminate Property Changes", *Composites*, July 1987, Vol. 14, Issue 3, pp. 227-232.

53. Phillips M.G., "Prediction of Long-term Stress-Rupture Life for Glass Fiber-Reinforced Polyester Composites in Air and in Aqueous Environments", *Composites*, July 1983, Vol. 14, Issue 3, pp. 270-275.

54. Wolff E.G., "Moisture Effects on Polymer Matrix Composites", *SAMPE Journal*, 1993, Vol. 29, Issue 3, pp. 11-19.

55. Karbhari V.M. and Zhang S., "E-glass/Vinylester Composites in Aqueous Environments – I: Experimental Results", *Applied Composite Materials*, 2003, Vol. 10, pp. 19-48.

56. Chin J.W., Nguyen T. and Aouadi K., "Sorption and Diffusion of Water, Salt Water and Concrete Pore Solution in Composite Matrices", *Journal of Applied Polymer Science*, 1999, Vol. 71, pp. 483-492.

57. Bonniau P. and Bunsell A.R., "A Comparative Study of Water Absorption Theories Applied to Composites", *Journal of Composite Materials*, 1981, Vol. 15, 272-293.

58. Holmberg J.A., "On Flexural and Tensile Strength for Composites manufactured by RTM", *Journal of Reinforced Plastics and Composites*, 1992, Vol. 11, pp. 1302-1320.

59. Whitney J.M. and Knight M., "The Relationship between Tensile Strength and Flexure Strength in Fiber-reinforced Composites", *(Journal Paper) Experimental Mechanics,* 1980, Vol. 20, Issue 6, pp. 211-216.

60. Springer G.S., Sanders B.A. and Tung R.W., "Environmental Effects on Glass Fiber Reinforced Polyester and Vinylester Composites", *Journal of Composite Materials*, July 1980, Vol. 14, pp. 213-232.

61. Loos A.C. and Springer G.S., "Moisture Absorption of Graphite-Epoxy Composites Immersed in Liquids and in Humid Air", *Journal of Composite Materials*, April 1979, Vol. 13, pp. 131-145.

62. Marsh L.L., Lasky R., Seraphim D.P. and Springer G.S., "Moisture Solubility and Diffusion in Epoxy and Epoxy-Glass Composites", *IBM Journal of Research and Development*, November1984, Vol. 28, Issue 6, pp. 655-661.

63. Chu W., "Investigation of Short-Term Aqueous Exposure on Pultruded E-Glass/Vinylester Composites", Master's Thesis, Department of Structural Engineering, University of California, San Diego**,** 2002**,** 222 pp.

64. Abanilla A., Master's Thesis, "Physico-Chemico Effects on T700 Based Fabric," Department of Structural Engineering, University of California, San Diego, 2004, 260 pp.

65. Wimolkiatisak A.S. and Bell J.P., "Interfacial Shear Strength and Failure Modes of Interphase-Modified Graphite/Epoxy Composites", *Polymer Composites*, June 1989, Vol. 10, Issue 3, pp. 162-172.

66. Parvatareddy H., Wang J.Z., Dillard D.A., Ward T.C. and Rogalski M.E., "Environmental Ageing of High-Performance Polymeric Composites: Effects on Durability", *Composites Science and Technology*, 1995, Vol. 53, pp. 399-409.

67. Karbhari V.M., "E-glass Vinylester Composites in Aqueous Environments: Effect on Short-Beam Shear Strength", *Journal of Composites for Construction*, March/April 2004, Vol. 8, Issue 2, pp. 148-156.

68. Mazor A., Broutman L.J. and Eckstein B.H., "Effect of Long-Term Water Exposure on Properties of Carbon and Graphite Fiber Reinforced Epoxies", *Polymer Engineering and Science*, April 1978, Vol. 18, Issue 5, pp. 341-349.

69. Reay J.T., Pantelides C.P., Reaveley L.D., Ring T.A., "Long Term Durability of Carbon FRP Composites Applied to RC Bridges: State Street Bridge on Interstate 80", *Report No. CVEEN-04/1*, University of Utah, Salt Lake City Utah, 2004.

70. Malvar L.J., "Durability of Composites in Reinforced Concrete", Proceedings of the First International Conference on Durability of Composites for Construction, Sherbrooke, Quebec, Canada, August 1998, pp. 361-372.

71. Han M. and Nairn J.A., "Hygrothermal Ageing of Polyimide Matrix Composites", *Composites: Part A*, 2003, Vol. 34, pp. 979-986.

72. Aveston J., Kelly A. and Sillwood J.M., "Advances in Composite Materials", Vol I, A. R. Bunsell, C.R. Bathias, A. Martrenchar, D. Henkes and G. Verchery Ed., Pergamon, Paris, 1980.

73. Harper J.F. and Naeem M., "The Moisture Absorption of Glass Fiber Reinforced Vinylester and Polyester composites", *Materials and Design*, December 1989, Vol. 10, Issue 6, pp. 297-300.

74. Karbhari V.M., Chu W. and Wu L., "Durability Evaluation of Moderate Temperature Cured E-glass/Vinylester Systems" *Composite Structures*, December 2004, Vol. 66, Issue 1-4, pp. 367-376.

Chapter 3

Materials and Test Procedures

3.1 Material Constituents

The composite system used in the study is a unidirectional E-glass/Vinylester composite with a volume fraction of 50-55 %. The E-glass/Vinylester composite specimens were manufactured by the Resin Infusion Process using the Dow Derakane 411-350 vinylester resin.

3.1.1 Glass Fiber Properties

The properties of E-glass fiber used to manufacture the unidirectional composites are listed in Table 3.1.

3.1.2 Vinylester Matrix Properties

Vinylester resins are being widely considered for use in civil infrastructure, marine vessels and offshore structures due to their ability to be easily fabricated through processes like resin infusion. The vinylester resin used for the composite is Dow Chemicals Derakane 411-350. Dow Derakane 411-350 is based on bisphenol-A epoxy resin and has been widely used in a wide range of end-use applications due to its ability to be used in a wide range of fabrication techniques. Derakane 411-350 provides resistance to acids, alkalis and organic compounds and also provides good corrosion resistance. The resin is characterized by superior elongation and toughness, which provides the composites with better impact resistance and less cracking due to cyclic temperature and mechanical shocks [2]. The

liquid resin properties of Dow Derakane 411-350 are listed in Table 3.2 [2]. Table 3.3 gives a list of properties of the post-cured clear cast resin.

3.1.3 Fabrication Method

The E-glass/Vinylester composites were fabricated using the Resin Infusion Process [1] and are of 2.54 mm (0.1 in) thickness each. The specimens were post-cured at 120 ^{o}C for 24 hours. The fiber volume fraction of the specimens was then assessed by burn-off tests and it was found to be 50-55 %.

3.2 Environmental Conditions

The E-glass/Vinylester test specimens were subjected to different environments encompassing immersion in deionized water and humidity at different temperatures. The list of the testing environments is given below:

1. Ambient conditions at 23 ^{o}C and 30 % Relative Humidity
2. Immersion in deionized water at 23 ^{o}C
3. Immersion in deionized water at 45 ^{o}C
4. Immersion in deionized water at 60 ^{o}C
5. Immersion in deionized water at 80 ^{o}C
6. Immersion in deionized water at 95 ^{o}C
7. Exposure to humid air with 0-5 % relative humidity at 23 ^{o}C
8. Exposure to humid air with 45 % relative humidity at 23 ^{o}C
9. Exposure to humid air with 60 % relative humidity at 23 ^{o}C
10. Exposure to humid air with 75 % relative humidity at 23 ^{o}C
11. Exposure to humid air with 98 % relative humidity at 23 ^{o}C
12. Exposure to humid air with 0-5 % relative humidity at 95 ^{o}C

13. Exposure to humid air with 45 % relative humidity at 95 ^{o}C
14. Exposure to humid air with 60 % relative humidity at 95 ^{o}C
15. Exposure to humid air with 75 % relative humidity at 95 ^{o}C
16. Exposure to humid air with 98 % relative humidity at 95 ^{o}C

The set of conditions were chosen to enable testing over a range og hygrothermal exposures which would also enable useof acceleration procedures.

Table 3.1 Properties of E-glass Fibers (Kaw [1])

Property	**Value (SI)**	**Value (FPS)**
Specific gravity	2.54	2.54
Young's modulus	72.40 GPa	10.5 Msi
Ultimate Tensile Strength	1447 MPa	210 Ksi
Coefficient of thermal expansion	5.04 μm/m/^{o}C	2.80 μ.in/in/^{o}F
Poisson's Ratio	0.2	0.2
Axial Shear Modulus	35.42 GPa	5.136 Msi
Shear strength	35 MPa	5.08 Ksi
Chemical Composition	54% Silicon oxide, 15% Aluminium oxide, 17% Calcium oxide, 4.5% Magnesium oxide, 8% Boron oxide	

Table 3.2 Typical Liquid Resin
Properties of Dow Derakane 411-350 Vinylester Resin *

Property	**Value**
Density 25 ^{o}C/ 77 ^{o}F	1.046 g/mL
Dynamic Viscosity 25 ^{o}C/ 77 ^{o}F	370 mPa. s
Kinematic Viscosity	350 centiStokes
Styrene content	45 % by weight
Shelf Life 25 ^{o}C/ 77 ^{o}F	7 months

*www.dow.com

Table 3.3 Typical Properties of Clear Resin Castings (From [2])

Property	Value (SI)	Value (FPS)
Tensile Strength	73 MPa	10500 psi
Tensile Modulus	2.8 GPa	4×10^5 psi
Tensile Elongation, Yield	4.8 %	4.8 %
Flexural Strength	122 MPa	17600 psi
Flexural Modulus	3.1 GPa	4.5×10^5 psi

3.3 Test Procedures

A brief account of the testing procedures followed for the moisture absorption tests and mechanical characterization tests is given in the subsequent sections.

3.3.1 Moisture Sorption

Moisture is known to react with one or more of the matrix constituents and can hydrolyze the polymer bonds leading to the dissolution and leaching of water-soluble components. Moisture affects polymeric composites physically by plasticizing the matrix and thus lowering its glass transition temperature [3]. Moisture absorption in FRP composites not only affects the dimensional stability but also affects the mechanical properties of the composites. Thus determination of the moisture content and the rate of moisture diffusion in composites after exposure to hygrothermal ageing is necessary because moisture sorption has profound effects on short-term and long-term durability of the composite system.

The measurement of moisture uptake was conducted by the gravimetric method. Five specimens with dimensions of 25.4 mm x 25.4 mm (0.1in x 0.1 in) and 2.54 mm (0.1

in) thickness were placed in each of the environments listed in section 3.3 and the uptake was measured at periodic intervals.

3.3.2 Tensile Characterization

Tensile tests are important because they are main characterizing element that defines the in-plane tensile properties of the composite specimen [4]. Tensile data on unidirectional composites are often used as one of the key factors in materials selection and also provide basic ply properties, which are used in laminate design [5]. The ultimate tensile strength and tensile modulus are the two important parameters that are obtained from this test in addition to other tensile properties. However the tensile tests carried out under controlled conditions and close observation can also yield additional information about failure initiation and development [4]. Polymeric composites being non-homogenous exhibit weakness in a particular loading direction, while having high strength in other directions. Therefore the direction of loading is of utmost importance for polymeric composites for the determination of tensile properties. The tensile tests on the E-glass/Vinylester composite specimens were performed in accordance with ASTM D 3039M [6]. The composite specimens measuring 254 mm x 25.4 mm x 2.54 mm (10 in x 1 in x 0.1 in) were tested in an Instron testing machine with the grips set to a gage length of 177.8 mm (7 in). The specimen was loaded at a rate of 1.27 mm/min (0.05 in/min).

3.3.3 Flexure Characterization

The use of flexural tests to determine the mechanical properties of polymeric composites is widely prevalent because of the relative simplicity of the test method, instrumentation and testing equipment required. Flexure mode tests can also be used to determine the interlaminar shear strength (using a short beam) and interlaminar fracture

toughness of the composite laminates. Although it is frequently found that the flexure tests give results, which are very similar to those from other tests (tension and compression), it is generally recognized that test methods applying flexure as a means of loading do not produce results of design data quality. But flexure tests continue to be used widely because of their relative simplicity [7].

The flexure tests for the E-glass/Vinylester specimens were done in accordance with ASTM D 790 [8]. The composite specimens used measured 12.7 mm (0.5 in) in width and 2.54 mm (0.1in) in thickness. The span of the specimen measures 152.4 mm (6 in) making the span to depth ratio 60:1. The specimen is loaded at a constant rate of 5.08 mm/min (0.2 in/min). The specimen is loaded until rupture occurs.

3.3.4 Short Beam Shear Characterization

Fiber-reinforced composite are known to exhibit poor resistance to shear deformation, especially in material planes dominated by matrix properties. Relatively low values of shear strength and shear modulus often leads to use of optimized arrangement of laminate stacking sequences to maximize shear resistance. This in turn can lead to the compromise of other mechanical properties [9]. Development of in-plane and out-of-plane shear test methods for the determination of shear modulus and strength of fiber-reinforced composites is difficult because a region of pure and uniform shear stress has to be provided in the test section of the specimen. The difficulty of inducing pure shear increases with increasing anisotropy and inhomogeneity of the material. Because of this there are a wide variety of methods employed to determine the shear characteristics of a fiber-reinforced composite specimen, which are listed below:

- $\pm 45^{o}$ Tension test – ASTM D 3518
- Rail Shear Test – ASTM D 4255

- V-notched beam test – ASTM D 5379
- Plate-twist test – ASTM D 3044
- Short Beam Shear test – ASTM D 2344

In this study, the short beam shear test ASTM D 2344 [10] was employed to find the shear characteristics of the E-glass/Vinylester composite specimens. Short beam shear tests are performed on composite specimens 12.7 mm (0.5 in) in width and 2.54 mm (0.1 in) in thickness and 12.7 mm (0.5 in) length (span). A span to depth ratio of 5:1 was employed for the test. The specimens were loaded at a rate of 32.25 mm/min.

3.3.5 Dynamic Mechanical Thermal Analysis

Dynamic Mechanical Thermal Analysis (DMTA) is used to determine the change in the mechanical properties of materials either under isothermal conditions or as a function of temperature. The technique is often used to measure the damping properties of materials and the glass transition temperature of polymers [11]. The technique uses measured natural frequencies of dynamically excited specimens to derive stiffness properties of the material.

DMTA tests were performed as per ASTM E1640 [12], using three-point bending. The DMTA test was performed on the composite specimens and the glass transition temperature was measured for the specimens immersed in water at 23 ^{o}C, 40 ^{o}C, 60 ^{o}C, 80 ^{o}C and 95 ^{o}C.

3.4 References

1. Kaw A.K, “Mechanics of Composites Materials” CRC Press, 1997.

2. V.M. Karbhari, unpublished results.

3. Marom G., “The Role of Water Transport in Composite Materials”, Polymer Permeability, Comyn J., Ed., Elsevier, New York, 1975, pp. 341-374.

4. Godwin E.W., “Tension”, Mechanical Testing of Advanced Fiber Composites, J.M. Hodgkinson Ed., Cambridge, England, CRC Press, 2000.

5. Whitney J.M. and Knight M., “The relationship between Tensile Strength Flexure Strength in Fiber-Reinforced Composites”, *Experimental Mechanics*, June 1980, pp. 211-216.

6. ASTM D3039M, “Standard Test Method for Tensile Properties of Polymer Matrix Composite Materials”, American Society of Testing Materials, 1997, Vol. 15.03.

7. Hodgkinson J.M., “Flexure”, Mechanical Testing of Advanced Fiber Composites, J.M. Hodgkinson Ed., Cambridge, England, CRC Press, 2000.

8. ASTM D790M, “Standard Test Methods for Flexural Properties of Unreinforced and Reinforced Plastics and Electrical Insulating Materials”, American Society of Testing Materials, 1993, Vol. 08.01.

9. Broughton W.R., “Shear”, Mechanical Testing of Advanced Fiber Composites, J.M. Hodgkinson Ed., Cambridge, England, CRC Press, 2000.

10. ASTM D2344M, “Standard Test Method for Apparent Interlaminar Shear Strength of Parallel Fiber Composites by Short-Beam Method”, American Society of Testing Materials, 2000.

11. Bank L.C., Gentry T.R. and Barkatt A., “Accelerated Test Methods to Determine the Long-Term Behavior of FRP composite Structures: Environmental Effects”, *Journal of Reinforced Plastics and Composites*, June 1995, Vol. 14, pp. 559-587.

12. ASTM E1640, “Standard Test Method for Assignment of the Glass Transtion Temperature by Dynamic Mechanical Analysis”, American Society of Testing Materials, 1999, Vol. 13.02.

Chapter 4

Experimental Results

This chapter reports data pertaining to moisture uptake and results of the mechanical characterization tests. For purposes of clarity, the results are listed separately by section. The results will be used in the subsequent chapters to develop predictive and correlative relationships.

4.1 Moisture Uptake Results

4.1.1 Immersion in Water

The moisture absorption data, reported as the average of five specimens per time period and set, for E-glass/vinylester composite specimens immersed in deionized water at different temperatures are shown in the Table 4.1 and represented graphically in Fig. 4.1.

4.1.2 Exposure to Humid Air

The moisture absorption data, reported as the average of five specimens per time period and set, for E-glass/vinylester composite specimens exposed to humid air at 23 ^{o}C and 95 ^{o}C are given in the Table 4.2 and Table 4.3 and represented graphically in Fig. 4.2 and Fig. 4.3 respectively. It is noted that at the lowest humidity level there is an overall mass loss due to further drying of samples under this exposure condition. The moisture picked up from the environment by the specimens is given up at this low level.

Table 4.1 Percentage weight gain for E-glass/Vinylester specimens immersed in deionized water at temperatures of 23 ^{o}C, 40 ^{o}C, 60 ^{o}C, 80 ^{o}C and 95 ^{o}C

Time (Days)	Temperature of Immersion				
	23 ^{o}C	40 ^{o}C	60 ^{o}C	80 ^{o}C	95 ^{o}C
0	0	0	0	0	0
0.031	-	0.030	0.040	0.050	-
0.042	-	0.049	0.104	0.121	0.180
1	0.090	0.090	0.125	0.145	0.235
2	0.103	0.106	0.133	0.176	0.248
6	-	0.130	0.142	0.184	-
7	0.138	0.153	0.163	-	0.280
9	-	0.165	0.179	0.203	-
12	0.154	0.174	0.182	-	0.310
14	0.164	0.183	0.195	0.226	-
16	0.17	0.192	-	-	0.370
20	0.173	-	0.217	0.240	-
23	-	0.216	0.231	0.284	0.410
27	0.180	0.218	-	0.326	-
33	0.192	-	0.268	0.335	0.450
40	0.210	0.262	0.276	0.358	0.480
47	0.235	0.262	0.294	0.361	0.530
54	0.250	0.263	0.302	0.385	-
61	0.257	0.263	0.316	-	0.572
68	0.264	-	0.327	0.396	0.579
78	0.268	0.276	0.335	-	0.613
89	0.278	0.285	0.342	0.426	-
96	0.281	0.296	-	-	0.624
117	0.292	0.314	0.364	0.446	-
130	0.303	0.326	0.381	0.458	0.631
150	0.314	-	0.397	-	-
189	0.317	-	0.403	0.477	0.635
216	-	0.368	-	0.516	0.642
225	0.344	0.372	0.419	0.534	0.648
248	0.365	0.385	0.427	0.538	0.669
269	0.377	0.396	0.435	0.552	0.683
301	0.381	0.403	0.448	0.563	0.717
335	0.387	0.405	0.453	0.573	0.719
380	0.389	0.409	0.462	0.589	0.728
450	0.393	0.415	0.481	0.603	0.714
600	0.395	0.421	0.498	0.616	0.692
708	0.398	0.425	0.516	0.619	0.686
900	0.401	0.433	0.520	0.624	0.670
1200	0.403	0.437	0.529	0.616	0.650
1500	0.405	0.438	0.533	0.601	0.621

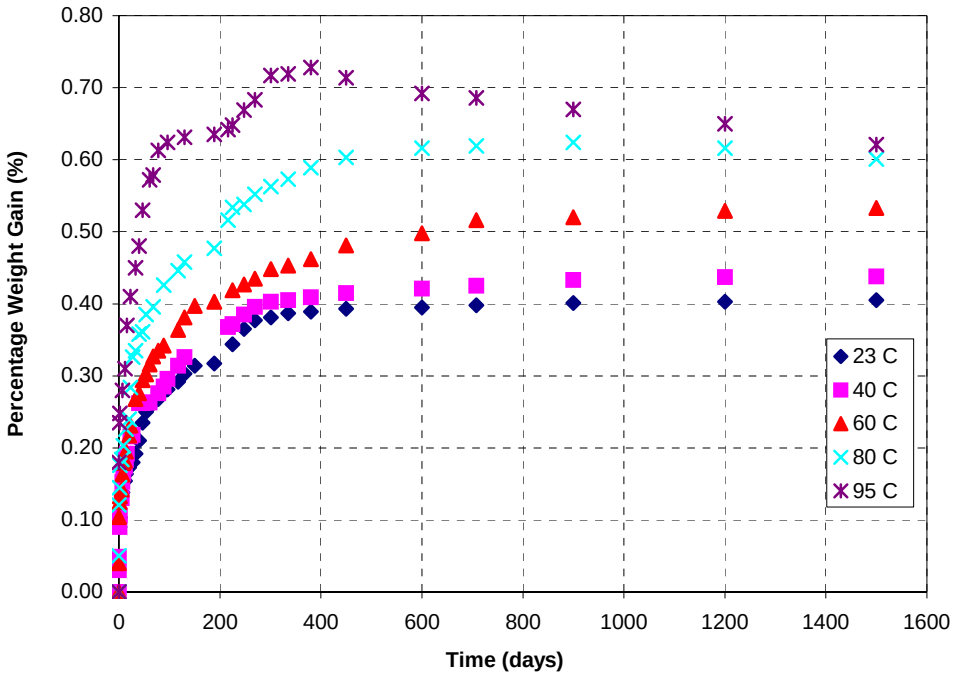

Fig. 4.1 Moisture uptake profiles of E-glass/Vinylester specimens immersed in deionized water at temperatures of 23 °C, 40 °C, 60 °C, 80 °C and 95 °C

Table 4.2 Percentage weight gain for E-glass/Vinylester specimens exposed to relative humidity levels of 0-5%, 45%, 60%, 80% and 98% at a constant temperature of 23 °C

Time (Days)	% Relative Humidity				
	0-5	45	60	80	98
0	0	0	0	0	0
2	0	0.002	0.015	0.025	0.073
5	0	0.004	0.024	0.040	0.084
8	-0.0076	0.005	0.031	0.043	0.100
13	-0.0079	0.006	0.040	0.051	0.128
20	-0.0081	0.007	0.066	0.078	0.126
26	-0.0086	0.020	0.088	0.101	0.146
33	-0.0088	0.024	0.098	0.118	0.172
41	-0.0094	0.041	0.111	0.129	0.177
48	-0.0097	0.054	0.109	0.142	0.207
54	-0.0100	0.056	0.119	0.157	0.210
71	-0.0103	0.063	0.130	0.178	0.222
91	-0.0112	0.067	0.152	0.188	0.265
130	-0.0114	0.111	0.179	0.228	0.288
159	-0.0119	0.118	0.168	0.220	0.293
182	-0.0121	0.122	0.173	0.222	0.295
200	-0.0120	0.130	0.182	0.227	0.310
221	-0.0124	0.134	0.184	0.235	0.318
250	-0.0133	0.136	0.183	0.237	0.314
272	-0.0129	0.138	0.185	0.239	0.313
305	-0.0128	0.137	0.183	0.238	0.312
330	-0.0126	0.139	0.187	0.236	0.310
365	-0.0126	0.141	0.19	0.239	0.315
450	-0.0128	0.149	0.195	0.241	0.318
600	-0.0127	0.154	0.203	0.240	0.321
800	-0.0128	0.158	0.210	0.245	0.325
1000	-0.0127	0.163	0.212	0.250	0.327
1500	-0.0128	0.164	0.215	0.253	0.329

Table 4.3 Percentage Weight Gain for E-glass/Vinylester specimens exposed to relative humidity levels of 0-5%, 45%, 60%, 80% and 98% at a constant temperature of 95 ^{o}C

Time (Days)	% Relative Humidity				
	0-5	45	60	80	98
0	0	0	0	0	0
1	0	0.002	0.013	0.0254	0.048
2	0	0.005	0.017	0.027	0.069
3	0	0.009	0.021	0.036	0.071
5	-0.00141	0.010	0.027	0.049	0.090
8	-0.00153	0.013	0.035	0.0495	0.119
11	-0.00120	0.017	0.041	0.054	0.123
13	-0.00136	0.019	0.045	0.055	0.139
18	-0.00137	0.020	0.055	0.080	0.154
24	-0.00158	0.028	0.063	0.103	0.164
34	-0.00140	0.038	0.102	0.122	0.187
55	-0.00168	0.059	0.123	0.165	0.232
70	-0.00185	0.064	0.137	0.187	0.253
98	-0.00190	0.078	0.158	0.189	0.273
113	-0.00201	0.093	0.167	0.206	0.285
130	-0.00207	0.116	0.183	0.235	0.298
151	-0.00214	0.119	0.189	0.239	0.309
172	-0.00217	0.127	0.192	0.242	0.318
195	-0.00220	0.131	0.197	0.244	0.325
219	-0.00225	0.137	0.201	0.247	0.337
240	-0.00225	0.141	0.205	0.251	0.35
261	-0.00220	0.146	0.211	0.251	0.357
290	-0.00215	0.153	0.216	0.255	0.365
315	-0.00219	0.157	0.219	0.259	0.371
330	-0.00217	0.159	0.225	0.263	0.376
365	-0.00218	0.163	0.229	0.266	0.379
450	-0.00219	0.176	0.236	0.278	0.382
600	-0.00227	0.188	0.238	0.283	0.386
800	-0.00217	0.193	0.239	0.289	0.392
1000	-0.00225	0.196	0.241	0.292	0.395
1500	-0.00217	0.203	0.241	0.293	0.397

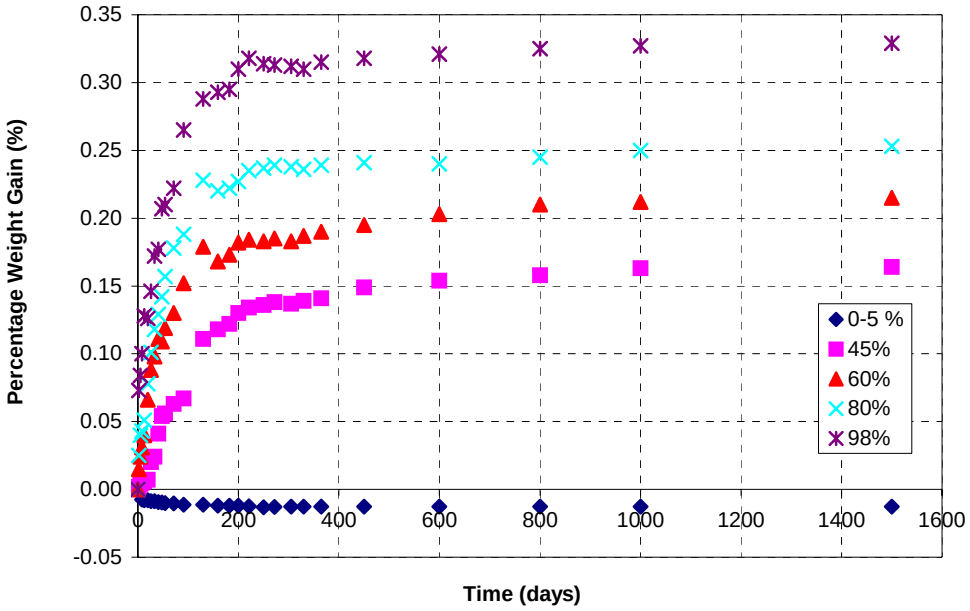

Fig. 4.2 Moisture uptake profiles of E-glass/Vinylester specimens exposed to relative humidity levels of 0-5 %, 45 %, 60 %, 80 % and 98 % at a constant temperature of 23 ^{o}C

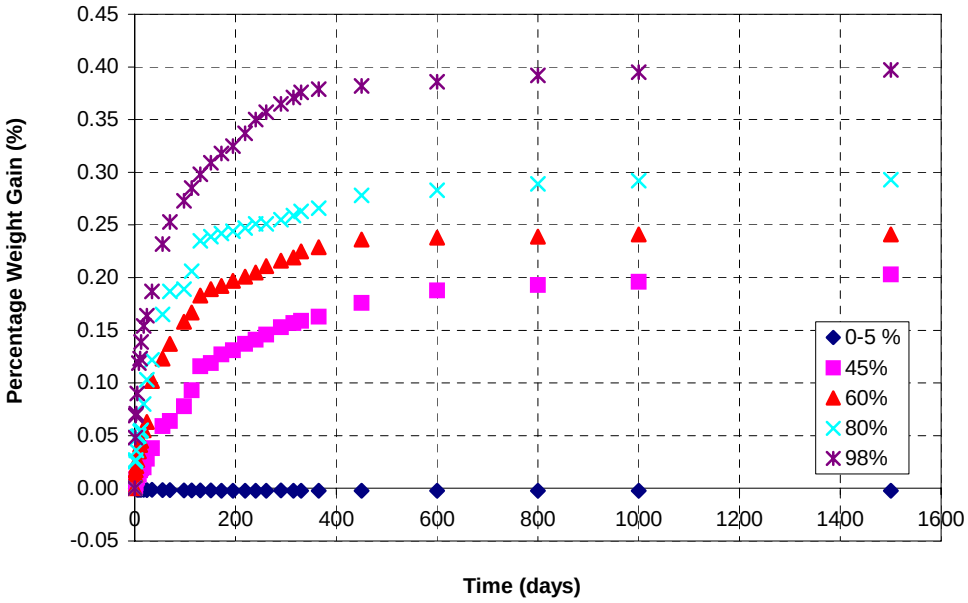

Fig. 4.3 Moisture uptake profiles of E-glass/Vinylester specimens exposed to relative humidity levels of 0-5 %, 45 %, 60 %, 80 % and 98 % at a constant temperature of 95 ^{o}C

4.2 Tensile Strength

The changes in the values of tensile strength of the E-glass/Vinylester composite specimens immersed in deionized water at different temperatures are listed in Table 4.4 and depicted graphically in Fig. 4.4.

4.3 Tensile Modulus

The changes in the values of tensile modulus of the E-glass/Vinylester composite specimens immersed in deionized water at different temperatures are listed in Table 4.5 and depicted graphically in Fig. 4.5.

4.4 Flexural Strength

The changes in the values of flexural strength of the E-glass/Vinylester composite specimens immersed in deionized water at different temperatures are listed in Table 4.6 and depicted graphically in Fig. 4.6.

4.5 Short Beam Shear Strength

The changes in the values of short beam shear strength of the E-glass/Vinylester composite specimens immersed in deionized water at different temperatures are listed in Table 4.7 and represented graphically in Fig. 4.7. Results pertaining to changes in short beam shear strength of the E-glass/Vinylester composite specimens exposed to humid air at 23 ^{o}C and 95 ^{o}C are shown in Fig 4.8 and Fig. 4.9 respectively and data is listed in Tables 4.8 and 4.9 respectively.

4.6 Glass Transition Temperature

Glass transition temperature (T_g) for the specimens exposed to immersion in deionized water was determined through Dynamic Mechanical Thermal Analysis (DMTA). Table 4.10 gives the changes in glass transition temperature for the specimens for a period of 1440 days. The changes in the T_g are represented graphically in Fig. 4.10.

Table 4.4 Tensile strength (MPa) data for E-glass/Vinylester specimens immersed in deionized water at temperatures of 23 °C, 40 °C, 60 °C, 80 °C and 95 °C and under "control" conditions of 30 % RH at 23 °C

Time (days)	Control		23°C water		40°C water		60°C water		80°C water		95°C water	
	Tensile Strength (MPa)	Standard Deviation (MPa)	Tensile Strength (MPa)	Standard Deviation (MPa)	Tensile Strength (MPa)	Standard Deviation (MPa)	Tensile Strength (MPa)	Standard Deviation (MPa)	Tensile Strength (MPa)	Standard Deviation (MPa)	Tensile Strength (MPa)	Standard Deviation (MPa)
0	684.65	63.50	684.65	63.50	684.65	63.50	684.65	63.50	684.65	63.50	684.65	63.50
30	690.86	71.15	686.03	84.67	686.79	71.71	469.67	45.64	277.52	20.62	263.59	11.10
90	740.50	55.50	686.65	24.13	534.83	52.19	406.45	51.92	272.97	10.69	233.04	41.44
180	726.71	43.58	675.69	51.30	511.32	46.26	397.83	19.31	258.35	27.99	231.87	25.37
270	755.67	50.61	689.41	37.23	525.18	5.31	326.81	34.47	255.18	20.62	229.32	23.17
360	792.90	37.78	642.94	18.06	467.12	27.92	311.58	13.93	251.04	34.06	210.77	5.38
540	782.56	15.10	617.64	26.34	394.18	29.65	309.02	39.65	241.80	31.58	204.43	24.13
720	809.45	44.33	575.37	14.96	362.60	7.17	301.79	51.64	232.91	25.92	195.47	22.61
1080	798.42	57.71	550.34	33.30	326.61	26.61	279.31	25.65	215.39	20.20	182.16	20.27
1440	818.41	30.06	515.94	21.99	291.17	33.92	262.90	33.16	197.12	30.13	172.03	27.30

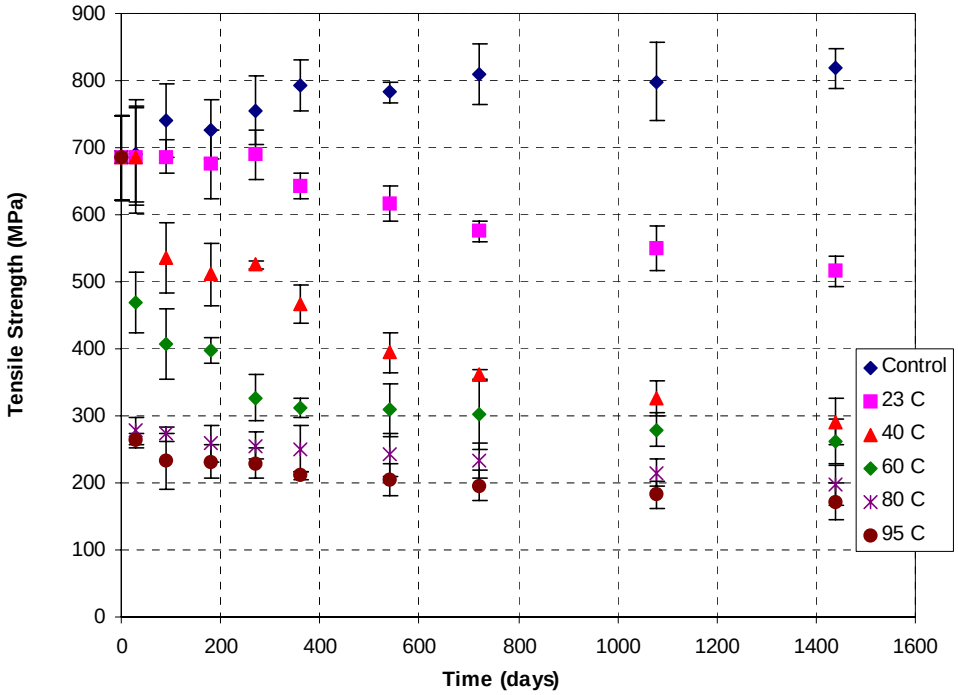

Fig 4.4 Tensile strength profiles of E-glass/Vinylesterspecimens immersed in deionized water at temperatures of 23 ^{o}C, 40 ^{o}C, 60 ^{o}C, 80 ^{o}C and 95 ^{o}C and "control" specimens

Table 4.5 Tensile modulus (GPa) data for E-glass/Vinylester specimens immersed in deionized water at temperatures of 23 ^{o}C, 40 ^{o}C, 60 ^{o}C, 80 ^{o}C and 95 ^{o}C and under "control" conditions of 30 % RH at 23 ^{o}C

Time (days)	Control		23^{0}C water		40^{0}C water		60^{0}C water		80^{0}C water		95^{0}C water	
	Tensile Modulus (GPa)	Standard Deviation (GPa)	Tensile Modulus (GPa)	Standard Deviation (GPa)	Tensile Modulus (GPa)	Standard Deviation (GPa)	Tensile Modulus (GPa)	Standard Deviation (GPa)	Tensile Modulus (GPa)	Standard Deviation (GPa)	Tensile Modulus (GPa)	Standard Deviation (GPa)
0	40.20	1.72	40.20	1.72	40.20	1.72	40.20	1.72	40.20	1.72	40.20	1.72
30	40.33	2.76	40.68	848.06	39.30	2.41	39.16	8.14	37.99	3.79	37.78	2.69
90	40.82	3.86	39.71	4.41	38.89	5.38	38.13	0.97	36.68	1.65	35.65	1.65
180	41.09	2.34	39.99	1.72	38.96	4.55	38.13	0.76	36.47	3.10	34.96	2.55
270	40.27	3.52	39.37	12.13	39.16	1.03	38.40	2.21	36.20	3.79	35.16	2.83
360	40.40	3.38	39.85	3.72	38.96	1.52	38.20	6.21	35.51	5.45	35.23	1.45
540	40.61	2.34	39.71	2.96	38.68	0.76	38.27	2.14	35.09	2.48	34.82	1.10
720	40.33	3.52	38.96	8.83	38.82	3.72	37.85	1.17	33.44	6.00	32.82	8.83
1080	40.54	3.31	38.68	4.96	37.85	2.14	36.68	1.65	31.92	4.07	31.37	3.10
1440	41.09	2.28	38.27	4.69	37.99	2.90	36.54	2.55	32.68	2.48	31.23	0.90

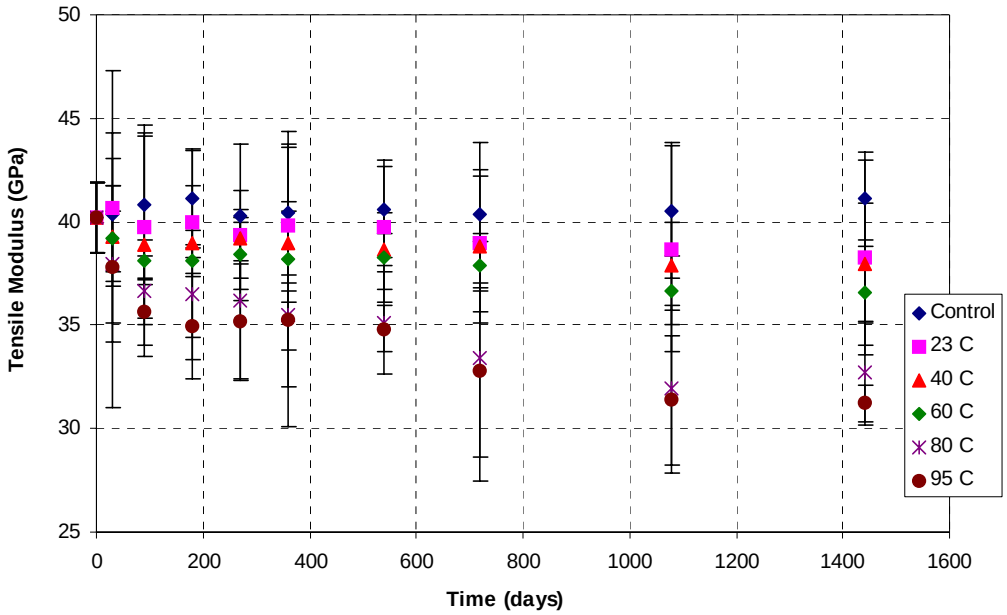

Fig 4.5 Tensile modulus profiles of E-glass/Vinylester composite specimens immersed in deionized water at temperatures of 23 ^{o}C, 40 ^{o}C, 60 ^{o}C, 80 ^{o}C and 95 ^{o}C and "control" specimens

Table 4.6 Flexural strength data for E-glass/Vinylester composite specimens immersed in deionized water at temperatures of 23 °C, 40 °C, 60 °C, 80 °C and 95 °C and under "control" conditions of 30 % RH at 23 °C

Time (days)	Control		23°C water		40°C water		60°C water		80°C water		95°C water	
	Flexural Strength (MPa)	Standard Deviation (MPa)	Flexural Strength (MPa)	Standard Deviation (MPa)	Flexural Strength (MPa)	Standard Deviation (MPa)	Flexural Strength (MPa)	Standard Deviation (MPa)	Flexural Strength (MPa)	Standard Deviation (MPa)	Flexural Strength (MPa)	Standard Deviation (MPa)
0	1106.89	60.19	1106.89	60.19	1106.89	60.19	1106.89	60.19	1106.89	60.19	1106.89	60.19
30	1133.85	73.91	1126.96	83.91	1092.34	13.65	913.01	59.50	526.21	70.46	459.12	47.37
90	1094.55	61.64	1104.96	31.17	772.08	80.47	670.86	62.40	423.96	77.29	426.86	51.50
180	1146.88	77.29	1086.83	57.16	748.36	65.78	556.07	89.29	402.93	66.67	373.84	71.29
270	1135.23	72.81	1064.83	72.26	726.92	43.09	512.42	70.46	381.21	38.89	347.29	49.71
360	1189.01	58.26	1036.70	24.55	744.22	51.37	471.81	45.09	369.84	50.13	314.95	56.47
540	1151.16	48.54	1001.68	40.89	591.44	42.68	409.83	38.27	336.40	3.93	260.35	8.48
720	1162.05	39.09	928.25	71.98	541.45	85.84	377.97	19.58	307.23	20.27	251.32	23.58
1080	1189.01	47.09	901.29	60.12	443.47	40.89	341.71	67.29	285.93	38.82	240.42	30.06
1440	1168.25	36.06	775.94	66.05	417.41	52.81	308.75	45.44	279.86	60.12	226.98	27.17

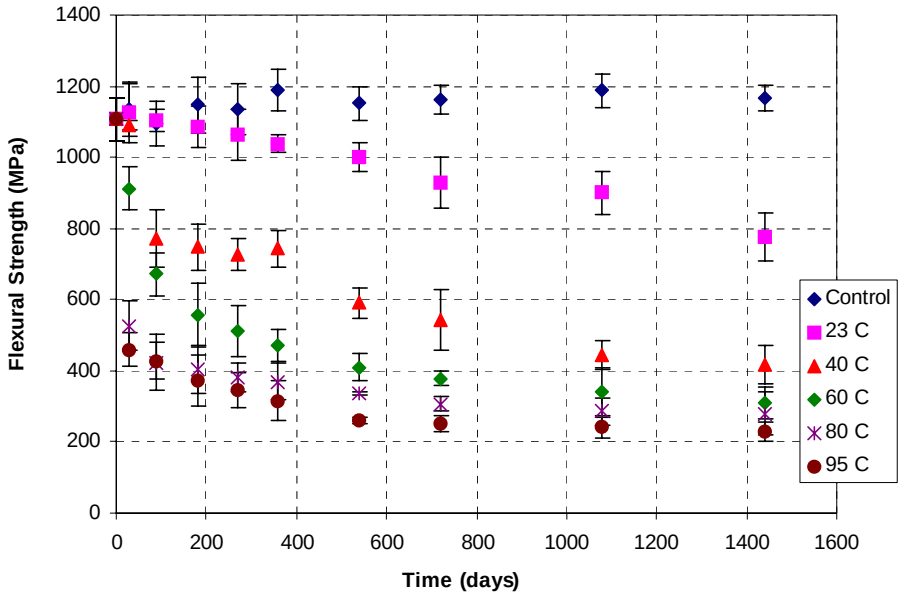

Fig 4.6 Flexural strength profiles of E-glass/Vinylester composite specimens exposed to immersion in deionized water at temperatures of 23 ^{o}C, 40 ^{o}C, 60 ^{o}C, 80 ^{o}C and 95 ^{o}C and "control" specimens

Table 4.7 Short beam shear strength data for E-glass/Vinylester composite specimens immersed in deionized water at temperatures of 23 °C, 40 °C, 60 °C, 80 °C and 95 °C and under "control" conditions of 30 % RH at 23 °C

Time (days)	Control		23°C water		40°C water		60°C water		80°C water		95°C water	
	SBS Strength (MPa)	Standard Deviation (MPa)	SBS Strength (MPa)	Standard Deviation (MPa)	SBS Strength (MPa)	Standard Deviation (MPa)	SBS Strength (MPa)	Standard Deviation (MPa)	SBS Strength (MPa)	Standard Deviation (MPa)	SBS Strength (MPa)	Standard Deviation (MPa)
0	55.30	1.38	55.30	1.38	55.30	1.38	55.30	1.38	55.30	1.38	55.30	1.38
30	55.30	1.79	57.16	4.14	55.71	3.38	46.47	5.45	44.40	7.31	31.65	5.10
90	57.09	1.86	50.40	2.00	53.99	5.17	46.75	4.62	34.27	2.55	22.75	1.24
180	56.40	2.69	50.40	3.72	48.47	5.10	37.58	2.62	33.51	1.31	24.34	2.62
270	57.50	1.45	50.06	6.07	44.82	6.48	37.85	4.76	29.37	2.76	23.58	1.10
360	57.57	2.76	49.23	1.31	43.58	5.86	30.89	3.72	26.06	0.28	18.89	1.10
540	57.16	2.34	44.54	4.34	42.61	1.65	30.20	1.65	23.72	1.45	14.27	1.93
720	57.71	2.28	42.89	2.62	39.51	4.34	28.34	2.62	19.65	1.31	12.62	3.59
1080	57.99	1.79	40.54	2.14	37.09	4.00	25.72	1.45	17.03	3.24	11.58	0.90
1440	57.71	1.93	38.47	3.10	35.78	2.34	24.20	1.65	16.20	2.62	10.96	1.65

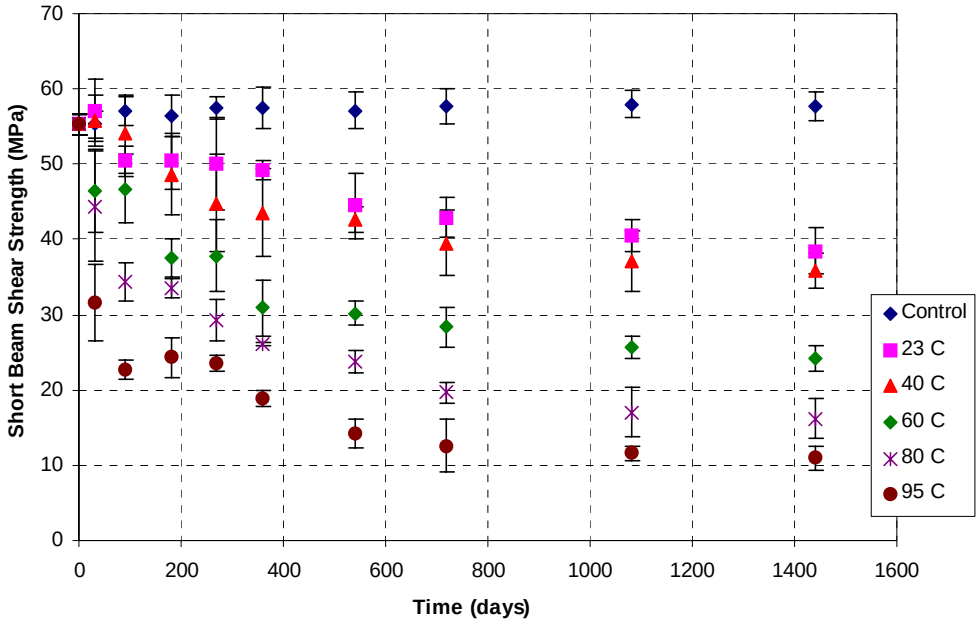

Fi

FIg. 4.7 Short beam shear strength profiles of E-glass/Vinylester composite specimens exposed to immersion in deionized water at temperatures of 23 °C, 40 °C, 60 °C, 80 °C and 95 °C and "control" specimens

Table 4.8 Short-beam shear strength data for E-glass/Vinylester composite specimens exposed to relative humidity levels of 0-5 %, 45 %, 60 %, 80 % and 98 % at a constant temperature 23 ^{o}C and under "control" conditions of 30 % RH at 23 ^{0}C

Time (days)	Control		0-5 % R.H.		45 % R.H.		60 % R.H.		75 % R.H.		98 % R.H.	
	SBS Strength (MPa)	Standard Deviation (MPa)	SBS Strength (MPa)	Standard Deviation (MPa)	SBS Strength (MPa)	Standard Deviation (MPa)	SBS Strength (MPa)	Standard Deviation (MPa)	SBS Strength (MPa)	Standard Deviation (MPa)	SBS Strength (MPa)	Standard Deviation (MPa)
0	55.30	1.38	55.30	1.38	55.30	1.38	55.30	1.38	55.30	1.38	55.30	1.38
30	55.30	1.79	60.26	4.34	57.99	4.48	57.57	4.34	53.43	4.76	53.43	1.72
90	57.09	1.86	58.40	2.69	57.30	0.97	55.43	3.38	53.30	3.52	52.06	4.07
180	56.40	2.69	56.26	5.03	55.02	0.62	54.54	2.14	53.92	3.17	50.88	6.76
270	57.50	1.45	55.85	1.10	54.06	3.10	53.78	1.24	53.64	2.14	48.82	6.62
360	57.57	2.76	55.30	5.65	53.92	1.93	53.78	2.90	53.30	3.59	46.95	4.34
540	57.16	2.34	55.50	6.27	53.71	2.07	53.16	1.59	51.78	0.97	44.89	3.10
720	57.71	2.28	55.37	4.62	53.99	1.17	52.61	3.52	50.19	1.24	43.99	2.14
1080	57.99	1.79	55.64	5.38	53.16	4.27	51.44	4.34	48.40	1.72	41.71	1.93
1440	57.71	1.93	55.23	5.72	52.95	1.24	50.40	1.72	47.09	3.03	40.40	4.27

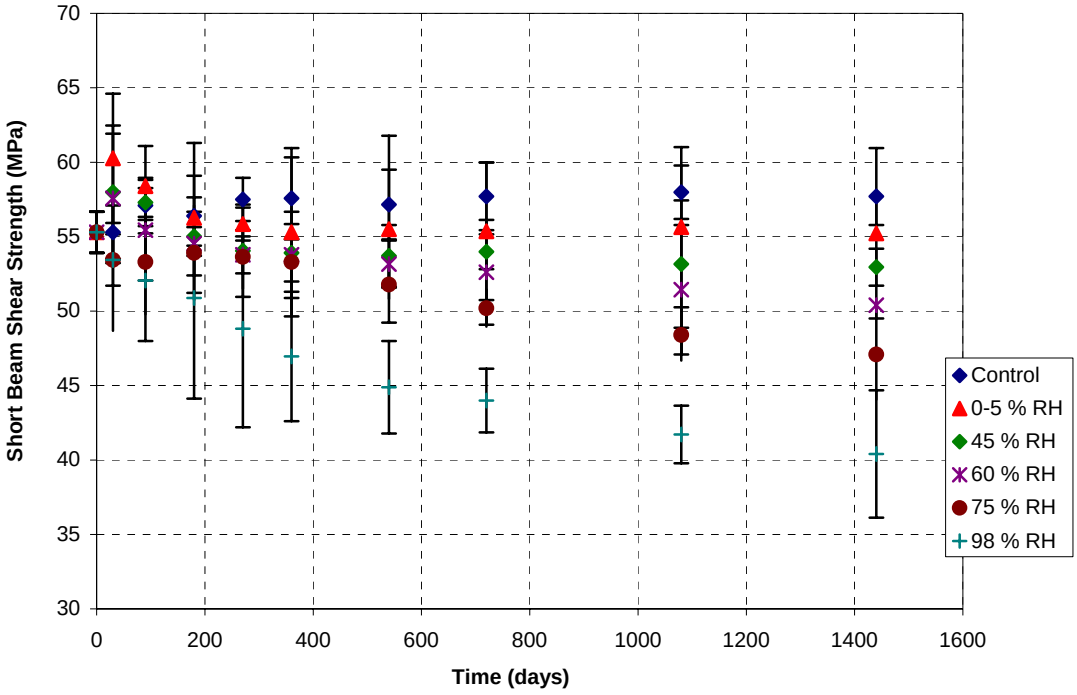

Fig 4.8 Short beam shear strength profiles of E-glass/Vinylester composite specimens exposed to relative humidity levels of 0-5 %, 45 %, 60 %, 80 % and 98 % at a constant temperature 23 ^{o}C and "control" specimens

Table 4.9 Short beam shear strength data for E-glass/Vinylester composite specimens exposed to relative humidity levels of 0-5 %, 45 %, 60 %, 80 % and 98 % at a constant temperature 95 ^{0}C and under "control" conditions of 30 % RH at 23 ^{0}C

Time (days)	Control		0-5 % R.H.		45 % R.H.		60 % R.H.		75 % R.H.		98 % R.H.	
	SBS Strength (MPa)	Std Dev (MPa)	SBS Strength (MPa)	Std Dev (MPa)	SBS Strength (MPa)	Std Dev (MPa)	SBS Strength (MPa)	Std Dev (MPa)	SBS Strength (MPa)	Std Dev (MPa)	SBS Strength (MPa)	Std Dev (MPa)
0	57.36	1.38	55.30	1.38	55.30	1.38	55.30	1.38	55.30	1.38	55.30	1.38
30	55.30	1.79	60.19	1.72	52.75	2.14	57.85	4.62	55.64	2.41	45.37	3.31
90	57.09	1.86	60.47	1.24	52.19	6.83	55.85	2.14	47.51	0.90	33.99	6.00
180	56.40	2.69	58.61	3.72	51.99	4.48	52.54	3.72	46.13	3.65	33.78	1.86
270	57.50	1.45	59.50	2.62	51.09	1.93	51.23	3.93	37.44	3.93	30.48	3.59
360	57.57	2.76	60.26	2.21	50.75	5.38	48.33	1.24	29.44	4.34	25.79	3.79
540	57.16	2.34	59.57	4.21	49.78	5.72	46.40	0.62	27.85	2.14	22.13	3.17
720	57.71	2.28	59.50	1.17	49.09	3.31	43.99	0.90	26.54	2.00	20.82	1.24
1080	57.99	1.79	59.85	4.27	48.33	2.14	42.13	1.86	25.92	3.52	18.82	0.76
1440	57.71	1.93	59.57	3.03	47.85	1.10	40.47	4.07	25.44	4.76	17.51	2.62

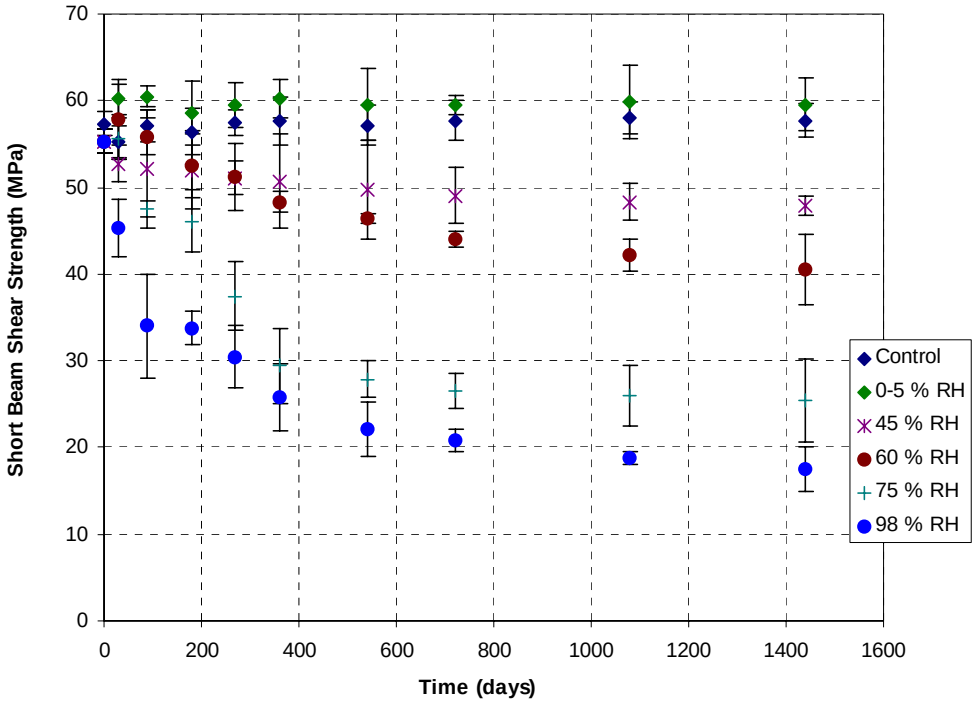

Fig 4.9 Short beam shear strength profiles of E-glass/Vinylester composite specimens exposed to relative humidity levels of 0-5 %, 45 %, 60 %, 80 % and 98 % at a constant temperature 95 ^{o}C and "control" specimens

Table 4.10 Glass Transition Temperature data for E-glass/Vinylester composite specimens immersed in deionized water at temperatures of 23 °C, 40 °C, 60°C, 80 °C and 95 °C and under "control" conditions of 30 % RH at 23 °C

Time (days)	Glass Transition Temperature (°C)											
	Control	Std Dev	23 °C (Water)	Std Dev	40 °C (Water)	Std Dev	60 °C (Water)	Std Dev	80 °C (Water)	Std Dev	95 °C (Water)	Std Dev
0	121.39	3.61	121.39	3.61	121.39	3.61	121.39	3.61	121.39	3.61	121.39	3.61
30	123.45	1.23	117.52	1.89	116.67	4.87	116.68	3.59	120.73	4.81	121.58	3.16
90	124.32	3.45	116.54	1.45	113.28	3.92	114.57	2.87	120.27	1.73	119.94	2.59
180	127.45	2.65	112.94	1.38	110.54	2.46	113.54	1.37	119.54	1.37	119.57	1.63
270	124.95	2.12	112.37	1.76	110.45	3.61	113.67	2.82	119.01	2.93	116.45	1.57
360	122.56	1.76	110.43	1.89	109.22	1.83	112.34	2.51	114.88	2.48	114.38	2.91
540	124.84	1.58	109.59	1.52	109.56	1.28	110.93	1.93	113.51	3.71	113.27	1.03
720	125.93	1.45	108.56	1.93	107.73	2.44	109.87	3.41	112.03	2.63	111.19	1.75
1080	122.45	2.63	106.45	2.65	105.76	2.39	108.52	3.73	111.54	1.54	111.06	3.28
1440	124.36	3.75	106.56	2.49	104.99	3.27	107.63	2.65	110.48	1.42	110.93	1.47

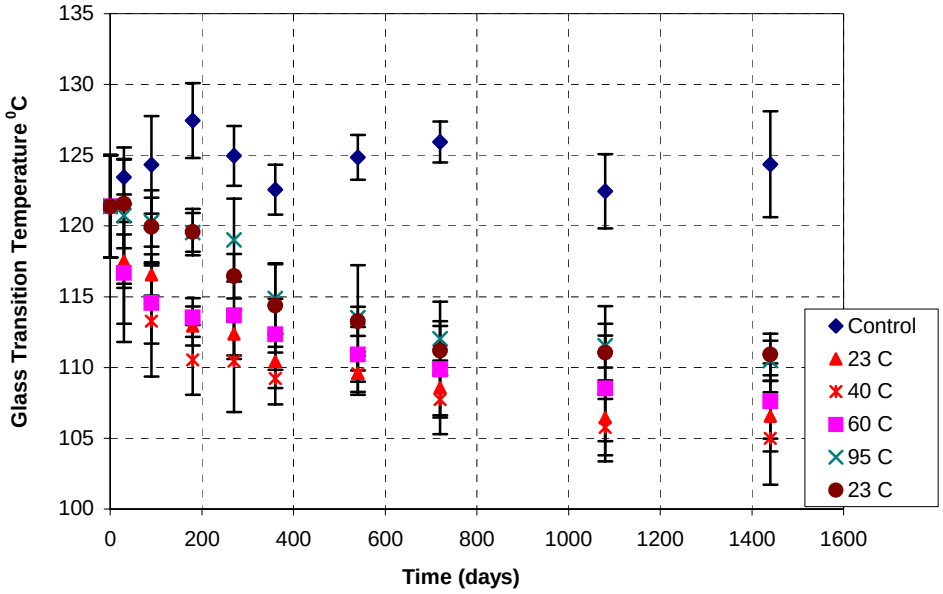

Fig 4.10 Changes in the glass transition temperature of the E-glass/Vinylester composite specimens immersed in deionized water at temperatures of 23 °C, 40 °C, 60°C, 80 °C and 95 °C and "control" specimens

Chapter 5

Moisture Absorption

5.1 Fickian Diffusion Model

Assuming that initially the temperature and moisture distributions inside the specimen are uniform and also that the temperature and the moisture content of environment are constant, the moisture content of the specimen at any time t [1, 2], as described by Fickian diffusion theory, M_t is

$$M_t = G\,(M_m - M_i) + M_i \qquad \text{(Equation 5.1)}$$

where M_t = Percentage moisture gain at time t

M_m = Maximum moisture content that can be attained under the given conditions

M_i = Initial moisture content of the specimen

G = Time dependent parameter and is given by

$$G = 1 - \frac{8}{\pi^2}\sum_{n=0}^{\infty}\frac{\exp\left[(2n+1)^2\pi^2\left(\frac{-Dt}{h^2}\right)\right]}{(2n+1)^2} \qquad \text{(Equation 5.2)}$$

where D = Diffusion Coefficient in the direction normal to the surface

h = thickness of the specimen

Since dry specimens were used in the moisture uptake experiments, M_i is equal to zero. Therefore the moisture content of the specimen at any time t, M_t is given by

$$M_t = M_m \left[1 - \frac{8}{\pi^2} \sum_{n=0}^{\infty} \frac{\exp\left[(2n+1)^2 \pi^2 \left(\frac{-Dt}{h^2} \right) \right]}{(2n+1)^2} \right] \qquad \text{(Equation 5.3)}$$

Equation 5.3 can be approximated for long term and short-term exposures. To do this, a non-dimensional time parameter Dt/h^2 is defined.

For $Dt/h^2 < 0.04$ (Short term approximation), Equation 5.3 reduces to

$$M_t = M_m \left[\frac{4}{\pi} \sqrt{\frac{Dt}{h^2}} \right] \qquad \text{(Equation 5.4)}$$

For $Dt/h^2 > 0.04$ (Long term approximation), Equation 5.3 reduces to

$$M_t = M_m \left[1 - \frac{8}{\pi^2} \exp\left(\frac{-Dt}{h^2} \pi^2 \right) \right] \qquad \text{(Equation 5.5)}$$

The moisture uptake curves for the E-glass Vinylester specimens immersed in deionized water and subjected to exposure to humidity at different temperatures are shown in chapter 4 in figures 4.1 through 4.3. The moisture uptake by the material is characterized by the two parameters: Maximum moisture content, M_m and the Diffusion Coefficient, D. These two parameters are calculated by using all three forms of the Fickian diffusion model. The values of the two parameters calculated with the aid of Mathcad tools are listed in Table 5.22.

5.2 Langmuir Diffusion Model

The Langmuir diffusion model assumes that the absorbed moisture consists of mobile and bound phases [3]. Molecules are emitted from the bound phase, thereby becoming mobile with a probability per unit time α and molecules of the mobile phase diffuse with a diffusion coefficient D and are absorbed thereby becoming bound with a probability per unit time of β at certain sites. The moisture content in the specimen approaches an equilibrium value, M_m, when the mobile molecules per unit volume, n, and the number of bound molecules per unit volume, N, approach values such that

$$\beta n = \alpha N \qquad \text{(Equation 5.6)}$$

The moisture content M_t in an initially dry one dimensional specimen, after a time t is given by,

$$M_t = M_m \left[1 - \frac{\alpha}{\alpha+\beta}\exp(-\alpha t) - \frac{\alpha}{\alpha+\beta}\frac{8}{\pi^2}\sum_{n=0}^{\infty}\frac{\exp\left[(2n+1)^2\pi^2\left(\frac{-Dt}{h^2}\right)\right]}{(2n+1)^2} \right]$$

(Equation 5.7)

For short term periods, $Dt/h^2 < 0.04$, Equation 5.7 can be approximated to

$$M_t = M_m \left[\frac{\alpha}{\alpha+\beta}\frac{4}{\pi}\sqrt{\frac{Dt}{h^2}} \right] \qquad \text{(Equation 5.8)}$$

For long periods of time, $Dt/h^2 < 0.04$, Equation 5.7 can be approximated to

$$M_t = M_m \left[1 - \frac{\alpha}{\alpha+\beta}\exp(-\alpha t) - \frac{\alpha}{\alpha+\beta} - \frac{8}{\pi^2}\exp\left(\frac{-Dt}{h^2}\pi^2\right) \right]$$

(Equation 5.9)

The Maximum Moisture Content Mm and Diffusion coefficient values obtained by applying the moisture uptake data to the Langmuir models have been tabulated in Tables 5.23, 5.24 and 5.25.

5.3 Correction for Edge Effects

The test specimens used for moisture absorption tests are made in the form a thin plate (l/h<<1 and l/n <<1) so that the moisture enters predominantly through the surface marked by n and h (Fig 5.1). But moisture actually penetrates through the edge surfaces also [2].

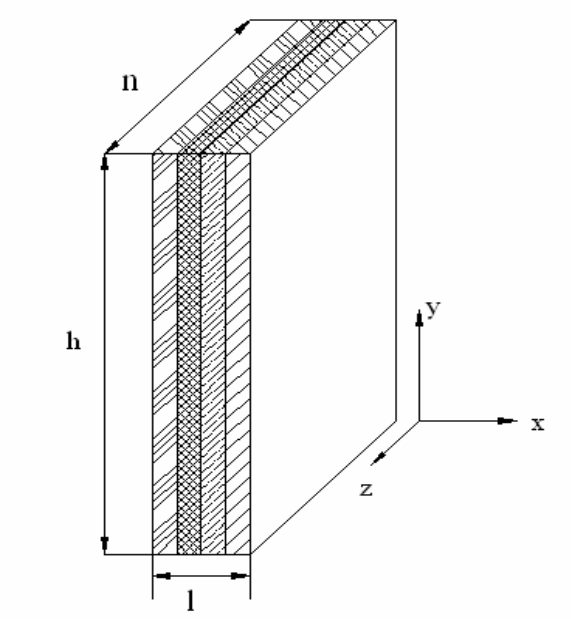

Fig. 5.1 Geometry of the test specimen

If the moisture entering the test specimen through the edges is neglected then the diffusion coefficient,

$$D_x = D$$

If the edge effects are considered, a correction has to applied to the diffusion coefficient obtained from the Fickian and Langmuir diffusion models, as follows,

$$D_x = D\left(1 + \frac{l}{h} + \frac{l}{n}\right)^{-2} \qquad \text{(Equation 5.10)}$$

Equation 5.10 is used to apply the edge effect correction to the diffusion coefficients obtained from the Fickian and Langmuir diffusion models hereafter.

5.4 Immersion in deionized water

Unidirectional E-glass Vinylester composite specimens measuring 25.4 mm X 25.4 mm X 2.54 mm were subjected to immersion in deionized water at five temperatures: 23 ^{o}C, 40 ^{o}C, 60 ^{o}C, 80 ^{o}C and 95 ^{o}C. Moisture absorption data was recorded at the following intervals: 45 minutes, 1 hour, 1 day, 2 days, 6 days, 7 days, 9 days, 12 days, 14 days and so on till 1500 days. The moisture absorption data is given in Table 5.1 (also in table 4.1). Percentage moisture gain of each of the specimens at different times is calculated from weight of the specimen after immersion W_i and its dry weight W.

$$M_t = \frac{(W_i - W)}{W} x100 \qquad \text{(Equation 5.11)}$$

where M_t = Percentage moisture gain at time t

W = Dry weight of the specimen

W_i = Weight of the specimen after immersion in water at time t.

Table 5.1 Moisture absorption (%) for E-glass/Vinylester specimens immersed in deionized water at temperatures 23 ^{o}C, 40 ^{o}C, 60 ^{o}C, 80 ^{o}C and 95 ^{o}C

Time (Days)	Temperature ^{o}C				
	23	40	60	80	95
0	0	0	0	0	0
0.031	-	0.030	0.040	0.050	-
0.042	-	0.049	0.104	0.121	0.180
1	0.090	0.090	0.125	0.145	0.235
2	0.103	0.106	0.133	0.176	0.248
6	-	0.130	0.142	0.184	-
7	0.138	0.153	0.163	-	0.280
9	-	0.165	0.179	0.203	-
12	0.154	0.174	0.182	-	0.310
14	0.164	0.183	0.195	0.226	-
16	0.17	0.192	-	-	0.370
20	0.173	-	0.217	0.240	-
23	-	0.216	0.231	0.284	0.410
27	0.180	0.218	-	0.326	-
33	0.192	-	0.268	0.335	0.450
40	0.210	0.262	0.276	0.358	0.480
47	0.235	0.262	0.294	0.361	0.530
54	0.250	0.263	0.302	0.385	-
61	0.257	0.263	0.316	-	0.572
68	0.264	-	0.327	0.396	0.579
78	0.268	0.276	0.335	-	0.613
89	0.278	0.285	0.342	0.426	-
96	0.281	0.296	-	-	0.624
117	0.292	0.314	0.364	0.446	-
130	0.303	0.326	0.381	0.458	0.631
150	0.314	-	0.397	-	-
189	0.317	-	0.403	0.477	0.635
216	-	0.368	-	0.516	0.642
225	0.344	0.372	0.419	0.534	0.648
248	0.365	0.385	0.427	0.538	0.669
269	0.377	0.396	0.435	0.552	0.683
301	0.381	0.403	0.448	0.563	0.717
335	0.387	0.405	0.453	0.573	0.719
380	0.389	0.409	0.462	0.589	0.728
450	0.393	0.415	0.481	0.603	0.714
600	0.395	0.421	0.498	0.616	0.692
708	0.398	0.425	0.516	0.619	0.686
900	0.401	0.433	0.520	0.624	0.670
1200	0.403	0.437	0.529	0.616	0.650
1500	0.405	0.438	0.533	0.601	0.621

5.4.1 Full Model

The moisture absorption data shown in Table 5.1 were fitted to equations 5.3 (Fickian Diffusion Model) and 5.7 (Langmuir Diffusion Model) using MathCAD tools. The details of the MathCAD programs used are given in Appendix B. Fitting the data to the equations results in the estimation of the Maximum moisture content, M_m and Diffusion Coefficient, D. The results of the analysis using the equations 5.3 and 5.7 are presented in the Figures 5.2 and 5.3. For brevity, moisture absorption curves are shown for the temperature 23 ^oC only. The moisture absorption curves for temperatures 40 ^oC, 60 ^oC, 80 ^oC and 95 ^oC are shown in Appendix A.

Figures 5.2 and 5.3 indicate that the Langmuir model fits the moisture absorption data for immersion in water, better than the Fickian Model. The maximum moisture content and the diffusion coefficients obtained from the Fickian and Langmuir diffusion models are listed in tables 5.2 and 5.3 respectively.

Table 5.2 Maximum moisture contents and diffusion coefficients obtained from Fickian Diffusion Model (FULL MODEL) for specimens immersed in water

Temp (^{0}C)	M_m %	Diffusion Coefficient (mm^2/sec)	
		Fickian Diffusion Model	Corrected for Edge Effects
23	0.405	1.304×10^{-7}	9.056×10^{-8}
40	0.438	1.969×10^{-7}	1.367×10^{-7}
60	0.533	2.139×10^{-7}	1.485×10^{-7}
80	0.624[a]	2.175×10^{-7}	1.510×10^{-7}
95	0.728[b]	2.414×10^{-7}	1.676×10^{-7}

[a] M_m at t = 900 days, followed by weight loss to M_m = 0.601 % at t =1500 days

[b] M_m at t = 380 days, followed by weight loss to M_m = 0.621 % at t =1500 days

Table 5.3 Maximum moisture contents and diffusion coefficients obtained from Langmuir Diffusion Model (FULL MODEL) for specimens immersed in water

Temp (^{0}C)	M_m %	Diffusion Coefficient (mm^2/s)		α	β
		Langmuir Diffusion Model	Corrected for Edge Effects		
23	0.405	8.945×10^{-8}	6.212×10^{-8}	1.761×10^{-4}	2.104×10^{-4}
40	0.438	1.048×10^{-7}	7.278×10^{-8}	1.530×10^{-4}	1.797×10^{-4}
60	0.533	1.257×10^{-7}	8.729×10^{-8}	3.300×10^{-4}	3.930×10^{-4}
80	0.624[a]	2.166×10^{-7}	1.504×10^{-7}	3.848×10^{-4}	5.177×10^{-3}
95	0.728[b]	2.384×10^{-7}	1.656×10^{-7}	3.540×10^{-4}	1.060×10^{-3}

[a] M_m at t = 900 days, followed by weight loss to M_m = 0.601 % at t =1500 days

[b] M_m at t = 380 days, followed by weight loss to M_m = 0.621 % at t =1500 days

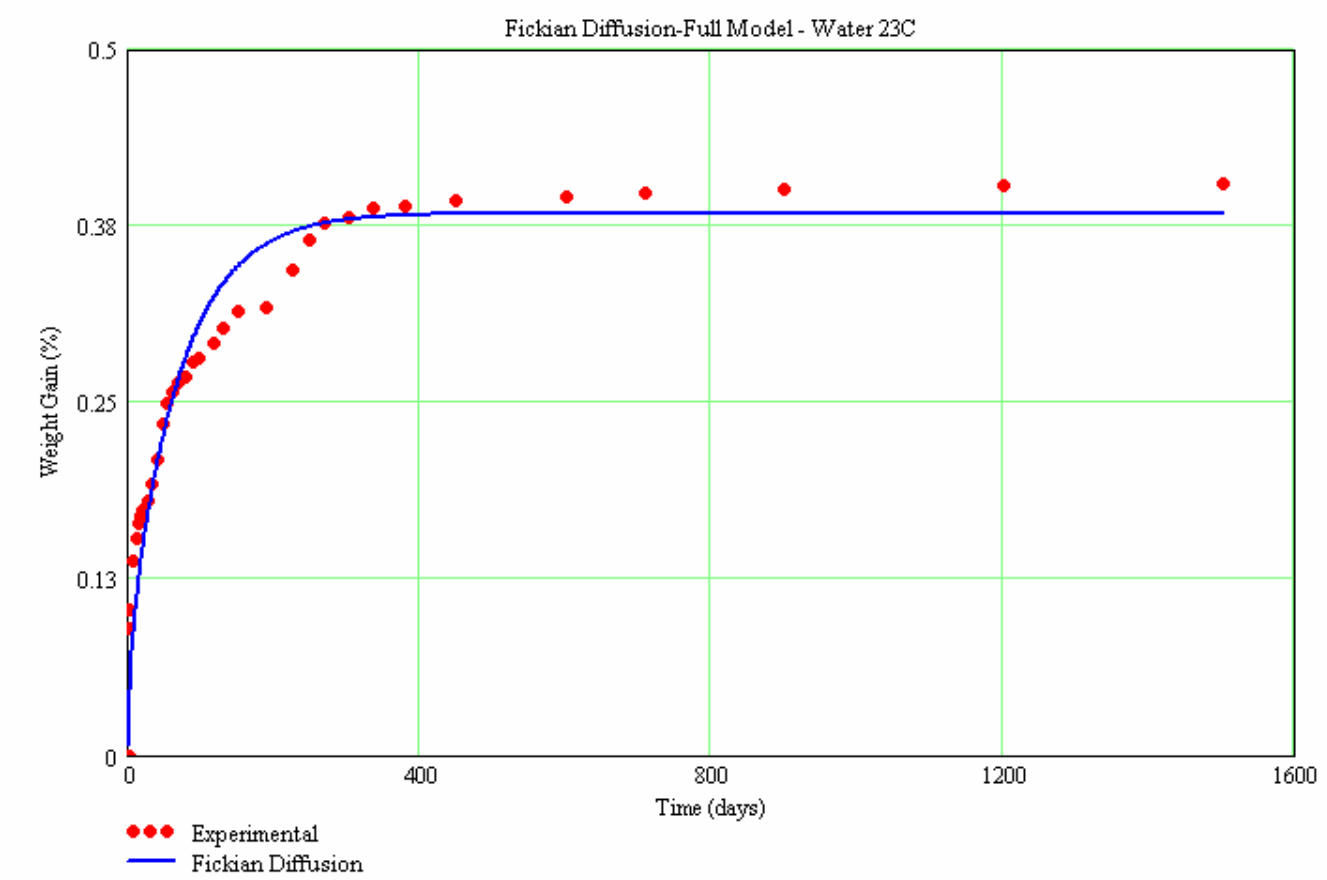

Fig. 5.2 Moisture absorption profile of E-glass vinylester composite specimens immersed in deionized water at 23 ^{o}C (Fickian Model)

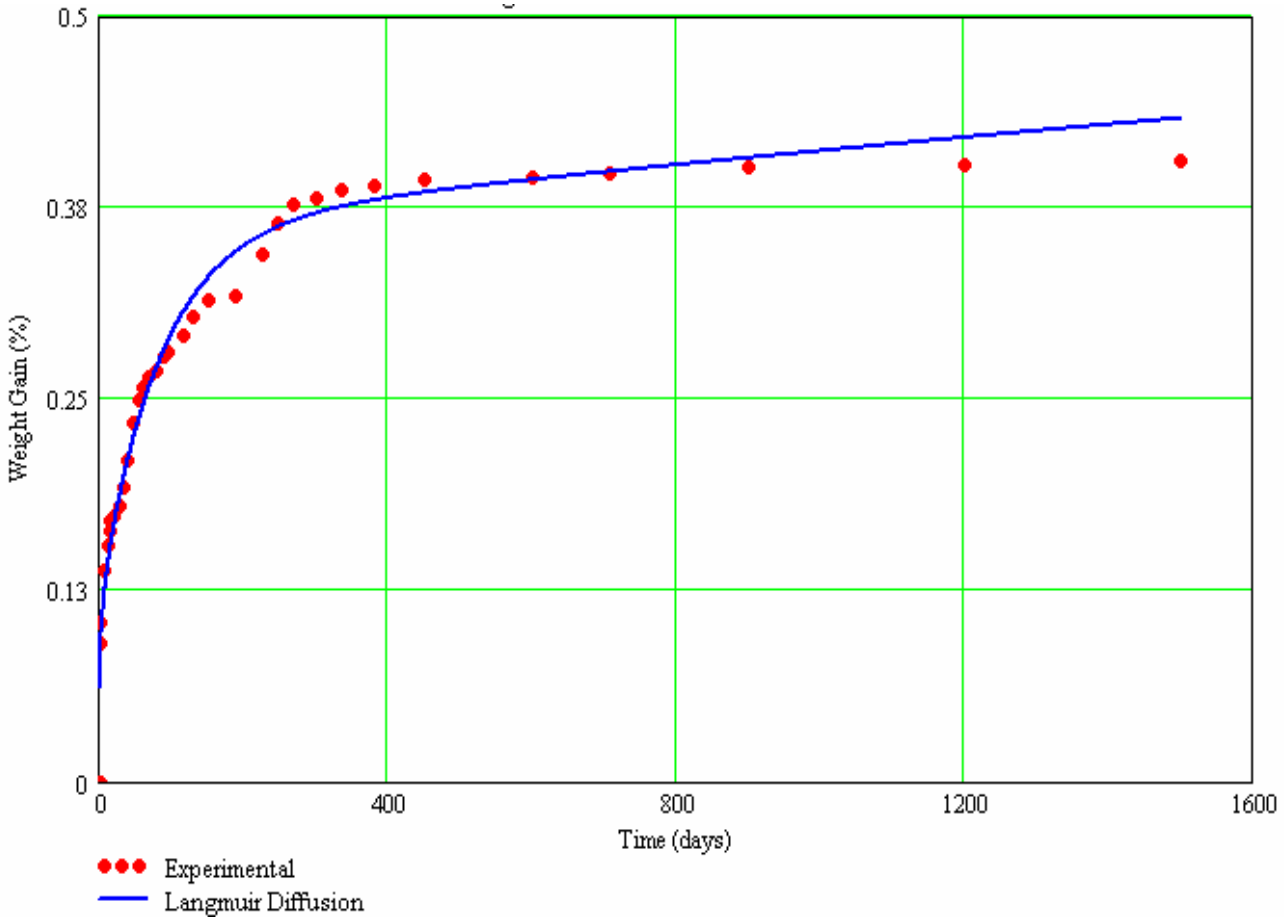

Fig. 5.3 Moisture absorption profile of E-glass vinylester composite specimens immersed in deionized water at 23 ^{o}C (Langmuir Model)

5.4.2 Long-term Approximation

Equations 5.5 and 5.9 are complicated and require elaborate procedures to fit the moisture absorption data. Long-term approximation given by equations 5.5 and 5.9 are often used in place of the elaborate full model. Results show that the values of maximum moisture content and diffusion coefficient obtained through long-term approximations of the Fickian and Langmuir models are rather close to those found employing the full models. These values are listed in table 5.4 and 5.5. For brevity, moisture absorption curves are shown for the case of immersion in deionized water at temperature of 23 ^{o}C only, in figure 5.4. The moisture absorption curves for immersion in deionzed water at temperatures of 40 ^{o}C, 60 ^{o}C, 80 ^{o}C and 95 ^{o}C are shown in Appendix A.

Table 5.4 Maximum moisture contents and diffusion coefficients obtainedfrom Fickian Diffusion Model (LONG-TERM APPROXIMATION) for specimens immersed in water

Temp (^{0}C)	M_m %	Diffusion Coefficient (mm^2/s)	
		Fickian Diffusion Model	Corrected for Edge Effects
23	0.405	1.186×10^{-7}	8.236×10^{-8}
40	0.438	2.024×10^{-7}	1.406×10^{-7}
60	0.533	2.135×10^{-7}	1.483×10^{-7}
80	0.624*	2.277×10^{-7}	1.581×10^{-7}
95	0.728**	2.513×10^{-7}	1.745×10^{-7}

* M_m at t = 900 days, followed by weight loss to M_m = 0.601 % at t =1500 days

** M_m at t = 380 days, followed by weight loss to M_m = 0.621 % at t =1500 days

Table 5.5 Maximum moisture contents and diffusion coefficients obtained from Langmuir Diffusion Model (LONG-TERM APPROXIMATION) for specimens immersed in water

Temp (^{0}C)	M_m %	Diffusion Coefficient (mm^2/s)		α	β
		Langmuir Diffusion Model	Corrected for Edge Effects		
23	0.405	9.509×10^{-8}	6.603×10^{-8}	-8.670×10^{-4}	2.200×10^{-2}
40	0.438	1.188×10^{-7}	8.250×10^{-8}	-1.308×10^{-4}	5.000×10^{-2}
60	0.533	1.538×10^{-7}	1.068×10^{-7}	-3.313×10^{-4}	1.030×10^{-1}
80	0.624*	2.019×10^{-7}	1.402×10^{-7}	-5.416×10^{-4}	1.060×10^{-1}
95	0.728**	2.472×10^{-7}	1.717×10^{-7}	-3.863×10^{-3}	9.300×10^{-2}

* M_m at t = 900 days, followed by weight loss to M_m = 0.601 % at t =1500 days

** M_m at t = 380 days, followed by weight loss to M_m = 0.621 % at t =1500 days

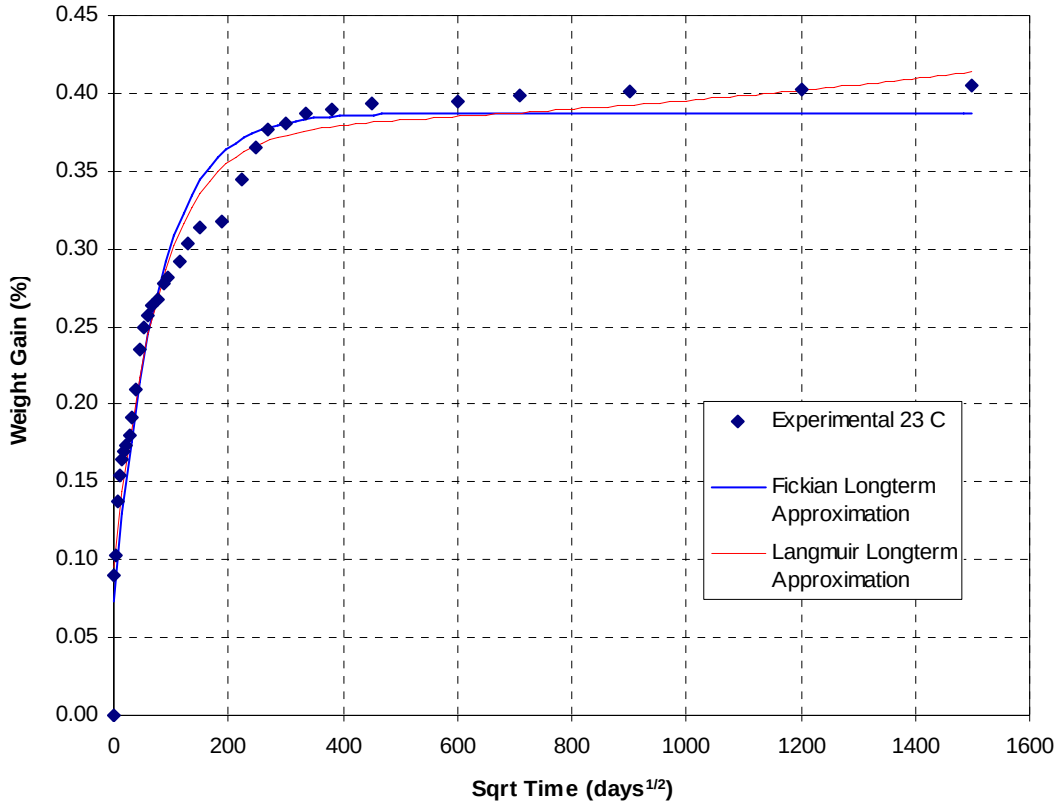

Fig. 5.4 Prediction of moisture absorption profile of E-glass vinylester composite specimens immersed in deionized water at 23 ^{o}C with long-term approximation terms

5.4.3 Short-term Approximation

For short times, equation 5.3 is reduced to

$$M_t = M_m \left[\frac{4}{\pi} \sqrt{\frac{Dt}{h^2}} \right] \qquad \text{(Equation 5.4)}$$

As seen in Fig. 5.5, the moisture absorption curve is linear till $t = t_L$.

When $t < t_L$ the slope is constant, and is given by

$$\frac{M_2 - M_1}{\sqrt{t_2} - \sqrt{t_1}} = \frac{4M_m}{l\sqrt{\pi}} \sqrt{D} \qquad \text{(Equation 5.12)}$$

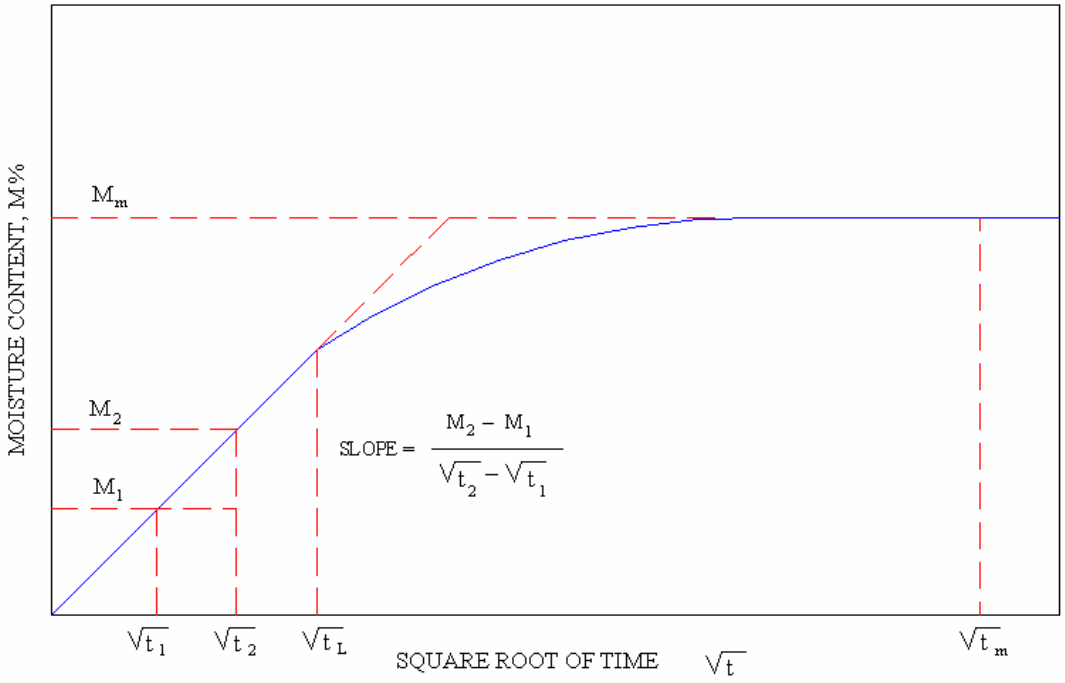

Fig. 5.5 Schematic of Classical Fickian Diffusion Process

The moisture absorption curve is plotted on the graph and the linear portion is determined by assuming that the curve ceases to be linear after 60% of the maximum

moisture content is reached. Here the maximum moisture content is the same as the highest moisture content reached for the specimen exposed to the harshest environment (In this case, immersion in 95 ^{o}C deionized water). Thus the slope of the curve is found and the diffusion coefficient is calculated as per equation 5.13.

$$D = \pi \left(\frac{l}{4M_m} \right)^2 \left(\frac{M_2 - M_1}{\sqrt{t_2} - \sqrt{t_1}} \right)^2 \qquad \text{(Equation 5.13)}$$

Similarly the short term approximation equation for Langmuir diffusion model is,

$$D = \pi \left(\frac{l}{4M_m} \right)^2 \left(\frac{\alpha + \beta}{\alpha} \right)^2 \left(\frac{M_2 - M_1}{\sqrt{t_2} - \sqrt{t_1}} \right)^2 \qquad \text{(Equation 5.14)}$$

The moisture absorption data is analyzed according to the procedure described above and the values of the diffusion coefficient for Fickian and Langmuir models are listed in Table 5.6 and 5.7 respectively.

Table 5.6 Maximum moisture contents and diffusion coefficients obtainedfrom Fickian Diffusion Model (SHORT-TERM APPROXIMATION) for specimens immersed in water

Temp (^{0}C)	M_m %	Diffusion Coefficient (mm^2/s)	
		Fickian Diffusion Model	Corrected for Edge Effects
23	0.405	1.041×10^{-7}	7.229×10^{-8}
40	0.438	1.086×10^{-7}	7.542×10^{-8}
60	0.533	1.392×10^{-7}	9.667×10^{-8}
80	0.624*	1.710×10^{-7}	1.187×10^{-7}
95	0.728**	2.003×10^{-7}	1.391×10^{-7}

* M_m at t = 900 days, followed by weight loss to M_m = 0.601 % at t =1500 days

** M_m at t = 380 days, followed by weight loss to M_m = 0.621 % at t =1500 days

Table 5.7 Maximum moisture contents and diffusion coefficients obtainedfrom Langmuir Diffusion Model (SHORT-TERM APPROXIMATION) for specimens immersed in water

Temp (^{0}C)	M_m %	Diffusion Coefficient (mm^2/s)		α	β
		Langmuir Diffusion Model	Corrected for Edge Effects		
23	0.405	5.013×10^{-7}	3.481×10^{-7}	1.761×10^{-4}	2.104×10^{-4}
40	0.438	5.137×10^{-7}	3.568×10^{-7}	1.530×10^{-4}	1.797×10^{-4}
60	0.533	6.682×10^{-7}	4.640×10^{-7}	3.300×10^{-4}	3.930×10^{-4}
80	0.624*	9.409×10^{-7}	6.534×10^{-7}	3.848×10^{-4}	5.177×10^{-3}
95	0.728**	3.195×10^{-6}	2.219×10^{-7}	3.540×10^{-4}	1.060×10^{-3}

* M_m at t = 900 days, followed by weight loss to M_m = 0.601 % at t =1500 days

** M_m at t = 380 days, followed by weight loss to M_m = 0.621 % at t =1500 days

5.5 Exposure to Relative Humidity at 23 ^{o}C

Unidirectional E-glass Vinylester composite specimens measuring 25.4 mm X 25.4 mm X 2.54 mm were subjected to different humidity levels of 0-5%, 45%, 60%, 75%, 98% at a temperature of 23 ^{o}C. Moisture absorption data was recorded at the following intervals: 2 days, 5 days, 8 days, 9 days, 13 days, 20 days and so on till 1500 days. The moisture absorption data is given in Table 5.8.

5.5.1 Full Model

The moisture absorption data shown in Table 5.8 were fitted to equations 5.3 (Fickian Diffusion Model) and 5.7 (Langmuir Diffusion Model) using MathCAD tools. The details of the MathCAD programs used are given in Appendix. Fitting the data to the equations results in the estimation of the maximum moisture content, M_m and diffusion coefficient, D. The results of the analysis using the equations 5.3 and 5.7 are presented in the Figures 5.6 and 5.7. For brevity, moisture absorption curves are shown for the 45 % relative humidity case only. The moisture absorption curves for the humidity levels of 0-5 %, 60 %, 75 % and 98 % are shown in Appendix A. The values of maximum moisture contents and diffusion coefficients obtained from the analyses are shown in Tables 5.9 and 5.10.

Table 5.8 Moisture absorption data of E-glass/Vinylester specimens exposed to relative humidity levels of 0-5%, 45%, 60%, 80% and 98% at a constant temperature of 23 ^{o}C

Time (Days)	Relative Humidity %				
	0-5	**45**	**60**	**80**	**98**
0	0	0	0	0	0
2	0	0.002	0.015	0.025	0.073
5	0	0.004	0.024	0.040	0.084
8	-0.0076	0.005	0.031	0.043	0.100
13	-0.0079	0.006	0.040	0.051	0.128
20	-0.0081	0.007	0.066	0.078	0.126
26	-0.0086	0.020	0.088	0.101	0.146
33	-0.0088	0.024	0.098	0.118	0.172
41	-0.0094	0.041	0.111	0.129	0.177
48	-0.0097	0.054	0.109	0.142	0.207
54	-0.0100	0.056	0.119	0.157	0.210
71	-0.0103	0.063	0.130	0.178	0.222
91	-0.0112	0.067	0.152	0.188	0.265
130	-0.0114	0.111	0.179	0.228	0.288
159	-0.0119	0.118	0.168	0.220	0.293
182	-0.0121	0.122	0.173	0.222	0.295
200	-0.0120	0.130	0.182	0.227	0.310
221	-0.0124	0.134	0.184	0.235	0.318
250	-0.0133	0.136	0.183	0.237	0.314
272	-0.0129	0.138	0.185	0.239	0.313
305	-0.0128	0.137	0.183	0.238	0.312
330	-0.0126	0.139	0.187	0.236	0.310
365	-0.0126	0.141	0.19	0.239	0.315
450	-0.0128	0.149	0.195	0.241	0.318
600	-0.0127	0.154	0.203	0.240	0.321
800	-0.0128	0.158	0.210	0.245	0.325
1000	-0.0127	0.163	0.212	0.250	0.327
1500	-0.0128	0.164	0.215	0.253	0.329

Table 5.9 Maximum moisture contents and diffusion coefficients obtainedfrom Fickian Diffusion Model (FULL MODEL) for specimens exposed to different relative humidity levels at 23 ^{0}C

Relative Humidity (%)	M_m %	Diffusion Coefficient (mm^2/s)	
		Fickian Diffusion Model	Corrected for Edge Effects
0-5	0.013 (WL)*	2.071×10^{-8}	1.438×10^{-8}
45	0.164	3.804×10^{-8}	2.642×10^{-8}
60	0.215	9.075×10^{-8}	6.302×10^{-8}
75	0.253	9.684×10^{-8}	6.725×10^{-8}
98	0.329	1.223×10^{-7}	8.496×10^{-8}

*WL – Weight Loss

Table 5.10 Maximum moisture contents and diffusion coefficients obtained from Langmuir Diffusion Model (FULL MODEL) for specimens exposed to different relative humidity levels at 23 ^{0}C

Relative Humidity (%)	M_m %	Diffusion Coefficient (mm^2/s)		α	β
		Langmuir Diffusion Model	Corrected for Edge Effects		
0-5	0.013(WL)	6.913×10^{-8}	4.801×10^{-8}	4.856×10^{-3}	5.039×10^{-3}
45	0.164	3.230×10^{-8}	2.243×10^{-8}	5.706×10^{-3}	5.040×10^{-3}
60	0.215	8.374×10^{-8}	5.816×10^{-8}	2.300×10^{-2}	2.300×10^{-2}
75	0.253	1.086×10^{-7}	7.541×10^{-8}	3.741×10^{-5}	3.502×10^{-5}
98	0.329	1.235×10^{-7}	8.576×10^{-8}	3.175×10^{-5}	3.367×10^{-5}

*WL – Weight Loss

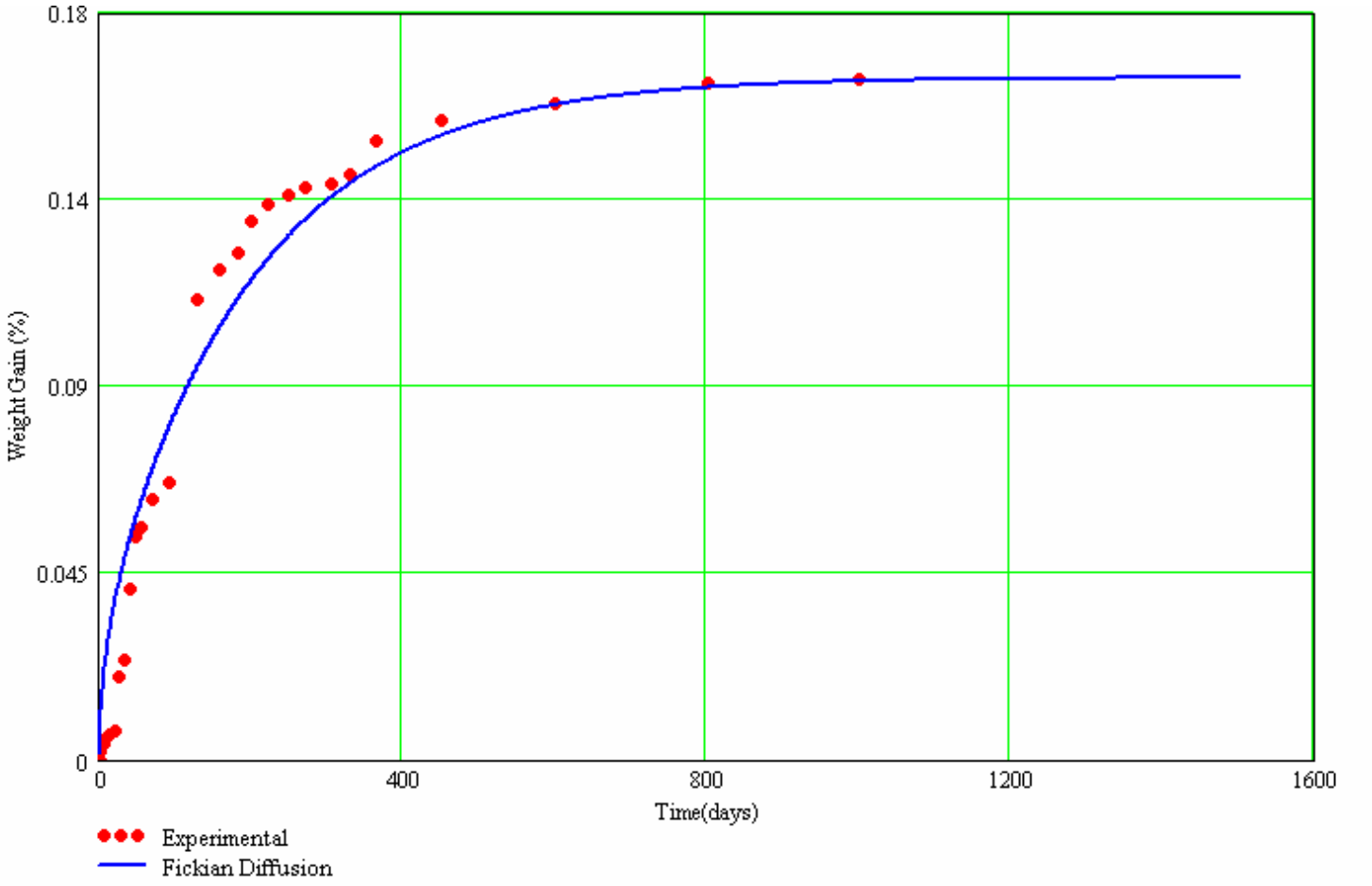

Fig. 5.6 Prediction of Moisture absorption profile of E-glass vinylester composite specimens exposed to Relative Humidity of 45 % at 23 ^{o}C with Fickian Model

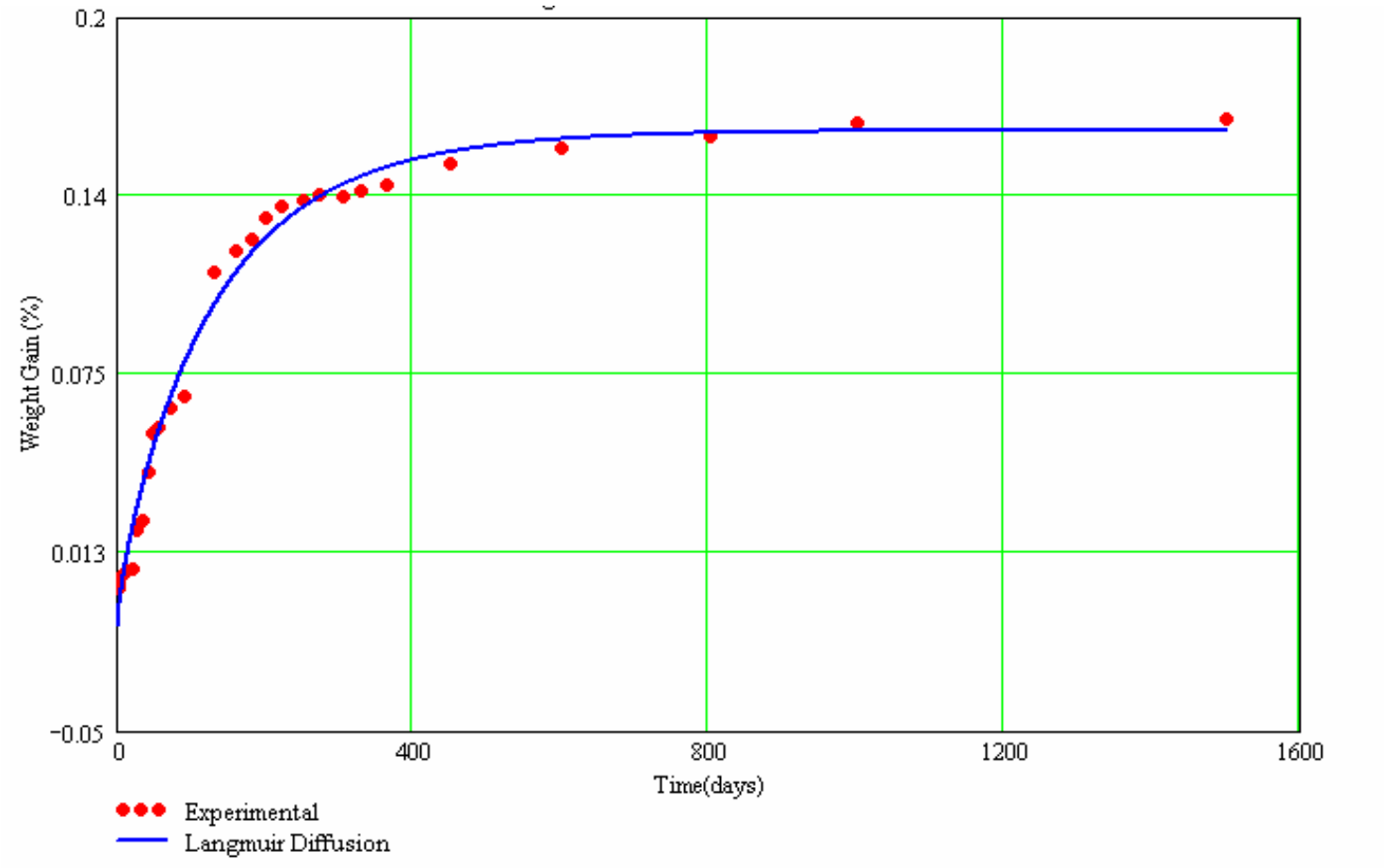

Fig. 5.7 Prediction of Moisture absorption profile of E-glass vinylester composite specimens exposed to Relative Humidity of 45 % at 23 ^{o}C with Langmuir Model

5.5.2 Long-term Approximation

Equations 5.5 and 5.9 are complicated and require elaborate procedures to fit the moisture absorption data. Long-term approximation given by equations 5.5 and 5.9 are often used in place of the elaborate full model. The values obtained by applying long-term approximation models to the moisture absorption data are listed in table 5.11 and 5.12. For brevity, moisture absorption curves are shown for the relative humidity 45 % only, in figure 5.8. The moisture absorption curves for relative humidity levels 0-5 %, 60 %, 75 % and 98 % are shown in Appendix A.

Table 5.11 Maximum moisture contents and Diffusion coefficients obtainedfrom Fickian Diffusion Model (LONG-TERM APPROXIMATION) for specimens exposed to different relative humidity levels at 23 ^{0}C

Relative Humidity (%)	M_m %	Diffusion Coefficient (mm^2/s)	
		Fickian Diffusion Model	Corrected for Edge Effects
0-5	0.013(WL)	2.128×10^{-8}	1.478×10^{-8}
45	0.164	5.654×10^{-8}	3.926×10^{-8}
60	0.215	1.181×10^{-7}	8.201×10^{-8}
75	0.253	1.287×10^{-7}	8.937×10^{-8}
98	0.329	1.404×10^{-7}	9.750×10^{-8}

*WL – Weight Loss

Table 5.12 Maximum moisture contents and diffusion coefficients obtainedfrom Langmuir Diffusion Model (LONG-TERM APPROXIMATION) for specimens exposed to different relative humidity levels at 23 ^{0}C

Relative Humidity (%)	M_m %	Diffusion Coefficient (mm^2/s)		α	β
		Langmuir Diffusion Model	Corrected for Edge Effects		
0-5	0.013(WL)	5.829×10^{-8}	4.048×10^{-8}	6.329×10^{-3}	3.500×10^{-2}
45	0.164	5.825×10^{-8}	4.045×10^{-8}	1.100×10^{-2}	2.200×10^{-2}
60	0.215	1.372×10^{-7}	9.528×10^{-8}	1.358×10^{-3}	5.600×10^{-2}
75	0.253	1.461×10^{-7}	1.014×10^{-7}	5.600×10^{-3}	6.900×10^{-2}
98	0.329	1.502×10^{-7}	1.043×10^{-7}	5.258×10^{-3}	2.730×10^{-1}

*WL – Weight Loss

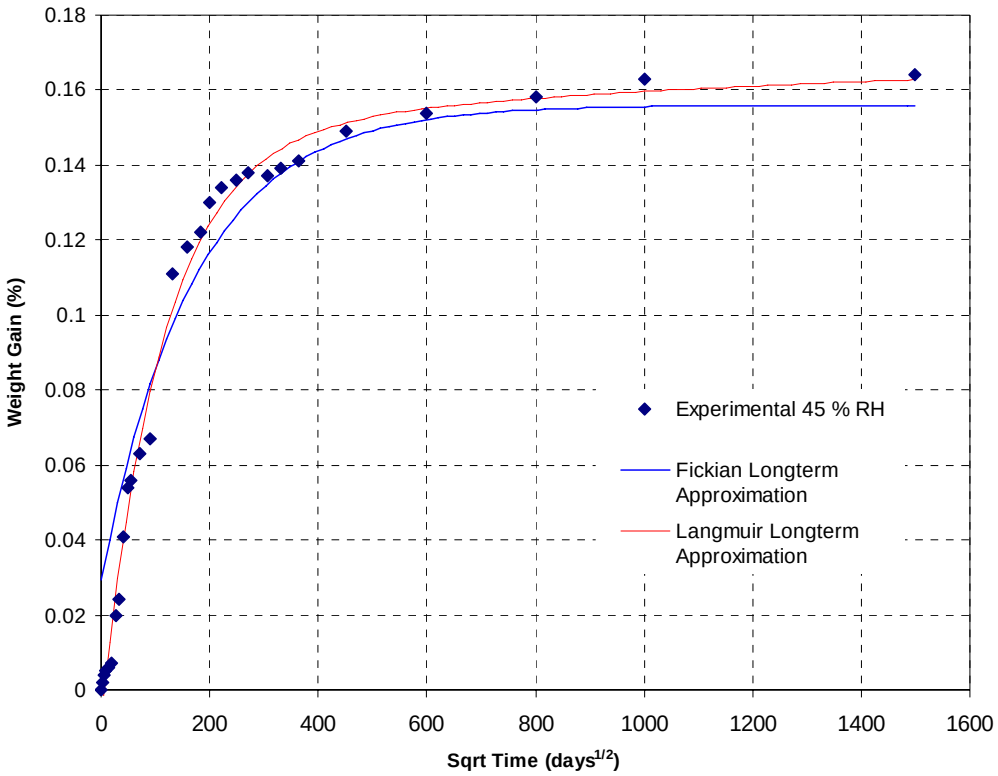

Fig. 5.8 Prediction of Moisture absorption profile of E-glass vinylester composite specimensexposed to Relative Humidity of 45 % at 23 ^{o}C with long-term approximation terms

5.5.3 Short-term Approximation

Short-term approximation of the moisture absorption data is performed according to the procedure described in section 5.4.3. The results are presented in Tables 5.13 and 5.14.

Table 5.13 Maximum moisture contents and diffusion coefficients obtainedfrom Fickian Diffusion Model (SHORT-TERM APPROXIMATION) for specimens exposed to different relative humidity levels at 23 ^{0}C

Relative Humidity (%)	M_m %	Diffusion Coefficient (mm^2/s)	
		Fickian Diffusion Model	Corrected for Edge Effects
0-5	0.013 (Weight Loss)	1.411×10^{-8}	9.800×10^{-9}
45	0.164	3.021×10^{-8}	2.098×10^{-8}
60	0.215	7.758×10^{-8}	5.387×10^{-8}
75	0.253	1.061×10^{-7}	7.368×10^{-8}
98	0.329	1.027×10^{-7}	7.132×10^{-8}

*WL – Weight Loss

Table 5.14 Maximum moisture contents and diffusion coefficients obtainedfrom Langmuir Diffusion Model (SHORT-TERM APPROXIMATION) for specimens exposed to different relative humidity levels at 23 ^{0}C

Relative Humidity (%)	M_m %	Diffusion Coefficient (mm^2/s)		α	β
		Langmuir Diffusion Model	Corrected for Edge Effects		
0-5	0.013(WL)	5.859×10^{-8}	4.069×10^{-8}	4.856×10^{-3}	5.039×10^{-3}
45	0.164	1.071×10^{-7}	7.439×10^{-8}	5.706×10^{-3}	5.040×10^{-3}
60	0.215	3.110×10^{-7}	2.160×10^{-7}	2.300×10^{-2}	2.300×10^{-2}
75	0.253	3.974×10^{-7}	2.760×10^{-7}	3.741×10^{-5}	3.502×10^{-5}
98	0.329	4.363×10^{-7}	3.030×10^{-7}	3.175×10^{-5}	3.367×10^{-5}

*WL – Weight Loss

5.6 Exposure to Relative Humidity at 95 ^{o}C

Unidirectional E-glass Vinylester composite specimens measuring 25.4 mm X 25.4 mm X 2.54 mm were subjected to humidity levels of 0-5%, 45%, 60%, 75%, 98% at a temperature 95 ^{o}C. Moisture absorption data was recorded at the following intervals: 2 days, 5 days, 8 days, 9 days, 13 days, 20 days and so on till 1500 days. The moisture absorption data is given in Table 5.15.

5.6.1 Full Model

The moisture absorption data shown in Table 5.15 were fir to equations 5.3 (Fickian Diffusion Model) and 5.7 (Langmuir Diffusion Model) MathCAD tools. The details of the MathCAD programs used are given in Appendix. using Mathcad tools. Fitting the data to the equations results in the estimation of the maximum moisture content, M_m and diffusion coefficient, D. The results of the analysis using the equations 5.3 and 5.7 are presented in the Figures 5.9 and 5.10. For brevity, moisture absorption curves are shown for the 45% relative humidity case only. The moisture absorption curves for humidity levels of 0-5 %, 60 %, 75 % and 98 % are shown in Appendix A. The values of maximum moisture contents and diffusion coefficients obtained from the analyses are shown in Tables 5.16 and 5.17.

Table 5.15 Moisture absorption data of E-glass/Vinylester specimens exposed to relative humidity levels of 0-5%, 45%, 60%, 80% and 98% at a constant temperature of 95 ^{o}C

Time (Days)	Relative Humidity %				
	0-5	45	60	80	98
0	0	0	0	0	0
1	0	0.002	0.013	0.0254	0.048
2	0	0.005	0.017	0.027	0.069
3	0	0.009	0.021	0.036	0.071
5	-0.00141	0.010	0.027	0.049	0.090
8	-0.00153	0.013	0.035	0.0495	0.119
11	-0.00120	0.017	0.041	0.054	0.123
13	-0.00136	0.019	0.045	0.055	0.139
18	-0.00137	0.020	0.055	0.080	0.154
24	-0.00158	0.028	0.063	0.103	0.164
34	-0.00140	0.038	0.102	0.122	0.187
55	-0.00168	0.059	0.123	0.165	0.232
70	-0.00185	0.064	0.137	0.187	0.253
98	-0.00190	0.078	0.158	0.189	0.273
113	-0.00201	0.093	0.167	0.206	0.285
130	-0.00207	0.116	0.183	0.235	0.298
151	-0.00214	0.119	0.189	0.239	0.309
172	-0.00217	0.127	0.192	0.242	0.318
195	-0.00220	0.131	0.197	0.244	0.325
219	-0.00225	0.137	0.201	0.247	0.337
240	-0.00225	0.141	0.205	0.251	0.35
261	-0.00220	0.146	0.211	0.251	0.357
290	-0.00215	0.153	0.216	0.255	0.365
315	-0.00219	0.157	0.219	0.259	0.371
330	-0.00217	0.159	0.225	0.263	0.376
365	-0.00218	0.163	0.229	0.266	0.379
450	-0.00219	0.176	0.236	0.278	0.382
600	-0.00227	0.188	0.238	0.283	0.386
800	-0.00217	0.193	0.239	0.289	0.392
1000	-0.00225	0.196	0.241	0.292	0.395
1500	-0.00217	0.203	0.241	0.293	0.397

Table 5.16 Maximum moisture contents and diffusion coefficients obtained from Fickian Diffusion Model (FULL MODEL) for specimens exposed to different relative humidity levels at 95 ^{0}C

Relative Humidity (%)	M_m %	Diffusion Coefficient (mm^2/s)	
		Fickian Diffusion Model	Corrected for Edge Effects
0-5	0.002(WL)	2.926×10^{-8}	2.032×10^{-8}
45	0.203	3.125×10^{-8}	2.170×10^{-8}
60	0.241	7.120×10^{-8}	4.944×10^{-8}
75	0.293	9.678×10^{-8}	6.721×10^{-8}
98	0.397	1.785×10^{-7}	1.240×10^{-7}

*WL – Weight Loss

Table 5.17 Maximum moisture contents and diffusion coefficients obtainedfrom Langmuir Diffusion Model (FULL MODEL) for specimens exposed to different relative humidity levels at 95 ^{0}C

Relative Humidity (%)	M_m %	Diffusion Coefficient (mm^2/s)		α	β
		Langmuir Diffusion Model	Corrected for Edge Effects		
0-5	0.0023(WL)*	1.107×10^{-7}	7.687×10^{-8}	4.249×10^{-3}	4.263×10^{-3}
45	0.203	5.424×10^{-8}	3.767×10^{-8}	3.701×10^{-3}	3.458×10^{-3}
60	0.241	1.065×10^{-7}	7.396×10^{-8}	3.701×10^{-3}	3.458×10^{-3}
75	0.293	1.992×10^{-7}	1.383×10^{-7}	6.092×10^{-3}	6.709×10^{-3}
98	0.397	2.978×10^{-7}	2.068×10^{-7}	4.062×10^{-3}	4.426×10^{-3}

*WL = Weight Loss

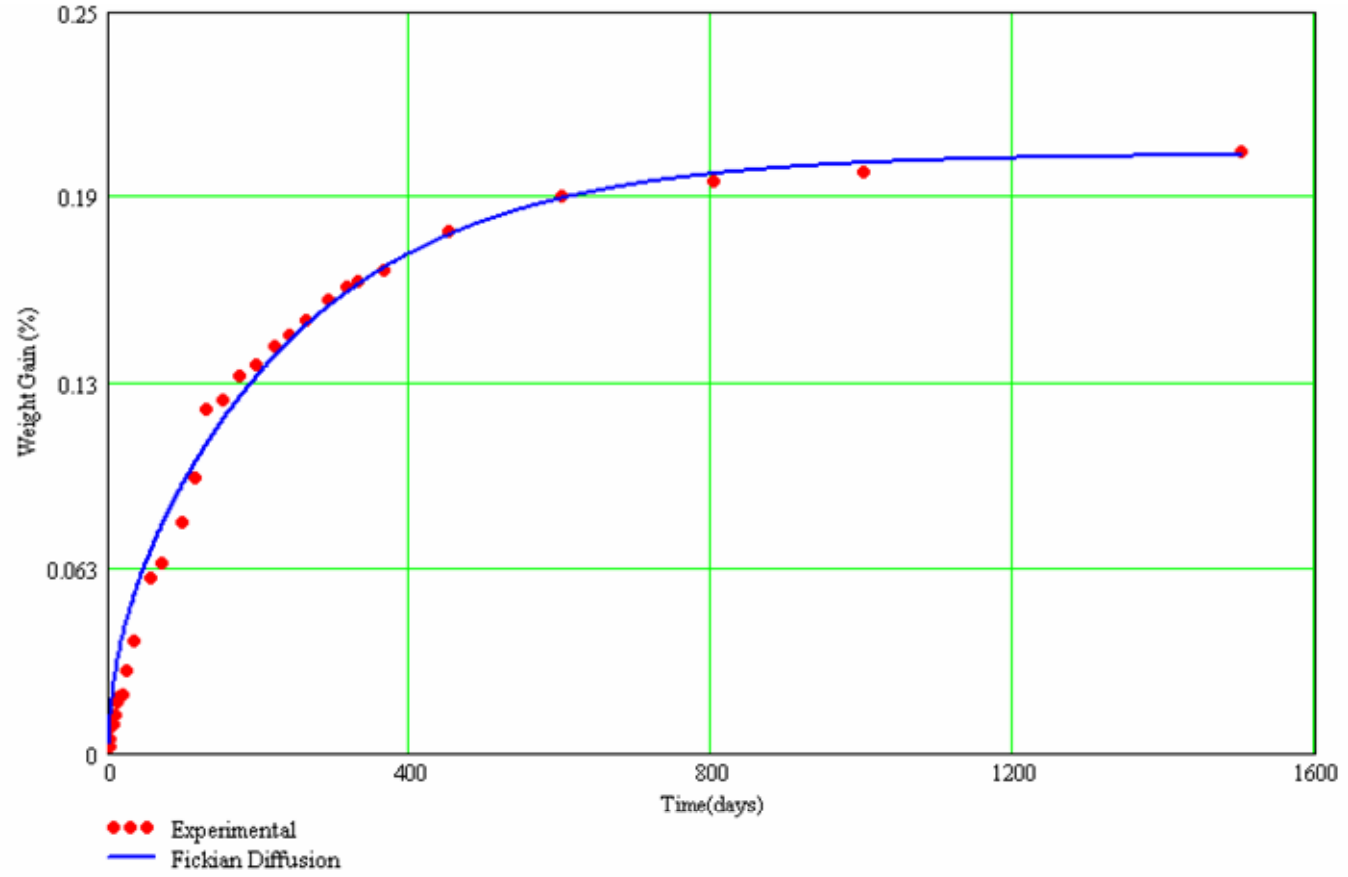

Fig. 5.9 Prediction of Moisture absorption profile of E-glass vinylester composite specimen exposed to a Relative Humidity of 45 % at 95 ^{o}C with Fickian Diffusion Model

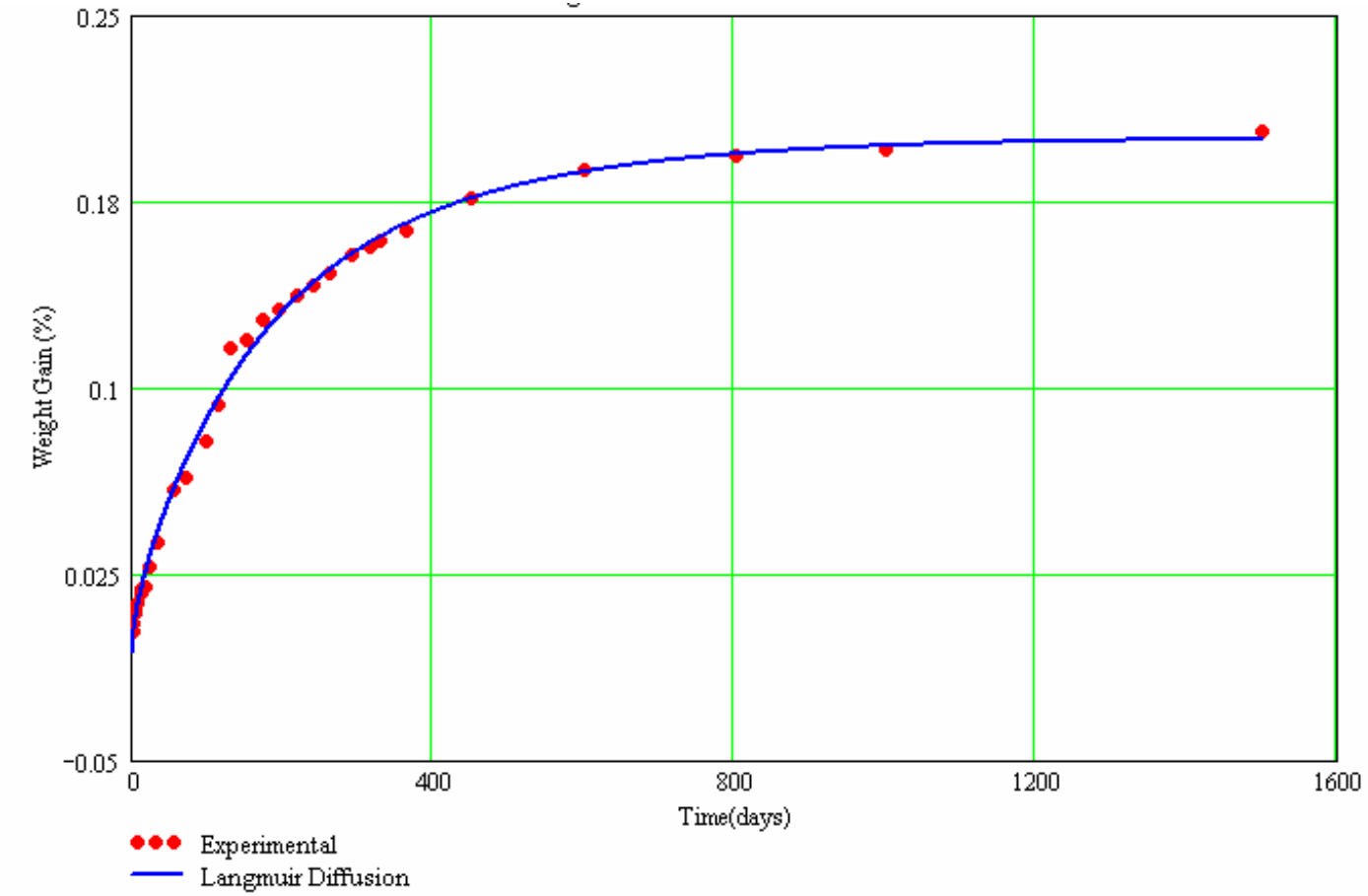

Fig. 5.10 Prediction of Moisture absorption profile of E-glass vinylester composite specimens exposed to a Relative Humidity of 45 % at 95 ^{o}C with Langmuir Diffusion Model

5.6.2 Long-term Approximation

Equations 5.5 and 5.9 are complicated and require elaborate procedures to fit the moisture absorption data. Long-term approximation given by equations 5.5 and 5.9 are often used in place of the elaborate full model. The values obtained by applying long-term approximation models are listed in table 5.18 and 5.19. For brevity, moisture absorption curves are shown for the relative humidity of 45 % only, in figure 5.11. The moisture absorption curves for relative humidity levels of 0-5 %, 60 %, 75 % and 98 % are shown in Appendix A.

Table 5.18 Maximum moisture contents and diffusion coefficients obtainedfrom Fickian Diffusion Model (LONG-TERM APPROXIMATION) for specimens exposed to different relative humidity levels at 95 ^{0}C

Relative Humidity (%)	M_m %	Diffusion Coefficient (mm^2/s)	
		Fickian Diffusion Model	Corrected for Edge Effects
0-5	0.0023(WL)	3.024×10^{-8}	2.100×10^{-8}
45	0.203	6.400×10^{-8}	4.444×10^{-8}
60	0.241	1.291×10^{-7}	8.965×10^{-8}
75	0.293	1.368×10^{-7}	9.500×10^{-8}
98	0.397	2.166×10^{-7}	1.504×10^{-7}

*WL – Weight Loss

Table 5.19 Maximum moisture contents and Diffusion coefficients obtained from Langmuir Diffusion Model (LONG-TERM APPROXIMATION) for specimens exposed to different relative humidity levels at 95 ^{0}C

Relative Humidity (%)	M_m %	Diffusion Coefficient (mm^2/s)		α	β
		Langmuir Diffusion Model	Corrected for edge effects		
0-5	0.0023(WL)	1.116×10^{-7}	7.750×10^{-8}	8.419×10^{-3}	3.900×10^{-3}
45	0.203	4.520×10^{-8}	3.139×10^{-8}	1.008×10^{-3}	1.000×10^{-3}
60	0.241	9.170×10^{-8}	6.368×10^{-8}	1.700×10^{-3}	2.300×10^{-2}
75	0.293	1.284×10^{-7}	8.917×10^{-8}	3.330×10^{-3}	5.000×10^{-2}
98	0.397	2.231×10^{-7}	1.549×10^{-7}	6.435×10^{-3}	2.910×10^{-1}

*WL – Weight Loss

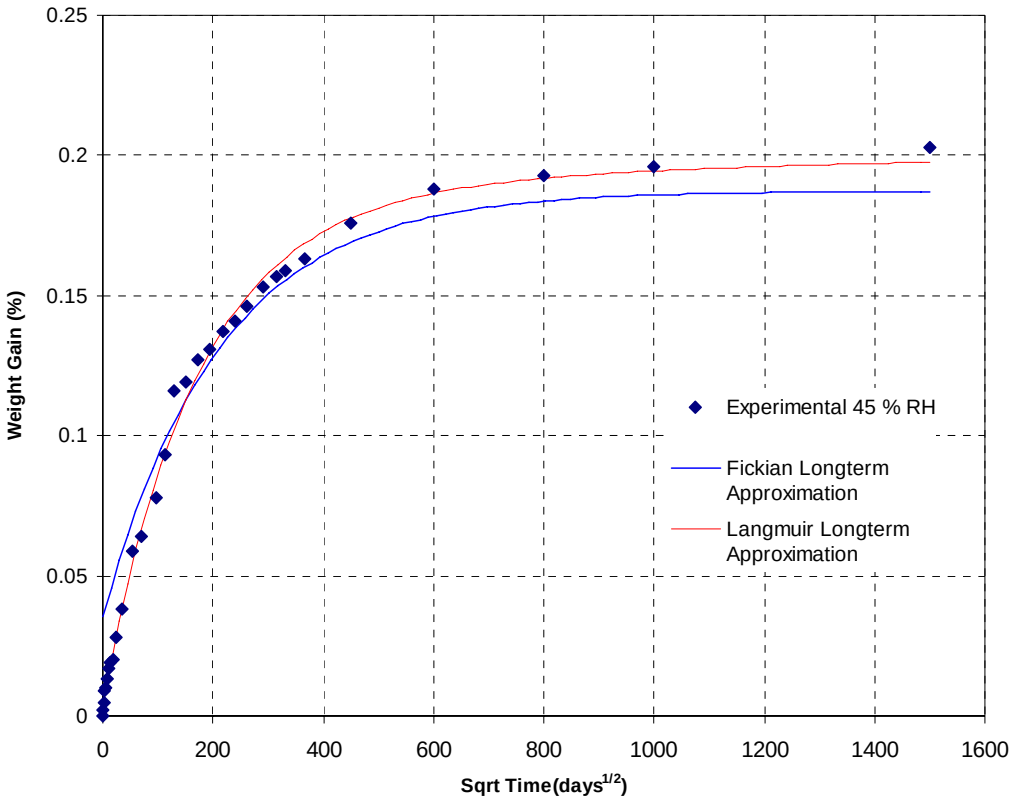

Fig. 5.11 Prediction of Moisture absorption profile of E-glass vinylester composite specimens exposed toRelative Humidity of 45 % at 95 ^{o}C with long-term approximation terms

5.6.3 Short-term Approximation

Short-term approximation of the moisture absorption data is performed according to the procedure described in section 5.4.3. The results are presented in Tables 5.20 and 5.21.

Table 5.20 Maximum moisture contents and diffusion coefficients obtainedfrom Fickian Diffusion Model (SHORT-TERM APPROXIMATION) for specimens exposed to different relative humidity levels at 95 ^{0}C

Relative Humidity (%)	M_m %	Diffusion Coefficient (mm^2/s)	
		Fickian Diffusion Model	Corrected for Edge Effects
0-5	0.0023(WL)	5.430×10^{-8}	3.771×10^{-8}
45	0.203	3.152×10^{-8}	2.189×10^{-8}
60	0.241	2.790×10^{-8}	1.937×10^{-8}
75	0.293	1.180×10^{-7}	8.194×10^{-8}
98	0.397	1.631×10^{-7}	1.133×10^{-7}

*WL – Weight Loss

Table 5.21 Maximum moisture contents and diffusion coefficients obtained from Langmuir Diffusion Model (SHORT-TERM APPROXIMATION) for specimens exposed to different relative humidity levels at 95 ^{0}C

Relative Humidity (%)	M_m %	Diffusion Coefficient (mm^2/s)		α	β
		Langmuir Diffusion Model	Corrected for Edge Effects		
0-5	0.0023(WL)	5.666×10^{-8}	3.935×10^{-8}	4.249×10^{-3}	4.263×10^{-3}
45	0.203	1.179×10^{-7}	8.190×10^{-8}	3.701×10^{-3}	3.458×10^{-3}
60	0.241	2.794×10^{-7}	1.940×10^{-7}	3.701×10^{-3}	3.458×10^{-3}
75	0.293	4.694×10^{-7}	3.260×10^{-7}	6.700×10^{-3}	6.870×10^{-3}
98	0.397	7.128×10^{-7}	4.950×10^{-7}	8.400×10^{-2}	9.900×10^{-2}

*WL – Weight Loss

5.7 Summary of Results

The summary of results from analyzing the moisture absorption data using Fickian diffusion model has been given in Table 5.22. The results from the Langmuir absorption theory have been summarized in Tables 5.23 through 5.25.

Table 5.22 Maximum moisture contents and diffusion coefficients of E-glass/vinylester composite specimens immersed in deionized water at various temperatures, obtained using Fickian diffusion theory

Immersion in Water							
Temp (^{0}C)	**M_m %**	**Diffusion Coefficients (mm^2/sec)**					
		Short term approximation	**Corrected for edge effects**	**Long term approximation**	**Corrected for edge effects**	**Full model**	**Corrected for edge effects**
23	0.405	1.041×10^{-7}	7.229×10^{-8}	1.186×10^{-7}	8.236×10^{-8}	1.304×10^{-7}	9.056×10^{-8}
40	0.438	1.086×10^{-7}	7.542×10^{-8}	2.024×10^{-7}	1.406×10^{-7}	1.969×10^{-7}	1.367×10^{-7}
60	0.533	1.392×10^{-7}	9.667×10^{-8}	2.135×10^{-7}	1.483×10^{-7}	2.139×10^{-7}	1.485×10^{-7}
80	0.624	1.710×10^{-7}	1.187×10^{-7}	2.277×10^{-7}	1.581×10^{-7}	2.175×10^{-7}	1.510×10^{-7}
95	0.728	2.003×10^{-7}	1.391×10^{-7}	2.513×10^{-7}	1.745×10^{-7}	2.414×10^{-7}	1.676×10^{-7}
Humidity at 23 ^{0}C							
Humidity (%)	**M_m %**	**Diffusion Coefficients (mm^2/sec)**					
		Short term approximation	**Corrected for edge effects**	**Long term approximation**	**Corrected for edge effects**	**Full model**	**Corrected for edge effects**
0-5	0.013 (Weight Loss)	1.411×10^{-8}	9.800×10^{-9}	2.128×10^{-8}	1.478×10^{-8}	2.071×10^{-8}	1.438×10^{-8}
45	0.164	3.021×10^{-8}	2.098×10^{-8}	5.654×10^{-8}	3.926×10^{-8}	3.804×10^{-8}	2.642×10^{-8}
60	0.215	7.758×10^{-8}	5.387×10^{-8}	1.181×10^{-7}	8.201×10^{-8}	9.075×10^{-8}	6.302×10^{-8}
75	0.253	1.061×10^{-7}	7.368×10^{-8}	1.287×10^{-7}	8.937×10^{-8}	9.684×10^{-8}	6.725×10^{-8}
98	0.329	1.027×10^{-7}	7.132×10^{-8}	1.404×10^{-7}	9.750×10^{-8}	1.223×10^{-7}	8.496×10^{-8}
Humidity at 95 ^{0}C							
Humidity (%)	**M_m %**	**Diffusion Coefficients (mm^2/sec)**					
		Short term approximation	**Corrected for edge effects**	**Long term approximation**	**Corrected for edge effects**	**Full model**	**Corrected for edge effects**
0-5	0.002(Weight Loss)	5.430×10^{-8}	3.771×10^{-8}	3.024×10^{-8}	2.100×10^{-8}	2.926×10^{-8}	2.032×10^{-8}
45	0.203	3.152×10^{-8}	2.189×10^{-8}	6.400×10^{-8}	4.444×10^{-8}	3.125×10^{-8}	2.170×10^{-8}
60	0.241	2.790×10^{-8}	1.937×10^{-8}	1.291×10^{-7}	8.965×10^{-8}	7.120×10^{-8}	4.944×10^{-8}
75	0.293	1.180×10^{-7}	8.194×10^{-8}	1.368×10^{-7}	9.500×10^{-8}	9.678×10^{-8}	6.721×10^{-8}
98	0.397	1.631×10^{-7}	1.133×10^{-7}	2.166×10^{-7}	1.504×10^{-7}	1.785×10^{-7}	1.240×10^{-7}

Table 5.23 Maximum moisture contents and diffusion coefficients of E-glass vinylester composite specimens immersed in deionized water at various temperatures, obtained using Langmuir diffusion theory

Immersion in Water - Full Model					
Temp (^{0}C)	M_m %	Diffusion Coefficients (mm^2/sec)		α	β
		Langmuir diffusion model	Corrected for edge effects		
23	0.405	8.945×10^{-8}	6.212×10^{-8}	1.761×10^{-4}	2.104×10^{-4}
40	0.438	1.045×10^{-7}	7.278×10^{-8}	1.530×10^{-4}	1.797×10^{-4}
60	0.533	1.257×10^{-7}	8.729×10^{-8}	3.300×10^{-4}	3.930×10^{-4}
80	0.624	2.166×10^{-7}	1.504×10^{-7}	3.848×10^{-4}	5.177×10^{-3}
95	0.728	2.384×10^{-7}	1.656×10^{-7}	3.540×10^{-4}	1.060×10^{-3}
Immersion in Water - Long term Approximation					
Temp (^{0}C)	M_m %	Diffusion Coefficients (mm^2/sec)		α	β
		Langmuir diffusion model	Corrected for edge effects		
23	0.405	9.509×10^{-8}	6.603×10^{-8}	-8.670×10^{-4}	2.200×10^{-2}
40	0.438	1.188×10^{-7}	8.250×10^{-8}	-1.308×10^{-4}	5.000×10^{-2}
60	0.533	1.538×10^{-7}	1.068×10^{-7}	-3.313×10^{-4}	1.030×10^{-1}
80	0.624	2.019×10^{-7}	1.402×10^{-7}	-5.416×10^{-4}	1.060×10^{-1}
95	0.728	2.472×10^{-7}	1.717×10^{-7}	-3.863×10^{-3}	9.300×10^{-2}
Immersion in Water - Short term Approximation					
Temp (^{0}C)	M_m %	Diffusion Coefficients (mm^2/sec)		α	β
		Langmuir diffusion model	Corrected for edge effects		
23	0.405	5.013×10^{-7}	3.481×10^{-7}	1.761×10^{-4}	2.104×10^{-4}
40	0.438	5.137×10^{-7}	3.568×10^{-7}	1.530×10^{-4}	1.797×10^{-4}
60	0.533	6.682×10^{-7}	4.640×10^{-7}	3.300×10^{-4}	3.930×10^{-4}
80	0.624	9.409×10^{-7}	6.534×10^{-7}	3.848×10^{-4}	5.177×10^{-3}
95	0.728	3.195×10^{-6}	2.219×10^{-6}	3.540×10^{-4}	1.060×10^{-3}

Table 5.24 Maximum moisture contents and Diffusion Coefficients of E-glass vinylester composite specimens exposed to relative humidity levels at 23 ^{o}C, obtained using Langmuir diffusion theory (WL- Weight Loss)

Humidity (23C) - Full Model					
RH %	**M_m %**	**D (mm^2/s)**		**α**	**β**
		Langmuir diffusion model	**Corrected for edge effects**		
0-5	0.013(WL)	6.913×10^{-8}	4.801×10^{-8}	4.856×10^{-3}	5.039×10^{-3}
45	0.164	3.230×10^{-8}	2.243×10^{-8}	5.706×10^{-3}	5.040×10^{-3}
60	0.215	8.374×10^{-8}	5.816×10^{-8}	2.300×10^{-2}	2.300×10^{-2}
75	0.253	1.086×10^{-7}	7.541×10^{-8}	3.741×10^{-5}	3.502×10^{-5}
98	0.329	1.235×10^{-7}	8.576×10^{-8}	3.175×10^{-5}	3.367×10^{-5}
Humidity (23C)- Long term Approximation					
RH %	**M_m %**	**D (mm^2/s)**		**α**	**β**
		Langmuir diffusion model	**Corrected for edge effects**		
0-5	0.013(WL)	5.829×10^{-8}	4.048×10^{-8}	6.329×10^{-3}	3.500×10^{-2}
45	0.164	5.825×10^{-8}	4.045×10^{-8}	1.100×10^{-2}	2.200×10^{-2}
60	0.215	1.372×10^{-7}	9.528×10^{-8}	1.358×10^{-3}	5.600×10^{-2}
75	0.253	1.461×10^{-7}	1.014×10^{-7}	5.600×10^{-3}	6.900×10^{-2}
98	0.329	1.502×10^{-7}	1.043×10^{-7}	5.258×10^{-3}	2.730×10^{-1}
Humidity (23C) - Short term Approximation					
RH %	**M_m %**	**D (mm^2/s)**		**α**	**β**
		Langmuir diffusion model	**Corrected for edge effects**		
0-5	0.013(WL)	5.859×10^{-8}	4.069×10^{-8}	4.856×10^{-3}	5.039×10^{-3}
45	0.164	1.071×10^{-7}	7.439×10^{-8}	5.706×10^{-3}	5.040×10^{-3}
60	0.215	3.110×10^{-7}	2.160×10^{-7}	2.300×10^{-2}	2.300×10^{-2}
75	0.253	3.974×10^{-7}	2.760×10^{-7}	3.741×10^{-5}	3.502×10^{-5}
98	0.329	4.363×10^{-7}	3.030×10^{-7}	3.175×10^{-5}	3.367×10^{-5}

Table 5.25 Maximum moisture contents and Diffusion Coefficients of E-glass vinylester composite specimens exposed to relative humidity levels at 95 ^{o}C, obtained using Langmuir diffusion theory (WL-Weight Loss)

Humidity (95C) - Full Model					
RH %	**M_m %**	**D (mm^2/s)**		**α**	**β**
		Langmuir diffusion model	**Corrected for edge effects**		
0-5	0.0023(WL)	1.107×10^{-7}	7.687×10^{-8}	4.249×10^{-3}	4.263×10^{-3}
45	0.203	5.424×10^{-8}	3.767×10^{-8}	3.701×10^{-3}	3.458×10^{-3}
60	0.241	1.065×10^{-7}	7.396×10^{-8}	3.701×10^{-3}	3.458×10^{-3}
75	0.293	1.992×10^{-7}	1.383×10^{-7}	6.092×10^{-3}	6.709×10^{-3}
98	0.397	2.978×10^{-7}	2.068×10^{-7}	4.062×10^{-3}	4.426×10^{-3}
Humidity (95C)- Long term Approximation					
RH %	**M_m %**	**D (mm^2/s)**		**α**	**β**
		Langmuir diffusion model	**Corrected for edge effects**		
0-5	0.0023(WL)	1.116×10^{-7}	7.750×10^{-8}	8.419×10^{-3}	3.900×10^{-3}
45	0.203	4.520×10^{-8}	3.139×10^{-8}	1.008×10^{-3}	1.000×10^{-3}
60	0.241	9.170×10^{-8}	6.368×10^{-8}	1.700×10^{-3}	2.300×10^{-2}
75	0.293	1.284×10^{-7}	8.917×10^{-8}	3.330×10^{-3}	5.000×10^{-2}
98	0.397	2.231×10^{-7}	1.549×10^{-7}	6.435×10^{-3}	2.910×10^{-1}
Humidity (95C) - Short term Approximation					
RH %	**M_m %**	**D (mm^2/s)**		**α**	**β**
		Langmuir diffusion model	**Corrected for edge effects**		
0-5	0.0023(WL)	5.666×10^{-8}	3.935×10^{-8}	4.249×10^{-3}	4.263×10^{-3}
45	0.203	1.179×10^{-7}	8.190×10^{-8}	3.701×10^{-3}	3.458×10^{-3}
60	0.241	2.794×10^{-7}	1.940×10^{-7}	3.701×10^{-3}	3.458×10^{-3}
75	0.293	4.694×10^{-7}	3.260×10^{-7}	6.700×10^{-3}	6.870×10^{-3}
98	0.397	7.128×10^{-7}	4.950×10^{-7}	8.400×10^{-2}	9.900×10^{-2}

5.8 Discussion

From the experimental results, it can be inferred that the level of moisture uptake is related to the temperature and relative humidity increase. From figures 4.1, 4.2 and 4.3, it can be seen that the specimens immersed in deionzied water at 95 ^{0}C absorbed the maximum amount of moisture of 0.728 %. The composite specimens immersed in deionzied water at 80 ^{0}C and 95 ^{0}C exhibit maximum moisture contents of 0.624 % and 0.728 % and from thereon the specimens begin to loose weight, indicating irreversible damage. These peak moisture contents were observed at 900 days and 380 days respectively. But the specimens at the lower temperatures of 23 ^{0}C, 40 ^{0}C and 60 ^{0}C continue to gain weight throughout the exposure time with maximum moisture contents of 0.405 %, 0.438 % and 0.533 % respectively at 1500 days.

The specimens exposed to a relative humidity of 0-5 % at both temperatures of 23 ^{0}C and 95 ^{0}C exhibited weight loss because of the dry conditions. But those exposed to higher levels of humidity of 45 %, 60 %, 80 % and 98 %, showed a steady weight gain and continue to do so throughout the exposure time. The maximum moisture content was recorded for the specimen exposed to 98 % relative humidity at 95 ^{0}C at 1500 days at 0.397 %. The specimens exposed to various relative humidity levels at 23 ^{0}C recorded less weight gain compared to those exposed to relative humidity at 95 ^{0}C, emphasizing that the rate of diffusion increases with temperature.

The diffusion coefficients for the moisture absorption process at 23 ^{0}C, immersion in water and exposed to a condition of 23 ^{0}C and 98 % R.H are comparable as seen from table 5.22. Similarly, the diffusion coefficients for the absorption process from immersion in water

at 95 ^{0}C and exposed to a condition of 95 ^{0}C and 98 % R.H are also comparable. This is because the relative humidity environment at 98 % R.H is comparable to immersion in water.

Comparison between Approximated Models and Full Model

From table 5.22, it can be seen that the Long-term Approximation Fickian Model and the Full Fickian Model yield similar diffusion coefficients. The percentage difference between the values obtained from these two models ranges from 0.14% to 9.05% for specimens immersed in deionized water. Looking at the diffusion coefficients from the Short-term Approximation model we can see that there is a significant difference between the short-term diffusion coefficient values and those obtained from the other two models. The percentage difference between the values obtained from Short-term Approximation Fickian model and Full Fickian model ranges from 17.0% to 44.8% for specimens immersed in deionized water.

A similar trend can be noticed with the Langmuir Models as well (refer to tables 5.23, 5.24, and 5.25). Long-term Langmuir Approximation and Full Langmuir Model yield similar diffusion coefficients. The percentage difference between the values obtained from the Long-term Langmuir Approximation and the Full Langmuir Model ranges from 3.73 % to 22.3 % for specimens immersed in deionized water. The Langmuir short-term diffusion coefficients are larger than those from the other models whereas the Fickian short-term diffusion coefficients for immersion in water were smaller than the Long-term and Full diffusion coefficients. The diffusion coefficients for specimens immersed in water obtained from the Short-term Langmuir Approximation Model are more than two times than those obtained from the Full Langmuir Model. Fickian diffusion coefficients for relative humidity exposure followed the same trends as the Langmuir diffusion Model.

5.8.1 Comparison between Fickian and Langmuir Models

The most commonly used methodology for modeling moisture diffusion is Fickian Diffusion theory applied to single free phase diffusion. Fick's law is based on the hypothesis that the rate of transfer of a diffusing substance through unit area of a section is proportional to the concentration gradient measured normal to the section [12]. The Langmuir Model retains the assumption that the diffusion coefficient remains independent of water concentration as in the Fickian Model, but the water is considered to be in two phases, one free to diffuse and the other trapped and hence not free to move in the absorbing medium [13].

For specimens immersed in deionized water, the Fickian and Langmuir models yield similar diffusion coefficients (Refer to Tables 5.22 and 5.23). The diffusion coefficients obtained from the Long-term Approximation and Full Langmuir Models are slightly less than those from Long-term Approximation and Full Fickian Models. But for the Short-term Langmuir diffusion coefficients, the reverse is true i.e. the diffusion coefficients from the Short-term Langmuir Approximation Model are larger than their Fickian counterparts.

Langmuir diffusion models applied to moisture gain data for humidity exposure yielded higher diffusion coefficients compared to the diffusion coefficients obtained from Fickian diffusion Models applied to the same data (Refer to Tables 5.22, 5.24, and 5.25).

5.8.2 Comparison with previously published data

The diffusion coefficients obtained are in close agreement with those reported by earlier researchers. Ghorbel and Valentin [1] investigated the effect of aging by immersion in water at 60 ^{0}C on polyester and vinylester resins and reinforced with glass fibers. They

reported a diffusion coefficient of 2.78 x 10^{-8} mm^2/sec for E-glass Vinylester composites immersed in water at 60 ^{0}C. The composites reported a higher maximum moisture uptake of 1.489 %. Vinylester specimens showed a maximum moisture uptake of 0.71 % and a diffusion coefficient of 8.47 x 10^{-5} mm^2/sec.

Springer et al [4] investigated the effects of humid air at 100% relative humidity (equivalent to immersion in water) at 23 ^{0}C and 93 ^{0}C on E-glass vinylester composites. They reported higher diffusion coefficients (compared to the present research) of 5 x 10^{-5} mm^2/sec and 5 x 10^{-4} mm^2/sec at 23 ^{0}C and 93 ^{0}C respectively. The maximum moisture uptakes were 0.63 %and 0.40 % at 23 ^{0}C and 93 ^{0}C respectively.

Chin et al [5] reported diffusion coefficient values of 6.88 x 10^{-7} mm^2/sec and 1.9 x 10^{-6} mm^2/sec for vinylester resins subjected to immersion in water at 22 ^{0}C and 60 ^{0}C respectively.

Chu et al [6] reported similar values of diffusion coefficients and maximum moisture contents for E-glass/vinylester composite specimens immersed in deionized water. The values are listed in Table 5.28. Karbhari and Zhang [7] reported diffusion coefficients of 4.5 x 10^{-7} mm^2/sec and 7.6 x 10^{-7} mm^2/sec for specimens subjected to immersion in deionized water at 23 ^{0}C and 60 ^{0}C respectively. The corresponding maximum moisture uptakes reported are 0.16 % and 0.25 % at 23 ^{0}C and 60 ^{0}C respectively. A list of diffusion coefficients reported for E-glass/Vinylester composites exposed to similar conditions are compiled in Table 5.26.

Table 5.26 Comparison of diffusion coefficients with previously published data

Source	Material Tested	Exposure Conditions	Diffusion Coefficient (mm^2/sec)	Maximum Moisture Content (%)
Chin et al. (1998) [5]	Epoxy	Distilled Water (22 ^{0}C)	0.59 x 10^{-7}	1.42
		Distilled Water (60 ^{0}C)	13.6 x 10^{-7}	2.00
	Vinylester	Distilled Water (22 ^{0}C)	6.88 x 10^{-7}	0.52
		Distilled Water (60 ^{0}C)	19.0 x 10^{-7}	0.62
	Iso-polyester	Distilled Water (22 ^{0}C)	8.93 x 10^{-7}	0.56
		Distilled Water (60 ^{0}C)	41.9 x 10^{-7}	0.50
Chu et al (2004) [6]	E-glass/Vinylester	Immersion in Alkali (23 ^{0}C)	2.17 x 10^{-7}	0.298
		Immersion in Alkali (40 ^{0}C)	3.26 x 10^{-7}	1.426
		Immersion in Alkali (60 ^{0}C)	4.42 x 10^{-7}	1.929
		Immersion in Alkali (80 ^{0}C)	5.95 x 10^{-7}	4.205
		Immersion in deionized water (23^{0}C)	1.39 x 10^{-7}	0.164
		Immersion in deionized water (40^{0}C)	2.17 x 10^{-7}	0.529
		Immersion in deionized water (60^{0}C)	2.70 x 10^{-7}	0.569
		Immersion in deionized water (80^{0}C)	3.14 x 10^{-7}	0.623

Table 5.26 contd.

Ghorbel and Valentin (1993)[1]	Polyester	Immersion in Water (60 ^{0}C)	2.29 x 10^{-5}	0.42
	Vinylester		8.47 x 10^{-5}	0.71
	E-glass/Polyester		9.44 x 10^{-7}	0.666
	E-glass/Vinylester		2.48 x 10^{-8}	1.489
Harper and Naeem (1989)[8]	411-45 (E-glass/Vinylester)	Immersion in Water (23 ^{0}C)	6.76 x 10^{-7}	0.279
		Immersion in Water (60 ^{0}C)	1.145 x 10^{-7}	0.433
		Relative Humidity 95 % (23 ^{0}C)	5.292 x 10^{-7}	0.262
		Relative Humidity 95 % (60 ^{0}C)	7.854 x 10^{-7}	0.477
	470-36 (E-glass/Vinylester)	Immersion in Water (23 ^{0}C)	4.001 x 10^{-7}	0.366
		Immersion in Water (60 ^{0}C)	9.258 x 10^{-7}	0.563
		Relative Humidity 95 % (23 ^{0}C)	3.981 x 10^{-7}	0.327
		Relative Humidity 95 % (60 ^{0}C)	9.044 x 10^{-7}	0.644
	272 (E-glass/Polyester)	Immersion in Water (23 ^{0}C)	6.749 x 10^{-7}	0.417
		Immersion in Water (60 ^{0}C)	9.993 x 10^{-7}	0.644
		Relative Humidity 95 % (23 ^{0}C)	6.218 x 10^{-7}	0.359
		Relative Humidity 95 % (60 ^{0}C)	9.258 x 10^{-7}	0.570

Table 5.26 contd.

Loos and Springer (1980) [9]	E-glass/Polyester (SMC-25)	Humid Air, 100% R.H, 32 ^{0}C	8.1 x 10^{-5}	3.25
		Humid Air, 100% R.H, 50 ^{0}C	20 x 10^{-5}	3.75
		Humid Air, 100% R.H, 65 ^{0}C	14 x 10^{-5}	3.40
		Humid Air, 60% R.H, 65 ^{0}C	40 x 10^{-5}	0.50
		Humid Air, 40% R.H, 65 ^{0}C	82 x 10^{-5}	0.35
		Distilled Water, 23 ^{0}C	12 x 10^{-5}	3.60
	E-glass/Polyester (SMC-65)	Humid Air, 100% R.H, 32 ^{0}C	3.1 x 10^{-5}	3.60
		Humid Air, 100% R.H, 50 ^{0}C	4.0 x 10^{-5}	4.00
		Humid Air, 100% R.H, 65 ^{0}C	7.4 x 10^{-5}	3.50
		Humid Air, 60% R.H, 65 ^{0}C	9.3 x 10^{-5}	1.25
		Humid Air, 40% R.H, 65 ^{0}C	15.0 x 10^{-5}	0.65
		Distilled Water, 23 ^{0}C	1.1 x 10^{-5}	3.50
	E-glass/Polyester (SMC-30 EA)	Humid Air, 100% R.H, 32 ^{0}C	1.0 x 10^{-5}	3.00
		Humid Air, 100% R.H, 50 ^{0}C	2.9 x 10^{-5}	3.00
		Humid Air, 100% R.H, 65 ^{0}C	8.3 x 10^{-5}	2.75
		Humid Air, 60% R.H, 65 ^{0}C	50 x 10^{-5}	0.45
		Humid Air, 40% R.H, 65 ^{0}C	160 x 10^{-5}	0.25
		Distilled Water, 23 ^{0}C	0.85 x 10^{-5}	2.95
Marshal et al. (1982) [10]	Vinylester Resin (411-45)	Distilled Water, 20 ^{0}C	2.03 x 10^{-6}	-
		Distilled Water, 50 ^{0}C	9.23 x 10^{-6}	-
	E-glass/Vinylester (411-45)	Distilled Water, 20 ^{0}C	3.40 x 10^{-6}	-
		Distilled Water, 50 ^{0}C	1.49 x 10^{-5}	-

Table 5.26 contd.

Springer et al. (1980)[4]	SMC –R25 (E-glass/Polyester)	Humid air 50 % (23 ^{0}C)	10 x 10^{-5}	0.17
		Humid air 50 % (93 ^{0}C)	50 x 10^{-5}	0.10
		Humid air 100 % (23 ^{0}C)	10 x 10^{-5}	1.00
		Humid air 100 % (93 ^{0}C)	50 x 10^{-5}	0.30
	SMC –R50 (E-glass/Polyester)	Humid air 50 % (23 ^{0}C)	30 x 10^{-5}	0.10
		Humid air 50 % (93 ^{0}C)	30 x 10^{-5}	0.22
		Humid air 100 % (23 ^{0}C)	9 x 10^{-5}	1.35
		Humid air 100 % (93 ^{0}C)	50 x 10^{-5}	0.56
	VE SMC –R50 (E-glass/Vinylester)	Humid air 50 % (23 ^{0}C)	10 x 10^{-5}	0.13
		Humid air 50 % (93 ^{0}C)	50 x 10^{-5}	0.10
		Humid air 100 % (23 ^{0}C)	5 x 10^{-5}	0.63
		Humid air 100 % (93 ^{0}C)	50 x 10^{-5}	0.40
Zhang and Karbhari (2003)[7]	Neat Resin (Vinylester)	Deionized Water (23 ^{0}C)	7.90 x 10^{-7}	0.37
		Deionized Water (60 ^{0}C)	11.5 x 10^{-7}	0.65
	E-glass/Vinylester (Uniaxial- UM2403)	Deionized Water (23 ^{0}C)	4.50 x 10^{-7}	0.16
		Deionized Water (60 ^{0}C)	7.60 x 10^{-7}	0.25
	E-glass/Vinylester (Biaxial- CM5005)	Deionized Water (23 ^{0}C)	4.70 x 10^{-7}	0.19
		Deionized Water (60 ^{0}C)	8.00 x 10^{-7}	0.31
	E-glass/Vinylester (Triaxial-TWM3408)	Deionized Water (23 ^{0}C)	4.80 x 10^{-7}	0.32
		Deionized Water (60 ^{0}C)	8.50 x 10^{-7}	0.50

5.9 Diffusion Coefficients

The diffusion coefficients are related to the maximum moisture content levels. The max moisture contents are set to the highest recorded levels for each exposure environments and the change in diffusion coefficients are examined in the following sections.

5.9.1 Comparison I

In this section, for each of the exposure conditions, the maximum moisture contents are set to values obtained for the harshest environment experimentally. The diffusion coefficients (both Fickian and Langmuir models) so obtained are listed in table 5.27.

5.9.2 Comparison II

In this section, for each humidity exposure at temperatures 23 ^{o}C and 95 ^{o}C, the maximum moisture content is set to values obtained for the specimens exposed to immersion in water at the corresponding temperatures. The diffusion coefficients (both Fickian and Langmuir models) so obtained are listed in table 5.28.

5.9.3 Comparison III

In this section, for each of the exposure conditions, the maximum moisture content is set to 0.728 %, which is the maximum moisture content obtained for the specimens exposed to immersion in water at 95 ^{o}C. The diffusion coefficients (both Fickian and Langmuir models) so obtained are listed in table 5.29.

Table 5.27 Diffusion Coefficients - Comparison I

Immersion in water (Fickian)					Immersion in water (Langmuir)				
Temperature ^{0}C	M_m = max for each temperature		$M_m = M_m$ at 95 ^{0}C		Temperature ^{0}C	M_m = max for each temperature		$M_m = M_m$ at 95 ^{0}C	
	M_m (%)	D (mm^2/sec)	M_m (%)	D (mm^2/sec)		M_m (%)	D (mm^2/sec)	M_m (%)	D (mm^2/sec)
23	0.405	7.229×10^{-8}	0.728	2.239×10^{-8}	23	0.405	3.481×10^{-7}	0.728	1.079×10^{-7}
40	0.438	7.542×10^{-8}	0.728	2.731×10^{-8}	40	0.438	3.568×10^{-7}	0.728	1.291×10^{-7}
60	0.533	9.667×10^{-8}	0.728	5.181×10^{-8}	60	0.533	4.640×10^{-7}	0.728	2.487×10^{-7}
80	0.624	1.187×10^{-7}	0.728	8.727×10^{-8}	80	0.624	6.534×10^{-7}	0.728	4.801×10^{-7}
95	0.728	1.391×10^{-7}	0.728	1.391×10^{-7}	95	0.728	2.219×10^{-6}	0.728	2.219×10^{-6}
Humidity 23 ^{0}C(Fickian)					Humidity 23 ^{0}C (Langmuir)				
Humidity %	M_m = max for each temperature		$M_m = M_m$ at 23 ^{0}C & 98% RH		Humidity %	M_m = max for each temperature		$M_m = M_m$ at 23 ^{0}C & 98% RH	
	M_m (%)	D (mm^2/sec)	M_m (%)	D (mm^2/sec)		M_m (%)	D (mm^2/sec)	M_m (%)	D (mm^2/sec)
45	0.164	2.098×10^{-8}	0.329	5.212×10^{-9}	45	0.164	7.439×10^{-8}	0.329	1.849×10^{-8}
60	0.215	5.387×10^{-8}	0.329	2.301×10^{-8}	60	0.215	2.160×10^{-7}	0.329	9.204×10^{-8}
75	0.253	7.368×10^{-8}	0.329	4.358×10^{-8}	75	0.253	2.760×10^{-7}	0.329	1.631×10^{-7}
95	0.329	7.138×10^{-8}	0.329	7.138×10^{-8}	95	0.329	3.030×10^{-7}	0.329	3.030×10^{-7}
Humidity 95 ^{0}C (Fickian)					Humidity 95^{0}C (Langmuir)				
Humidity %	M_m = max for each temperature		$M_m = M_m$ at 95 ^{0}C & 98% RH		Humidity %	M_m = max for each temperature		$M_m = M_m$ at 95 ^{0}C & 98% RH	
	M_m (%)	D (mm^2/sec)	M_m (%)	D (mm^2/sec)		M_m (%)	D (mm^2/sec)	M_m (%)	D (mm^2/sec)
45	0.203	2.189×10^{-8}	0.397	5.723×10^{-9}	45	0.203	8.190×10^{-8}	0.397	2.141×10^{-8}
60	0.241	1.937×10^{-8}	0.397	1.912×10^{-8}	60	0.241	1.940×10^{-7}	0.397	7.152×10^{-8}
75	0.293	8.194×10^{-8}	0.397	4.446×10^{-8}	75	0.293	3.260×10^{-7}	0.397	1.774×10^{-7}
95	0.397	1.133×10^{-7}	0.397	1.133×10^{-7}	95	0.397	4.950×10^{-7}	0.397	4.948×10^{-7}

Table 5.28 Diffusion Coefficients - Comparison II

Humidity 23 ^{0}C (Fickian)					Humidity 23 ^{0}C (Langmuir)				
Humidity %	M_m = max for each temperature		M_m = M_m at 23 ^{0}C & 100 % RH		Humidity %	M_m = max for each temperature		M_m = M_m at 23 ^{0}C & 100% RH	
	M_m (%)	D (mm^2/sec)	M_m (%)	D (mm^2/sec)		M_m (%)	D (mm^2/sec)	M_m (%)	D (mm^2/sec)
45	0.164	2.098×10^{-8}	0.405	3.440×10^{-9}	45	0.164	7.439×10^{-8}	0.405	1.220×10^{-8}
60	0.215	5.387×10^{-8}	0.405	1.518×10^{-8}	60	0.215	2.160×10^{-7}	0.405	6.074×10^{-8}
75	0.253	7.368×10^{-8}	0.405	2.876×10^{-8}	75	0.253	2.760×10^{-7}	0.405	1.076×10^{-7}
95	0.329	7.138×10^{-8}	0.405	4.711×10^{-8}	95	0.329	3.030×10^{-7}	0.405	2.000×10^{-7}
Humidity 95 ^{0}C (Fickian)					Humidity 95^{0}C (Langmuir)				
Humidity %	M_m = max for each temperature		M_m = M_m at 95 ^{0}C & 100 % RH		Humidity %	M_m = max for each temperature		M_m = M_m at 95 ^{0}C & 100% RH	
	M_m (%)	D (mm^2/sec)	M_m (%)	D (mm^2/sec)		M_m (%)	D (mm^2/sec)	M_m (%)	D (mm^2/sec)
45	0.203	2.189×10^{-8}	0.728	1.702×10^{-9}	45	0.203	8.190×10^{-8}	0.728	6.368×10^{-9}
60	0.241	1.937×10^{-8}	0.728	5.685×10^{-9}	60	0.241	1.940×10^{-7}	0.728	2.127×10^{-8}
75	0.293	8.194×10^{-8}	0.728	1.322×10^{-8}	75	0.293	3.260×10^{-7}	0.728	5.277×10^{-8}
95	0.397	1.133×10^{-7}	0.728	3.370×10^{-8}	95	0.397	4.950×10^{-7}	0.728	1.472×10^{-7}

Table 5.29 Diffusion Coefficients - Comparison III

Immersion in water (Fickian)					Immersion in water (Langmuir)				
Temperature ^{0}C	M_m = max for each temperature		$M_m = M_m$ at 95 ^{0}C		Temperature ^{0}C	M_m = max for each temperature		$M_m = M_m$ at 95 ^{0}C	
	M_m (%)	D (mm^2/sec)	M_m (%)	D (mm^2/sec)		M_m (%)	D (mm^2/sec)	M_m (%)	D (mm^2/sec)
23	0.405	7.229×10^{-8}	0.728	2.239×10^{-8}	23	0.405	3.481×10^{-7}	0.728	1.079×10^{-7}
40	0.438	7.542×10^{-8}	0.728	2.731×10^{-8}	40	0.438	3.568×10^{-7}	0.728	1.291×10^{-7}
60	0.533	9.667×10^{-8}	0.728	5.181×10^{-8}	60	0.533	4.640×10^{-7}	0.728	2.487×10^{-7}
80	0.624	1.187×10^{-7}	0.728	8.727×10^{-8}	80	0.624	6.534×10^{-7}	0.728	4.801×10^{-7}
95	0.728	1.391×10^{-7}	0.728	1.391×10^{-7}	95	0.728	2.219×10^{-6}	0.728	2.219×10^{-6}
Humidity 23 ^{0}C (Fickian)					Humidity 23 ^{0}C (Langmuir)				
Humidity %	M_m = max for each temperature		$M_m = M_m$ at 95 ^{0}C & 100 % RH		Humidity %	M_m = max for each temperature		$M_m = M_m$ at 95 ^{0}C &100 % RH	
	M_m (%)	D (mm^2/sec)	M_m (%)	D (mm^2/sec)		M_m (%)	D (mm^2/sec)	M_m (%)	D (mm^2/sec)
45	0.164	2.098×10^{-8}	0.728	1.065×10^{-9}	45	0.164	7.439×10^{-8}	0.728	3.776×10^{-9}
60	0.215	5.387×10^{-8}	0.728	4.699×10^{-9}	60	0.215	2.160×10^{-7}	0.728	1.880×10^{-8}
75	0.253	7.368×10^{-8}	0.728	8.901×10^{-9}	75	0.253	2.760×10^{-7}	0.728	3.330×10^{-8}
95	0.329	7.138×10^{-8}	0.728	1.458×10^{-8}	95	0.329	3.030×10^{-7}	0.728	6.189×10^{-8}
Humidity 95 ^{0}C (Fickian)					Humidity 95^{0}C (Langmuir)				
Humidity %	M_m = max for each temperature		$M_m = M_m$ at 95 ^{0}C & 100% RH		Humidity %	M_m = max for each temperature		$M_m = M_m$ at 95 ^{0}C & 100 % RH	
	M_m (%)	D (mm^2/sec)	M_m (%)	D (mm^2/sec)		M_m (%)	D (mm^2/sec)	M_m (%)	D (mm^2/sec)
45	0.203	2.189×10^{-8}	0.728	1.702×10^{-9}	45	0.203	8.190×10^{-8}	0.728	6.368×10^{-9}
60	0.241	1.937×10^{-8}	0.728	5.685×10^{-9}	60	0.241	1.940×10^{-7}	0.728	2.127×10^{-8}
75	0.293	8.194×10^{-8}	0.728	1.322×10^{-8}	75	0.293	3.260×10^{-7}	0.728	5.277×10^{-8}
95	0.397	1.133×10^{-7}	0.728	3.370×10^{-8}	95	0.397	4.950×10^{-7}	0.728	1.472×10^{-7}

5.10 Activation Energy

According to the Arrhenius life-stress relationship, the rate of a reaction is proportional to the stimulus (e.g. temperature) [11],

$$R(T) = Ae^{-\frac{E_a}{KT}} \qquad \text{(Equation 5.12)}$$

where R(T) is the rate of the reaction,

E_a is the Activation Energy,

T is the temperature,

A is an unknown thermal constant and

K is the Boltzmann's constant.

Activation energy is a measure of the effect that temperature has on the reaction. The diffusion coefficient for the moisture absorption process, is a function of temperature which follows the classical Arrhenius relationship,

$$D = D_0 \exp\left(-\frac{E_a}{RT}\right) \qquad \text{(Equation 5.13)}$$

where D is the diffusion coefficient,

D_0 is a constant,

E_a is the activation energy in J/mol ^{0}K,

R is the universal gas constant, 8.3144 Jmol^{-1} K^{-1}

T is the absolute temperature in Kelvin.

Taking natural logarithms on both sides, equation 5.13 becomes,

$$\ln(D) = \ln(D_0) - \frac{E_a}{RT} \qquad \text{(Equation 5.14)}$$

The natural logarithms of the diffusion coefficients are plotted against the inverse temperature to find the activation energy of the diffusion process. The plots are shown in figures 5.12 and 5.13. The plots show a linear relationship between the diffusion coefficients and the inverse of temperature thus showing the diffusion coefficient depends on temperature as demonstrated by Arrhenius equation 5.14. Figure 5.12 employs the diffusion coefficients obtained from the Fickian diffusion theory whereas Figure 5.13 uses the diffusion coefficients obtained from the Langmuir diffusion theory. The activation energies obtained from the two plots are different and are listed below in table 5.30.

Activation energy denotes the minimum energy required for a reaction to occur. In other words, it is a measure of energy barrier to be overcome for the diffusion process to occur. A high activation energy level indicates a strong energy barrier for the moisture diffusion process to take place and the converse is also true. The value of activation energy obtained by plotting the Langmuir diffusion coefficients is 11.991 KJ/mol ^{0}K, which close to the value, reported by Karbhari and Zhang [7], of 11.719 KJ/mol ^{0}K for unidirectional E-glass/411-350 vinylester composite. Harper and Naeem [8] reported activation energy values of 12.618 KJ/mol ^{0}K and 17.160 KJ/mol ^{0}K for Eglass/411-45 vinylester and E-glass/470-36 vinylester respectively. Chu et al. [6] reported activation energy values of 12.141 KJ/mol ^{0}K and 15.147 KJ/mol ^{0}K for E-glass/441-400 Vinylester composites immersed in deionized water and alkaline solution respectively.

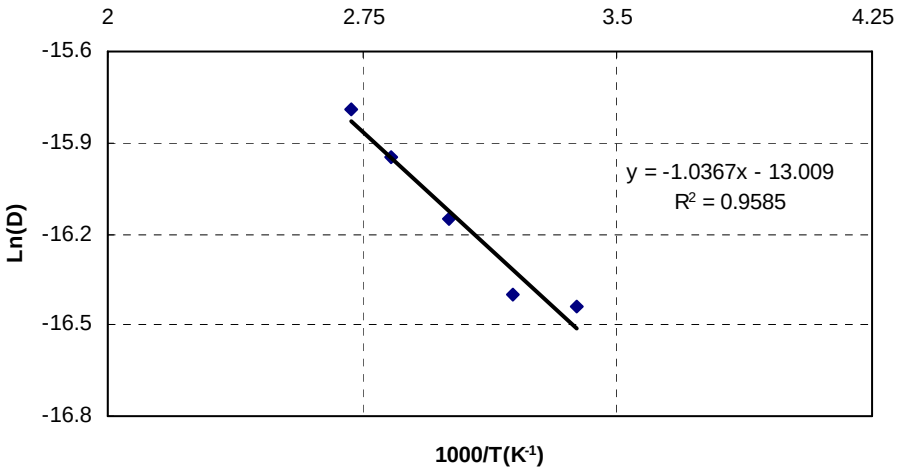

Fig.5.12 Activation energy for specimens immersed in deionized water –Fickian diffusion model

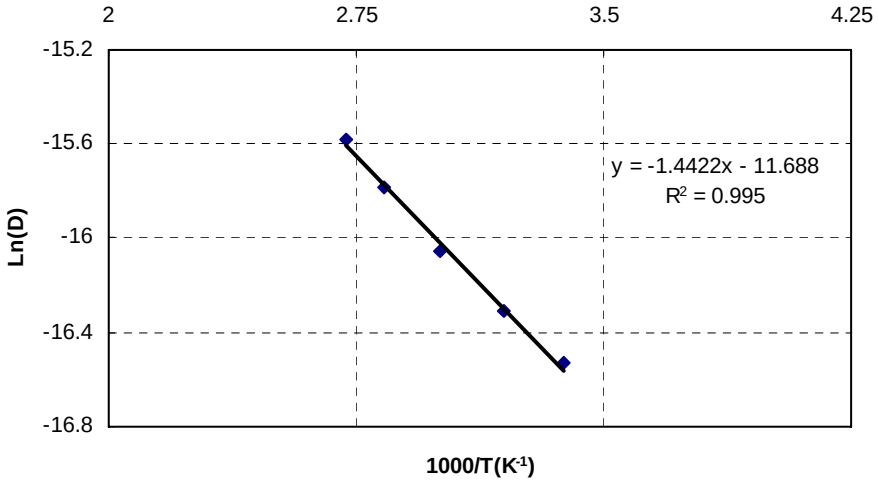

Fig. 5.13 Activation energy for specimens immersed in deionized water -Langmuir Diffusion Model

Table 5.30 Activation Energy (Immersion in Water)

Diffusion Theory	Value of Activation Energy (KJ/mol ^{0}K)
Fickian	8.619
Langmuir	11.991

Diffusion coefficients obtained for the relative humidity exposure were also plotted as shown in figures 5.14 to 5.18. Diffusion coefficient values obtained for each of the relative humidities, at temperatures of 23 ^{0}C and 95 ^{0}C are plotted in figures 5.14 to 5.18. The activation energies thus calculated are tabulated in table 5.31. The Diffusion coefficients utilized in figures 5.14 to 5.18 were obtained from Langmuir diffusion theory.

The activation energy value obtained for 98 % relative humidity (11.072 KJ/mol ^{0}K) is similar to that reported by Harper and Naeem [8] of 10.104 KJ/mol ^{0}K for E-glass/ 411-45 vinylester composite exposed to 95 % relative humidity at various temperatures.

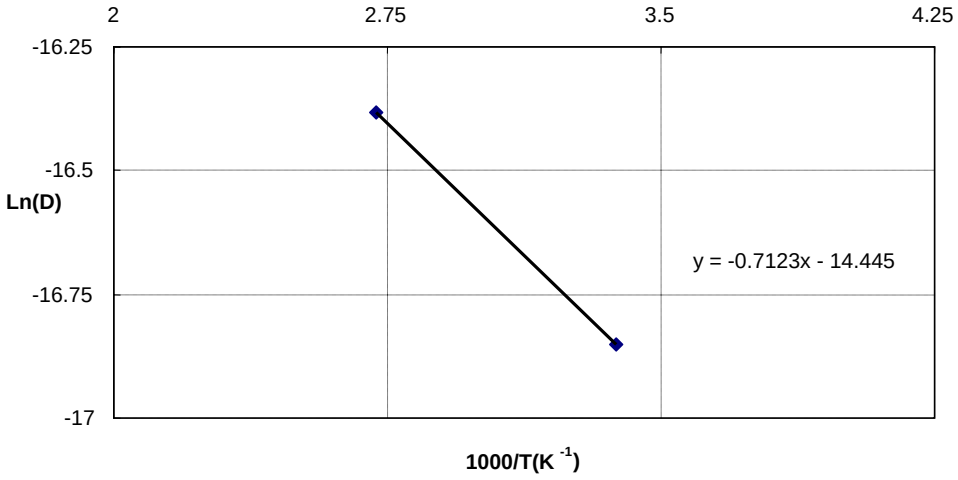

Fig. 5.14 Activation Energy (Relative Humidity 0-5%)

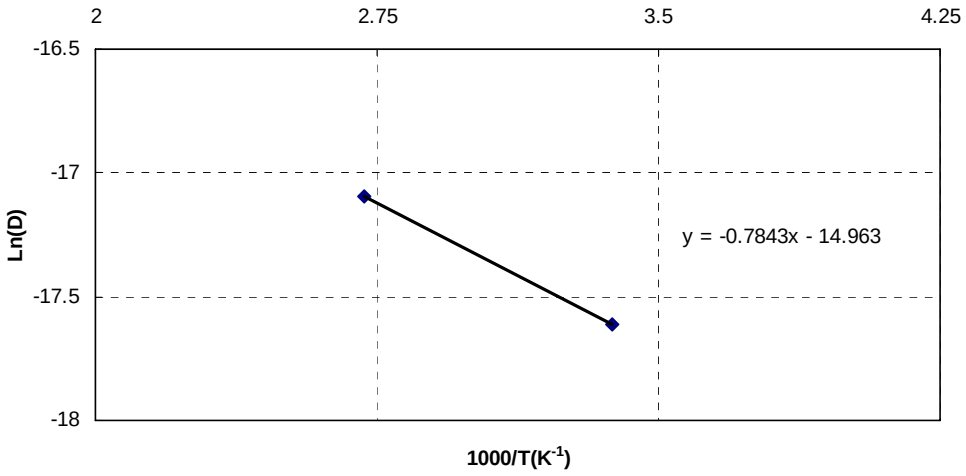

Fig. 5.15 Activation Energy (Relative Humidity 45%)

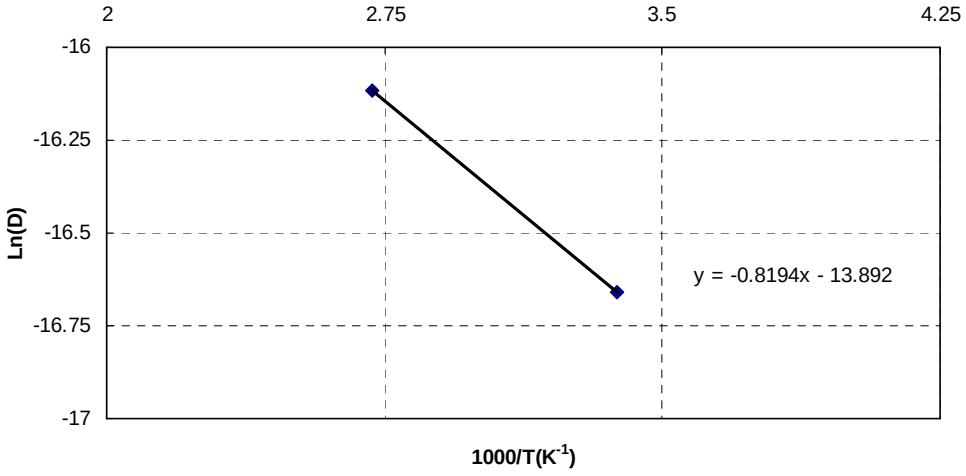

Fig. 5.16 Activation Energy (Relative Humidity 60%)

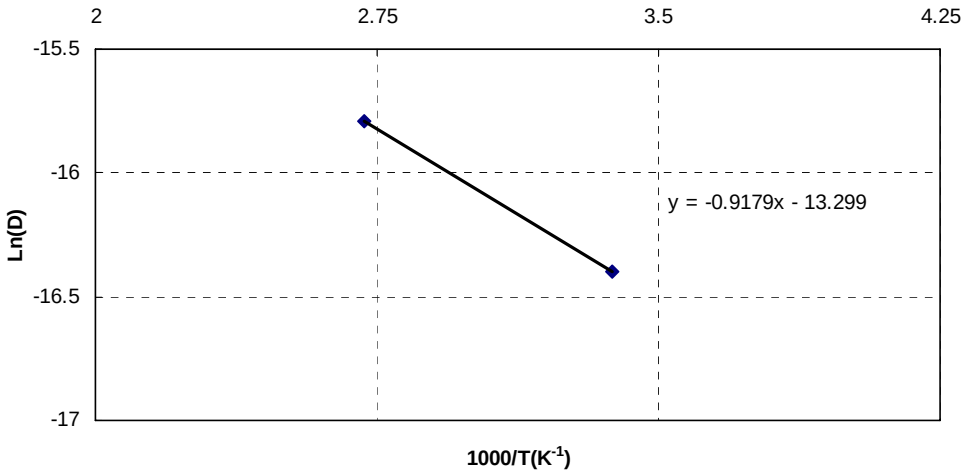

Fig. 5.17 Activation Energy (Relative Humidity 75%)

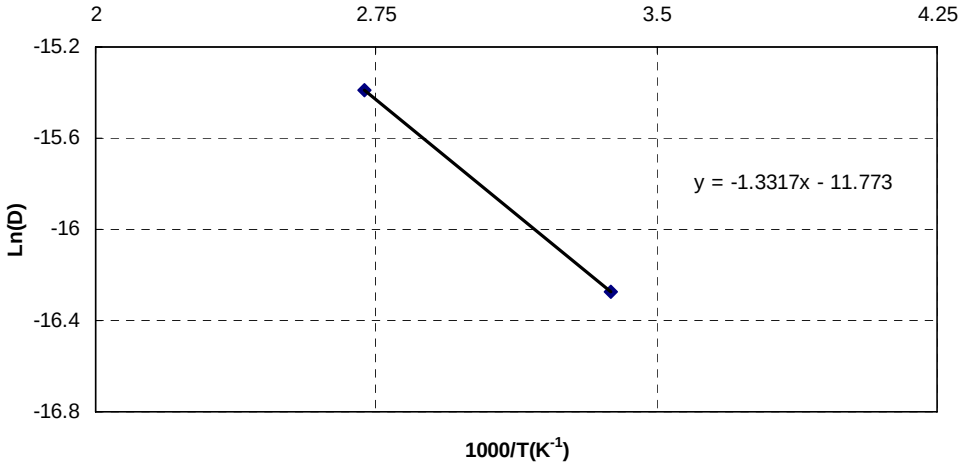

Fig. 5.18 Activation Energy (Relative Humidity 98%)

Table 5.31 Activation Energy (Relative Humidity Exposure)

Relative Humidity (%)	Value of Activation Energy (KJ/mol ^{0}K)
0-5	5.922
45	6.520
60	6.813
75	7.631
98	11.072

5.11 References

1. Ghorbel I. and Valentin D., "Hydrothermal Effects on the Physico-Chemical Properties of Pure and Glass Fiber Reinforced Polyester and Vinylester Resins", *Polymer Composites*, 1993, Vol. 14, Issue 4, pp. 324-334.

2. Shen C. and Springer G.S., "Moisture Absorption and Desorption of Composite Materials", Environmental effects on Composite Materials, 1988, Ed., Springer G.S., Vol. 3, pp. 15-34.

3. Carter H.G. and Kibler K.G., "Langmuir Type Model for Anomalous Moisture Diffusion in Composite Resins", *Journal of Composite Materials*, 1978, Vol.12, pp. 118-131.

4. Springer G.S., Sanders B.A. and Tung R.W., "Environmental Effects on Glass Fiber Reinforced Polyester and Vinylester Composites", *Journal of Composite Materials*, July 1980, Vol. 14, pp. 213-232.

5. Chin J.W., Nguyen T., Aouadi K., "Sorption and Diffusion of Water, Salt Water and Concrete Pore Solution in Composite Matrices", *Journal of Applied Polymer Science*, 1999, Vol. 71, pp. 483-492.

6. Karbhari V.M., Chu W. and Wu L., "Durability Evaluation of Moderate Temperature Cured E-glass/Vinylester Systems" *Composite Structures*, December 2004, Vol. 66, Issue 1-4, pp. 367-376.

7. Karbhari V.M. and Zhang S., "E-glass Vinylester composites in Aqueous Environments-I: Experimental Results", *Applied Composite Materials,* January 2003, Vol. 10, Issue 1, pp. 19-48.

8. Harper J.F. and Naeem M., "The Moisture Absorption of Glass Fiber Reinforced Vinylester and Polyester Composites", *Materials and Design*, December 1989, Vol. 10, Issue 6, pp. 297-300.

9. Loos A.C, and Springer G.S., "Moisture Absorption of Graphite-Epoxy Composites Immersed in Liquids and in Humid Air", *Journal of Composite Materials*, April 1979, Vol. 13, pp. 131-145.

10. Marshall J.P., Marshall G.P. and Pinzelli R.F., "The Diffusion of Liquids into Resins and Composites", *Polymer Composites*, July 1982, Vol. 3, Issue 3, pp. 131-137.

11. Reliasoft Corporation Website, www.reliasoft.com

12. Bunsell A.R. and Dewimille B., "The Modeling of Hydrothermal Aging in Glass Fiber-Reinforced Epoxy Composites", *Applied Physics Journal*, 1982, Vol. 15, pp. 2079-2091.

13. Crank J. and Park G.S., Diffusion in Polymers, Academic Press, New York, 1968.

Chapter 6

Correlation between Tension and Flexure Results

6.1 Introduction

The characterization of materials for purposes of specification and assessment of durability can be a time-consuming and expensive process. Hence there is substantial impetus to either develop unique tests that can yield multiple performance attributes or to develop analytical approaches that would enable use of data from a series of tests aimed at characterizing one metric of performance that can be used for the prediction of other metrics.

Tensile strength data is a significant criterion in materials selection and preliminary design of composite laminates and hence the tensile test is routinely performed. Although flexural tests are easier to conduct, tensile strength data generated from flexure data yield higher strength values than that observed from a standard tensile coupon [1] and hence flexure tests are not considered useful for design purposes. The ultimate strength measured in bending tests is often 30 % to 100 % higher than the strength measured from pure tension [2]. According to the statistical strength theory based on Weibull distribution, the presence of a stress gradient in the flexure tests leads to an increase in the tensile strength as compared to the tensile test under uniform stress. The establishment of a correlation between the simpler flexure test and the tensile test would provide a basis for the use of flexure test data for design purposes [1].

This chapter aims at correlating data from a 3-point flexure test and a standard tensile coupon test for the material in consideration – unidirectional E-glass/vinylester composites. A

two parameter Weibull distribution model was used to generate theoretical results and the results are compared with the experimental data for tensile and flexural strength.

6.2 Weibull Statistical Strength Model

According to the Weibull theory, the probability that a specimen containing a distribution of flaws throughout its volume can survive the application of a stress distribution σ (x,y,z) is given by [3],

$$P(S) = \exp\left\{-\int_V \left[\frac{\sigma(x,y,z) - \sigma_u}{S_0}\right]^{\alpha}\right\} dxdydz \quad \text{(Equation 6.1)}$$

where P(S) is the probability of survival, α is the flaw-density exponent that determines the scatter of the strength for the material (also known as the shape parameter) and is related to the relative variance of the distribution, S_0 is the normalizing scale parameter that locates the strength distribution, σ_u is the threshold stress below which the material will never fail (usually taken as zero) and V is the volume of the specimen under stress.

For tensile tests where the stress is uniform throughout the specimen, and taking σ_u as zero, equation 6.1 takes the simpler form,

$$P(S_t) = \exp\left[-V_t\left(\frac{\sigma_t}{S_0}\right)^{\alpha}\right] \quad \text{(Equation 6.2)}$$

where the subscript t denotes tension and V_t is the volume of the tensile coupon used in the tensile tests. It has to be noted that the gage length of the coupon is used for the calculation of its volume.

For three-point bending flexure tests where the stress is non-uniform throughout the rectangular specimen, equation 6.1 can be written as,

$$P(S_f) = \exp\left[-V_f \left(\frac{\sigma_f}{S_0} \right)^{\alpha} \left(\frac{1}{2(\alpha+1)^2} \right) \right] \quad \text{(Equation 6.3)}$$

where the subscript f denotes flexure, V_f is the volume of the specimen used in the flexure tests and the factor $\frac{1}{2(\alpha+1)^2}$ is used to account for the non-uniform stress distribution. The length of the specimen between the supports is used for the calculation of the volume of the flexural specimen. The ratio of the median failure stress in three-point flexure to that in tension is obtained from equations 6.2 and 6.3, by setting $P(S_t) = P(S_f)$, such that,

$$\frac{\sigma_f}{\sigma_t} = \left[2(\alpha+1)^2 \frac{V_t}{V_f} \right]^{\frac{1}{\alpha}} \quad \text{(Equation 6.4)}$$

The shape parameter, α, can be correlated to the coefficient of variation (COV) as follows [4],

$$COV = \left\{ \frac{\Gamma\left(1+\frac{2}{\alpha}\right)}{\Gamma^2\left(2+\frac{1}{\alpha}\right)} - 1 \right\}^{0.5} \quad \text{(Equation 6.5)}$$

where Γ represents the gamma function.

Equation 6.5 can be further approximated and two different approximations are often used to express the relationship between the shape parameter and COV with a high degree of accuracy, as follows,

$$\text{COV} \approx \alpha^{-0.926} \quad \text{(Equation 6.6)}$$

$$\text{COV} \approx \frac{1.2}{\alpha} \qquad \text{(Equation 6.7)}$$

The relationship between the scale parameter and shape parameter can be expressed as follows,

$$\mu = S_0 \Gamma\left(1 + \frac{1}{\alpha}\right) \qquad \text{(Equation 6.8)}$$

where μ is the mean value of the data set.

6.3 Prediction of Flexural Strength from Tensile Tests

As a first step of this procedure, the Weibull parameters for each of the tensile test data sets are evaluated. For purposes of this investigation, equation 6.7 is used to determine the shape parameter, using the coefficient of variation for each data set. The average of the shape parameters for each exposure condition is then determined. The values of the shape parameter and the tensile strength are then substituted in equation 6.4 to evaluate the values of flexural strength at each time step for each of the exposure conditions.

Table 6.1 lists the values of shape parameters calculated from the tensile test data, for each of the exposure environments. Tables 6.2 through 6.7 show the values of flexural strength determined from the tensile strength data as described by the procedure above. Figure 6.1 compares the predicted and the experimental flexural strength values graphically.

Table 6.1 Values of shape parameters for the different exposure conditions calculated from tensile tests

Exposure Condition	Shape Parameter
Air at 23°C	19.43
Immersion in Water at 23°C	21.37
Immersion in Water at 40°C	19.08
Immersion in Water at 60°C	13.66
Immersion in Water at 80°C	13.51
Immersion in Water at 95°C	15.69
Average value of shape parameter for specimens immersed in deionized water	16.62
Overall average value of shape parameter	17.12

The tables also depict the percentage error between the predicted and experimental values of flexural strength. The percentage error is calculated according to the following equation,

$$\%\ Error = \frac{\text{Predicted Value - Experimental Value}}{Experimental\ Value} x100 \qquad \text{(Equation 6.9)}$$

Table 6.2 Values of flexural strength predicted from tensile tests of composite specimens exposed to air at 23^0C

Time(days)	Tensile Strength (MPa)	Predicted Flexural Strength (MPa)	Experimental Flexural Strength (MPa)	Std. Deviation (MPa)	Percentage error
0	684.65	1011.05	1106.89	60.19	-8.66
30	690.86	1020.21	1133.85	73.91	-10.02
90	740.50	1093.52	1094.55	61.64	-0.09
180	726.71	1073.16	1146.88	77.29	-6.43
270	755.67	1115.92	1135.23	72.81	-1.70
360	792.90	1170.91	1189.01	58.26	-1.52
540	782.56	1155.63	1151.16	48.54	0.39
720	809.45	1195.34	1162.05	39.09	2.86
1080	798.42	1179.05	1189.01	47.09	-0.84
1440	818.41	1208.58	1168.25	36.06	3.45

Table 6.3 Values of flexural strength predicted from tensile tests of composite specimens immersed in deionized water at 23^0C

Time(days)	Tensile Strength (MPa)	Predicted Flexural Strength (MPa)	Experimental Flexural Strength (MPa)	Std. Deviation (MPa)	Percentage error
0	684.65	984.22	1106.89	60.19	-11.08
30	686.03	986.20	1126.96	83.91	-12.49
90	686.65	987.09	1104.96	31.17	-10.67
180	675.69	971.33	1086.83	57.16	-10.63
270	689.41	991.06	1064.83	72.26	-6.93
360	642.94	924.25	1036.70	24.55	-10.85
540	617.64	887.88	1001.68	40.89	-11.36
720	575.37	827.12	928.25	71.98	-10.89
1080	550.34	791.14	901.29	60.12	-12.22
1440	515.94	741.68	775.94	66.05	-4.42

Table 6.4 Values of flexural strength predicted from tensile tests of composite specimens immersed in deionized water at 40^0C

Time(days)	Tensile Strength (MPa)	Predicted Flexural Strength (MPa)	Experimental Flexural Strength (MPa)	Std. Deviation (MPa)	Percentage error
0	684.65	1016.46	1106.89	60.19	-8.17
30	686.79	1019.64	1092.34	13.65	-6.66
90	534.83	794.03	772.08	80.47	2.84
180	511.32	759.12	748.36	65.78	1.44
270	525.18	779.70	726.92	43.09	7.26
360	467.12	693.51	744.22	51.37	-6.81
540	394.18	585.21	591.44	42.68	-1.05
720	362.60	538.33	541.45	85.84	-0.58
1080	326.61	484.89	443.47	40.89	9.34
1440	291.17	432.28	417.41	52.81	3.56

Table 6.5 Values of flexural strength predicted from tensile tests of composite specimens immersed in deionized water at 60^0C

Time(days)	Tensile Strength (MPa)	Predicted Flexural Strength (MPa)	Experimental Flexural Strength (MPa)	Std. Deviation (MPa)	Percentage error
0	684.65	1135.49	1106.89	60.19	2.58
30	469.67	778.95	913.01	59.50	-14.68
90	406.45	674.09	670.86	62.40	0.48
180	397.83	659.80	556.07	89.29	18.65
270	326.81	542.02	512.42	70.46	5.78
360	311.58	516.75	471.81	45.09	9.52
540	309.02	512.51	409.83	38.27	25.06
720	301.79	500.51	377.97	19.58	32.42
1080	279.31	463.23	341.71	67.29	35.56
1440	262.90	436.01	308.75	45.44	41.22

Table 6.6 Values of flexural strength predicted from tensile tests of composite specimens immersed in deionized water at 80^0C

Time(days)	Tensile Strength (MPa)	Predicted Flexural Strength (MPa)	Experimental Flexural Strength (MPa)	Std. Deviation (MPa)	Percentage error
0	684.65	1140.15	1106.89	60.19	3.00
30	277.52	462.15	526.21	70.46	-12.17
90	272.97	454.57	423.96	77.29	7.22
180	258.35	430.23	402.93	66.67	6.77
270	255.18	424.94	381.21	38.89	11.47
360	251.04	418.05	369.84	50.13	13.04
540	241.80	402.67	336.40	3.93	19.70
720	232.91	387.86	307.23	20.27	26.24
1080	215.39	358.69	285.93	38.82	25.45
1440	197.12	328.27	279.86	60.12	17.30

Table 6.7 Values of flexural strength predicted from tensile tests of composite specimens immersed in deionized water at 95^0C

Time(days)	Tensile Strength (MPa)	Predicted Flexural Strength (MPa)	Experimental Flexural Strength (MPa)	Std. Deviation (MPa)	Percentage error
0	684.65	1081.27	1106.89	60.19	-2.31
30	263.59	416.29	459.12	47.37	-9.33
90	233.04	368.05	426.86	51.50	-13.78
180	231.87	366.20	373.84	71.29	-2.04
270	229.32	362.17	347.29	49.71	4.28
360	210.77	332.88	314.95	56.47	5.69
540	204.43	322.86	260.35	8.48	24.01
720	195.47	308.70	251.32	23.58	22.83
1080	182.16	287.69	240.42	30.06	19.66
1440	172.03	271.68	226.98		19.69

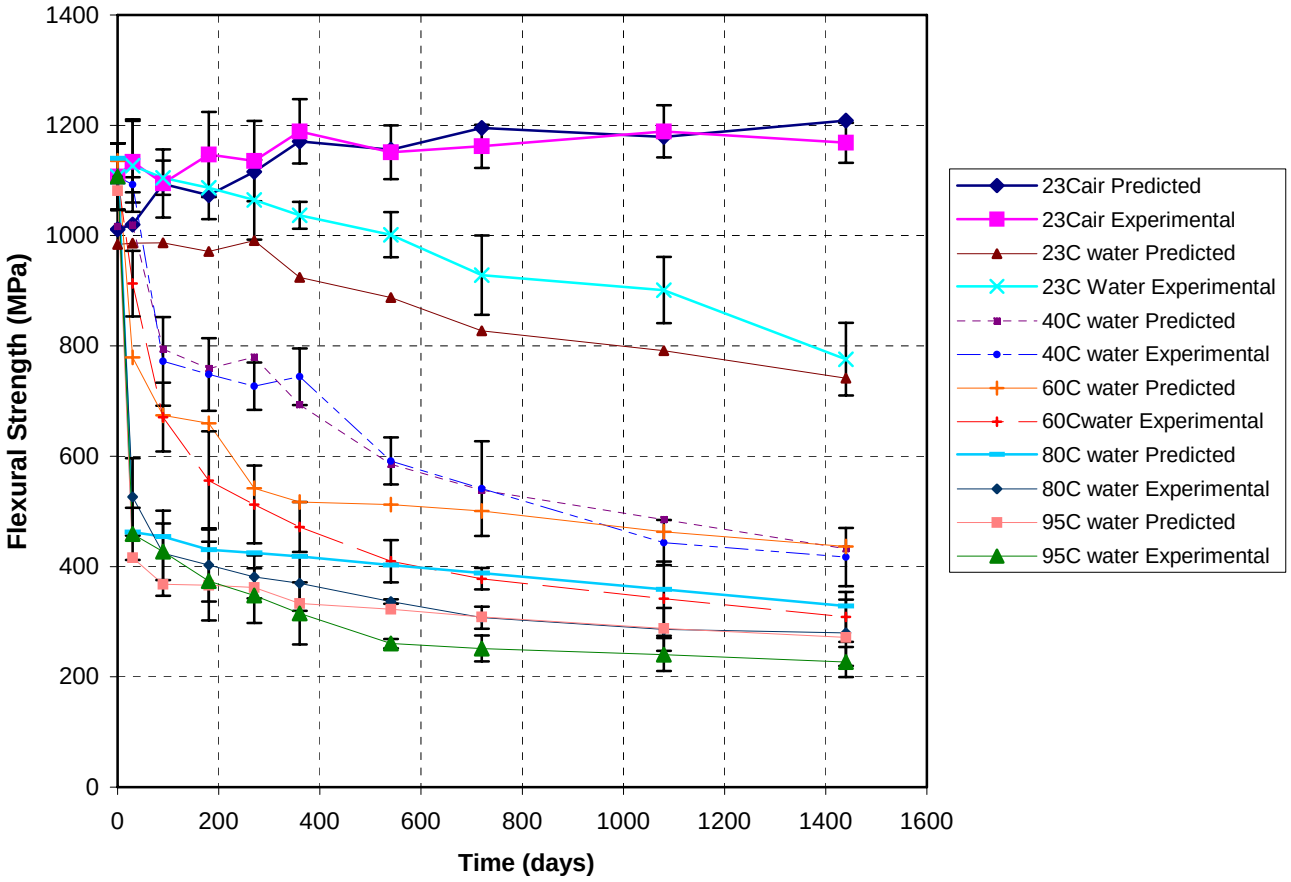

Fig. 6.1 Values of flexural strength predicted from tensile test data

6.4 Prediction of Tensile Strength from Flexural Tests

As seen in the previous section, there is overall a fairly good correlation between the experiment and the predictions, especially if scatter is considered. Although this implicitly shows that the reverse can also be done, results are elucidated in this section. As a first step of this procedure, the Weibull parameters for each of the flexural test data sets are evaluated. For purposes of this investigation, equation 6.7 is used to determine the shape parameter. To evaluate the shape parameter, the coefficient of variation for each data set is found. Then equation 6.7 is used to determine the value of the shape parameter. The average of the shape parameters for each exposure condition is determined. The values of the shape parameter and the flexural strength are then substituted in equation 6.4 to evaluate the values of tensile strength at each time step for each of the exposure conditions.

Table 6.8 lists the values of shape parameters calculated from the flexural test data, for each of the exposure environments. Tables 6.9 through 6.14 show the values of tensile strength evaluated from the flexural strength data as described by the procedure above. Figure 6.2 compares the predicted and the experimental tensile strength values graphically. The tables also depict the percentage error between the predicted and experimental values of tensile strength. The percentage error is calculated according to the equation 6.9.

Table 6.8 Values of shape parameters for the different exposure conditions calculated from flexural tests

Exposure Condition	Shape Parameter
"Control" Conditions at 23°C	25.61
Immersion in Water at 23°C	22.02
Immersion in Water at 40°C	14.62
Immersion in Water at 60°C	13.24
Immersion in Water at 80°C	20.08
Immersion in Water at 95°C	13.43
Average value of shape parameter for specimens immersed in deionized water	16.68
Overall average value of shape parameter	18.17

Table 6.9 Values of tensile strength predicted from flexural tests of composite specimens exposed to air at 23^0C

Time(days)	Flexural Strength (MPa)	Predicted Tensile Strength (MPa)	Experimental Tensile Strength (MPa)	Std. Deviation (MPa)	Percentage error
0	1106.89	806.67	684.65	63.50	17.82
30	1133.85	826.31	690.86	71.15	19.61
90	1094.55	797.67	740.50	55.50	7.72
180	1146.88	835.81	726.71	43.58	15.01
270	1135.23	827.32	755.67	50.61	9.48
360	1189.01	866.51	792.90	37.78	9.28
540	1151.16	838.92	782.56	15.10	7.20
720	1162.05	846.86	809.45	44.33	4.62
1080	1189.01	866.51	798.42	57.71	8.53
1440	1168.25	851.39	818.41	30.06	4.03

Table 6.10 Values of tensile strength predicted from flexural tests of composite specimens immersed in deionized water at 23^0C

Time(days)	Flexural Strength (MPa)	Predicted Tensile Strength (MPa)	Experimental Tensile Strength (MPa)	Std. Deviation (MPa)	Percentage error
0	1106.89	776.26	684.65	63.50	13.38
30	1126.96	790.33	686.03	84.67	15.20
90	1104.96	774.91	686.65	24.13	12.85
180	1086.83	762.19	675.69	51.30	12.80
270	1064.83	746.77	689.41	37.23	8.32
360	1036.70	727.04	642.94	18.06	13.08
540	1001.68	702.47	617.64	26.34	13.74
720	928.25	650.98	575.37	14.96	13.14
1080	901.29	632.07	550.34	33.30	14.85
1440	775.94	544.17	515.94	21.99	5.47

Table 6.11 Values of tensile strength predicted from flexural tests of composite specimens immersed in deionized water at 40^0C

Time(days)	Flexural Strength (MPa)	Predicted Tensile Strength (MPa)	Experimental Tensile Strength (MPa)	Std. Deviation (MPa)	Percentage error
0	1106.89	683.99	684.65	63.50	-0.10
30	1092.34	675.00	686.79	71.71	-1.72
90	772.08	477.10	534.83	52.19	-10.79
180	748.36	462.44	511.32	46.26	-9.56
270	726.92	449.19	525.18	5.31	-14.47
360	744.22	459.89	467.12	27.92	-1.55
540	591.44	365.47	394.18	29.65	-7.28
720	541.45	334.58	362.60	7.17	-7.73
1080	443.47	274.04	326.61	26.61	-16.09
1440	417.41	257.93	291.17	33.92	-11.41

Table 6.12 Values of tensile strength predicted from flexural tests of composite specimens immersed in deionized water at 60^0C

Time(days)	Flexural Strength (MPa)	Predicted Tensile Strength (MPa)	Experimental Tensile Strength (MPa)	Std. Deviation (MPa)	Percentage error
0	1106.89	659.67	684.65	63.50	-3.65
30	913.01	544.13	469.67	45.64	15.85
90	670.86	399.81	406.45	51.92	-1.63
180	556.07	331.40	397.83	19.31	-16.70
270	512.42	305.39	326.81	34.47	-6.56
360	471.81	281.19	311.58	13.93	-9.75
540	409.83	244.24	309.02	39.65	-20.96
720	377.97	225.26	301.79	51.64	-25.36
1080	341.71	203.65	279.31	25.65	-27.09
1440	308.75	184.01	262.90	33.16	-30.01

Table 6.13 Values of tensile strength predicted from flexural tests of composite specimens immersed in deionized water at 80^0C

Time(days)	Flexural Strength (MPa)	Predicted Tensile Strength (MPa)	Experimental Tensile Strength (MPa)	Std. Deviation (MPa)	Percentage error
0	1106.89	756.71	684.65	63.50	10.52
30	526.21	359.74	277.52	20.62	29.63
90	423.96	289.83	272.97	10.69	6.18
180	402.93	275.46	258.35	27.99	6.62
270	381.21	260.61	255.18	20.62	2.13
360	369.84	252.83	251.04	34.06	0.71
540	336.40	229.97	241.80	31.58	-4.89
720	307.23	210.03	232.91	25.92	-9.82
1080	285.93	195.47	215.39	20.20	-9.25
1440	279.86	191.32	197.12	30.13	-2.94

Table 6.14 Values of tensile strength predicted from flexural tests of composite specimens immersed in deionized water at 95^0C

Time(days)	Flexural Strength (MPa)	Predicted Tensile Strength (MPa)	Experimental Tensile Strength (MPa)	Std. Deviation (MPa)	Percentage error
0	1106.89	663.21	684.65	63.50	-3.13
30	459.12	275.09	263.59	11.10	4.36
90	426.86	255.76	233.04	41.44	9.75
180	373.84	223.99	231.87	25.37	-3.40
270	347.29	208.09	229.32	23.17	-9.26
360	314.95	188.71	210.77	5.38	-10.47
540	260.35	155.99	204.43	24.13	-23.69
720	251.32	150.58	195.47	22.61	-22.96
1080	240.42	144.05	182.16	20.27	-20.92
1440	226.98	136.00	172.03	27.30	-20.94

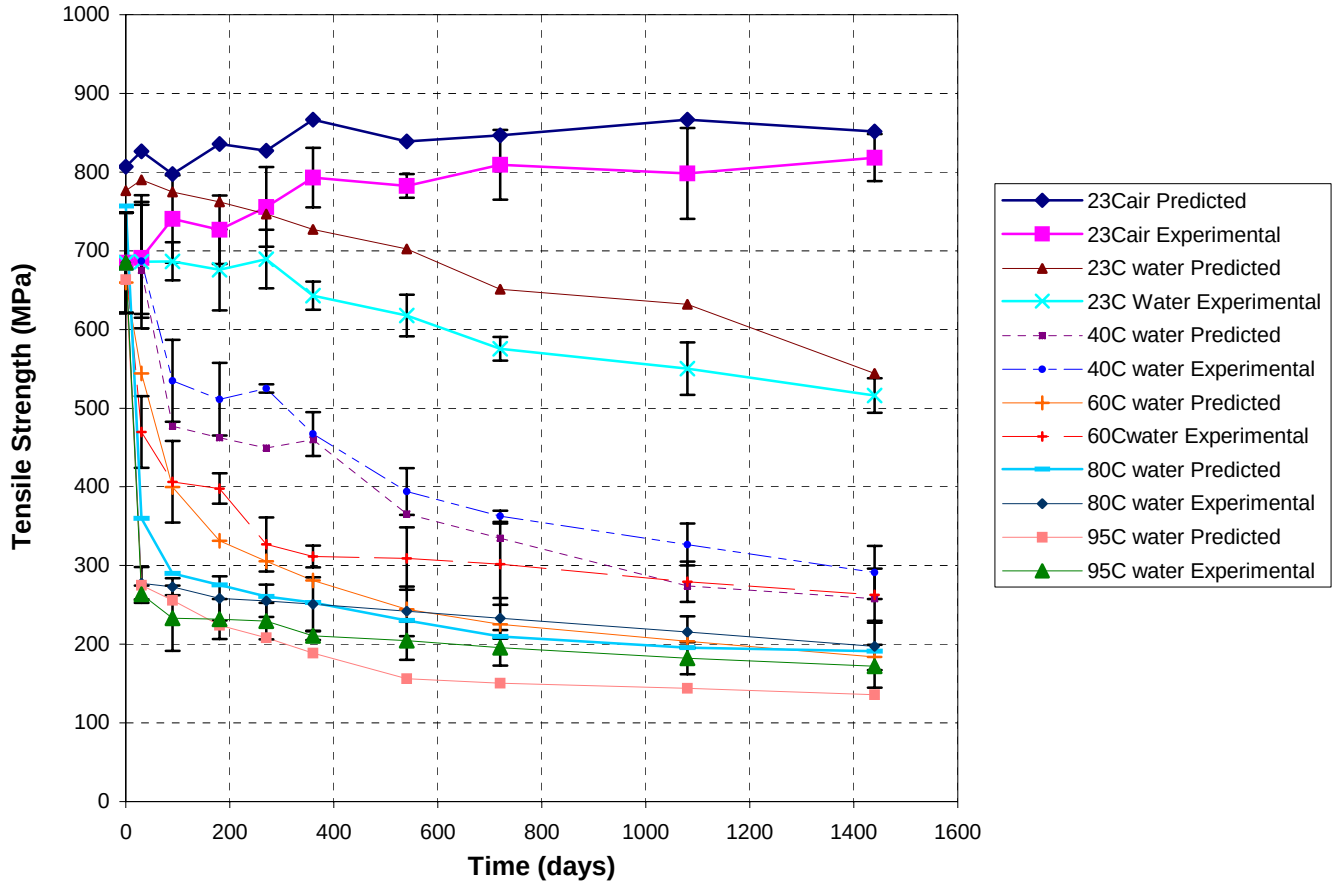

Fig. 6.2 Values of tensile strength predicted from flexural test data

6.5 Discussion

It can be seen from figures 6.1 and 6.2 that predictions of flexural strength and tensile strength are fairly close to the experimental values of flexural strength and tensile strength, respectively. Except for the predictions of tensile strength for specimens exposed to air at 23^{o}C and immersed in deionized water at 23^{o}C, the predicted values of tensile strength and flexural strength are conservative estimates. It can be noted from tables 6.1 and 6.8 that although the individual flexure-shape parameters and tension-shape parameters are different, perhaps indicating that their failures are governed by different flaw distributions, the average values across sets immersed in water are actually very close indicating overall similarity.

6.6 References

1. Whitney J.M. and Knight M., "The Relationship between Tensile Strength and Flexure Strength in Fiber-reinforced Composites", *Experimental Mechanics*, June 1980, Vol. 20, Issue 6, pp. 211-216.

2. Holmberg J.A., "On Flexural and Tensile Strength for Composites Manufactured by RTM", *Journal of Reinforced Plastics and Composites*, November 1992, Vol. 11, pp. 1302-1320.

3. Bullock R.E., "Strength Ratios of Composite Materials in Flexure and Tension", *Journal of Composite Materials*, April 1974, Vol. 8, pp. 200-206.

4. Karbhari V.M. and Abanilla M.A., "Durability Characterization of Wet Layup Carbon/Epoxy Used in External Strengthening III: Design Factors, Reliability, and Durability Prediction" *Composites B*, submitted 2005.

5. Leon M. and Kittl P., "On the Estimation of Weibull's Parameters in Brittle Materials", *Journal of Materials Science*, 1985, Vol. 20, pp. 3778-3782.

Chapter 7

Performance Prediction: Immersion in Deionized Water

7.1 Introduction

Exposure to humidity, water, elevated temperatures and other harsh environments can induce physical, chemical and mechanical changes in polymer composites. Moisture absorption in FRP composites cannot only affect their dimensional stability but also can affect the mechanical properties of the composites. As a result of this, the determination of the rate of degradation of mechanical properties and the consequent estimation of remaining service life is of utmost importance to engineers and designers. The effects of immersion in water and exposure to humidity at different temperatures on the mechanical properties of unidirectional E-glass Vinylester composites are studied as a part of this research. Long-term durability characteristics of E-glass Vinylester composites in these environments are then studied by employing suitable life prediction models. For the purposes of this study, the Arrhenius and Phani-Bose based prediction methods were used. The following sections describe the analysis procedures and present the results of the analysis.

7.2 Arrhenius Prediction Model

The Arrhenius Prediction Model is a commonly used life prediction model in accelerated life testing [1]. The model is derived from the Arrhenius reaction rate equation proposed by the Swedish Chemist Svandte Arrhenius in 1887. The Arrhenius reaction rate equation for a phenomenon under consideration is given by,

$$R(T) = A\exp\left[\frac{-E_a}{RT}\right] \qquad \text{(Equation 7.1)}$$

where R(T) is the rate of the reaction, A is a non-thermal constant, E_a is the activation energy in J/mol K, T is the absolute temperature (Kelvin) and R is the universal gas constant (8.3144 J/mol K).

The Arrhenius life-stress relationship is formulated by assuming that the life is proportional to the inverse reaction rate of the process.

$$L(T) = C\exp\left[\frac{B}{T}\right] \qquad \text{(Equation 7.2)}$$

where L(T) represents the quantifiable measure of life, T is the temperature in degrees Kelvin, C is one of the model parameters to be determined and B is another model parameter to be determined.

The Arrhenius relationship can be plotted on a life vs. temperature plot, also called the Arrhenius plot. The Arrhenius life-stress relationship is linearized by taking natural logarithms on both sides of the equation 7.2,

$$\ln\left[L(T)\right] = \ln(C) + \frac{B}{T} \qquad \text{(Equation 7.3)}$$

Equation 7.3 represents a line in the slope-intercept form, where B is the slope of the line, ln (C) is the intercept and the variable on the horizontal axis is the inverse of temperature.

From equations 7.1 and 7.2 it can be seen that the constant B has the same properties as the activation energy, which implies that B is the measure of the effect that the stressing or forcing, function (e.g. temperature) has on the life of the material. The larger the value of B, the higher the dependency of the life on the stress (temperature).

7.2.1 Analysis Procedure

The use of the Arrhenius rate analysis procedure described in the previous section is demonstrated with an example in this section. Table 7.1 shows the tensile strength of the composite specimens immersed in deionized water. Details pertaining to the tensile strength data have previously been reported in chapter 4. Fig 7.1 shows the percentage retention of tensile strength of the composite specimens immersed in deionized water at temperatures of 23 ^{o}C, 40 ^{o}C, 60 ^{o}C, 80 ^{o}C and 95 ^{o}C.

Since the strength of the unexposed "control" specimens is seen to increase with time due to the slow progression of cure, the final value of strength was used for the calculation of percentage retention. This results in a more conservative estimate since it assumes that post-cure effects would dominate over deterioration mechanisms in the early stages of exposure.

Table 7.1 Tensile Strength data for E-glass/Vinylester composite specimens immersed in deionized water and "control" specimens at 23 ^{o}C and 30 % RH

Time (days)	Control		23^{0}C		40^{0}C		60^{0}C		80^{0}C		95^{0}C	
	Tensile Strength (MPa)	Standard Deviation (MPa)	Tensile Strength (MPa)	Standard Deviation (MPa)	Tensile Strength (MPa)	Standard Deviation (MPa)	Tensile Strength (MPa)	Standard Deviation (MPa)	Tensile Strength (MPa)	Standard Deviation (MPa)	Tensile Strength (MPa)	Standard Deviation (MPa)
0	684.65	63.50	684.65	63.50	684.65	63.50	684.65	63.50	684.65	63.50	684.65	63.50
30	690.86	71.15	686.03	84.67	686.79	71.71	469.67	45.64	277.52	20.62	263.59	11.10
90	740.50	55.50	686.65	24.13	534.83	52.19	406.45	51.92	272.97	10.69	233.04	41.44
180	726.71	43.58	675.69	51.30	511.32	46.26	397.83	19.31	258.35	27.99	231.87	25.37
270	755.67	50.61	689.41	37.23	525.18	5.31	326.81	34.47	255.18	20.62	229.32	23.17
360	792.90	37.78	642.94	18.06	467.12	27.92	311.58	13.93	251.04	34.06	210.77	5.38
540	782.56	15.10	617.64	26.34	394.18	29.65	309.02	39.65	241.80	31.58	204.43	24.13
720	809.45	44.33	575.37	14.96	362.60	7.17	301.79	51.64	232.91	25.92	195.47	22.61
1080	798.42	57.71	550.34	33.30	326.61	26.61	279.31	25.65	215.39	20.20	182.16	20.27
1440	818.41	30.06	515.94	21.99	291.17	33.92	262.90	33.16	197.12	30.13	172.03	27.30

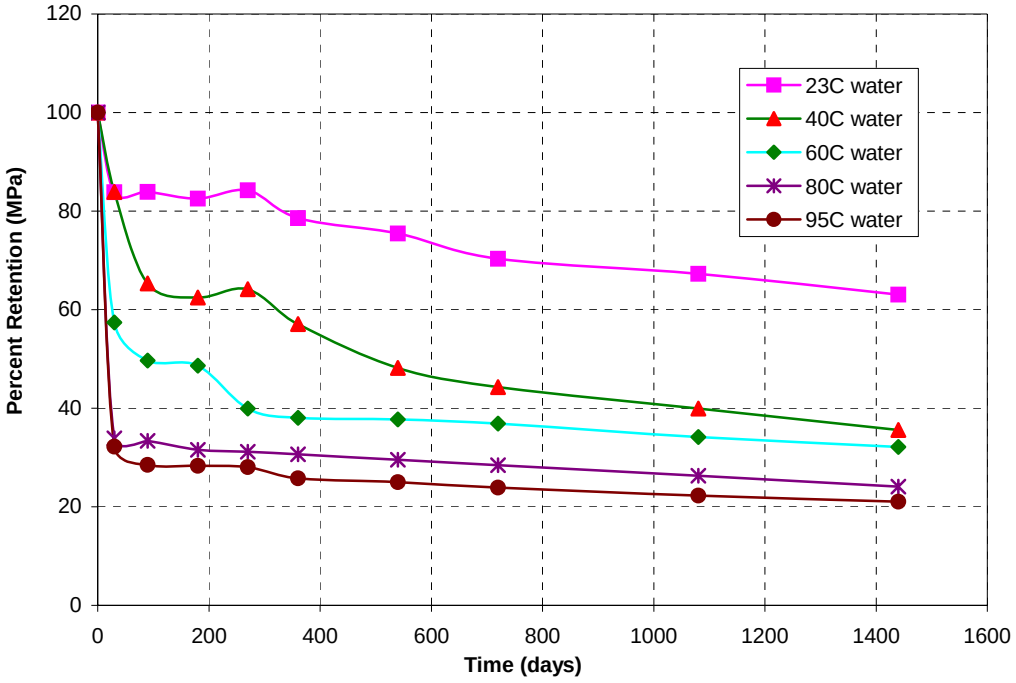

Fig. 7.1 Percent retention of tensile strength for E-glass/Vinylester composite specimens

The relationship between percent retention of the tensile strength and time is linearized by taking the natural logarithm of the time (in days) and plotting it against the percent retention. This is illustrated in Fig 7.2. Since the natural logarithm of time at zero days is mathematically undefined, the value of "0 days" is approximated, for the purposes of this calculation, to "1 day" assuming that degradation in properties on the first day is minimal.

The straight lines in figure 7.2 represent the linear curve fits obtained from linear regression analysis, and these are tabulated in table 7.2.

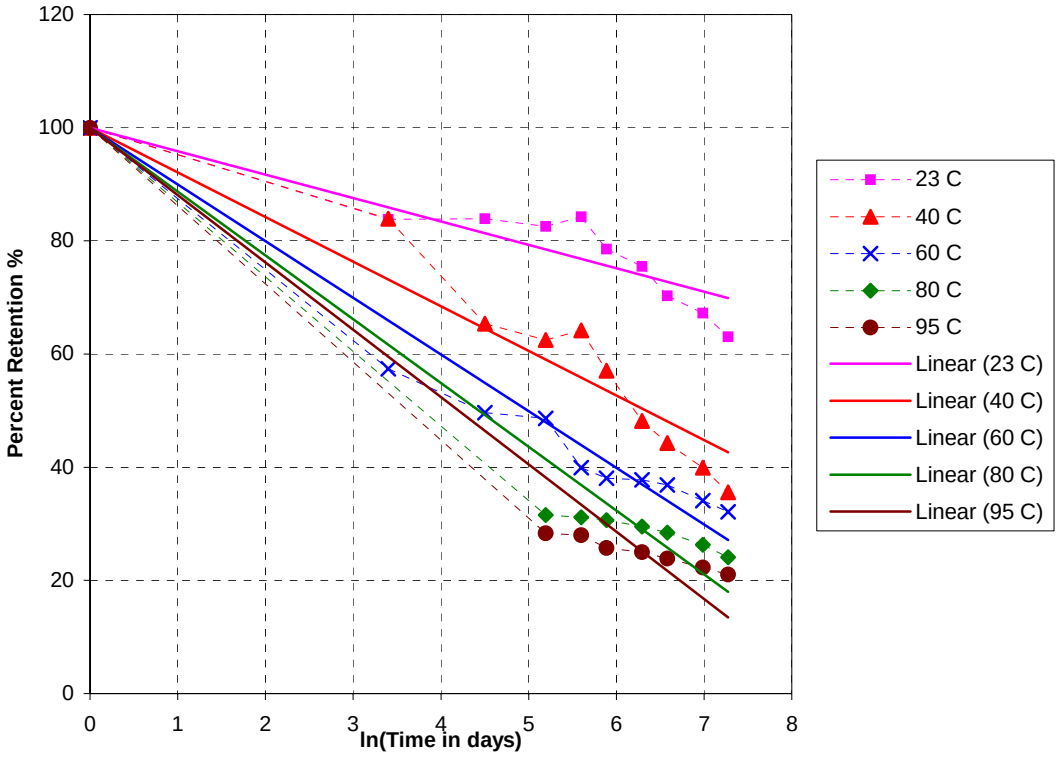

Fig. 7.2 Arrhenius plot for decrease in percent retention oftensile strength for E-glass/Vinylester composite specimens

Table 7.2. Linear relationship between tensile strength and time forE-glass/Vinylester composite specimens immersed in deionized water

Temperature (^{o}C)	Linear Relationship	R^2
23	y(t) = -4.1374* ln (t) + 100	0.8407
45	y(t) = -7.8868* ln (t) + 100	0.9161
60	y(t) = -10.021* ln (t) + 100	0.9516
80	y(t) = -11.277* ln (t) + 100	0.9534
95	y(t) = -11.900* ln (t) + 100	0.9529

The equations in Table 7.2 predict the response of the composite specimens with time. Therefore they can be used to predict the tensile strength of the specimens for longer times at different temperatures.

The percent retention values are used to establish a relationship between percentage strength retention and temperature. The relationship between strength retention and temperature is different for each time step. As discussed in section 7.2 the life of the material is proportional to the inverse reaction rate of the process. Therefore, the percent retention values, determined in the previous step in the analysis, are plotted against the inverse of temperature (1000/T (K)). This is illustrated in Fig. 7.3. To predict the response of the material immersed in deionized water at 23 ^{o}C the equations for predicted response of immersion at temperatures of 40 ^{o}C, 60 ^{o}C, 80 ^{o}C and 95 ^{o}C are considered, thereby using the 23 ^{o}C case as a basis of comparison.

Regression analysis is performed for each of the time steps and this yields a set of linear relationships between the percent strength retention and inverse of temperature. The relationships so obtained are listed in table 7.3. The relationships in Table 7.3 can be used to determine the tensile strength of the composite specimen at different time steps for a particular temperature. For predictions of response due to immersion in deionized water at 23 ^{o}C, the values of tensile strength at each time step are obtained by substituting the temperature of 23 ^{o}C (296 K) in the equations in Table 7.3. The values of predicted tensile strength thus obtained are tabulated in Table 7.4 and compared to experimentally obtained data. The percentage error between the experimental and predicted values is also tabulated in Table 7.4. The percentage error is calculated according to the equation,

$$\text{Percentage Error} = \frac{\text{Predicted Value - Experimental Value}}{\text{Experimental Value}} x100$$

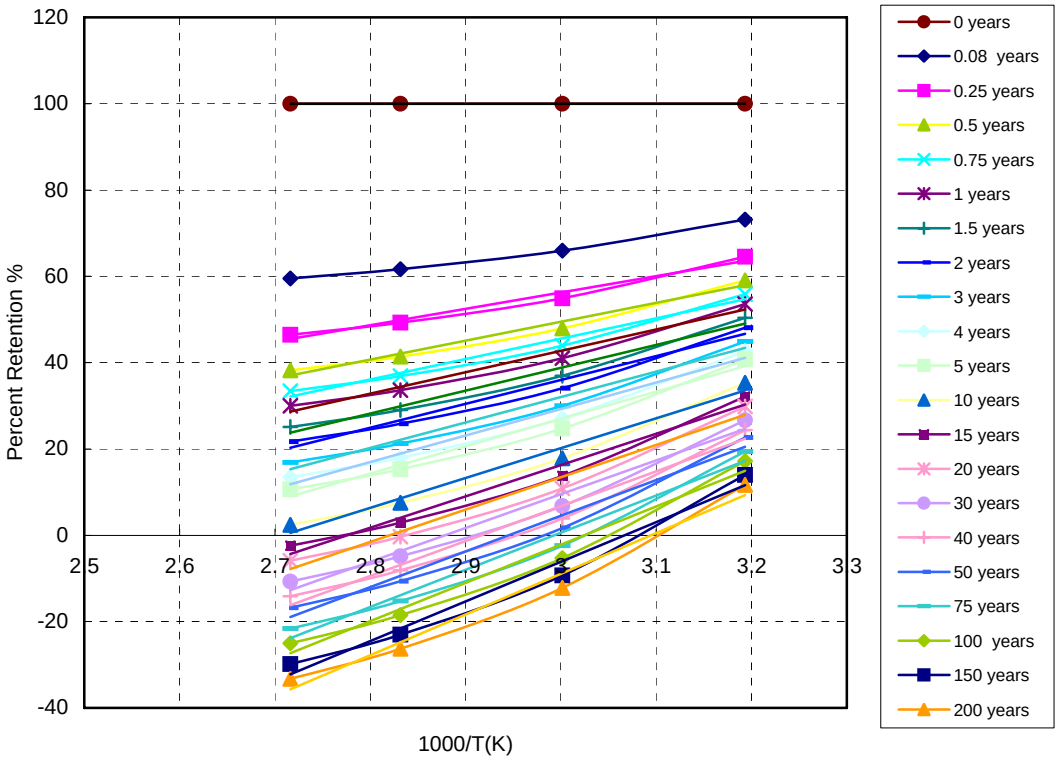

Fig. 7.3 Percent retention of tensile strength Vs. Inverse of temperature (1000/T (K))

Table 7.3 Linear Relationship between percent retention of tensile strength and the inverse of temperature

Time (years)	Linear relationship between percent retention and 1/T
0	y (T) = 100
0.08	y (T) = 28.568 * (1000/T) – 19.068
0.25	y (T) = 37.915 * (1000/T) – 57.528
0.5	y (T) = 43.756 * (1000/T) – 81.793
0.75	y (T) = 47.172 * (1000/T) – 95.987
1	y (T) = 49.596 * (1000/T) – 106.06
1.5	y (T) = 53.013 * (1000/T) – 120.25
2	y (T) = 55.437 * (1000/T) – 130.32
3	y (T) = 58.853 * (1000/T) – 144.52
4	y (T) = 61.277 * (1000/T) – 154.59
5	y (T) = 63.273 * (1000/T) – 162.88
10	y (T) = 69.114 * (1000/T) – 187.15
15	y (T) = 72.530 * (1000/T) – 201.34
20	y (T) = 74.954 * (1000/T) – 211.41
30	y (T) = 78.371 * (1000/T) – 225.61
40	y (T) = 80.795 * (1000/T) – 235.68
50	y (T) = 82.675 * (1000/T) – 243.49
75	y (T) = 86.091 * (1000/T) – 257.69
100	y (T) = 88.515 * (1000/T) – 267.76
150	y (T) = 91.932 * (1000/T) – 281.95
200	y (T) = 94.356 * (1000/T) – 292.02

Table 7.4 Predicted values of tensile strength in comparison with experimentally obtained values for specimens immersed in deionized water at 23 ^{o}C

Time (years)	Predicted values of percent retention	Experimentally obtained average values	Percentage error
0	100.00	100.00	0.00
0.08	77.70	83.82	-7.31
0.25	70.50	83.90	-15.97
0.5	65.96	82.56	-20.11
0.75	63.30	84.24	-24.86
1	62.62	78.56	-20.28
1.5	58.76	75.47	-22.14
2	56.87	70.30	-19.10
3	54.21	67.25	-19.39
4	52.32	63.04	-17.00
5	50.77	-	-
10	46.22	-	-
15	43.57	-	-
20	41.68	-	-
30	39.02	-	-
40	37.14	-	-
50	35.68	-	-
75	33.01	-	-
100	31.13	-	-
150	28.47	-	-
200	26.59	-	-

From the data listed in the Table 7.4 and Fig 7.4 it is obvious that the Arrhenius model predicts a slightly higher rate of degradation when compared to the tensile strength values obtained from the experiment, which is partly attributable to the higher value used for the “unexposed” final strength. In comparing the values and assessing the percentage error it should be kept in mind that the comparison is on the basis of average values, and

that the experimental values have a level of scatter which in many cases minimizes the actual error. This results in the predictions being well within the experimental scatter bounds in figure 7.4.

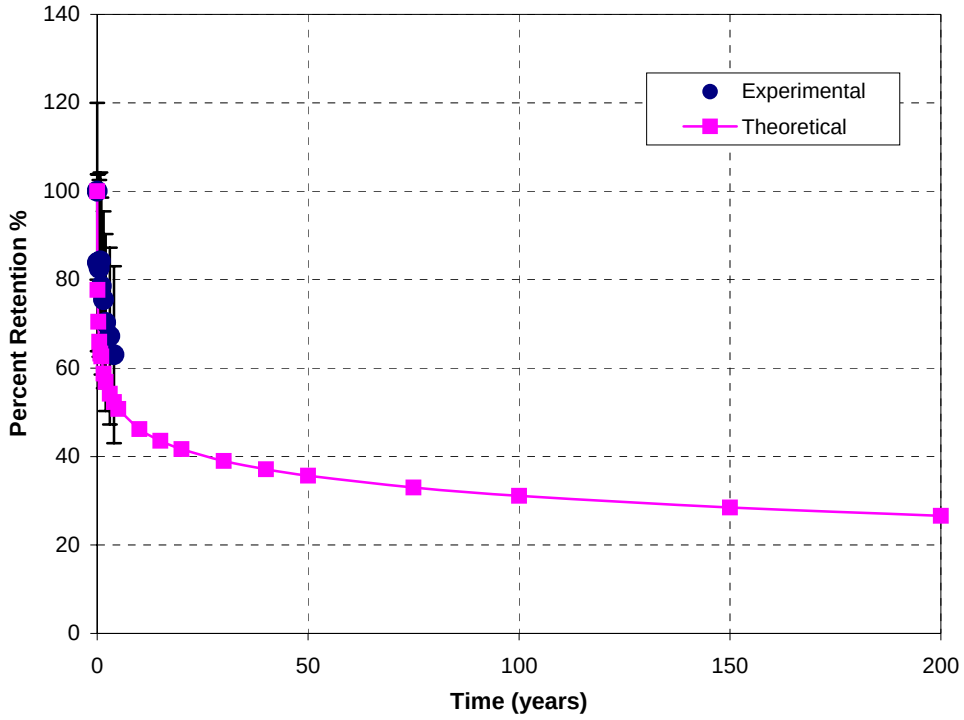

Fig. 7.4 Comparison between the experimental and predicted values of tensile strength for specimens immersed in deionized water at 23 ^{o}C

The overall predictive equation describing the relationship between the tensile strength and exposure time is given by:

$$y(t) = - 6.9588 \ \ln(t) + 103.52$$

where t is the time in days and y (t) is the percent retention of tensile strength.

It should be noted that the above expression is valid for all times except zero. At time zero, it is suggested that y =100 % be used, because the composite specimen has 100

% of its cured strength before exposure to hygrothermal ageing, but this could not be considered mathematically due to the use of the "ln" function at time t = 0.

Similar expressions can be derived for other test temperatures, by substituting the absolute temperatures in the equations listed in Table 7.3 and plotting the values of the predicted tensile strength against time.

The analysis procedure described above was applied to data from all the tensile, flexural and short beam shear tests and results are presented in the following sections. All the predictions shown below are for composites immersed in deionized water at 23 ^{o}C.

7.2.2 Tensile Strength Prediction

The Arrhenius prediction of tensile strength, for the specimens exposed to deionized water at 23 ^{o}C is summarized in the table 7.4 and figure7.4. The predicted values of tensile strength are smaller than the experimental values as seen from the table 7.4.

Table 7.4 shows percentage errors ranging from –7.31% to 24.86%. Higher percentage errors are observed for exposure times of 0.5, 0.75, 1 and 1.5 years. In reality, the tensile strength of the composite specimen increases with time due to residual post-cure. But the Arrhenius Rate model is based on degradation trends, which leads to larger errors in the prediction of the strength during the post-cure period. But the error percentages decrease starting with the 2-year prediction, indicating the domination of degradation mechanisms after the initial post-cure. Further, as noted earlier, overall experimental scatter bounds need to be considered in assessing the accuracy of the predictions.

Table 7.4 Predicted values of tensile strength in comparison with experimentally obtained values for immersed in deionized water at 23 ^{o}C

Time (years)	Predicted values of percent retention– Arrhenius rate model	Experimentally obtained average values	Percentage error
0	100.00	100.00	0.00
0.08	77.70	83.82	-7.31
0.25	70.50	83.90	-15.97
0.5	65.96	82.56	-20.11
0.75	63.30	84.24	-24.86
1	62.62	78.56	-20.28
1.5	58.76	75.47	-22.14
2	56.87	70.30	-19.10
3	54.21	67.25	-19.39
4	52.32	63.04	-17.00
5	50.77	-	-
10	46.22	-	-
15	43.57	-	-
20	41.68	-	-
30	39.02	-	-
40	37.14	-	-
50	35.68	-	-
75	33.01	-	-
100	31.13	-	-
150	28.47	-	-
200	26.59	-	-

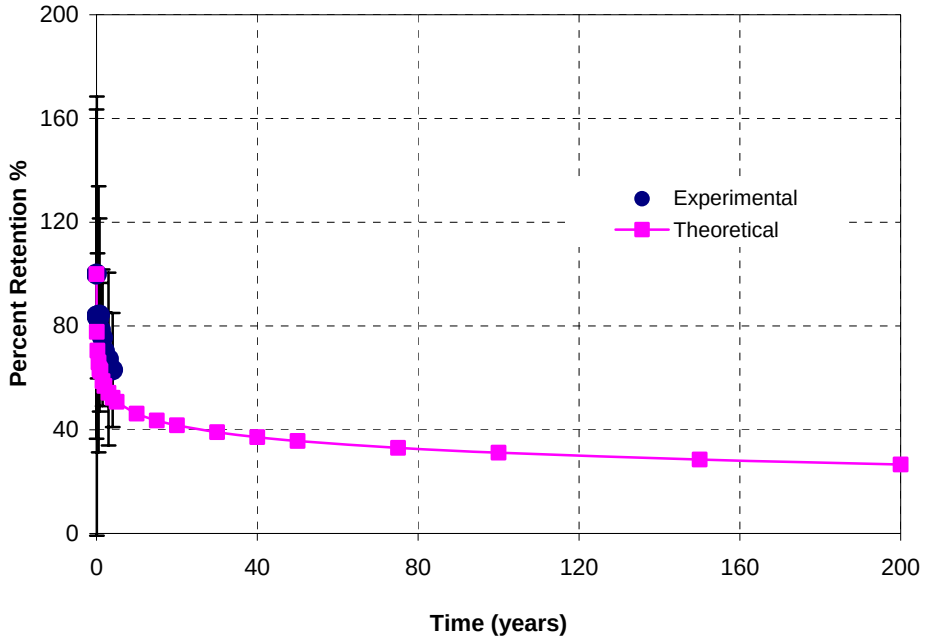

Fig. 7.4 Comparison between the experimental and predicted values of tensile strength for specimens immersed in deionized water at 23^0C

7.2.3 Tensile Modulus

The Arrhenius prediction of tensile modulus, for the specimens immersed in deionized water at 23 ^{o}C is summarized in the table 7.5 and figure 7.5. Similar to the tensile strength predictions, the tensile modulus predictions are slightly lower than the experimental values. It has to be noted that the rate of decrease of the tensile modulus is slower than that of tensile strength.

Table 7.5 Predicted values of tensile modulus in comparison with experimentally obtained values for specimens immersed in deionized water at 23^0C

Time (years)	Predicted values of percent retention– Arrhenius rate model	Experimentally obtained average values	Percentage error
0	100.00	100.00	0.00
0.08	96.39	98.99	-2.63
0.25	95.22	96.64	-1.47
0.5	94.48	97.32	-2.91
0.75	94.05	95.81	-1.83
1	93.75	96.98	-3.33
1.5	93.32	96.64	-3.44
2	93.01	94.80	-1.89
3	92.58	94.13	-1.64
4	92.58	93.12	-0.58
5	92.02	-	-
10	91.29	-	-
15	90.86	-	-
20	90.55	-	-
30	90.12	-	-
40	89.82	-	-
50	89.58	-	-
75	89.15	-	-
100	88.84	-	-
150	88.41	-	-
200	88.11	-	-

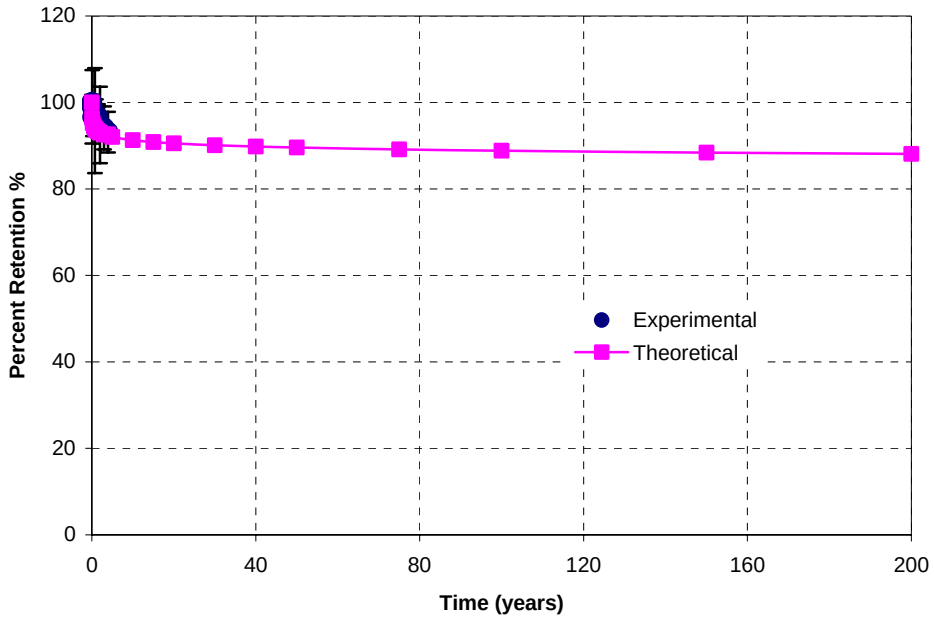

Fig. 7.5 Comparison between the experimental and predicted values of tensile modulus for specimens immersed in deionized water at 23^0C

7.2.4 Flexural Strength

The Arrhenius prediction of flexural strength, for the specimens immersed in deionized water at 23 ^oC is summarized in the table 7.6 and figure7.6. As seen from the figure 7.6, the flexural strength of the specimen decreases much more rapidly than the tensile strength or tensile modulus. It can also be observed that Arrhenius model provides rather conservative estimates for the flexural strength.

Table 7.6 Predicted values of flexural strength in comparison with experimentally obtained values for specimens immersed in deionized water at 23^0C

Time (years)	Predicted values of percent retention– Arrhenius rate model	Experimentally obtained average values	Percentage error
0	100.00	100.00	0.00
0.08	79.74	96.46	-17.34
0.25	65.36	94.58	-30.90
0.5	58.61	93.03	-37.00
0.75	54.66	91.15	-40.03
1	51.87	88.74	-41.55
1.5	47.92	85.74	-44.11
2	45.12	79.46	-43.22
3	41.17	77.15	-46.63
4	38.38	66.42	-42.22
5	36.07	-	-
10	29.32	-	-
15	25.38	-	-
20	22.58	-	-
30	18.63	-	-
40	15.84	-	-
50	13.66	-	-
75	9.71	-	-
100	5.92	-	-
150	2.96	-	-
200	0.17	-	-

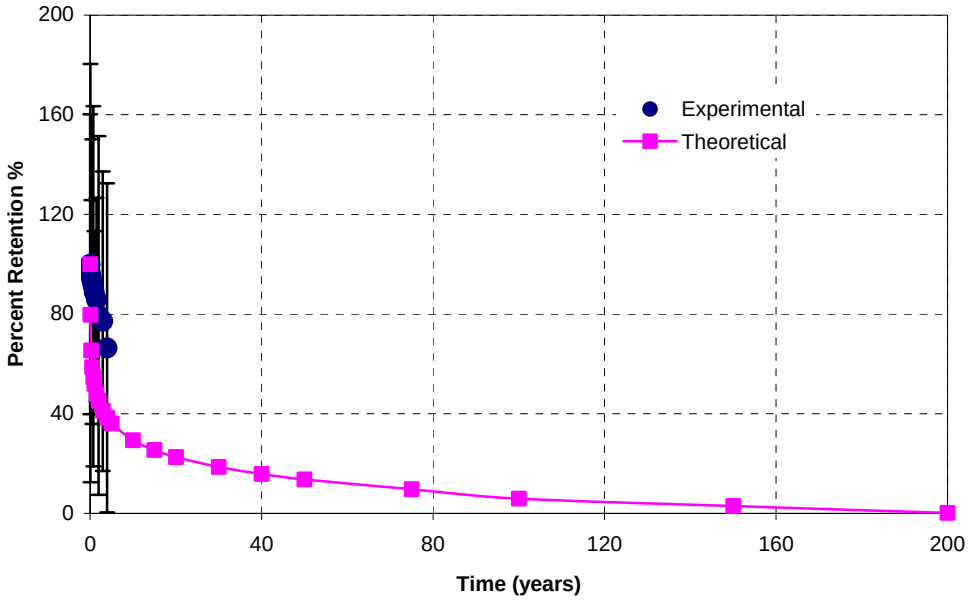

Fig. 7.6 Comparison between the experimental and predicted values of flexural strength for specimens immersed in deionized water at 23^0C

7.2.5 Short-Beam Shear Strength

The Arrhenius prediction of short beam shear strength, for the specimens immersed in deionized water at 23 ^{o}C is summarized in table 7.7 and figure 7.7. Similar to flexural strength, the short beam shear strength declines rapidly with time.

Table 7.7 Predicted values of short-beam shear strength in comparison with experimentally obtained values for specimens immersed in deionized water at 23^0C

Time (years)	Predicted values of percent retention– Arrhenius rate model	Experimentally obtained average values	Percentage error
0	100.00	100.00	0.00
0.08	97.19	99.04	-1.87
0.25	73.70	87.34	-15.62
0.5	67.40	87.34	-22.83
0.75	63.71	86.74	-26.54
1	61.10	85.30	-28.38
1.5	57.41	77.18	-25.61
2	54.80	74.31	-26.26
3	51.12	70.25	-27.24
4	48.50	66.67	-27.25
5	46.35	-	-
10	40.05	-	-
15	36.36	-	-
20	33.75	-	-
30	30.07	-	-
40	27.45	-	-
50	25.42	-	-
75	21.74	-	-
100	19.12	-	-
150	15.44	-	-
200	12.83	-	-

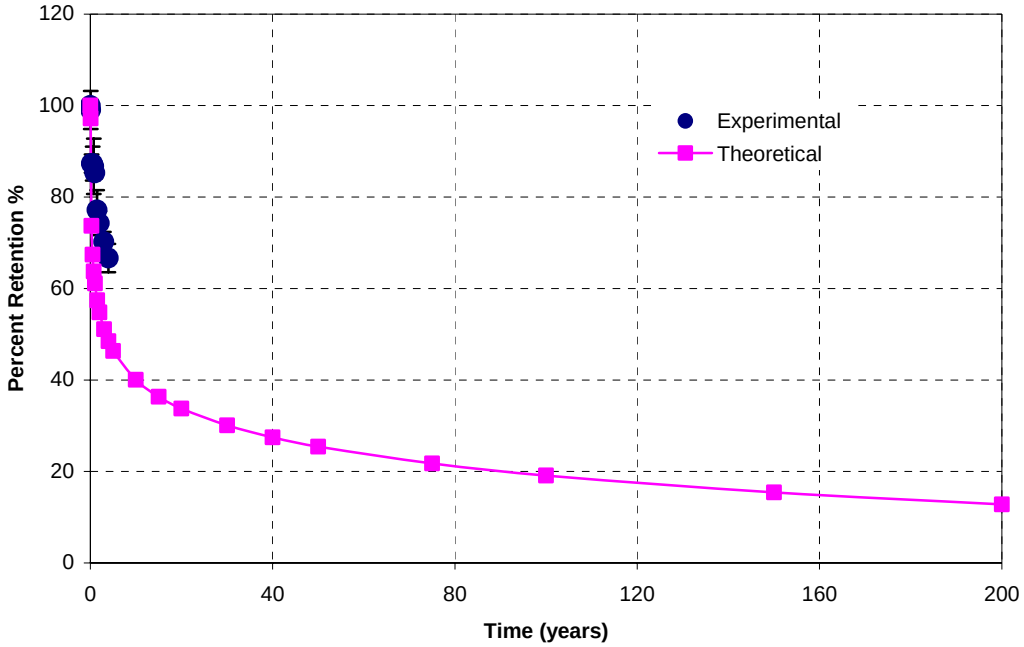

Fig. 7.7 Comparison between the experimental and predicted values of short-beam shear strength for specimens immersed in deionized water at 23^0C

7.2.6 Summary – Arrhenius Prediction Model

The results of the application of Arrhenius Prediction Model to tensile strength, tensile modulus, flexural strength and short-beam shear strength data, for the different exposure conditions is summarized in table 7.8 and figures 7.8 through 7.11. Table 7.8 lists the Arrhenius equations relating the strength characteristic to time, for each of the exposure conditions. Figures 7.8, 7.9, 7.10 and 7.11 compare the predicted and experimental values of tensile strength, tensile modulus, flexural strength and short-beam shear strength respectively.

Table 7.8 Arrhenius equations for prediction of properties of E-glass/Vinylester composites immersed in deionized water

Property	Temperature of immersion ^{o}C	Arrhenius equation*
Tensile Strength	23	y(t) = -6.9588 ln (t) + 103.52
	45	y(t) = -8.5942 ln (t) + 104.30
	60	y(t) = -10.304 ln (t)+ 105.11
	80	y(t) = -11.821 ln (t) + 105.84
	95	y(t) = -12.850 ln (t) + 106.33
Tensile Modulus	23	y(t) = -1.1257 ln (t) + 100.56
	45	y(t) = -1.6668 ln (t) + 100.83
	60	y(t) = -2.2328 ln (t) + 101.11
	80	y(t) = -2.7346 ln (t) + 101.36
	95	y(t) = -3.0752 ln (t) + 101.53
Flexural Strength	23	y(t) = -10.217 ln (t) + 112.57
	45	y(t) = -10.855 ln (t) + 109.75
	60	y(t) = -11.523 ln (t) + 106.81
	80	y(t) = -12.115 ln (t) + 104.20
	95	y(t) = -12.517 ln (t) + 102.43
Short Beam Shear Strength	23	y(t) = -9.3715 ln (t) + 117.27
	45	y(t) = -9.1098 ln (t) + 113.02
	60	y(t) = -8.8361 ln (t) + 108.57
	80	y(t) = -10.250 ln (t) + 104.95
	95	y(t) = -12.104 ln (t) + 105.84

* t = time in days

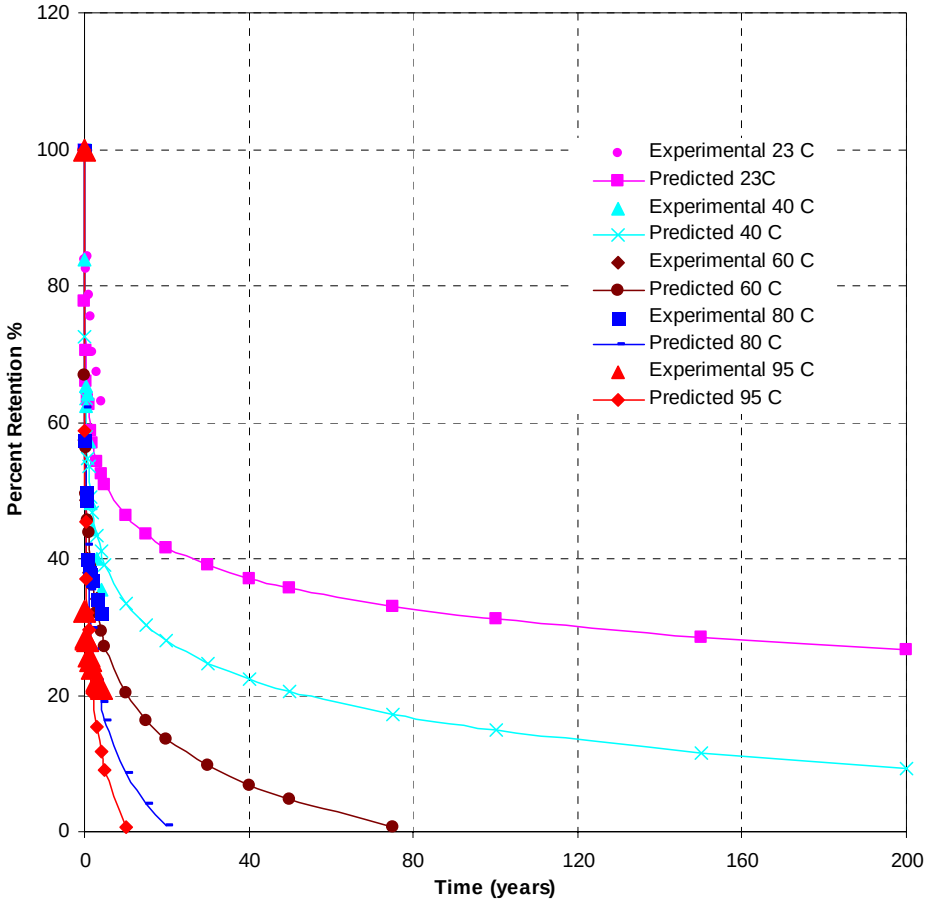

Fig. 7.8 Predicted values of tensile strength immersed in deionized water at different temperatures – Arrhenius Rate Method

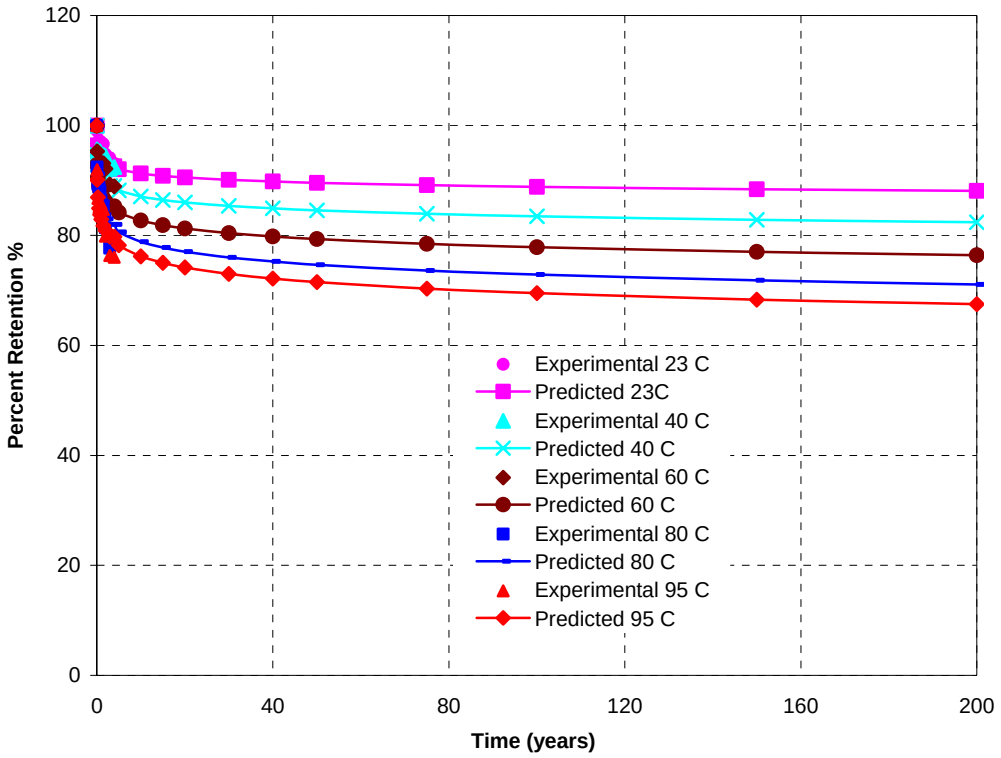

Fig. 7.9 Predicted values of tensile modulus immersed in deionized water at different temperatures – Arrhenius Rate Method

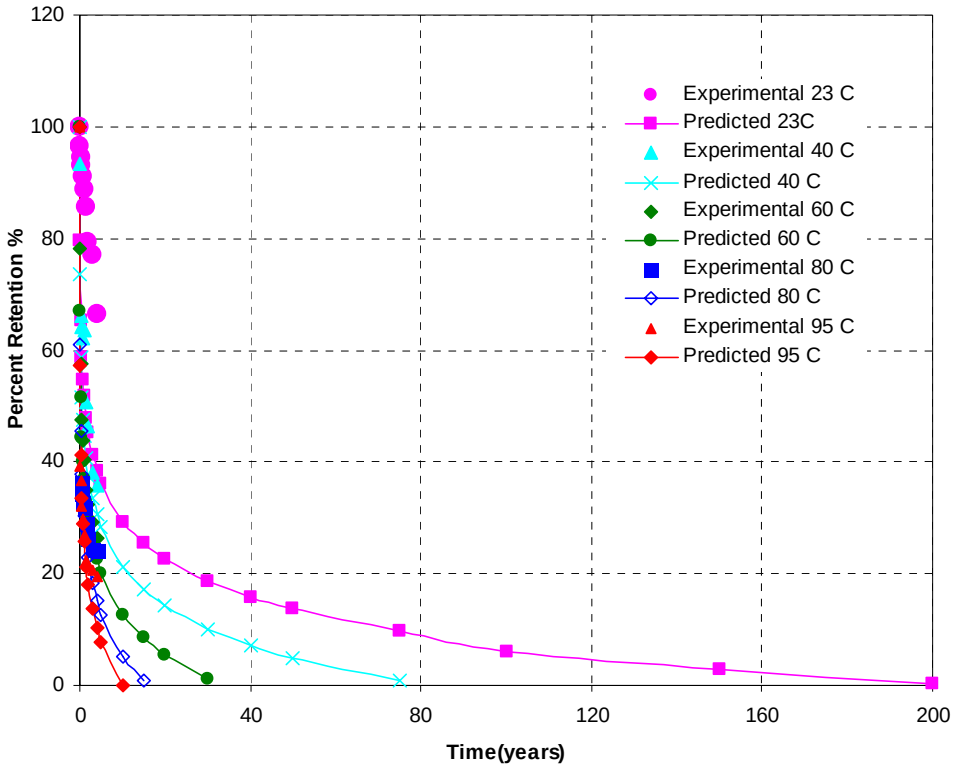

Fig.7.10. Predicted values of flexural strength immersed in deionized water at different temperatures – Arrhenius Rate Method

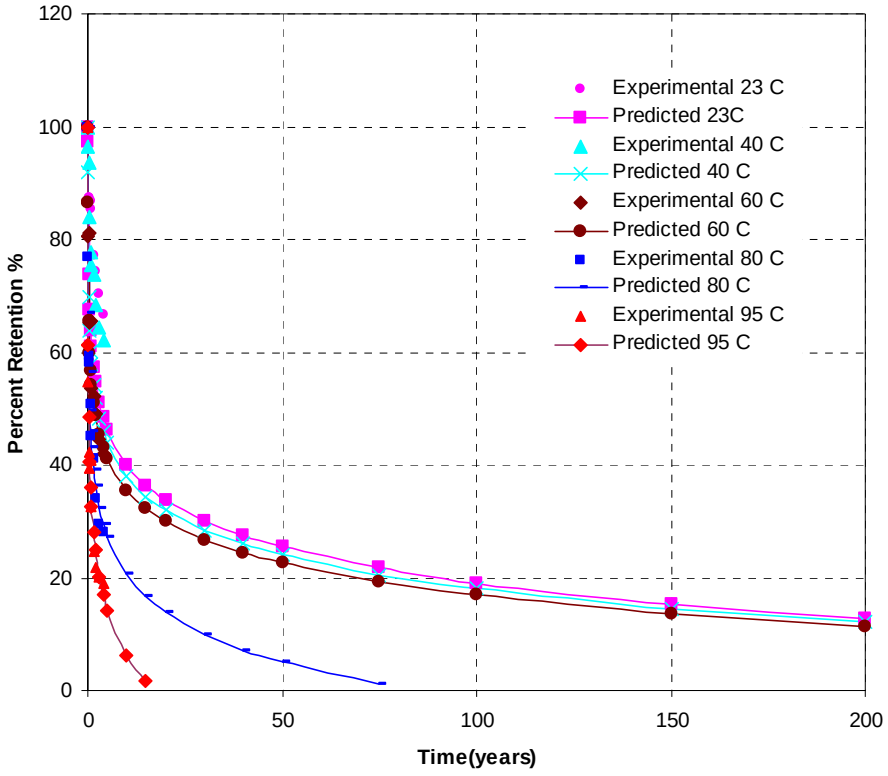

Fig. 7.11 Predicted values of short-beam shear strength immersed in deionized water at different temperatures – Arrhenius Rate Method

7.3 Phani and Bose Model

Phani and Bose investigated the hydrothermal ageing behavior of E-glass/ Polyester chopped strand mat (CSM) laminates and suggested that three distinct but inter-related processes may occur [2]

- Water plasticizes the matrix in the absence of inorganic impurities. In the presence of traces of impurities the matrix acts as a semi-permeable membrane and the resulting osmotic pressure within the matrix leads to cracking.
- Penetration of water into the resin promotes crack growth in the individual fibers resulting in weakness. Radial stresses due to resin swelling along with osmotic pressure caused by penetration of water lead to fiber debonding, increase in transfer length and consequent weakening of the composite.
- Increase in viscoelasticity due to plasticization of matrix results in further increase in transfer length decreasing the efficiency of load transfer at the interface.

Phani and Bose [2] studied the hydrothermal ageing characteristics of the laminates and proposed a model for the degradation of flexural strength of the composite. The material under investigation was a three-layer chopped strand E-glass/polyester mat, which was subjected to immersion in distilled water at different temperatures ranging from 23 ^{o}C to 90 ^{o}C. The analysis procedure used for the prediction of flexural strength of the composite is described in the next section.

7.3.1 Analysis Procedure

The assessment of hydrothermal ageing of the laminates by use of acousto-ultrasonic techniques showed that the flexural strength σ_t after exposure time t is given by the relation [2],

$$\sigma_t = (\sigma_0 - \sigma_\infty)\exp[-t/\tau] + \sigma_\infty \qquad \text{(Equation 7.4)}$$

where σ_0 and σ_∞ are the flexural strength at times 0 and ∞ respectively and τ is a characteristic time dependent on temperature. It was found that the reduction of the strength of CSM laminates due to hydrothermal effects is a rate process for which the temperature influences only the rate constant. The rate constant follows the Arrhenius equation [3], such that,

$$\frac{1}{\tau} = \frac{1}{\tau_0}\exp\left[\frac{-E_a}{RT}\right] \qquad \text{(Equation 7.5)}$$

where $1/\tau$ is the rate constant, τ_0 is a constant, E_a is the activation energy in J/mol K, R is the universal gas constant (8.314 J/mol K), and T is the temperature (Kelvin).

Equation 7.4 is fitted to the percent retention data using regression analysis by estimating an initial value for σ_∞. A least squares analysis is performed on the data and the values of σ_∞ are iterated to get the minimum least squares sum. The values of τ and σ_∞ are thus found from the regression analysis. The values of $1/\tau$ and $1/T$ are plotted and a least squares analysis is performed to find the activation energy, E_a, and the constant $1/\tau_0$. Equations 7.4 and 7.5 are combined to give the strength degradation with time and temperature for the prediction of the behavior of the material.

$$\sigma_t = (\sigma_0 - \sigma_\infty)\exp\left[\frac{-t}{\tau_0}\exp\left(\frac{-E}{RT}\right)\right] + \sigma_\infty \qquad \text{(Equation 7.6)}$$

The values of σ_∞, E_a and $1/\tau_0$ found from the regression analysis are used in the above equation. It is obvious from the expression that the strength of the material is a function of $1/\tau$ and T. Since the temperature influences only the rate constant, the use of the Time and Temperature Superposition principle (TTSP) [5,6] is possible for this process. The amount by which the data must be shifted along the time axis to obtain a master curve for this process is given by,

$$\ln\left(\frac{\tau_R}{\tau}\right) = -\ln a_D \qquad \text{(Equation 7.7)}$$

where $\ln a_D$ is the shift distance along the time scale

$1/\tau_R$ is the rate constant at the reference temperature, T_R

Combining equation 7.7 and 7.5, we have,

$$-\ln a_D = -\frac{E_a}{R\left[\frac{1}{T} - \frac{1}{T_R}\right]} \qquad \text{(Equation 7.8)}$$

If the activation energy for the degradation process is determined from other experiments, the shift distance can be calculated from equation 7.8. The shift distance can be used for estimations of the rate of degradation at different temperatures. Thus it is sufficient to conduct experiments at only one temperature to predict the long-term properties at other temperatures.

7.3.2 Flexural Strength

The analysis procedure described in the previous section has been applied to the flexural strength data for the E-glass vinylester composites. Table 7.9 shows the flexural strength of the composite specimens immersed in deionized water at different temperatures.

Table 7.9. Flexural strength data for E-glass/Vinylester composite specimens immersed in deionized water attemperatures of 23 ^{o}C, 40 ^{o}C, 60 ^{o}C, 80 ^{o}C and 95 ^{o}C and under "control" conditions of 30 % RH at 23 ^{o}C

Time (days)	Control		23^{0}C		40^{0}C		60^{0}C		80^{0}C		95^{0}C	
	Flexural Strength (MPa)	Standard Deviation (MPa)	Flexural Strength (MPa)	Standard Deviation (MPa)	Flexural Strength (MPa)	Standard Deviation (MPa)	Flexural Strength (MPa)	Standard Deviation (MPa)	Flexural Strength (MPa)	Standard Deviation (MPa)	Flexural Strength (MPa)	Standard Deviation (MPa)
0	1106.89	60.19	1106.89	60.19	1106.89	60.19	1106.89	60.19	1106.89	60.19	1106.89	60.19
30	1133.85	73.91	1126.96	83.91	1092.34	13.65	913.01	59.50	526.21	70.46	459.12	47.37
90	1094.55	61.64	1104.96	31.17	772.08	80.47	670.86	62.40	423.96	77.29	426.86	51.50
180	1146.88	77.29	1086.83	57.16	748.36	65.78	556.07	89.29	402.93	66.67	373.84	71.29
270	1135.23	72.81	1064.83	72.26	726.92	43.09	512.42	70.46	381.21	38.89	347.29	49.71
360	1189.01	58.26	1036.70	24.55	744.22	51.37	471.81	45.09	369.84	50.13	314.95	56.47
540	1151.16	48.54	1001.68	40.89	591.44	42.68	409.83	38.27	336.40	3.93	260.35	8.48
720	1162.05	39.09	928.25	71.98	541.45	85.84	377.97	19.58	307.23	20.27	251.32	23.58
1080	1189.01	47.09	901.29	60.12	443.47	40.89	341.71	67.29	285.93	38.82	240.42	30.06
1440	1168.25	36.06	775.94	66.05	417.41	52.81	308.75	45.44	279.86	60.12	226.98	27.17

Equation 7.4 is fitted to the data in table 7.9 by using regression analysis. The lowest recorded value of the flexural strength for the harshest environment (95 ^{o}C deionized water, in this case) is taken as the initial estimation for σ_{∞}. The value of σ_{∞} is adjusted to find the minimum least squares sum. Analysis of the data using this technique yielded the following relationships:

$$\sigma_{23^0C} = 911.12 \exp\left(\frac{-t}{3071.6}\right) + 226.98 \qquad \text{(Equation 7.9 (a))}$$

$$\sigma_{40^0C} = 619.12 \exp\left(\frac{-t}{1139.9}\right) + 226.98 \qquad \text{(Equation 7.9 (b))}$$

$$\sigma_{60^0C} = 373.12 \exp\left(\frac{-t}{860.85}\right) + 226.98 \qquad \text{(Equation 7.9 (c))}$$

$$\sigma_{80^0C} = 216.37 \exp\left(\frac{-t}{831.94}\right) + 226.98 \qquad \text{(Equation 7.9 (d))}$$

$$\sigma_{95^0C} = 254.76 \exp\left(\frac{-t}{345.18}\right) + 226.98 \qquad \text{(Equation 7.9(e))}$$

The values of $1/\tau$ for the temperatures have been listed in Table 7.10. The values of $1/\tau$ are plotted against 1/T to find the values of E_a and $1/\tau_0$. Figure 7.12 shows the plot of $1/\tau$ against 1/T.

Equation 7.5 is fitted to the plot in the figure 7.12. The values of the activation energy and $1/\tau_0$ are calculated from the curve fit and are found to be,

E_a = 25.949 KJ/mol K

$1/\tau_0$ = 0.06894 days $^{-1}$

Combining equations 7.4 and 7.5 and substituting the values of the constants above, the Phani and Bose equations for different temperatures are determined. Equations 7.10 (a) through 7.10 (e) describe the Phani and Bose equations for different temperatures.

$$\sigma_{23^0C} = 474.90\exp\left(-3.823*10^{-4}t\right)+226.98 \qquad \text{(Equation 7.10 (a))}$$

$$\sigma_{45^0C} = 474.90\exp\left(-6.777*10^{-4}t\right)+226.98 \qquad \text{(Equation 7.10 (b))}$$

$$\sigma_{60^0C} = 474.90\exp\left(-1.234*10^{-3}t\right)+226.98 \qquad \text{(Equation 7.10 (c))}$$

$$\sigma_{80^0C} = 474.90\exp\left(-2.098*10^{-3}t\right)+226.98 \qquad \text{(Equation 7.10 (d))}$$

$$\sigma_{95^0C} = 474.90\exp\left(-3.008*10^{-3}t\right)+226.98 \qquad \text{(Equation 7.10 (e))}$$

The equation set 7.10 (a)-(e) gives the relationships between the flexural strength and the time at different temperatures. The predicted values of the flexural strength at different temperatures is compared with the experimental values in Table 7.11 and the experimental and predicted values for each temperature are plotted in Figs 7.13 through 7.17 to demonstrate the accuracy of the fit.

Table 7.10 Values of the characteristic time and the corresponding temperatures

Temperature of immersion (^{o}C)	Temperature of immersion (K)	1000/T(K)	$1/\tau$ (days $^{-1}$)
23	296	3.378	0.00032556
40	313	3.195	0.00087727
60	333	3.003	0.00116164
80	353	2.833	0.00120201
95	368	2.717	0.00289704

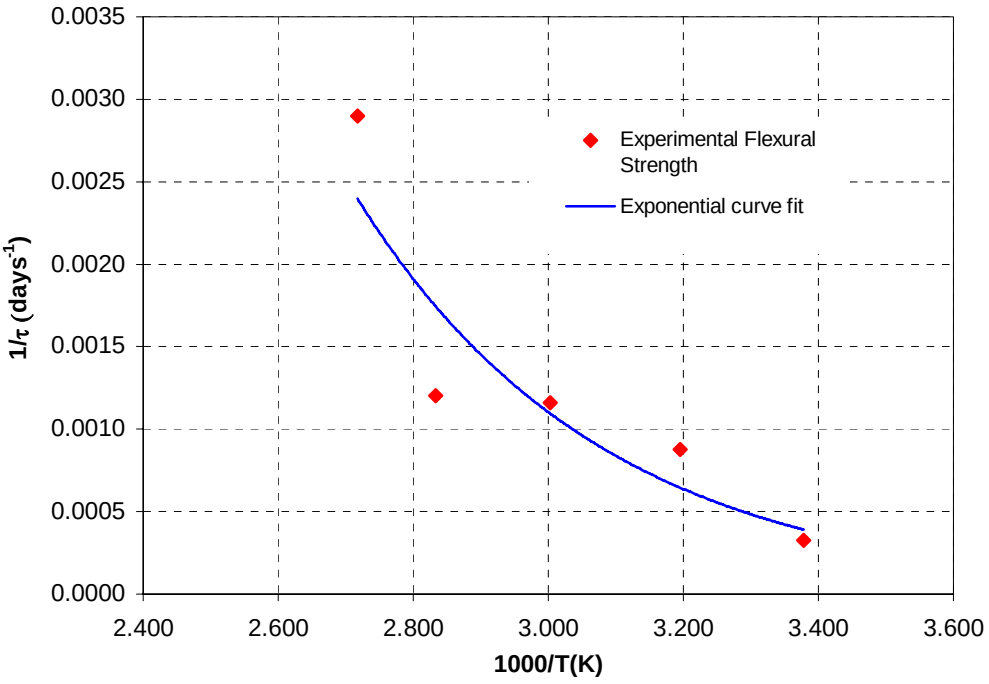

Fig. 7.12 (1/τ) Vs. (1/T)

Table 7.11 Comparison of experimental values of flexural strength with the predicted values using the Phani and Bose equations

Time (days)	23 °C			40 °C			60 °C			80 °C			90 °C		
	Exp *	Pred **	% Error	Exp	Pred	% Error	Exp	Pred	% Error	Exp	Pred	% Error	Exp	Pred	% Error
0	1106.9	1106.9	0.0	1106.9	1106.9	0.0	1106.9	1106.9	0.0	1106.9	1106.9	0.0	1106.9	1106.9	0.0
30	1106.9	696.4	-37.0	1092.3	692.3	-36.6	913.0	684.6	-25.0	526.2	672.9	27.8	459.1	660.9	43.9
90	1104.9	685.8	-37.9	772.0	673.7	-12.7	670.8	651.9	-2.8	423.9	620.1	46.2	426.5	589.2	38.0
180	1086.8	670.3	-38.3	748.3	647.3	-13.5	556.0	607.2	9.2	402.9	552.5	37.1	373.8	503.3	34.6
270	1064.8	655.3	-38.4	726.9	622.4	-14.3	512.4	567.3	10.7	381.2	496.5	30.2	347.2	437.7	26.0
360	1036.7	640.8	-38.1	744.2	599.0	-19.5	471.8	531.5	12.6	369.8	450.1	21.7	314.9	387.7	23.1
540	1001.7	613.3	-38.7	591.4	556.3	-5.9	409.8	470.8	14.9	336.4	379.9	12.9	260.3	320.5	23.1
720	928.2	587.6	-36.7	541.4	518.5	-4.2	377.9	422.3	11.7	307.2	331.8	8.0	251.3	281.4	11.9
1080	901.2	541.2	-39.9	443.4	455.4	2.6	341.7	352.2	3.0	285.9	276.2	-3.3	240.4	245.4	2.0
1440	775.9	500.8	-35.4	417.4	405.9	-2.7	308.7	307.3	-0.4	279.8	250.1	-10.6	226.9	233.2	2.7
1500	-	494.6		-	398.8		-	301.5		-	247.3		-	232.1	
2000	-	448.0		-	349.4		-	267.2		-	234.1		-	228.1	
4000	-	329.8		-	258.5		-	230.3		-	227.0		-	226.9	
8000	-	249.2		-	229.0		-	227.0		-	226.9		-	226.9	
10000	-	237.3		-	227.5		-	226.9		-	226.9		-	226.9	
20000	-	227.2		-	226.9		-	226.9		-	226.9		-	226.9	
30000	-	226.9		-	226.9		-	226.9		-	226.9		-	226.9	
40000	-	226.9		-	226.9		-	226.9		-	226.9		-	226.9	
50000	-	226.9		-	226.9		-	226.9		-	226.9		-	226.9	

* Exp – Experimental ** Pred – Predicted

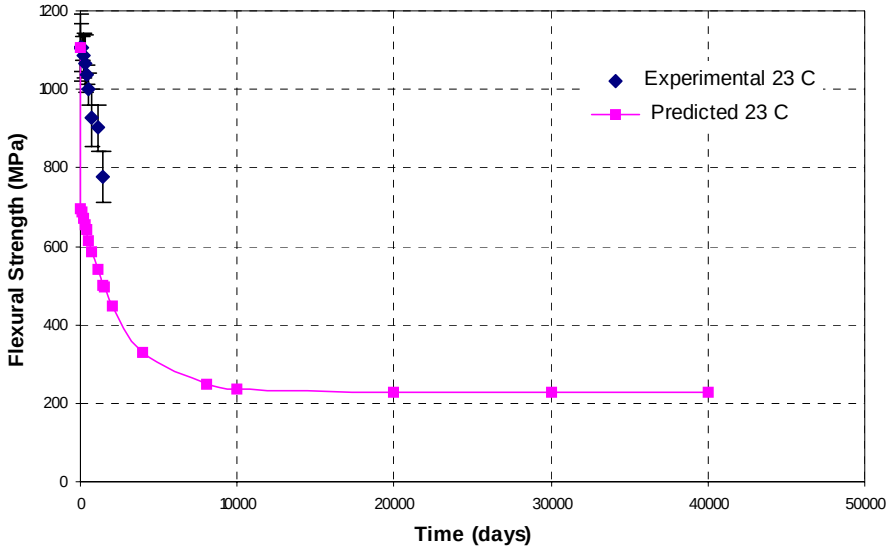

Fig. 7.13 Comparison of experimental values of flexural strength for specimens immersed in deionized water at 23 °C with the predicted values using the Phani and Bose equations

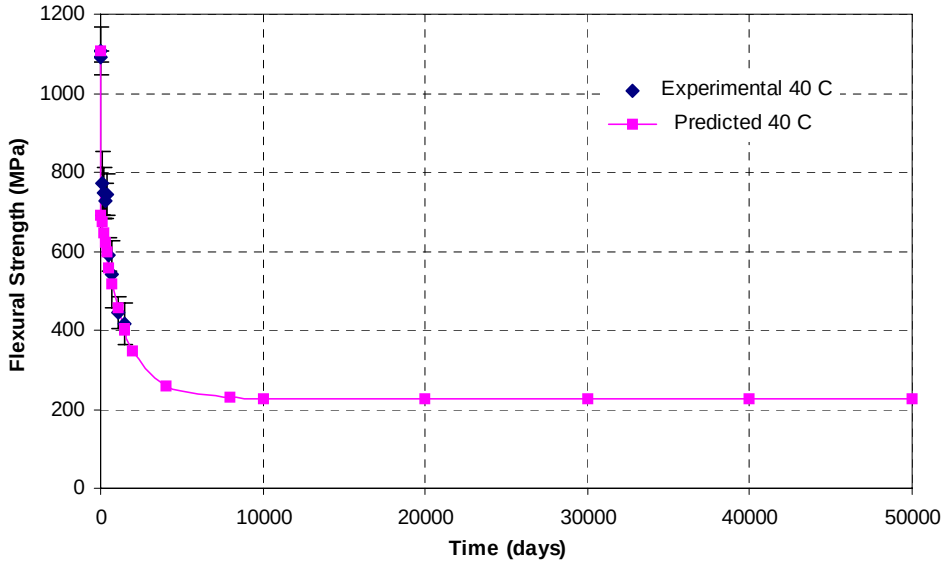

Fig. 7.14 Comparison of experimental values of flexural strength for specimens immersed in deionized water at 40 °C with the predicted values using the Phani and Bose equations

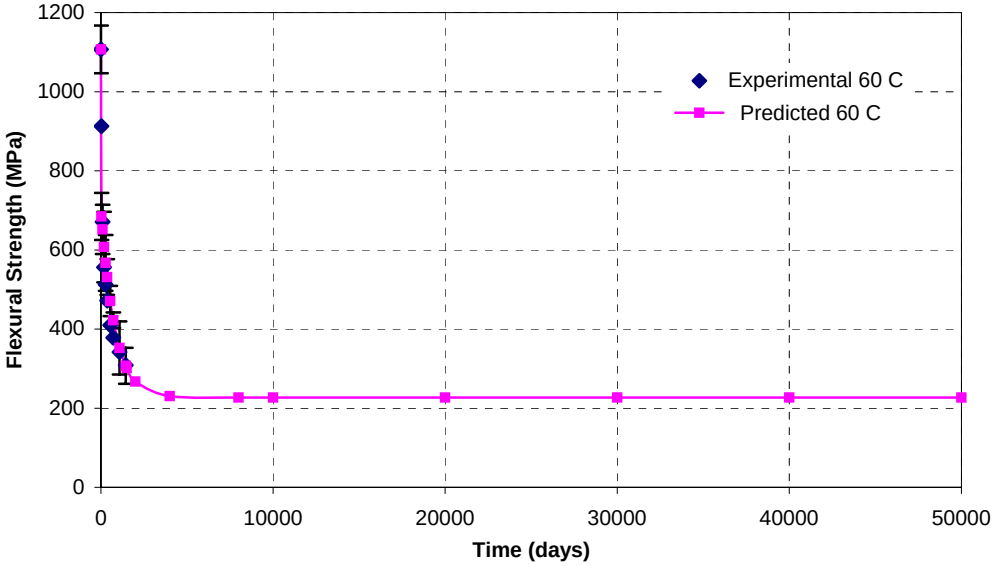

Fig. 7.15 Comparison of experimental values of flexural strength for specimens immersed in deionized water at 60 ^{o}C with the predicted values using the Phani and Bose equations

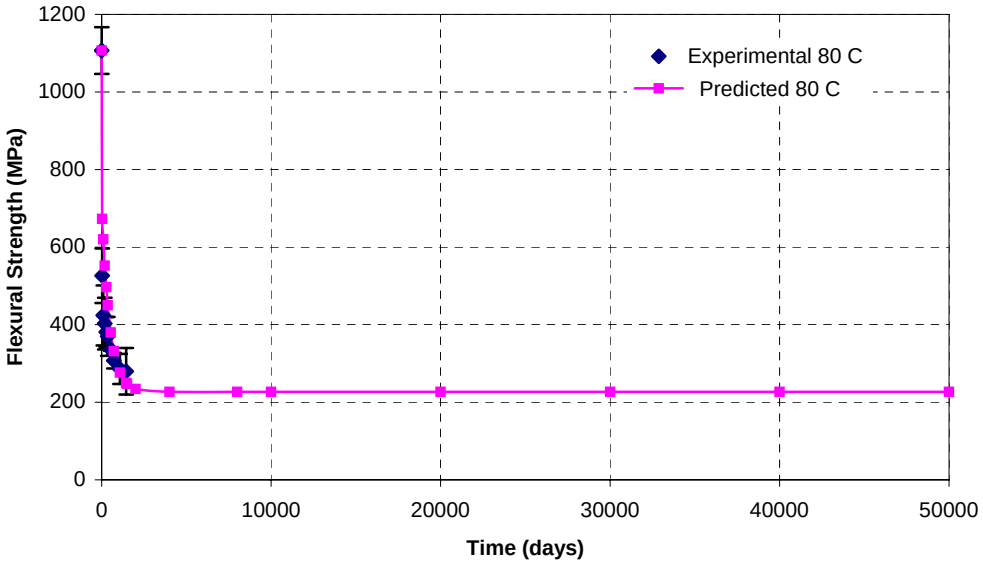

Fig. 7.16 Comparison of experimental values of flexural strength for specimens immersed in deionized water at 80 ^{o}C with the predicted values using the Phani and Bose equations

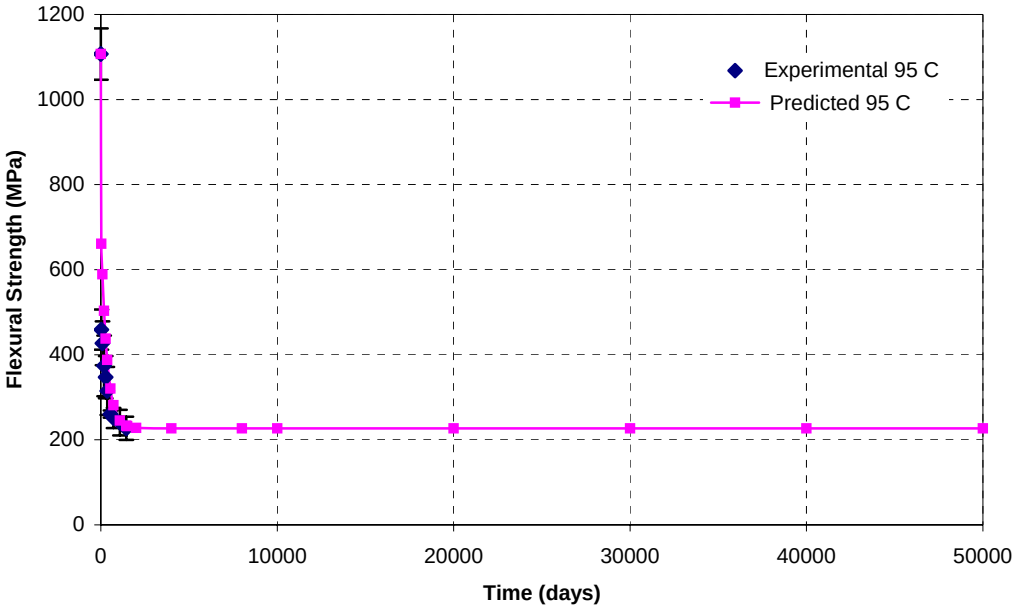

Fig. 7.17 Comparison of experimental values of flexural strength for specimens immersed in deionized water at 95 ^{o}C with the predicted values using the Phani and Bose equations

It is possible to predict the values of the flexural strength for all temperatures from data recorded at one temperature. This is done by applying the Time Temperature Superposition Principle to the data. The shift factors for each temperature are calculated from equations 7.7 and 7.8 by taking 23 ^{o}C (296 K) as the reference temperature. The shift factors calculated are listed below in Table 7.12.

The flexural strength values at different temperatures are plotted against $\ln(t/a_D)$ along with equations 7.10 (a)-(e) to obtain give the master curve for hygrothermal degradation of the E-glass/Vinylester composites (Fig 7.18).

Table 7.12 TTSP shift factors for flexural strength predictions

Temperature of immersion (^{o}C)	Temperature of immersion (K)	Shift factor a_D
40	313	0.5617
60	333	0.3074
80	353	0.1802
95	368	0.1254

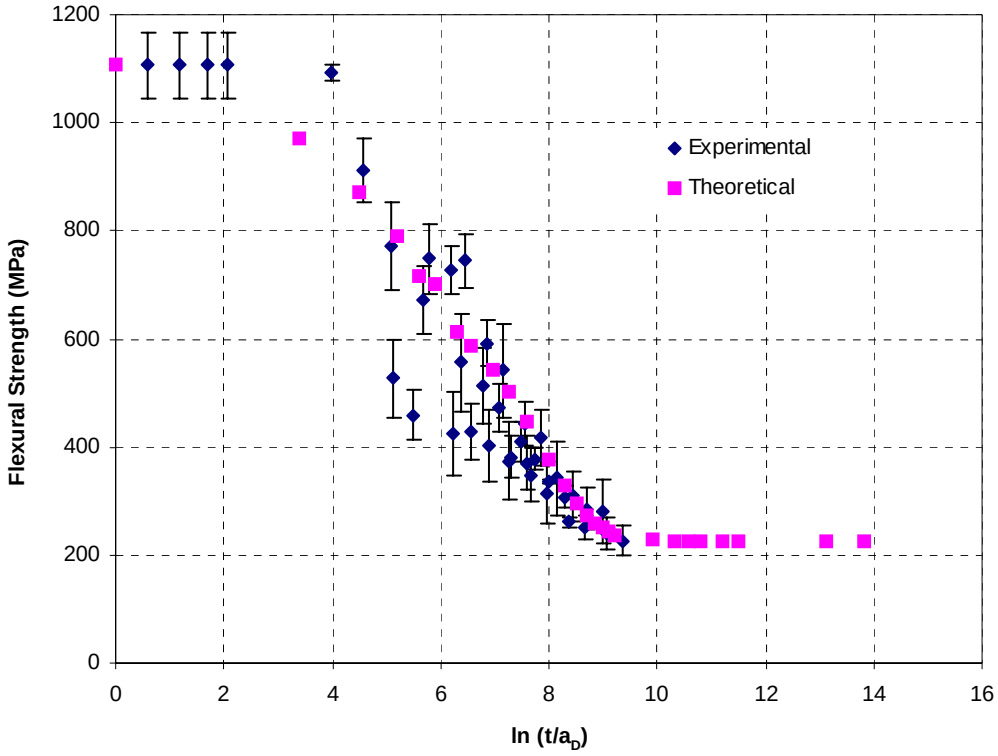

Fig. 7.18 TTSP – Master curve for long term predictions of flexural strength using the Phani and Bose method

7.3.3 Tensile Strength

The analysis procedure described in the previous section was applied to tensile strength data and the results are presented below. Table 7.13 gives the Phani and Bose equations corresponding to the tensile strength data. Table 7.14 compares the predicted values of tensile strength to the measured values at each temperature. Figures 7.19 through 7.23 display the accuracy of the Phani and Bose fit. Fig 7.24 shows the master curve for the prediction of tensile strength, obtained from Time and Temperature Superposition.

Table 7.13 Phani and Bose equations for tensile strength predictions at different temperatures

Temperature of immersion (^{o}C)	Phani and Bose Equation
23	$\sigma_{23C} = 275.03 \exp(-3.277 \times 10^{-4} t) + 172.02$
40	$\sigma_{40C} = 275.03 \exp(-5.141 \times 10^{-4} t) + 172.02$
60	$\sigma_{60C} = 275.03 \exp(-8.232 \times 10^{-4} t) + 172.02$
80	$\sigma_{80C} = 275.03 \exp(-1.250 \times 10^{-3} t) + 172.02$
95	$\sigma_{95C} = 275.03 \exp(-1.269 \times 10^{-3} t) + 172.02$

Table 7.14 Comparison of experimental values of tensile strength with the predicted values using the Phani and Bose equations

Time (days)	23 °C			40 °C			60 °C			80 °C			90 °C		
	Exp *	Pred **	% Error	Exp	Pred	% Error	Exp	Pred	% Error	Exp	Pred	% Error	Exp	Pred	% Error
0	684.65	684.65	0.00	684.65	684.65	0.00	684.65	684.65	0.00	684.65	684.65	0.00	684.65	684.65	0.00
30	686.03	444.36	-35.23	686.79	442.84	-35.52	469.67	440.34	-6.24	277.51	428.33	54.35	263.59	424.51	61.05
90	686.65	439.06	-36.06	534.83	434.61	-18.74	406.45	427.41	5.16	272.96	394.62	44.57	233.04	384.83	65.13
180	675.69	431.30	-36.17	511.32	422.74	-17.32	397.83	409.17	2.85	258.35	352.19	36.32	231.87	336.68	45.20
270	689.41	423.76	-38.53	525.17	411.41	-21.66	326.81	392.24	20.02	255.17	317.84	24.56	229.32	299.43	30.57
360	642.94	416.45	-35.23	467.12	400.58	-14.24	311.57	376.51	20.84	251.04	290.04	15.54	210.77	270.60	28.39
540	617.63	402.45	-34.84	394.17	380.38	-3.50	309.02	348.35	12.73	241.8	249.33	3.12	204.43	231.04	13.02
720	575.37	389.25	-32.35	362.6	361.97	-0.17	301.78	324.06	7.38	232.9	222.67	-4.39	195.47	207.36	6.08
1080	550.34	365.08	-33.66	326.6	329.88	1.00	279.31	285.06	2.06	215.39	193.75	-10.05	182.16	184.69	1.39
1440	515.93	343.60	-33.40	291.17	303.21	4.13	262.9	256.07	-2.60	197.12	181.35	-8.00	172.02	176.56	2.64
1500	-	340.26		-	299.22		-	252.02		-	180.12		-	175.85	
2000	-	314.84		-	270.39		-	225.03		-	174.52		-	172.94	
4000	-	246.18		-	207.21		-	182.24		-	172.04		-	172.02	
8000	-	192.02		-	176.52		-	172.40		-	172.02		-	172.02	
10000	-	182.40		-	173.63		-	172.09		-	172.02		-	172.02	
20000	-	172.41		-	172.03		-	172.02		-	172.02		-	172.02	
30000	-	172.03		-	172.02		-	172.02		-	172.02		-	172.02	
40000	-	172.02		-	172.02		-	172.02		-	172.02		-	172.02	
50000	-	172.02		-	172.02		-	172.02		-	172.02		-	172.02	

* Exp – Experimental ** Pred – Predicted

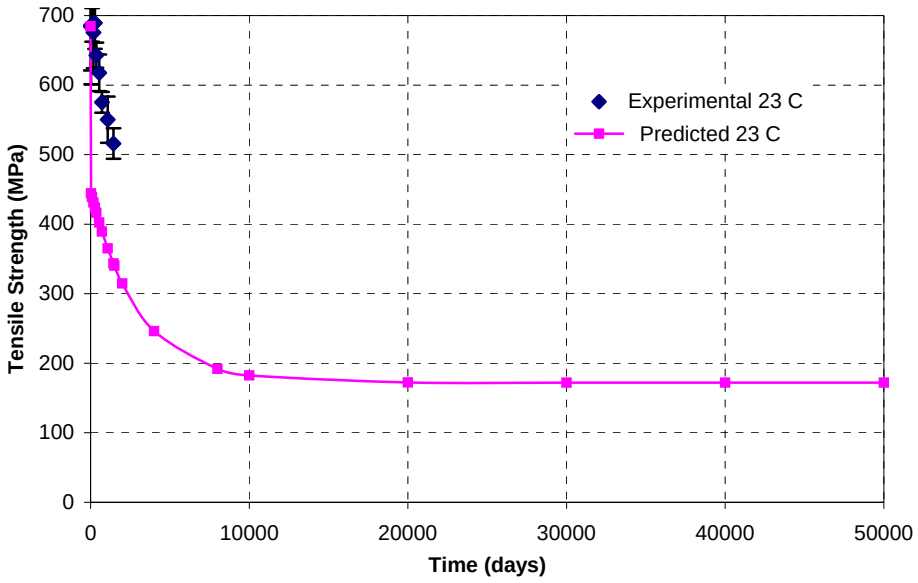

Fig. 7.19 Comparison of experimental values of tensile strength for specimens immersed in deionized water at 23 °C with the predicted values using the Phani and Bose equations

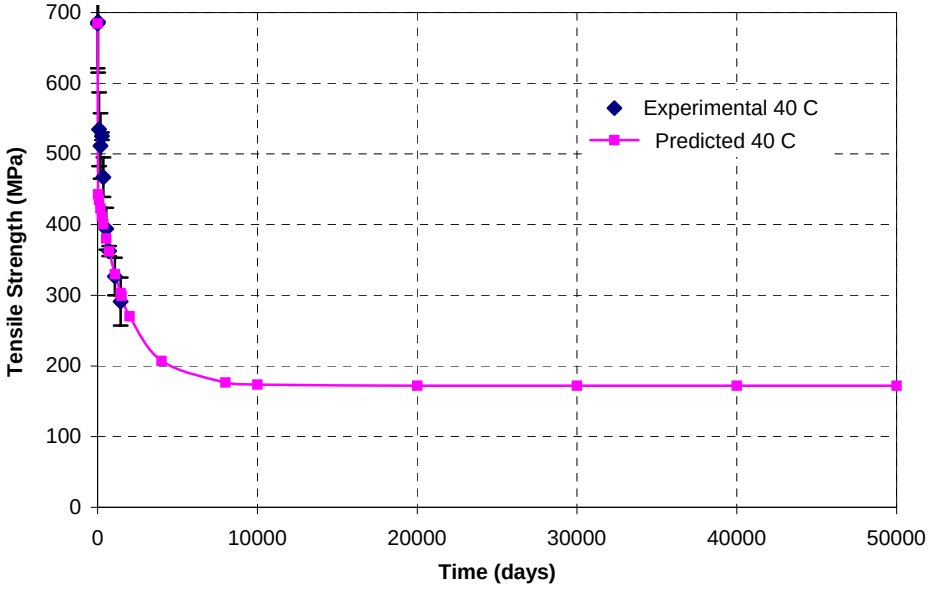

Fig. 7.20 Comparison of experimental values of tensile strength for specimens immersed in deionized water at 40 °C with the predicted values using the Phani and Bose equations

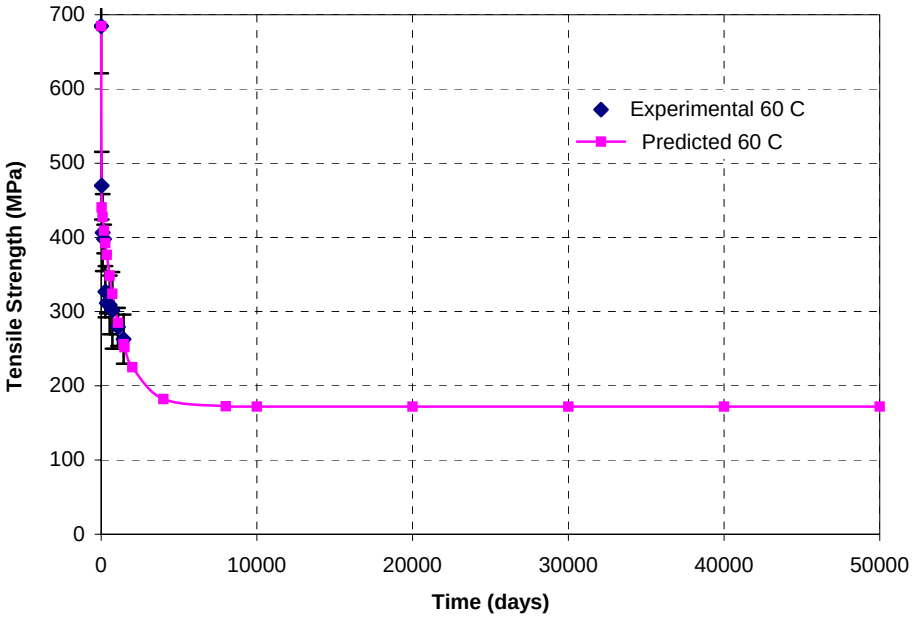

Fig. 7.21 Comparison of experimental values of tensile strength for specimens immersed in deionized water at 60 ^{o}C with the predicted values using the Phani and Bose equations

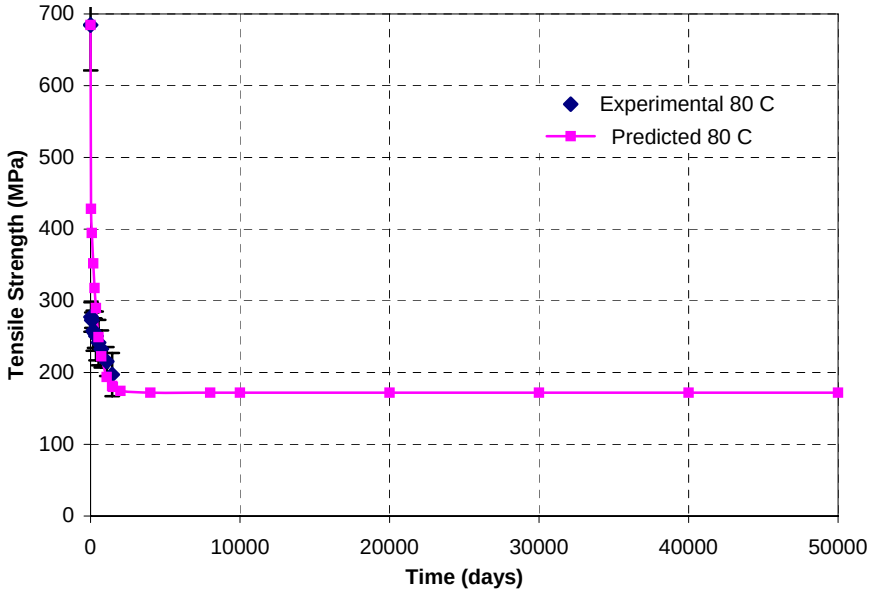

Fig. 7.22 Comparison of experimental values of tensile strength for specimens immersed in deionized water at 80 ^{o}C with the predicted values using the Phani and Bose equations

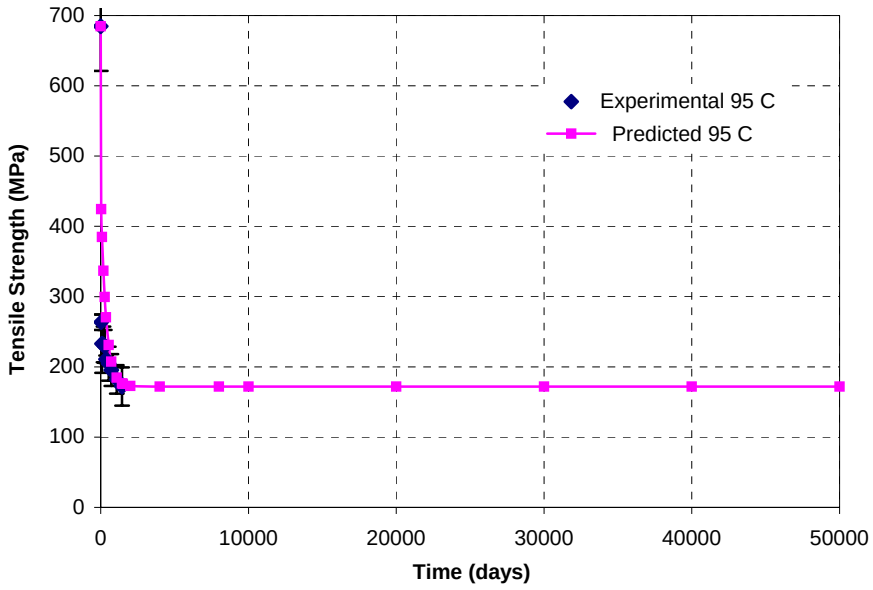

Fig 7.23 Comparison of experimental values of tensile strength for specimens immersed in deionized water at 95 ^{o}C with the predicted values using the Phani and Bose equations

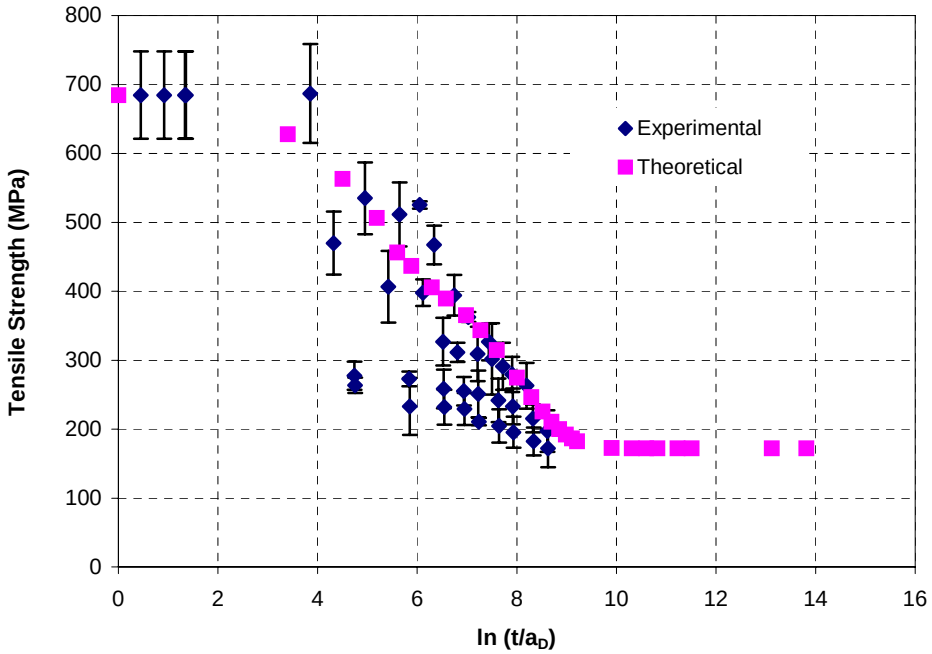

Fig. 7.24 TTSP – Master curve for long term predictions of tensile strength using the Phani and Bose method

7.3.4 Tensile Modulus

The analysis procedure described in the previous section was applied to tensile modulus data and the results are presented below. Table 7.15 gives the Phani and Bose equations corresponding to the tensile modulus data. Table 7.16 compares the predicted values of tensile modulus to the measured values at each temperature. Figures 7.25 through 7.29 display the accuracy of the Phani and Bose fit. Fig 7.30 shows the master curve for the prediction of tensile modulus, obtained from Time and Temperature Superposition.

Table 7.15 Phani and Bose equations for tensile modulus predictions at different temperatures

Temperature of Immersion (^{o}C)	Phani and Bose Equation
23	$E_{23C} = 7.657 \exp(-1.021 \times 10^{-4} t) + 31.23$
40	$E_{40C} = 7.657 \exp(-2.3123 \times 10^{-4} t) + 31.23$
60	$E_{60C} = 7.657 \exp(-5.4337 \times 10^{-4} t) + 31.23$
80	$E_{80C} = 7.657 \exp(-1.1591 \times 10^{-3} t) + 31.23$
95	$E_{95C} = 7.657 \exp(-1.9382 \times 10^{-3} t) + 31.23$

Table 7.16 Comparison of experimental values of tensile modulus with the predicted values using the Phani and Bose equations

Time (days)	23 °C			40 °C			60 °C			80 °C			90 °C		
	Exp *	Pred **	% Error	Exp	Pred	% Error	Exp	Pred	% Error	Exp	Pred	% Error	Exp	Pred	% Error
0	40.2	40.2	0.00	40.2	40.2	0.00	40.2	40.2	0.00	40.2	40.2	0.00	40.2	40.2	0.00
30	40.68	38.86	-4.46	39.3	38.83	-1.18	39.16	38.76	-1.01	37.99	38.63	1.67	37.78	38.45	1.79
90	39.71	38.82	-2.25	38.89	38.73	-0.41	38.13	38.52	1.03	36.68	38.13	3.95	35.65	37.66	5.64
180	39.99	38.75	-3.11	38.96	38.58	-0.99	38.13	38.17	0.12	36.47	37.45	2.67	34.96	36.63	4.78
270	39.37	38.68	-1.75	39.16	38.42	-1.88	38.4	37.84	-1.45	36.2	36.83	1.74	35.16	35.77	1.73
360	39.85	38.61	-3.11	38.96	38.28	-1.76	38.2	37.53	-1.76	35.51	36.27	2.15	35.23	35.04	-0.54
540	39.71	38.48	-3.11	38.68	37.99	-1.79	38.27	36.94	-3.47	35.09	35.32	0.67	34.82	33.92	-2.59
720	38.96	38.34	-1.58	38.82	37.71	-2.85	37.85	36.41	-3.81	33.44	34.55	3.33	32.82	33.13	0.93
1080	38.68	38.09	-1.53	37.85	37.20	-1.73	36.68	35.49	-3.25	31.92	33.42	4.70	31.37	32.17	2.56
1440	38.27	37.84	-1.12	37.99	36.72	-3.35	36.54	34.73	-4.95	32.68	32.67	-0.02	31.23	31.70	1.50
1500	-	37.80		-	36.64		-	34.62		-	32.58		-	31.65	
2000	-	37.47		-	36.05		-	33.81		-	31.98		-	31.39	
4000	-	36.32		-	34.27		-	32.10		-	31.30		-	31.23	
8000	-	34.61		-	32.43		-	31.33		-	31.23		-	31.23	
10000	-	33.99		-	31.99		-	31.26		-	31.23		-	31.23	
20000	-	32.22		-	31.31		-	31.23		-	31.23		-	31.23	
30000	-	31.59		-	31.24		-	31.23		-	31.23		-	31.23	
40000	-	31.36		-	31.23		-	31.23		-	31.23		-	31.23	
50000	-	31.28		-	31.23		-	31.23		-	31.23		-	31.23	

* Exp – Empirical ** Pred – Predicted

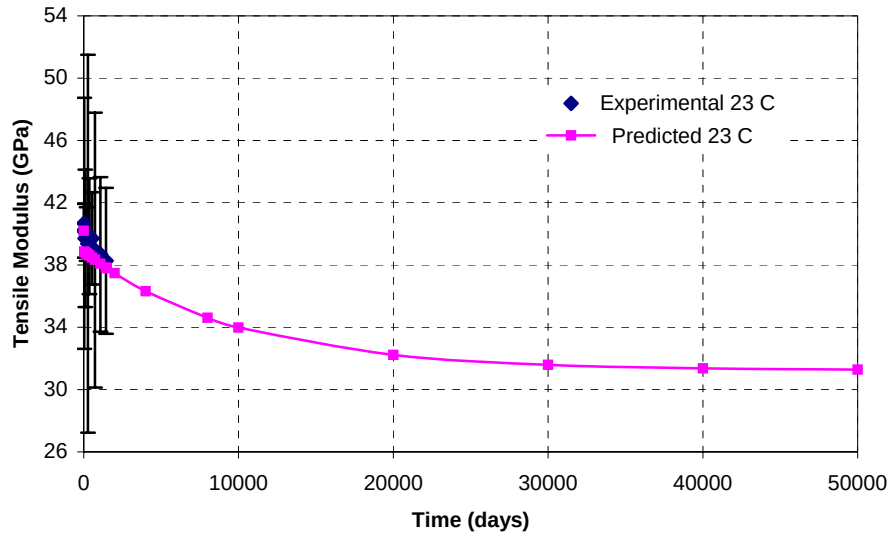

Fig. 7.25 Comparison of experimental values of tensile modulus for specimens immersed in deionized water at 23 °C with the predicted values using the Phani and Bose equations

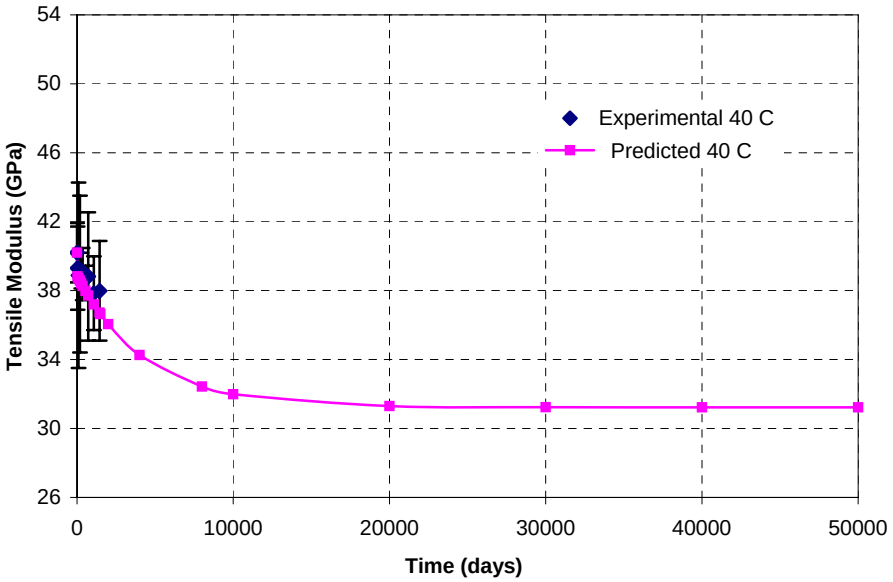

Fig. 7.26 Comparison of experimental values of tensile modulus for specimens immersed in deionized water at 40 °C with the predicted values using the Phani and Bose equations

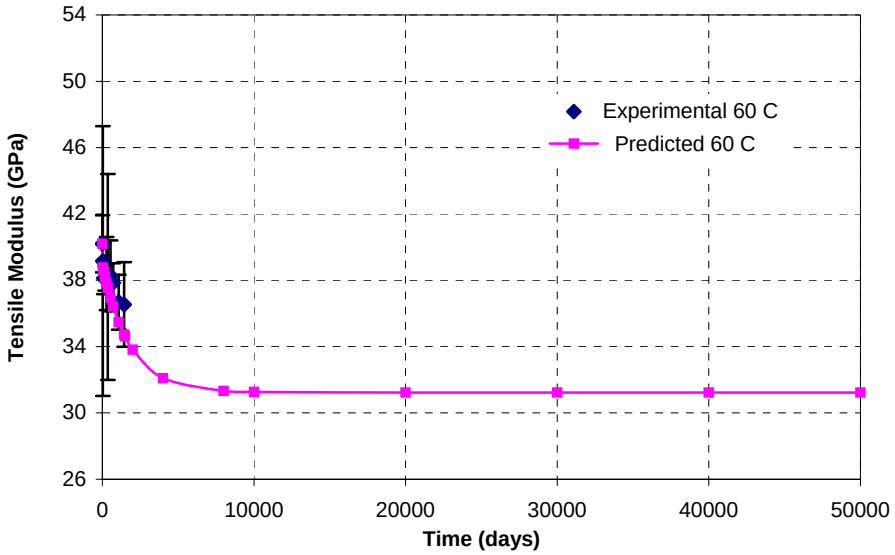

Fig. 7.27 Comparison of experimental values of tensile modulus for specimens immersed in deionized water at 60 ^{o}C with the predicted values using the Phani and Bose equations

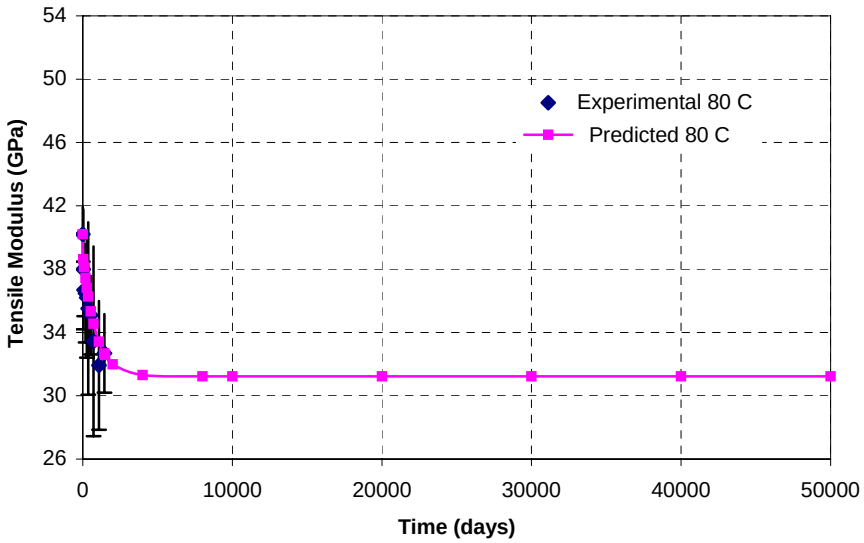

Fig. 7.28 Comparison of experimental values of tensile modulus for specimens mmersed in deionized water at 80 ^{o}C with the predicted values using the Phani and Bose equations

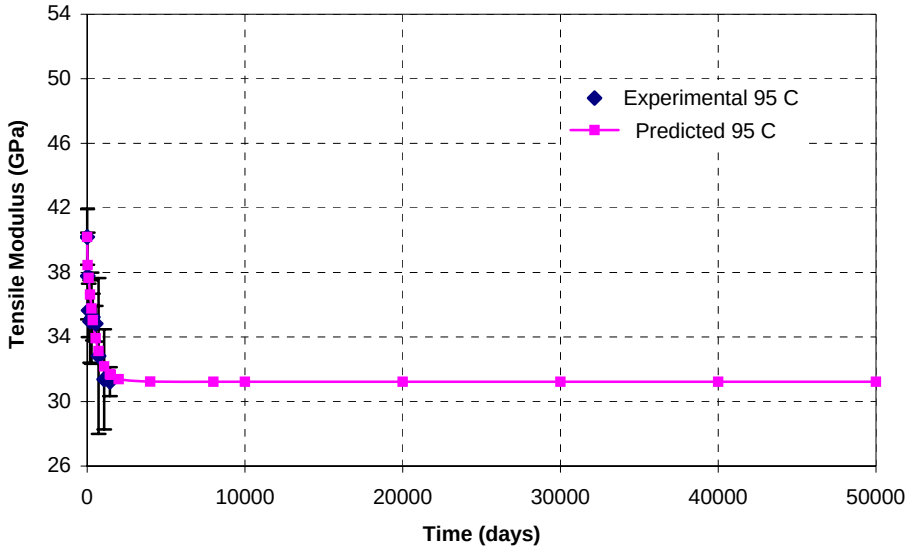

Fig. 7.29 Comparison of experimental values of tensile modulus for specimens immersed in deionized water at 95 ^{o}C with the predicted values using the Phani and Bose equations

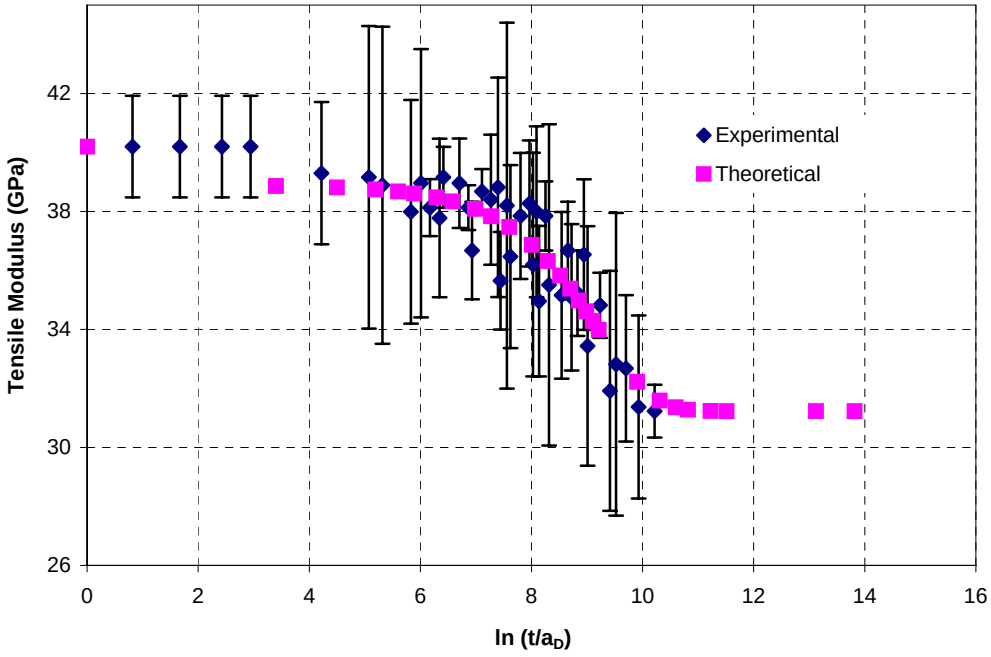

Fig. 7.30 TTSP – Master curve for long term predictions of tensile modulus using the Phani and Bose method

7.3.5 Short-Beam Shear Strength

The analysis procedure described in the previous section was applied to short-beam shear strength data and the results are presented below. Table 7.17 gives the Phani and Bose equations corresponding to the short-beam shear strength data. Table 7.18 compares the predicted values of short-beam shear strength to the measured values at each temperature. Figures 7.31 through 7.35 display the accuracy of the Phani and Bose fit. Fig 7.36 shows the master curve for the prediction of short-beam shear strength, obtained from Time and Temperature Superposition.

Table 7.17 Phani and Bose equations for short-beam shear strength predictions at different temperatures

Temperature of Immersion (^{o}C)	Phani and Bose Equation
23	$\sigma_{23C} = 41.84 \exp(-2.809 \times 10^{-4} t) + 10.96$
40	$\sigma_{40C} = 41.84 \exp(-6.013 \times 10^{-4} t) + 10.96$
60	$\sigma_{60C} = 41.84 \exp(-1.332 \times 10^{-3} t) + 10.96$
80	$\sigma_{80C} = 41.84 \exp(-2.698 \times 10^{-3} t) + 10.96$
95	$\sigma_{95C} = 41.84 \exp(-4.356 \times 10^{-3} t) + 10.96$

Table 7.18 Comparison of experimental values of short-beam shear strength with the predicted values using the Phani and Bose equations

Time (days)	23 °C			40 °C			60 °C			80 °C			90 °C		
	Exp *	Pred **	% Error	Exp	Pred	% Error	Exp	Pred	% Error	Exp	Pred	% Error	Exp	Pred	% Error
0	55.30	55.30	0.01	55.30	55.30	0.01	55.30	55.30	0.01	55.30	55.30	0.01	55.30	55.30	0.00
30	57.16	52.45	-8.24	55.71	52.05	-6.57	46.47	51.16	10.09	44.40	49.55	11.59	31.65	47.67	50.65
90	50.40	51.76	2.69	53.99	50.60	-6.28	46.75	48.07	2.84	34.27	43.78	27.76	22.75	39.23	72.42
180	50.40	50.74	0.67	48.47	48.51	0.08	37.58	43.88	16.78	33.51	36.70	9.54	24.34	30.06	23.51
270	50.06	49.74	-0.62	44.82	46.53	3.82	37.85	40.16	6.10	29.37	31.15	6.07	23.58	23.87	1.21
360	49.23	48.78	-0.92	43.57	44.66	2.48	30.89	36.86	19.34	26.06	26.80	2.83	18.89	19.68	4.18
540	44.54	46.91	5.32	42.61	41.20	-3.31	30.20	31.34	3.78	23.72	20.71	-12.70	14.27	14.94	4.69
720	42.89	45.14	5.25	39.51	38.10	-3.57	28.34	27.00	-4.74	19.65	16.96	-13.70	12.62	12.78	1.27
1080	40.54	41.85	3.23	37.09	32.82	-11.53	25.72	20.89	-18.78	17.03	13.23	-22.31	11.58	11.34	-2.11
1440	38.47	38.88	1.06	35.78	28.56	-20.18	24.20	17.11	-29.32	16.20	11.82	-27.05	10.96	11.04	0.70
1500	-	38.41		-	27.94		-	16.63		-	11.69		-	11.02	
2000	-	34.82		-	23.53		-	13.87		-	11.15		-	10.97	
4000	-	24.56		-	14.74		-	11.16		-	10.96		-	10.96	
8000	-	15.38		-	11.30		-	10.96		-	10.96		-	10.96	
10000	-	13.48		-	11.06		-	10.96		-	10.96		-	10.96	
20000	-	11.11		-	10.96		-	10.96		-	10.96		-	10.96	
30000	-	10.97		-	10.96		-	10.96		-	10.96		-	10.96	
40000	-	10.96		-	10.96		-	10.96		-	10.96		-	10.96	
50000	-	10.96		-	10.96		-	10.96		-	10.96		-	10.96	

* Exp- Empirical, ** Pred – Predicted

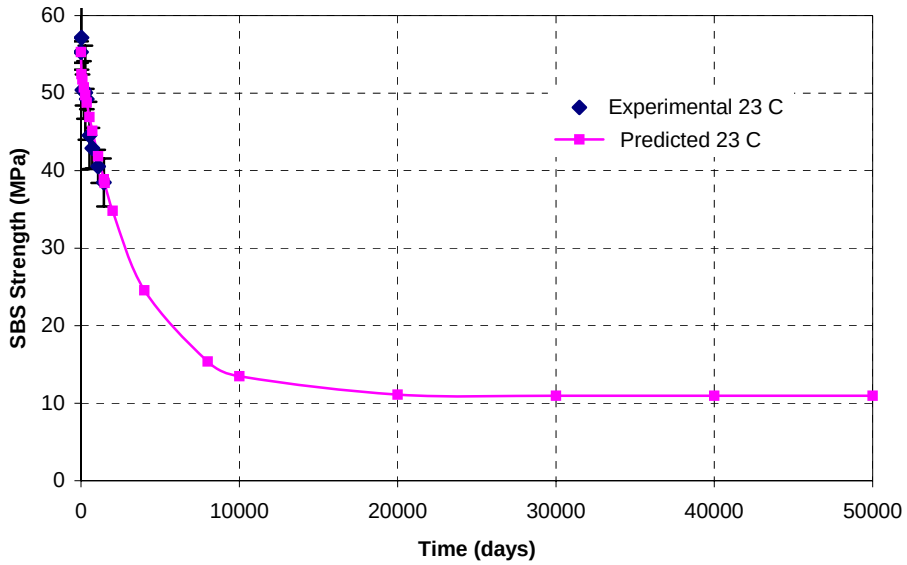

Fig. 7.31 Comparison of experimental values of short-beam shear strength for specimens immersed in deionized water at 23 ^{o}C with the predicted values using the Phani and Bose equations

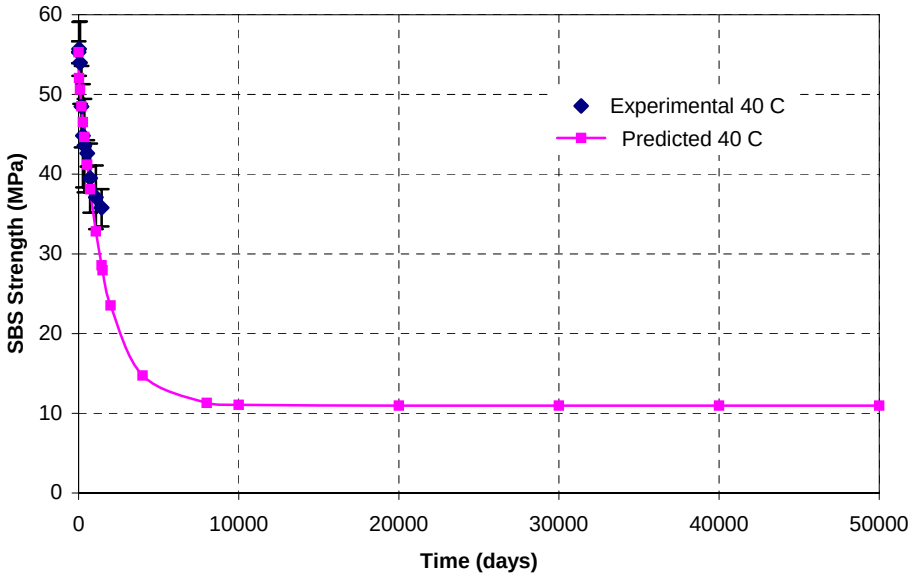

Fig 7.32 Comparison of experimental values of short-beam shear strength for specimens immersed in deionized water at 40 ^{o}C with the predicted values using the Phani and Bose equations

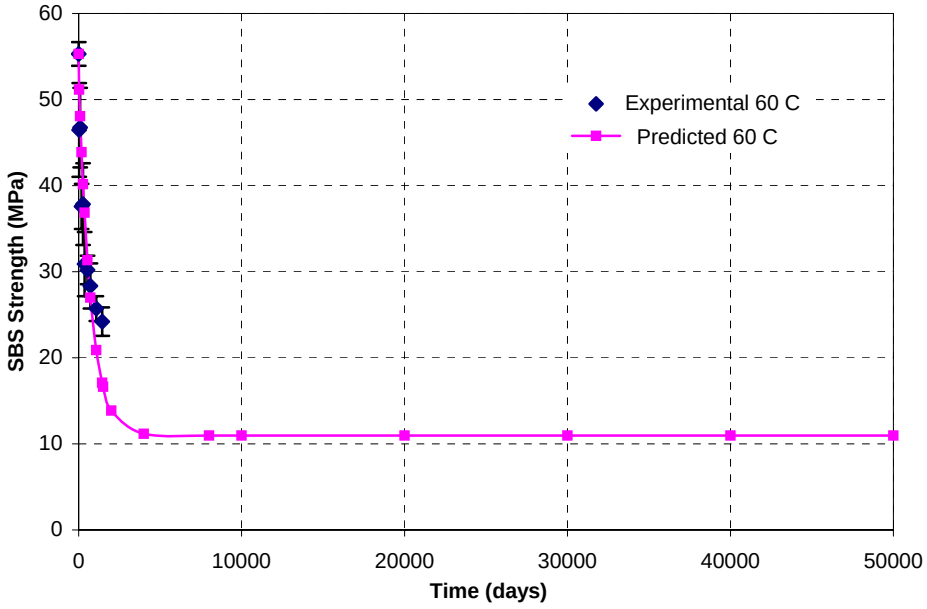

Fig. 7.33 Comparison of experimental values of short-beam shear strength for specimens immersed in deionized water at 60 ^{o}C with the predicted values using the Phani and Bose equations

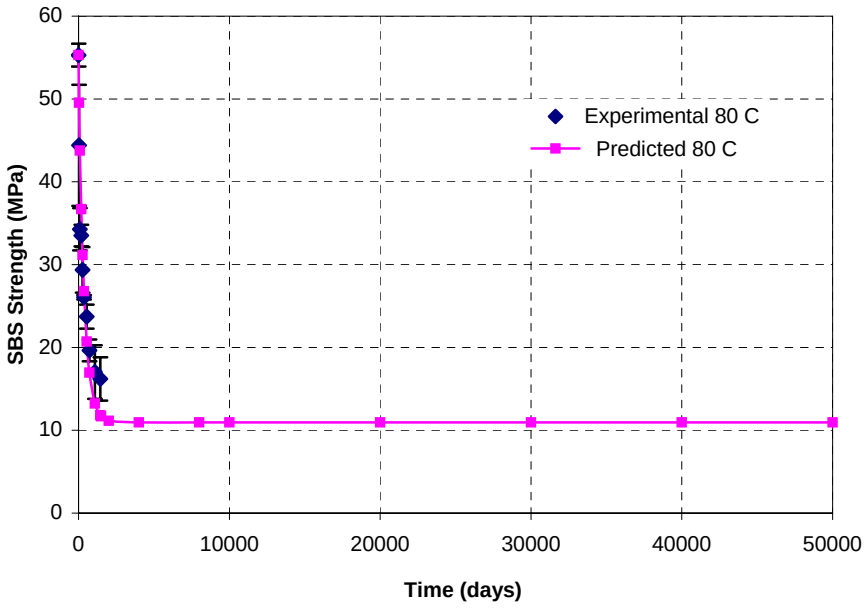

Fig 7.34 Comparison of experimental values of short-beam shear strength for specimens immersed in deionized water at 80 ^{o}C with the predicted values using the Phani and Bose Equations

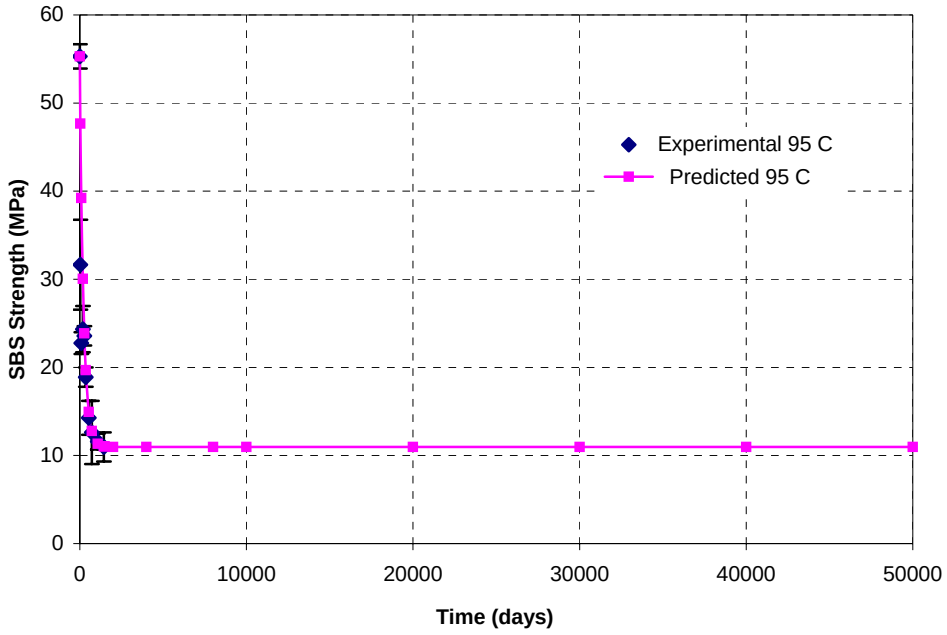

Fig. 7.35 Comparison of experimental values of short-beam shear strength for specimens immersed in deionized water at 95 °C with the predicted values using the Phani and Bose equations

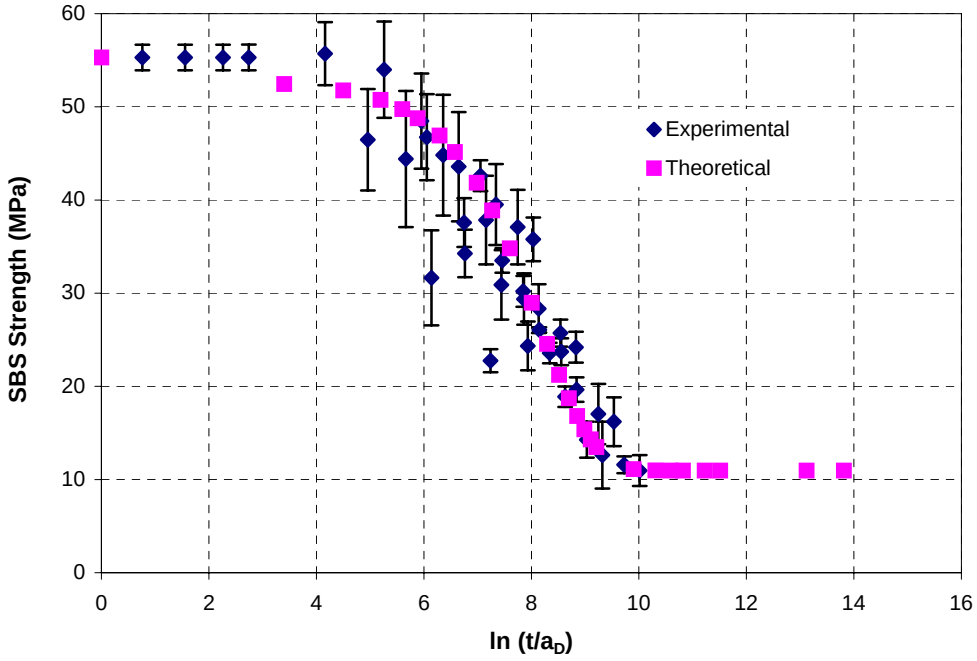

Fig. 7.36 TTSP – Master curve for long term predictions of short-beam shear strength using the Phani and Bose method

7.3.6 Summary – Phani and Bose Prediction

It can be noted from the tables 7.11, 7.14 and 7.18 that the Phani and Bose theory predicts a very steep initial decrease in flexural, tensile and short-beam shear strength. It can also be seen from the figures 7.13 through 7.31 that the use of Phani and Bose method predicts that the strength reaches a constant value after a period of time. This can be seen from the figures 7.13 through 7.31. The Phani and Bose model does not account for increase in performance characteristic initially, before the onset of degradation. This is reflected in the larger deviations from the experimental values of strength, in the initial periods of exposure (Tables 7.11, 7.14, 7.16 and 7.18).

7.4 Comparison of Predictive Models

The Arrhenius Rate Model and the Phani and Bose Method used to predict the long-term mechanical properties are compared in this section. The Arrhenius Rate Model is a rate-based model specifically meant for temperature-dependence and therefore can be used only for temperature-accelerated tests. The Arrhenius Rate Model assumes that there is a continuous loss of properties throughout the exposure time. But the current investigation suggests that the composite specimens experience an initial increase in performance due to initial post-cure. Due to this, the Arrhenius Rate Model may not be suitable to predict strength properties for short-term exposures. The Arrhenius model also assumes that the degradation occurs only due a single process.

The Phani and Bose Model also does not take into account the initial post-cure at ambient conditions. Using the Time and Temperature superposition principle and the activation energy of the degradation process, the mechanical strength of the composite

specimen at any temperature can be calculated from experiments conducted only at one temperature.

Tables 7.19, 7.20, 7.21 and 7.22 compare the predictions of tensile strength, tensile modulus, flexural strength and short-beam shear strength respectively from the two models. Figures 7.37 through 7.40 compare the results from the two models graphically. By examining the comparison tables the following can be inferred. For tensile strength and tensile modulus, both the models seems to agree with the experimental data very well at least for the short-term exposures, with the Arrhenius predictions being more conservative than those of the Phani and Bose model. The Arrhenius model predicts 52 % retention in tensile strength and the Phani and Bose model predicts 50 % retention at the end of 4 years (Experimental – 63% at the end of 4 years). For the tensile modulus, the Arrhenius model predicts 93% retention and the Phani and Bose model predicts 94 % retention at the end of 4 years (Experimental – 93 % at the end of 4 years).

On the other hand, for flexural and short-beam shear strength, the Arrhenius model predictions do not agree as well as the Phani and Bose predictions. This can be seen from the relatively high error percentages for the predictions of the Arrhenius model. The Arrhenius model predicts 38 % retention in flexural strength and the Phani and Bose model predicts 45 % retention at the end of 4 years (Experimental – 66% at the end of 4 years). For the short-beam shear strength, the Arrhenius model predicts 48.5 % retention and the Phani and Bose model predicts 70 % retention at the end of 4 years (Experimental – 67 % at the end of 4 years).

Table 7.19 Comparison of predictions for tensile strength retention for specimens immersed in 23 ^{0}C deionized water

Time (years)	Experimental values	Predicted values- Arrhenius method	% Error	Predicted values- Phani and Bose method	% Error
0	100.00	100.00	0.00	100.00	0.00
0.08	83.82	77.70	-7.31	64.91	-22.56
0.25	83.90	70.50	-15.97	64.11	-23.58
0.5	82.56	65.96	-20.11	62.96	-23.74
0.75	84.24	63.30	-24.86	61.85	-26.58
1	78.56	62.62	-20.28	60.77	-22.65
1.5	75.47	58.76	-22.14	58.70	-22.22
2	70.30	56.87	-19.10	56.75	-19.28
3	67.25	54.21	-19.39	53.19	-20.91
4	63.04	52.32	-17.00	50.02	-20.65
5	-	50.77	-	47.22	-
10	-	46.22	-	37.27	-
15	-	43.57	-	31.81	-
20	-	41.68	-	28.80	-
30	-	39.02	-	26.24	-
40	-	37.14	-	25.46	-
50	-	35.68	-	25.23	-
75	-	33.01	-	25.13	-
100	-	31.13	-	25.13	-
150	-	28.47	-	25.13	-
200	-	26.59	-	25.13	-

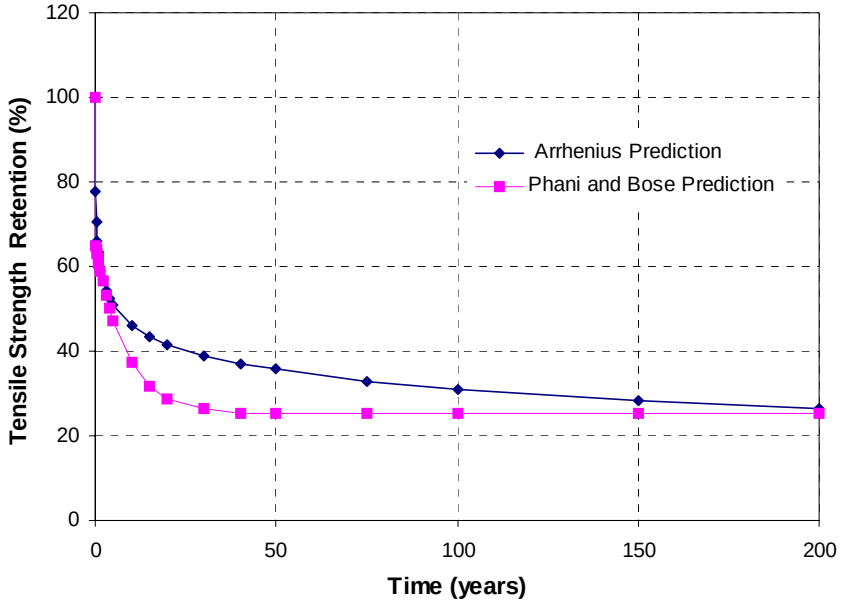

Fig. 7.37 Comparison of predictions for tensile strength retention for specimens immersed in 23 ^{0}C deionized water

Table 7.20 Comparison of predictions for tensile modulus retention for specimens immersed in 23 ^{0}C deionized water

Time (years)	Experimental values	Predicted values- Arrhenius method	% Error	Predicted values- Phani and Bose method	% Error
0	100.00	100.00	0.00	100.00	0.00
0.08	98.99	96.39	-2.63	96.68	-2.34
0.25	96.64	95.22	-1.47	96.56	-0.09
0.5	97.32	94.48	-2.91	96.38	-0.96
0.75	95.81	94.05	-1.83	96.21	0.42
1	96.98	93.75	-3.33	96.04	-0.97
1.5	96.64	93.32	-3.44	95.70	-0.98
2	94.80	93.01	-1.89	95.37	0.60
3	94.13	92.58	-1.64	94.72	0.63
4	93.12	92.58	-0.58	94.10	1.05
5	-	92.02	-	93.50	-
10	-	91.29	-	90.81	-
15	-	90.86	-	88.58	-
20	-	90.55	-	86.73	-
30	-	90.12	-	83.91	-
40	-	89.82	-	81.98	-
50	-	89.58	-	80.64	-
75	-	89.15	-	78.85	-
100	-	88.84	-	78.15	-
150	-	88.41	-	77.76	-
200	-	88.11	-	77.70	-

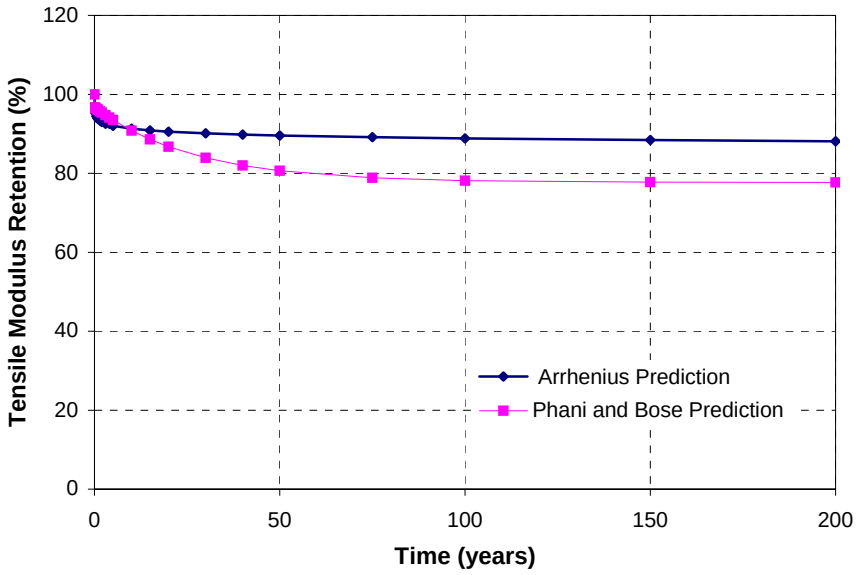

Fig. 7.38 Comparison of predictions for tensile modulus retention for specimens immersed in 23 ^{0}C deionized water

Table 7.21 Comparison of predictions for flexural strength retention for specimens immersed in 23 ^{0}C deionized water

Time (years)	Experimental values	Predicted values-Arrhenius method	% Error	Predicted values-Phani and Bose method	% Error
0	100.00	100.00	0.00	100.00	0.00
0.08	96.46	79.74	-17.34	62.93	-34.76
0.25	94.58	65.36	-30.90	61.94	-34.51
0.5	93.03	58.61	-37.00	60.52	-34.95
0.75	91.15	54.66	-40.03	59.15	-35.11
1	88.74	51.87	-41.55	57.82	-34.84
1.5	85.74	47.92	-44.11	55.31	-35.50
2	79.46	45.12	-43.22	52.96	-33.34
3	77.15	41.17	-46.63	48.73	-36.83
4	66.42	38.38	-42.22	45.06	-32.16
5	-	36.07	-	41.86	-
10	-	29.32	-	31.13	-
15	-	25.38	-	25.80	-
20	-	22.58	-	23.14	-
30	-	15.84	-	21.16	-
40	-	13.66	-	20.67	-
50	-	9.71	-	20.55	-
75	-	6.92	-	20.51	-
100	-	5.92	-	20.51	-
150	-	2.96	-	20.51	-

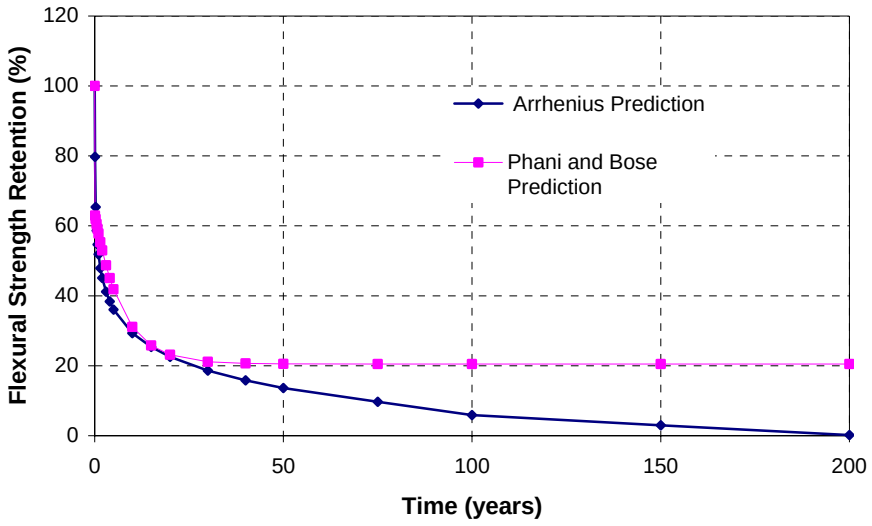

Fig. 7.39 Comparison of predictions for flexural strength retention for specimens immersed in 23 ^{0}C deionized water

Table 7.22 Comparison of predictions for short-beamshear strength retention for specimens immersed in 23 ^{0}C deionized water

Time (years)	Experimental values	Predicted values- Arrhenius method	% Error	Predicted values- Phani and Bose method	% Error
0	100.00	100.00	0.00	100.00	0.00
0.08	99.04	97.19	-1.87	94.86	-4.22
0.25	87.34	73.70	-15.62	93.56	7.13
0.5	87.34	67.40	-22.83	91.70	5.00
0.75	86.74	63.71	-26.54	89.88	3.62
1	85.30	61.10	-28.38	88.11	3.28
1.5	77.18	57.41	-25.61	84.69	9.73
2	74.31	54.80	-26.26	81.45	9.61
3	70.25	51.12	-27.24	75.45	7.39
4	66.67	48.50	-27.25	70.03	5.04
5	-	46.35	-	65.13	-
10	-	40.05	-	46.96	-
15	-	36.36	-	36.07	-
20	-	33.75	-	29.55	-
30	-	30.07	-	23.31	-
40	-	27.45	-	21.07	-
50	-	25.42	-	20.27	-
75	-	21.74	-	19.85	-
100	-	19.12	-	19.82	-

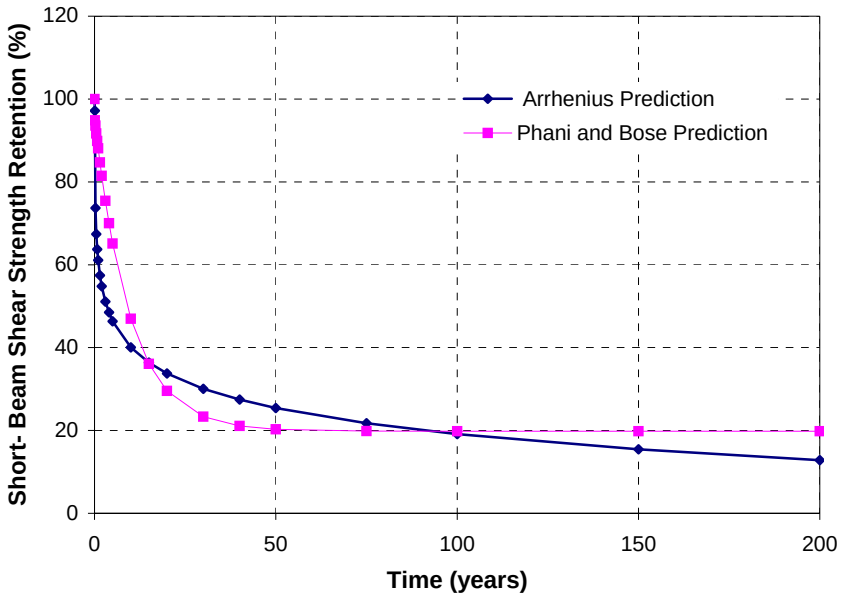

Fig. 7.40 Comparison of predictions for short-beam shear strength retention for specimens immersed in 23 ^{0}C deionized water

7.5 References

1. Reliasoft Corporation Website, www.reliasoft.com

2. Phani K.K. and Bose N.R., "Hydrothermal Ageing of CSM- Laminate During Water Immersion- An Acousto-Ultrasonic Study", *Journal of Materials Science*, October 1986, Vol. 21, Issue10, pp. 3633-3637.

3. Phani K.K. and Bose N.R., "Temperature Dependence of Hydrothermal Ageing of CSM- Laminate During Water Immersion", *Composites Science and Technology*, 1987, Vol. 29, Issue 2, pp. 79-87.

4. Abanilla M.A., "Physico-Chemico Effects on T700 Based Fabric," Master's Thesis, Department of Structural Engineering, University of California, San Diego, 2004, 260 pages.

5. Kuraishi A., "Durability Analysis of Composite Structures Using the Accelerated Testing Methodology", Doctoral Dissertation, Department of Aeronautics and Astronautics, Stanford, California, Stanford University, 2001, 143 pages.

6. Fesko D.G., "Time-Temperature Superposition for Block Copolymers", Doctoral Dissertation, Department of Materials Science, Pasadena, California, California Institute of Technology**,** 1971**,** 202 pages.

7. Nguyen V.T., "Durability of E-glass/vinylester composites in a marine environment", Master's Thesis, Department of Structural Engineering, University of California, San Diego, 2004, 282 pages.

8. Aveston J., Kelly A., and Sillwood J.M., "Long-term Strength of Glass Reinforced Plastics in Wet Environment ", Advances in Composite Materials, Vol I, A. R. Bunsell, C.R. Bathias, A. Martrenchar, D. Henkes and G. Verchery Ed., Pergamon Press, Paris, 1980, pp. 557-568.

Chapter 8

Prediction of Life under Varying Conditions of Humidity Exposure

8.1 Introduction

The long-term durability characteristics of E-glass Vinylester composites in humid environments are studied by the Arrhenius Rate prediction model in this section. The Arrhenius Model is used to predict the short-beam shear strength for the E-glass vinylester composites exposed to relative humidity levels between 0 and 98 % RH at temperatures of 23 ^{0}C and 95 ^{0}C. The relationship between relative humidity and dew point temperature is used in integration with the Arrhenius model.

The predictions are made using relative humidity in place of temperature in the Arrhenius Model. The Arrhenius Rate equation is given by Equation 8.1 [1].

$$k=A\exp\left[\frac{-E_a}{RT}\right] \qquad \text{Equation 8.1}$$

where k is the rate coefficient, A is a constant, E_a is the activation energy in kJ/mol , R is the universal gas constant (8.314 x 10^{-3} kJ $mol^{-1}K^{-1}$) and T is the temperature in Kelvin.

The relative humidity ϕ and the dew point temperature T_d are two widely used indicators of the amount of moisture in air. The relationship between relative humidity and dew point temperature is given by the equation 8.2 [2].

$$T_d=\frac{b*\gamma(T,\varphi)}{a-\gamma(T,\varphi)} \qquad \text{Equation 8.2}$$

where $$\gamma(T,\varphi)=\frac{aT}{b+T}+\ln(\varphi)$$ Equation 8.2 a

where T is the air temperature in degrees Celsius, ϕ is the relative humidity as a fraction, T_d is the dew point temperature in degrees Celsius, a is a constant (with a value of 17.27) and b is another constant (with a value of 237.7 ^{0}C). Equation 8.2 is valid only for following conditions: 0 ^{0}C < T < 60 ^{0}C, 0.01 < ϕ < 1.0 and 0 ^{0}C < T_d < 50 ^{0}C.

Equation 8.2 can be approximated with good accuracy [2] as

$$T_d=T-\frac{(1-\varphi)}{0.05}$$ Equation 8.3

where T is the air temperature in degrees Kelvin and T_d is the dew point temperature in degrees Kelvin and ϕ is the relative humidity as a fraction. Given that the dew point temperature does not change for a given air temperature and relative humidity, equation 8.3 can be substituted in the Arrhenius Model and the relative humidity can be used in place of temperature such that,

$$k = A\exp\left[\frac{-E_a}{R\left[T_d+\frac{1-\varphi}{0.05}\right]}\right]$$ Equation 8.4

The above approach is combined with the procedure described in section 7.2 of chapter 7 and the short-beam shear strength is predicted for the composite specimens in humid air at 23 ^{0}C and 95 ^{0}C. It has to be noted that equation 8.2 is not strictly valid for the temperature of 95 ^{0}C. Nevertheless, the same procedure is followed in this chapter as a first approximation. As a result of the exposure temperature being outside the validity range of the equation, the short-

beam shear strength predictions for the 95 ^{0}C exposure can be expected to yield comparatively larger errors, as is seen in the following discussion of the results.

8.2 Predictions for exposure conditions of humid air at 23 ^{0}C

The Arrhenius prediction of short-beam shear strength, for the specimens exposed to relative humidities at 23 ^{o}C is summarized in tables 8.1 to 8.4 and figures 8.1 to 8.4. The predicted values of short-beam shear strength agree well with the experimental values for the humidity levels of 45%, 60% and 75%. For the 98% humidity specimen, the model predicts a faster rate of decrease in the short-beam shear strength than seen experimentally. .

Table 8.1 Predicted values of short-beam shear strengthin comparison with experimentally obtained values forspecimens exposed to 45% relative humidity at 23 ^{o}C

Time (years)	Predicted values of percent retention– Arrhenius rate model	Experimentally obtained average values	Percentage error
0	100.00	100.00	0.00
0.08	97.76	100.48	-2.71
0.25	97.03	99.28	-2.27
0.5	96.58	95.34	1.30
0.75	96.31	93.67	2.82
1	96.12	93.43	2.88
1.5	95.85	93.07	2.99
2	95.66	93.55	2.26
3	95.40	92.11	3.56
4	95.21	91.76	3.76
5	95.35	-	-
10	94.59	-	-
15	94.33	-	-
20	94.13	-	-
30	93.87	-	-
40	93.68	-	-
50	93.53	-	-
75	93.26	-	-
100	93.07	-	-
150	92.81	-	-
200	92.62	-	-

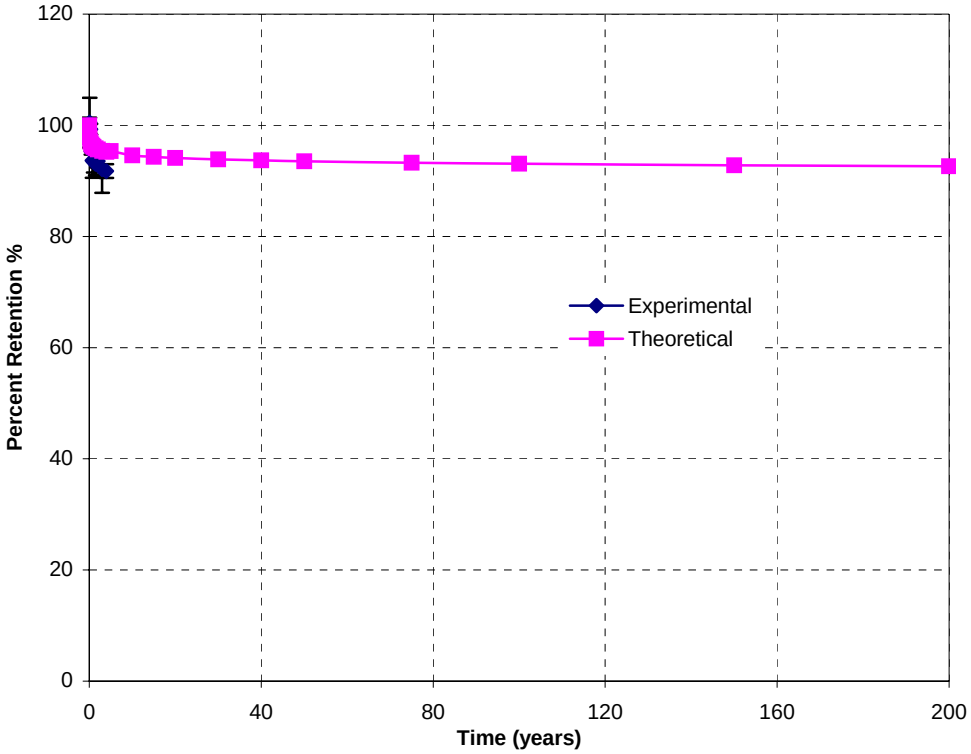

Fig. 8.1 Comparison between the experimental and predicted values of short-beam shear strength for specimens exposed to 45% relative humidity at 23 ^{o}C

Table 8.2 Predicted values of short-beam shear strength in comparison with experimentally obtained values for specimens exposed to 60% relative humidity at 23 °C

Time (years)	Predicted values of percent retention– Arrhenius rate model	Experimentally obtained average values	Percentage error
0	100.00	100.00	0.00
0.08	94.30	99.76	-5.47
0.25	92.46	96.06	-3.74
0.5	91.30	94.50	-3.39
0.75	90.62	93.19	-2.75
1	90.14	93.19	-3.27
1.5	89.46	92.11	-2.88
2	88.98	91.16	-2.39
3	88.30	89.13	-0.92
4	87.82	87.34	0.56
5	87.73	-	-
10	86.26	-	-
15	85.59	-	-
20	85.10	-	-
30	84.42	-	-
40	83.94	-	-
50	83.57	-	-
75	82.89	-	-
100	82.41	-	-
150	81.73	-	-
200	81.25	-	-

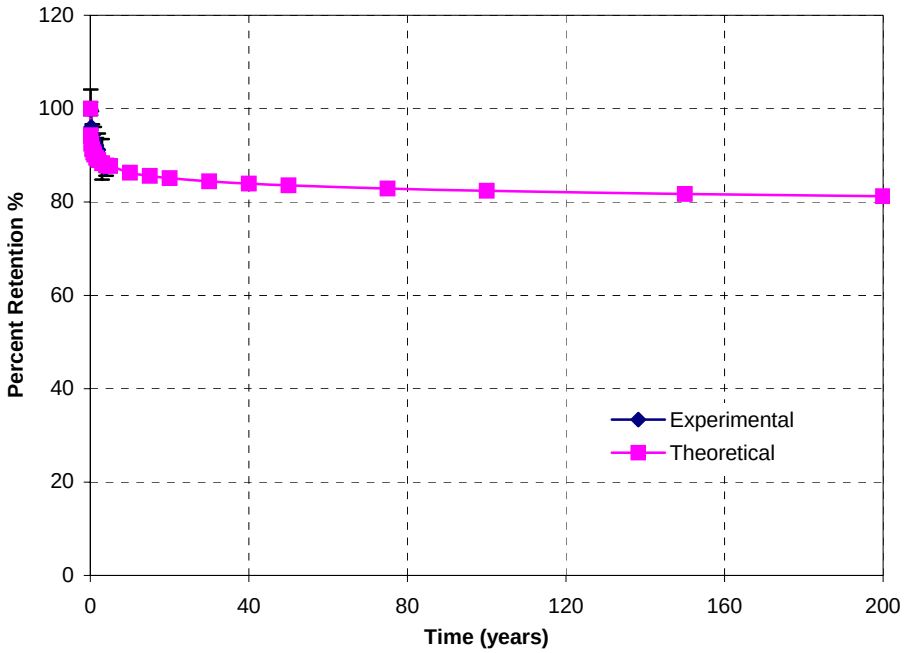

Fig. 8.2 Comparison between the experimental and predicted values of short-beam shear strength for specimens exposed to 60% relative humidity at 23 ^{o}C

Table 8.3 Predicted values of short-beam shear strength in comparison with experimentally obtained values forspecimens exposed to 75% relative humidity at 23 ^{o}C

Time (years)	Predicted values of percent retention– Arrhenius rate model	Experimentally obtained average values	Percentage error
0	100.00	100.00	0.00
0.08	92.23	92.59	-0.39
0.25	89.72	92.35	-2.85
0.5	88.14	93.43	-5.66
0.75	87.21	92.95	-6.17
1	86.56	92.35	-6.28
1.5	85.63	89.73	-4.56
2	84.97	86.98	-2.30
3	84.05	83.87	0.21
4	83.39	81.60	2.19
5	83.15	-	-
10	81.27	-	-
15	80.34	-	-
20	79.68	-	-
30	78.76	-	-
40	78.10	-	-
50	77.59	-	-
75	76.66	-	-
100	76.01	-	-
150	75.08	-	-
200	74.42	-	-

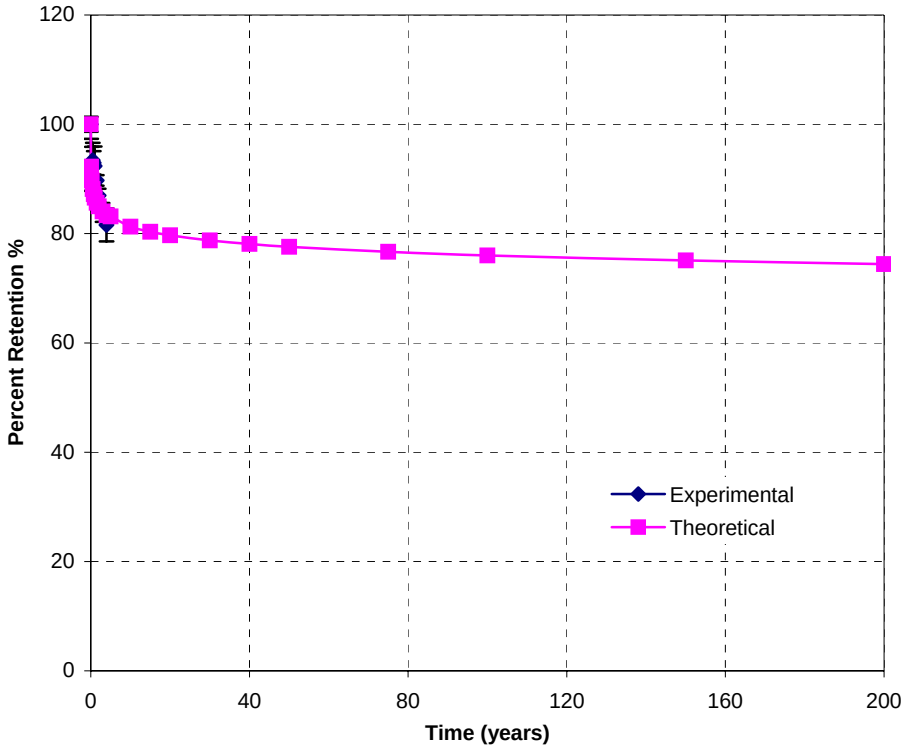

Fig. 8.3 Comparison between the experimental and predicted values of short-beam shear strength for specimens exposed to 75% relative humidity at 23 ^{o}C

Table 8.4 Predicted values of short-beam shear strength in comparison with experimentally obtained values for specimens exposed to 98% relative humidity at 23 ^{o}C

Time (years)	Predicted values of percent retention– Arrhenius rate model	Experimentally obtained average values	Percentage error
0	100.00	100.00	0.00
0.08	88.62	92.59	-4.29
0.25	84.95	90.20	-5.82
0.5	82.63	88.17	-6.29
0.75	81.24	84.59	-3.95
1	80.31	81.36	-1.29
1.5	78.96	77.78	1.51
2	77.99	76.22	2.32
3	76.64	72.28	6.02
4	75.67	70.01	8.09
5	74.88	-	-
10	72.56	-	-
15	71.21	-	-
20	70.25	-	-
30	68.89	-	-
40	67.93	-	-
50	67.18	-	-
75	65.82	-	-
100	64.86	-	-
150	63.51	-	-
200	62.54	-	-

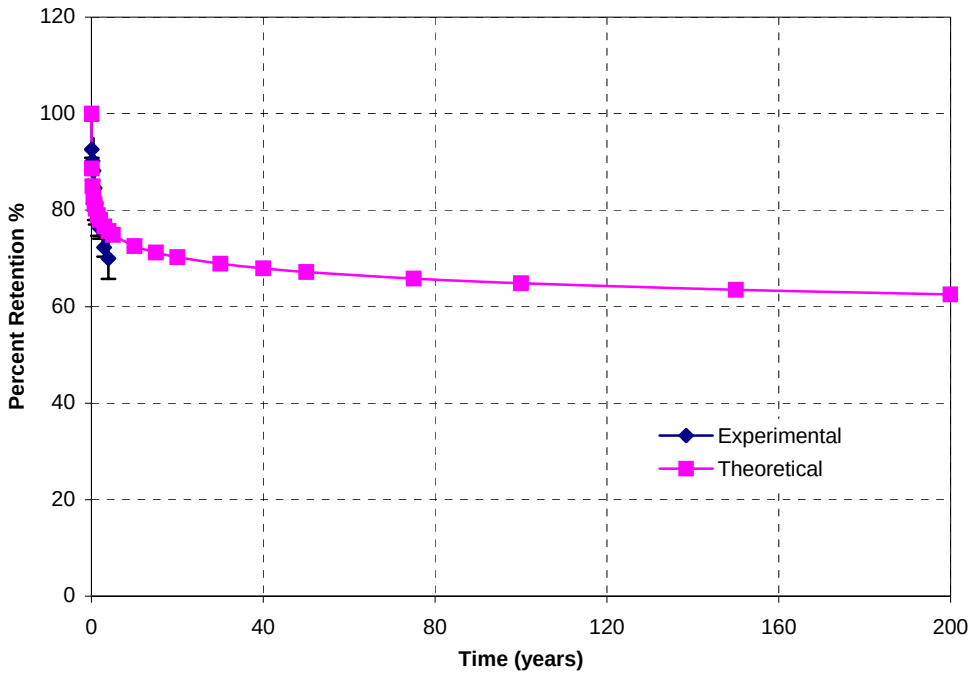

Fig. 8.4 Comparison between the experimental and predicted values of short-beam shear strength for specimens exposed to 98% relative humidity at 23 ^{o}C

8.3 Predictions for exposure conditions of humid air at 95 ^{0}C

The Arrhenius prediction of short-beam shear strength, for the specimens exposed to relative humidities at 95 ^{o}C is summarized in tables 8.5 to 8.8 and figures 8.5 to 8.8.

Table 8.5 Predicted values of short-beam shear strength incomparison with experimentally obtained values for specimensexposed to 45% relative humidity at 95 ^{o}C

Time (years)	Predicted values of percent retention– Arrhenius rate model	Experimentally obtained average values	Percentage error
0	100.00	100.00	0.00
0.08	95.49	91.40	4.48
0.25	94.04	90.44	3.98
0.5	93.12	90.08	3.37
0.75	93.03	88.53	5.08
1	92.20	87.93	4.85
1.5	91.66	86.26	6.26
2	91.28	85.07	7.31
3	90.74	83.75	8.35
4	90.36	82.92	8.98
5	90.05	-	-
10	89.13	-	-
15	88.59	-	-
20	88.21	-	-
30	87.67	-	-
40	87.29	-	-
50	87.00	-	-
75	86.46	-	-
100	86.08	-	-
150	85.54	-	-
200	85.16	-	-

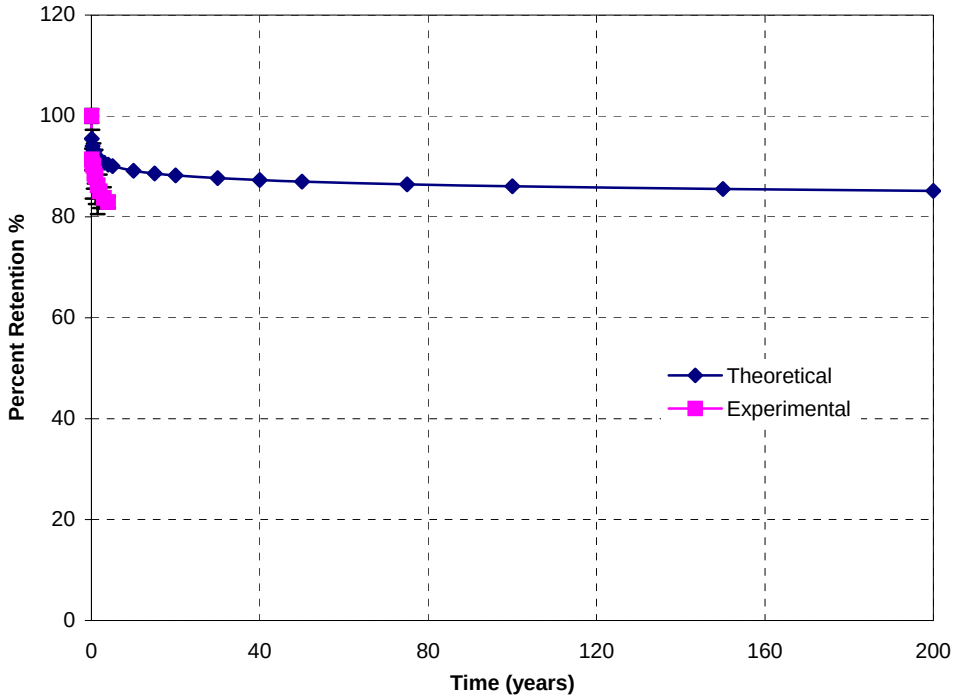

Fig. 8.5 Comparison between the experimental and predicted values of short-beam shear strength for specimens exposed to 45% relative humidity at 95 ^{o}C

Table 8.6 Predicted values of short-beam shear strengthin comparison with experimentally obtained values forspecimens exposed to 60% relative humidity at 95 ^{o}C

Time (years)	Predicted values of percent retention– Arrhenius rate model	Experimentally obtained average values	Percentage error
0	100.00	100.00	0.00
0.08	84.47	100.24	-15.73
0.25	79.45	96.77	-17.90
0.5	76.29	91.04	-16.20
0.75	74.44	88.77	-16.15
1	73.12	83.75	-12.69
1.5	71.27	80.41	-11.36
2	69.96	76.22	-8.22
3	68.11	73.00	-6.70
4	66.79	70.13	-4.76
5	65.71	-	-
10	62.55	-	-
15	60.69	-	-
20	59.38	-	-
30	57.53	-	-
40	56.22	-	-
50	55.20	-	-
75	53.35	-	-
100	52.03	-	-
150	50.18	-	-
200	48.87	-	-

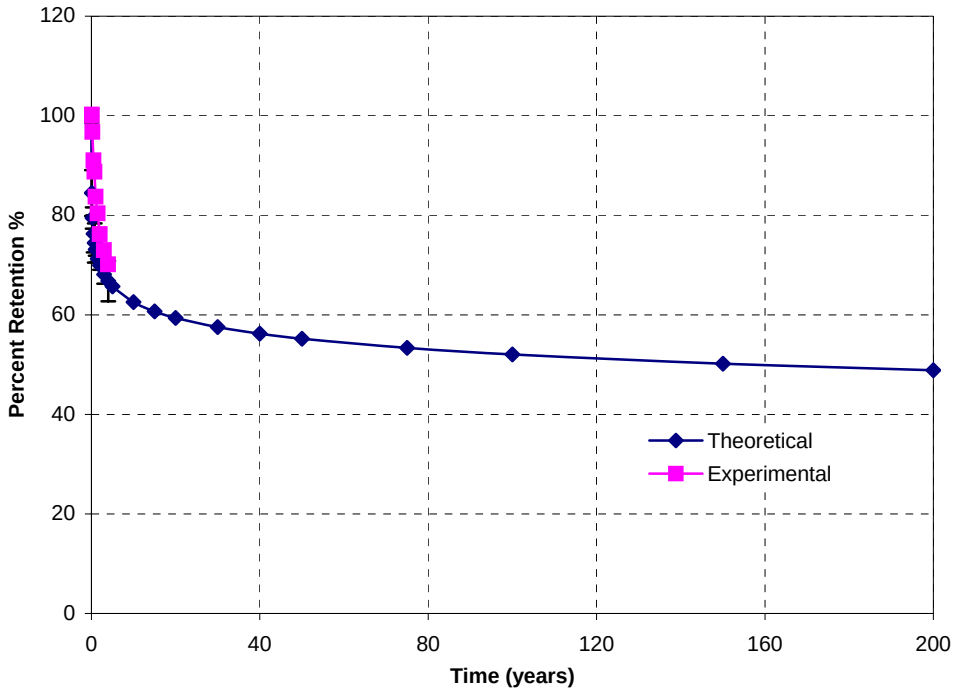

Fig. 8.6 Comparison between the experimental and predicted values of short-beam shear strength for specimens exposed to 60% relative humidity at 95 ^{o}C

Table 8.7 Predicted values of short-beam shear strength in comparison with experimentally obtained values for specimens exposed to 75% relative humidity at 95 ^{o}C

Time (years)	Predicted values of percent retention– Arrhenius rate model	Experimentally obtained average values	Percentage error
0	100.00	100.00	0.00
0.08	76.33	96.42	-20.84
0.25	68.68	82.32	-16.57
0.5	63.85	79.93	-20.11
0.75	61.03	64.87	-5.93
1	59.03	51.02	15.71
1.5	56.21	48.27	16.45
2	54.20	46.00	17.84
3	51.38	44.92	14.38
4	49.38	44.09	12.01
5	47.73	-	-
10	42.91	-	-
15	40.08	-	-
20	38.08	-	-
30	35.26	-	-
40	33.26	-	-
50	31.70	-	-
75	28.88	-	-
100	26.88	-	-
150	24.06	-	-
200	22.05	-	-

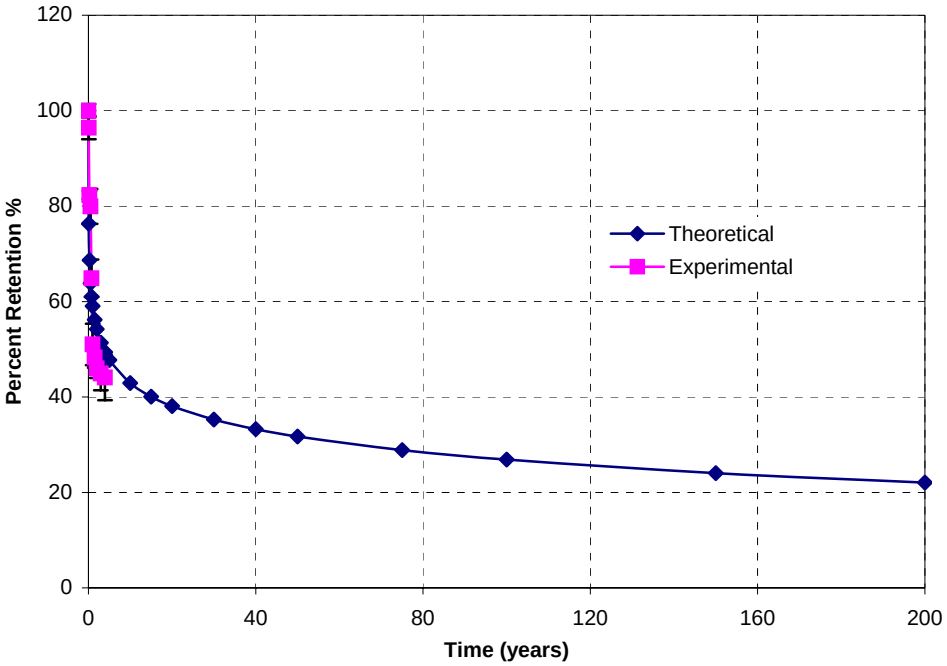

Fig. 8.7 Comparison between the experimental and predicted values of short-beam shear strength for specimens exposed to 75% relative humidity at 95 ^{o}C

Table 8.8 Predicted values of short-beam shear strengthin comparison with experimentally obtained values forspecimens exposed to 98% relative humidity at 95 ^{o}C

Time (years)	Predicted values of percent retention– Arrhenius rate model	Experimentally obtained average values	Percentage error
0	100.00	100.00	0.00
0.08	68.68	78.61	-12.64
0.25	58.56	58.90	-0.57
0.5	52.18	58.54	-10.87
0.75	48.45	52.81	-8.26
1	45.80	44.68	2.49
1.5	42.06	38.35	9.68
2	39.41	36.08	9.24
3	35.68	32.62	9.40
4	33.03	30.35	8.85
5	30.85	-	-
10	24.47	-	-
15	20.73	-	-
20	18.08	-	-
30	14.35	-	-
40	11.70	-	-
50	9.65	-	-
75	5.91	-	-
100	3.26	-	-
150	-0.47	-	-
200	-3.12	-	-

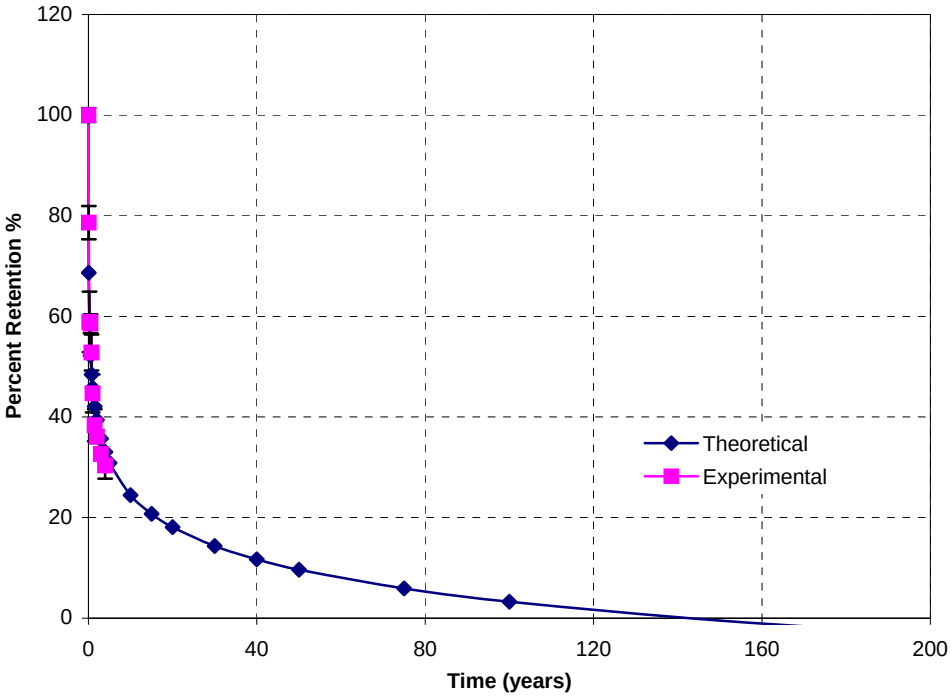

Fig. 8.8 Comparison between the experimental and predicted values of short-beam shear strength for specimens exposed to 98% relative humidity at 95 ^{o}C

8.4 Conclusions

The rate of degradation increases with the increase in relative humidity and temperature. The predicted values of short-beam shear strength agree well with the experimental values in for the specimens exposed to 23 ^{o}C, but not as well for those exposed to 95 ^{o}C. For instance, the error percentages between the experimental and predicted values of short-beam shear strength for the specimens at 23 ^{o}C and 60% relative humidity range between 0.56% to –5.47%. In contrast, the error percentages, for the same humidity exposure at 95 ^{o}C, range from –4.76% to 15.73%. This could be attributed to the fact that the equation 8.2 is valid only between 0 to 60 ^{o}C. Further, it should be noted that these values are compared to the means without consideration of experimental scatter bounds, consideration of which makes the error level much smaller.

8.5 References

1. Reliasoft Corporation Website, www.reliasoft.com.

2. Lawrence G.M., "The Relationship between Relative Humidity and the Dewpoint Temperature in Moist Air, A Simple Conversion and Applications", *American Meteorologist Society*, February 2005, pp. 225-233.

3. Shen C. and Springer G.S., "Moisture Absorption and Desorption of Composite Materials", Environmental effects on Composite Materials, 1988, Ed., Springer G. S., Vol. 3, 15-34.

4. Bonniau P. and Bunsell A.R., "A Comparative Study of Water Absorption Theories Applied to Composites", *Journal of Composite Materials*, 1981, Vol. 15, pp. 272-293.

5. Aditya P.K., and Sinha P.K., "Diffusion Coefficients of Polymeric Composites Subjected to Periodic Hygrothermal Exposure", *Journal of Reinforced Plastics and Composites*, 1992, Vol. 11, pp. 1035-1047.

Chapter 9

Summary and Conclusions

9.1 Overview

In almost all instances fiber reinforced polymer (FRP) composites used in applications pertaining to civil infrastructure systems will be subjected to extended periods of environmental exposure. The environmental conditions are likely to range from exposure to sunlight and humidity to immersion in water and solutions, as well as being in contact with concrete and other conventional materials. Due to cost and processing exigencies the FRP systems used in civil infrastructure are likely to be dramatically different from the well characterized systems used in the aerospace industry. The increasing use of E-glass systems (which are inherently susceptible to moisture and alkali solution induced deterioration, as well as stress rupture) and the use of non-autoclave processes such as wet layup and resin infusion (wherein cure is conducted under ambient conditions and without compaction beyond that of vacuum pressure under a thin bag) raise challenges related to the assurance of long-term durability. Thus the characterization of these materials and the development of an understanding of the fundamental mechanisms related to common environmental conditions such as moisture and humidity is essential.

9.2 Restatement of Goals and Rationale

While the primary objective of this research was the investigation of durability of E-glass/vinylester systems under conditions of immersion in water and exposure to varying

humidity levels, three specific goals were set. These goals and the rationale for each as related to civil infrastructure applications are given below.

1. Characterization of kinetics of moisture uptake

Since the presence of moisture is likely to be a constant in most civil environments it is essential that effects of moisture uptake in terms of diffusion coefficients and maximum moisture content are established since these form the basis for future modeling efforts.

2. Prediction of condition specific long-term durability

The further use of FRP composites in civil infrastructure applications is predicated both on the availability of validated data bases and the predictability of environmental effects on changes in various performance characteristics. At the base level it is essential that simple predictive equations that are amenable to use by designers be developed such that rates of deterioration can be predicted and compared with performance thresholds.

3. Correlation between immersion and humidity

While most published studies focus on the effects of immersion in water and various solutions, a more common environmental exposure is that of humidity and hence it is important to be able to develop methods that will enable correlation between the two based on common facets such as those related to the kinetics of moisture uptake.

4. Development and validation for test interchangeability

In most cases the validity of field-fabricated FRP is specified to be tested through the use of tensile tests. While these tests are accurate and provide a good representation of fiber dominated properties they need to be conducted in laboratories using specific equipment. In order to enable rapid field testing for purposes of inspection and validation simpler protocols need to be established and flexural tests provide the means for rapid field based testing using

portable equipment. However, the development of a correlation between the results of flexural testing and tensile characterization is necessary to enable this.

9.3 Summary and Conclusions

The results from the analysis of the data can be summarized as follows:

- The drop in the tensile strength is maximum for the highest temperature of immersion 95 ^{o}C and is equal to 79% loss at the end of 1440 days.
- The drop in the tensile modulus is maximum for the highest temperature of immersion 95 ^{o}C and is equal to 69% loss at the end of 1440 days.
- The drop in the flexural strength is maximum for the highest temperature of immersion 95 ^{o}C and is equal to 81% loss at the end of 1440 days.
- The drop in the short-beam shear strength is maximum for the highest temperature of immersion 95 ^{o}C and is equal to 80% loss at the end of 1440 days.
- The effects of high humidity levels is approximately same as the effects due to immersion i.e. the drop in short-beam shear strength of specimens exposed to relative humidity of 98% at 23 ^{o}C is 30% whereas the drop in short-beam shear strength of specimens immersed in deionized water at 23 ^{o}C is 33%.
- Similarly, the drop in short-beam shear strength of specimens exposed to relative humidity of 98% at 95 ^{o}C is 70% whereas the drop in short-beam shear strength of specimens immersed in deionized water at 95 ^{o}C is 80%.
- The percentage moisture gain for specimens exposed to high humidity levels is approximately same as that for specimens immersed in deionized water i.e. the percentage moisture gain for specimens exposed to relative humidity of 98% at 23 ^{o}C

is 0.329% whereas the percentage moisture gain for specimens immersed in deionized water at 23 ^{o}C is 0.405%.

As reported in Chapters 4, 7 and 8, the predictive methods show generally good agreement. Table 9.1 shows predictions for the property retention as a function of time. The periods of 5, 15, 25 and 50 years are selected to provide examples of rehabilitation service life.

Based on the research conducted in this investigation the following primary findings can be reported:

- Detailed characterization of moisture kinetics using both Fickian and Langmuir models was completed and it is concluded that while the Fickian model remains the simplest method in many cases the use of the Langmuir model more closely replicates actual response in FRP composites. The coefficient of diffusion is seen to be related to both temperature and humidity level with the effects of humidity being lower than those due to immersion under constant temperature regimes. Both conditions follow the Arrhenius rate equation and a correlation can be established between humidity and temperature through use of simple predictive formulae.
- A comprehensive data base is presented for change in mechanical properties as a result of immersion in deionized water and long-term predictive capability is established through both the Arrhenius approach and the Phani and Bose approach. Predictive equations that can be implemented in existing design procedures are provided for each of the mechanical characteristics.
- The use of Weibull characteristics to develop a correlation between tensile and flexural characteristics is validated thus enabling field based flexural test results to be correlated to specifications for performance on the basis of tensile characteristics.

- A correlation between rates of deterioration using the Arrhenius approach between moisture immersion and humidity exposure is enabled thereby providing the context for further development of durability prediction based on limited data sets under single environments.

9.4 Implementation

Since durability prediction and its integration with design vis-à-vis renewal of civil infrastructure is a major current concern, the following primary conclusions are made regarding the implementation of results of the current research.

- Predictive results based on both immersion and humidity conditions as reported in Chapter 8 can be immediately implemented for durability based design. Thus rather than using a single number based either on "as-received" properties (which is likely to be unconservative) or factored properties as suggested by ACI-440 (which are excessively conservative) a time based approach can be used enabling designers to select characteristics or thresholds based on intended service-life.
- Rather than waiting for extended periods of time for process panels to be sent to laboratories for tensile testing, flexural testing can be conducted in the field using simple tools as already developed in the marine industry for purposes of process validation, and results can be correlated to required tensile characteristics. This makes it possible to complete characterization in the field without long delays and is thus an important advantage for field inspection.
- Effects of humidity can be assessed based on the Arrhenius principles and correlated to those due to water immersion thereby providing a better tool for design and life estimation.

Table 9.1 Summary of predictions

Property	Percentage retention %							
	Immersion in water at 23 ^{o}C				Humidity exposure at 23 ^{o}C and 45 % RH			
	5 yrs	15 yrs	30 yrs	50 yrs	5 yrs	15 yrs	30 yrs	50 yrs
Tensile Strength	50.70	43.57	39.02	35.68	-	-	-	-
Tensile Modulus	92.02	90.86	90.12	89.58	-	-	-	-
Flexural Strength	36.07	25.38	18.63	13.66	-	-	-	-
SBS Strength	46.35	36.36	30.07	25.42	95.35	94.33	93.87	93.53

9.5 Future Research

The following suggestions are made for future research

- Development of a simplified predictive procedure for durability based on correlation of moisture kinetics thereby allowing for combined and/or changing exposures of immersion and humidity.
- Development of “equivalent” temperatures to characterize long-term ageing and to allow for consideration of cyclic exposures.
- Incorporation of effects due to sustained stresses or straining acting synergistically with moisture.
- Development of a web based data-base that can be used directly by DOT engineers to select materials and use time-based material characteristics in design.

APPENDIX A

A.1 Immersion in Water

A.1.1 Full Model

The moisture absorption data shown in Table 5.1 were fitted to equations A.1 (Fickian Diffusion Model) and A.2 (Langmuir Diffusion Model) using Mathcad Programming Methods. Fitting the data, using the least squares method, to the equations results in the estimation of the Maximum moisture content, M_m and Diffusion Coefficient, D. The results of the analysis using the equations A.1 and A.2 are presented in the Figures A.1 through A.10. Correction for edge effects was applied as described in section 5.3 of chapter 5.

$$M_t = M_m \left[1 - \frac{8}{\pi^2} \sum_{n=0}^{\infty} \frac{\exp\left[(2n+1)^2 \pi^2 \left(\frac{-Dt}{h^2} \right) \right]}{(2n+1)^2} \right] \qquad \text{Equation A.1}$$

$$M_t = M_m \left[1 - \frac{\alpha}{\alpha+\beta} \exp(-\alpha t) - \frac{\alpha}{\alpha+\beta} \frac{8}{\pi^2} \sum_{n=0}^{\infty} \frac{\exp\left[(2n+1)^2 \pi^2 \left(\frac{-Dt}{h^2} \right) \right]}{(2n+1)^2} \right]$$

Equation A.2

where M_t = Percentage moisture uptake at time t in seconds, M_m = Maximum moisture content that can be attained under the given conditions, D = Diffusion Coefficient in the direction normal to the surface in mm^2/sec, h = thickness of the specimen in mm, α = the probability of a trapped water molecule being released related to the Langmuir Model, β = the probability of a free water molecule being trapped related to the Langmuir Model.

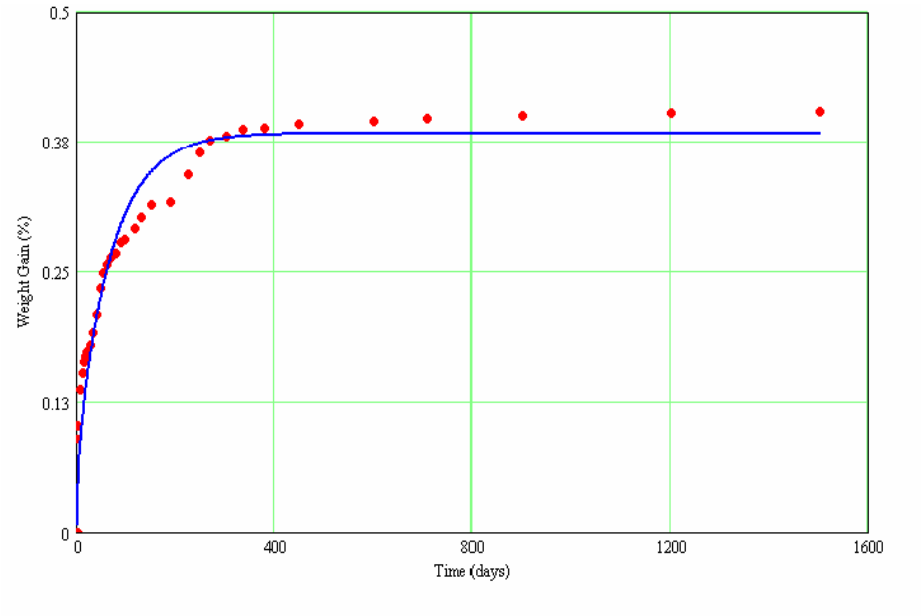

Fig. A.1 Comparison of experimental and predicted moistureabsorption profile of E-glass vinylester composite specimen immersed indeionized water at 23 ^{o}C using Fickian Full Model

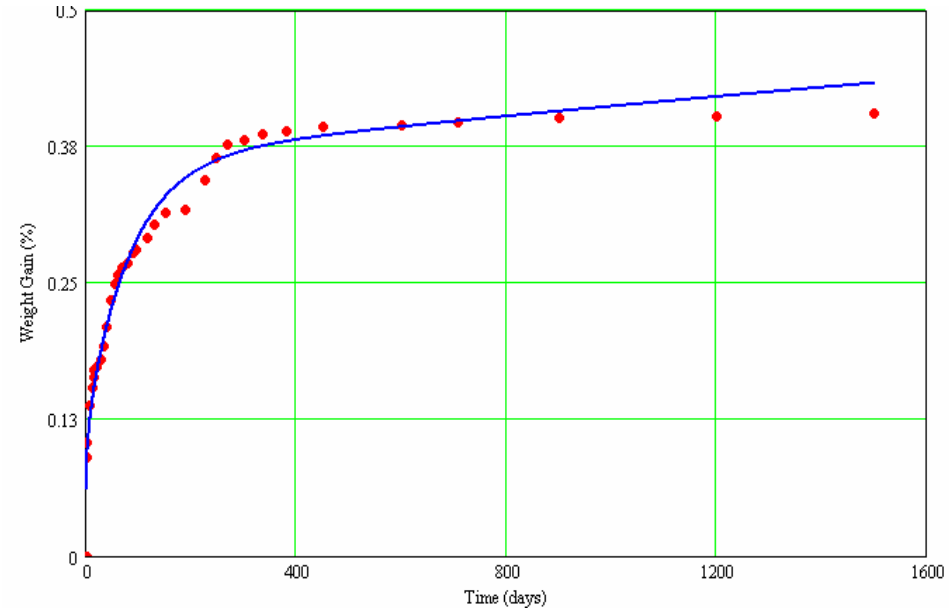

Fig. A.2 Comparison of experimental and predicted moisture absorption profile of E-glass vinylester composite specimens immersed in deionized water at 23 ^{o}C using Langmuir Full Model

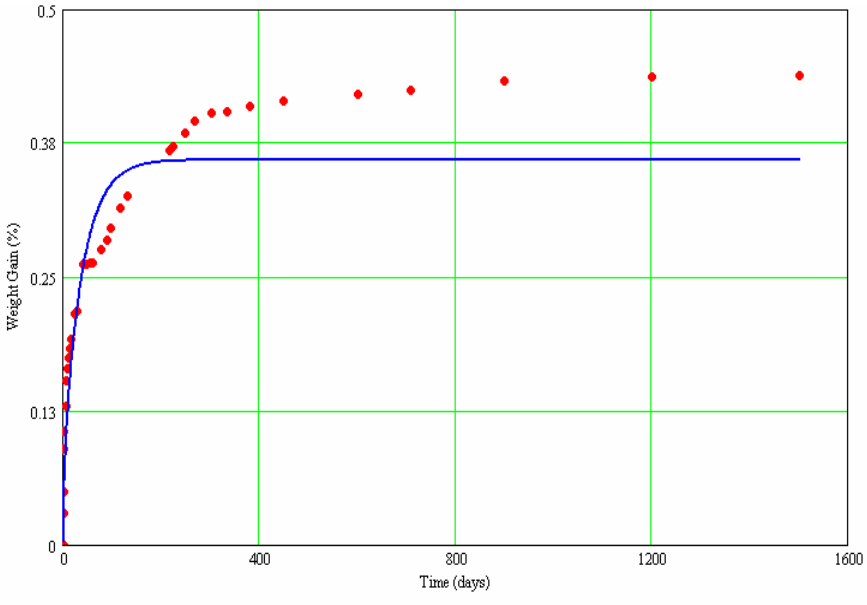

Fig. A.3 Comparison of experimental and predicted moisture absorption profile of E-glass vinylester composite specimen immersed in deionized water at 40^{o}C using Fickian Full Model

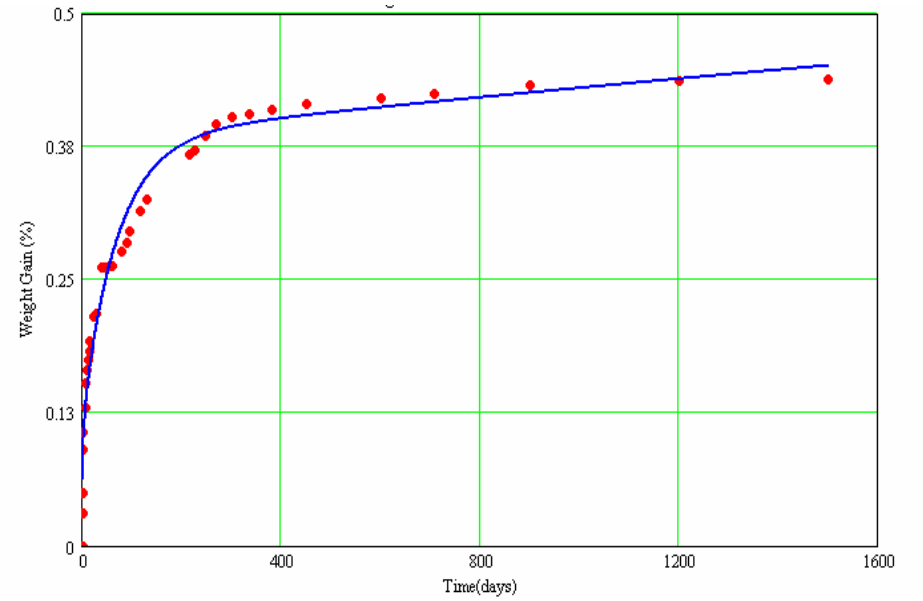

Fig. A.4 Comparison of experimental and predicted of moisture absorption profile of E-glass vinylester composite specimens immersed indeionized water at 40 ^{o}C using Langmuir Full Model

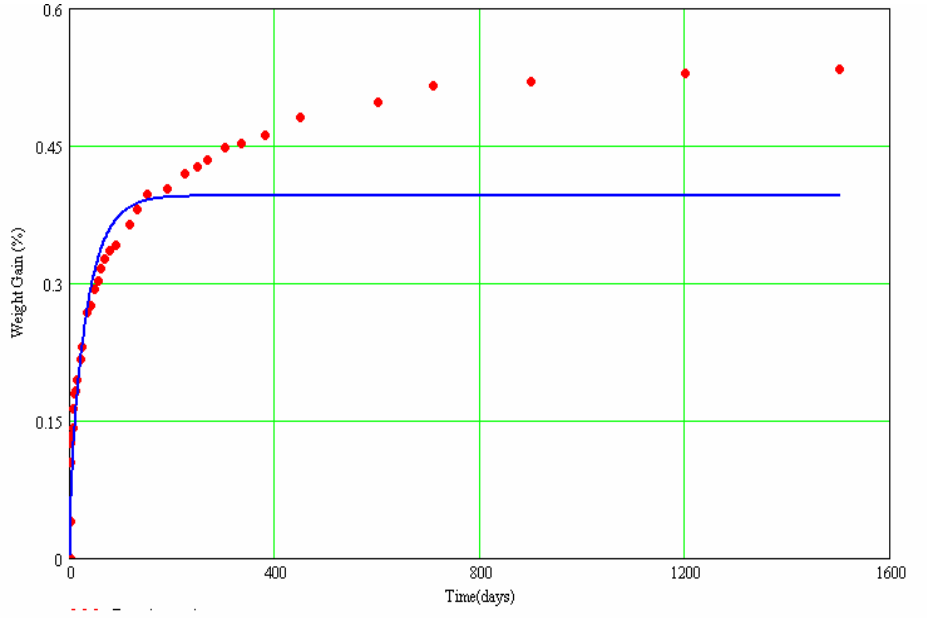

Fig. A.5 Comparison of experimental and predicted moistureabsorption profile of E-glass vinylester composite specimens immersed in deionized water at 60 ^{o}C using Fickian Full Model

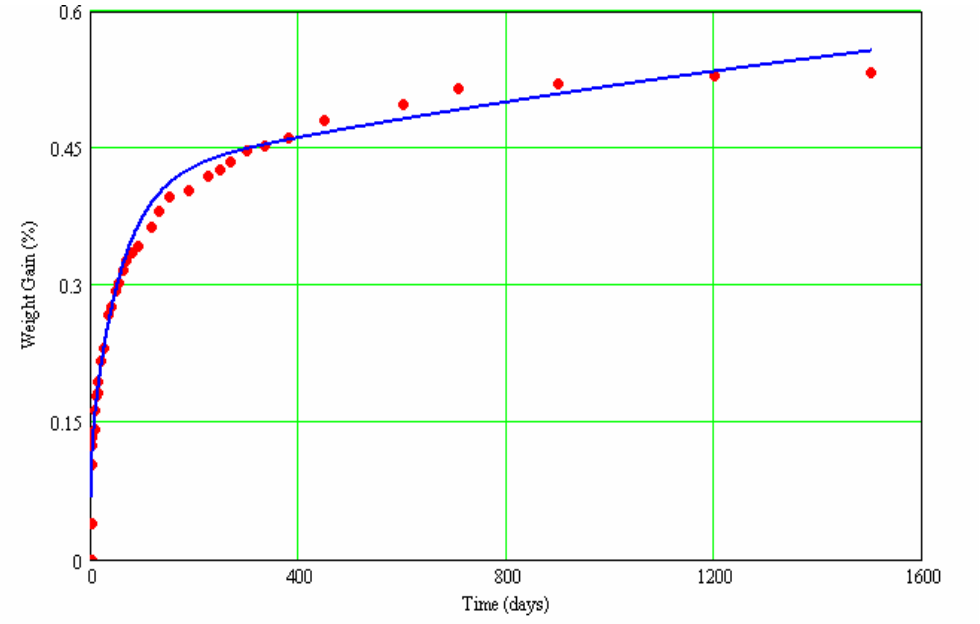

Fig. A.6 Comparison of experimental and predicted moisture absorption profile of E-glass vinylester composite specimen immersed in deionized water at 60 ^{o}C using Langmuir Full Model

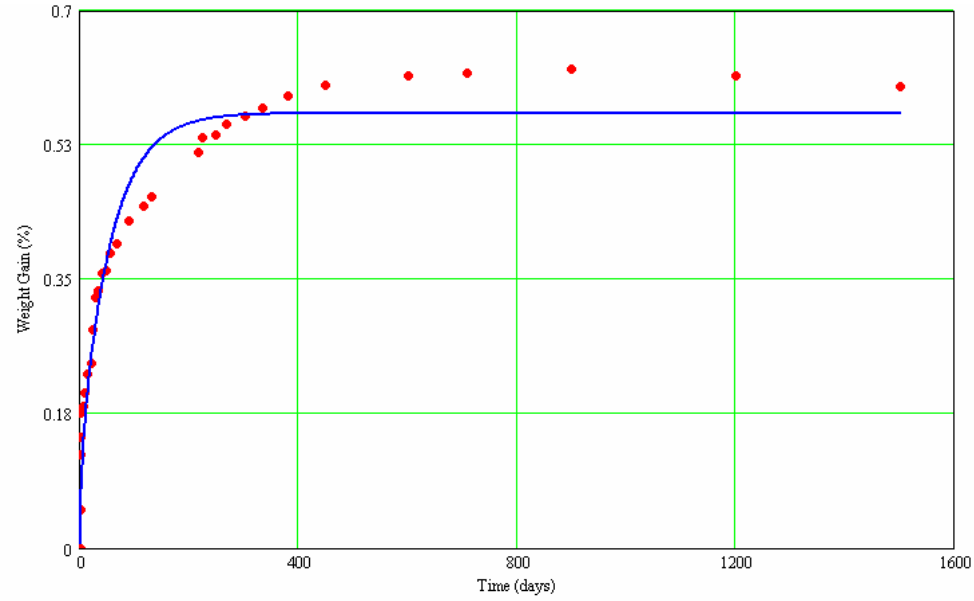

Fig. A.7 Comparison of experimental and predicted moistureabsorption profile of E-glass vinylester composite specimens immersed in deionized water at 80 ^{o}C using Fickian Full Model

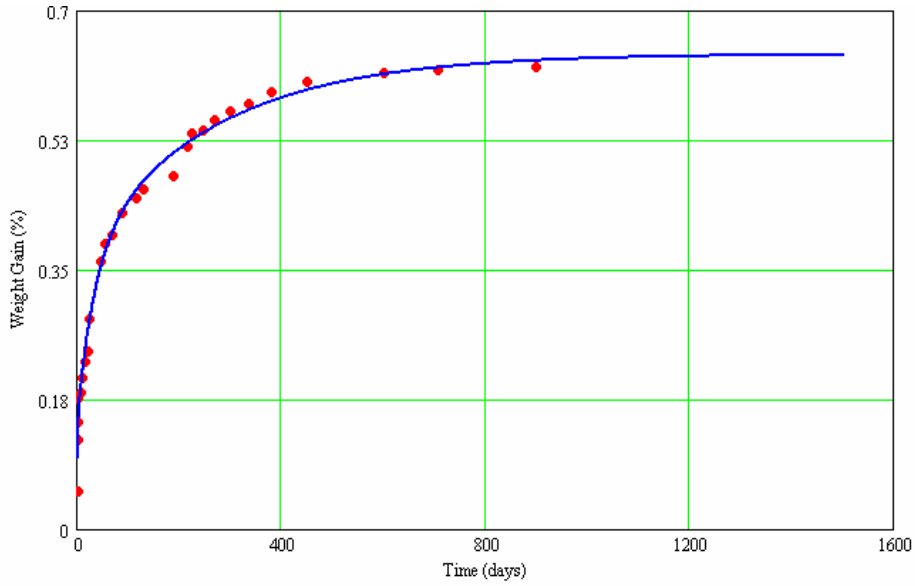

Fig. A.8 Comparison of experimental and predicted moistureabsorption profile of E-glass vinylester composite specimen immersed in deionized water at 80 ^{o}C using Langmuir Full Model

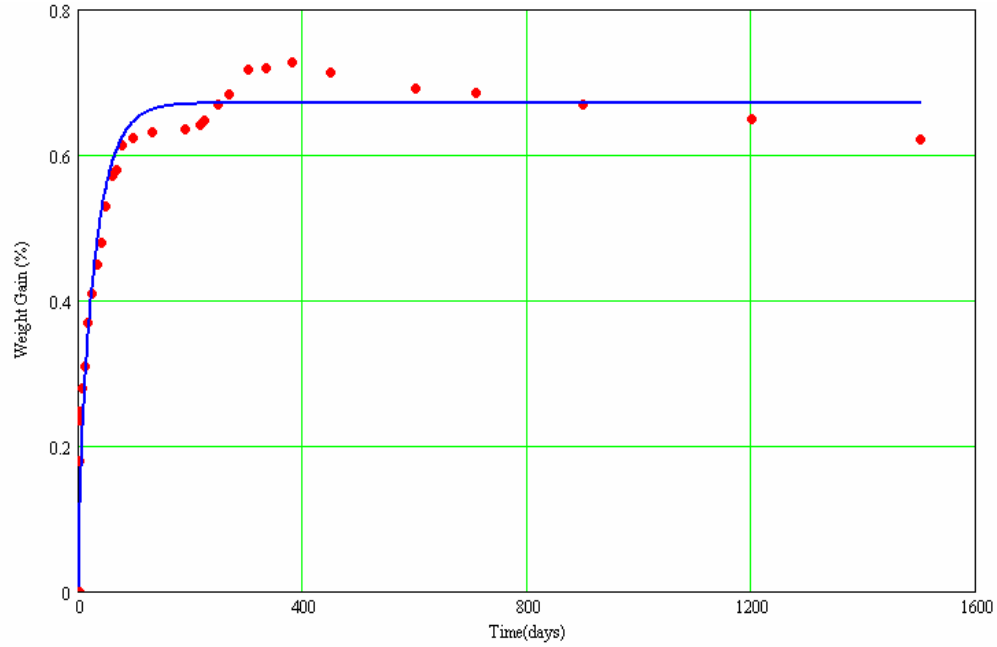

Fig. A.9 Comparison of experimental and predicted moistureabsorption profile of E-glass vinylester composite specimen immersed in deionized water at 95 ^{o}C using Fickian Full Model

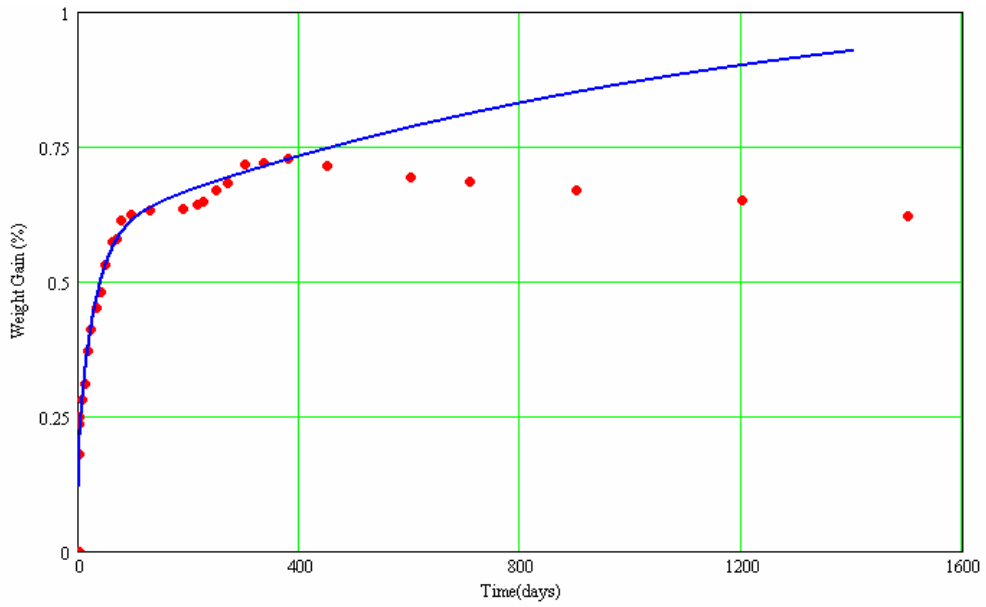

Fig. A.10 Comparison of experimental and predicted moistureabsorption profile of E-glass vinylester composite specimen immersed in deionized water at 95 ^{o}C using Langmuir Full Model

A.1.2 Long-term Approximation

The moisture absorption data in table 5.1 is fitted to equations A.3 (Fickian Long-Term Approximation) and A.4 (Langmuir Long-term Approximation). The results are presented in figures 11 through 15.

$$M_t = M_m\left[1-\frac{8}{\pi^2}\exp\left(\frac{-Dt}{h^2}\pi^2\right)\right] \qquad \text{Equation A.3}$$

$$M_t = M_m\left[1-\frac{\alpha}{\alpha+\beta}\exp(-\alpha t)-\frac{\alpha}{\alpha+\beta}-\frac{8}{\pi^2}\exp\left(\frac{-Dt}{h^2}\pi^2\right)\right] \qquad \text{Equation A.4}$$

where M_t = Percentage moisture gain at time t

M_m = Maximum moisture content that can be attained under the given conditions

D = Diffusion Coefficient in the direction normal to the surface

h = thickness of the specimen

α = the probability of a trapped water molecule being released (Langmuir Model)

β = the probability of a free water molecule being trapped (Langmuir Model)

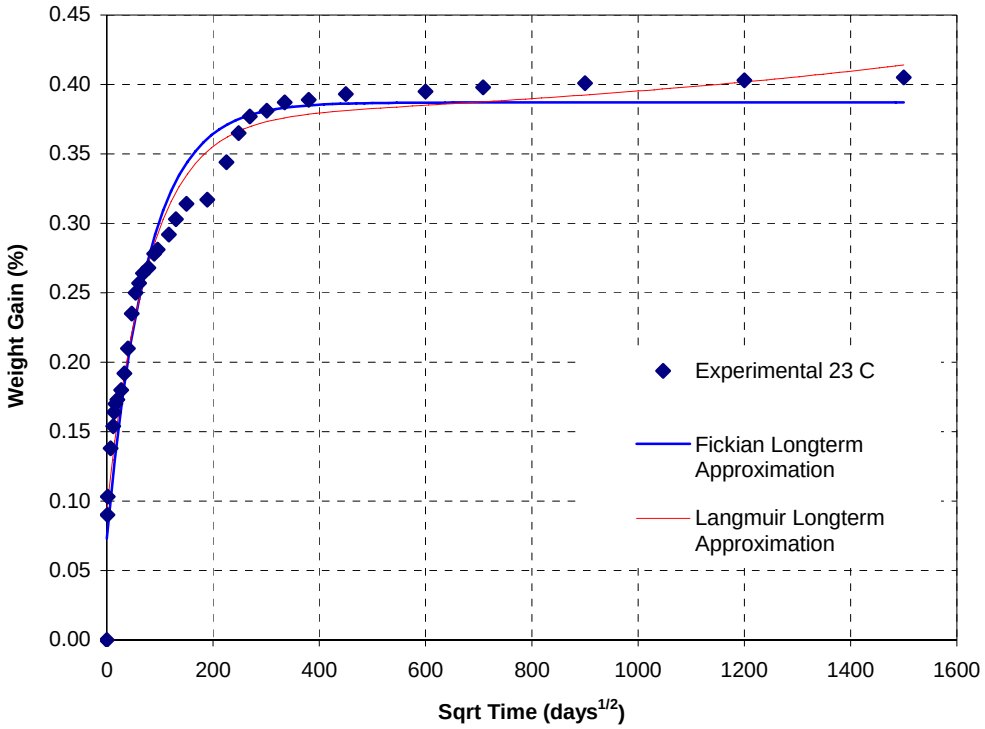

Fig. A.11 Comparison of experimental and predicted moisture absorption profiles of E-glass vinylester composite specimen immersed in deionized water at 23 ^{o}C using long-term approximations

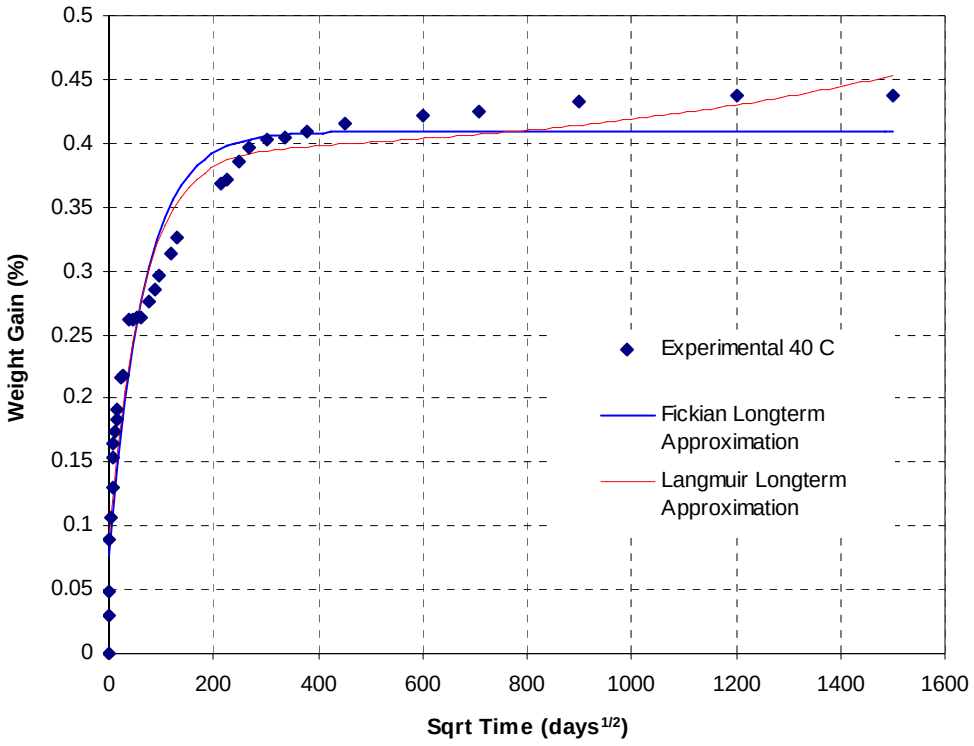

Fig. A.12 Comparison of experimental and predicted moisture absorption profile of E-glass vinylester composite specimen immersed in deionized water at 40 ^{o}C using long-term approximations

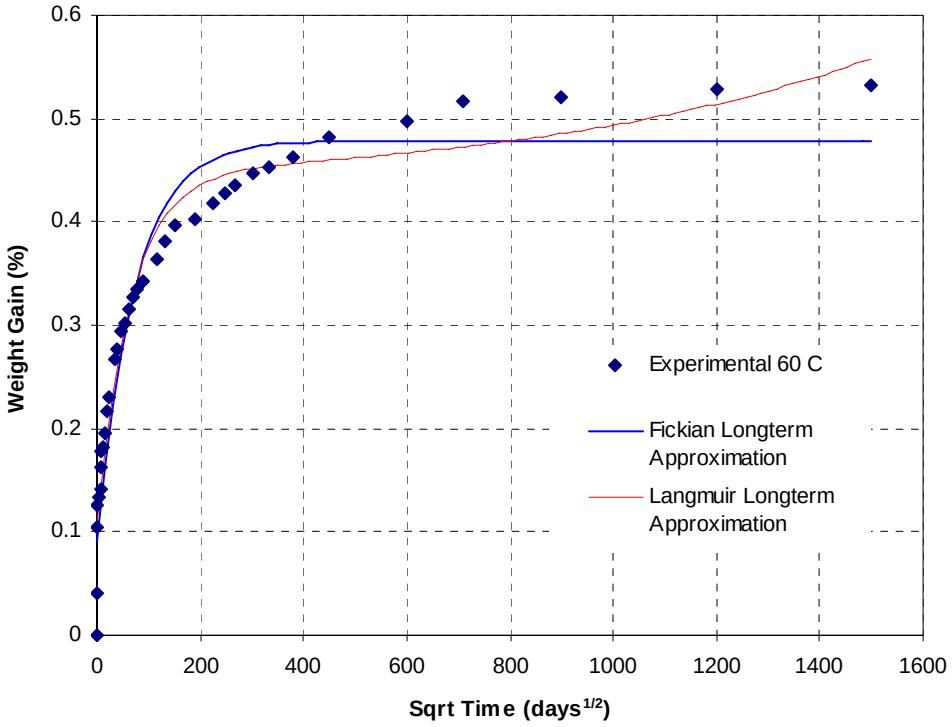

Fig. A.13 Comparison of experimental and predicted moisture absorption profile of E-glass vinylester composite specimen immersed in deionized water at 60 ^{o}C using long-term approximations

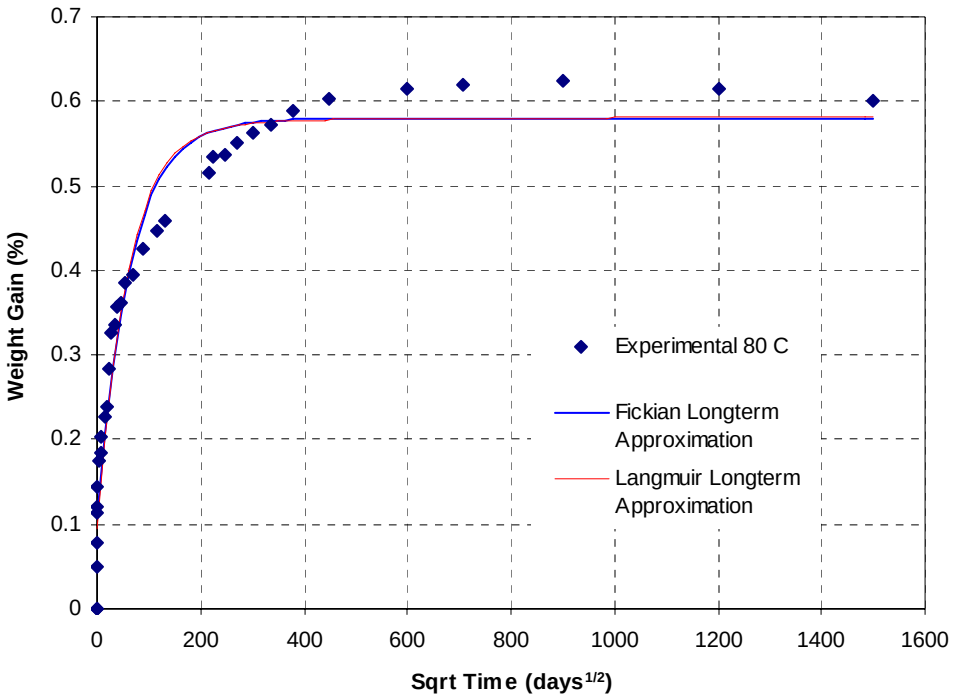

Fig. A.14 Comparison of experimental and predicted moisture absorption profile of E-glass vinylester composite specimen immersed in deionized water at 80 ^{o}C using long-term approximations

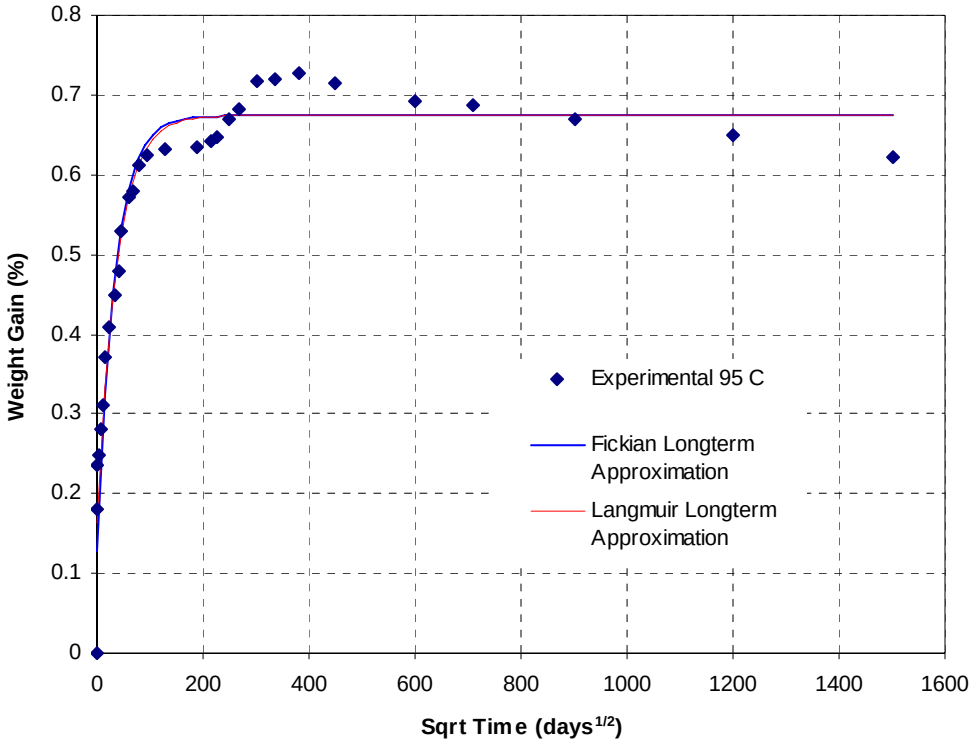

Fig. A.15 Comparison of experimental and predicted moisture absorption profile of E-glass vinylester composite specimen immersed in deionized water at 95 ^{o}C using long-term approximations

A.2 Exposure to Humidity at 23 C

A.2.1 Full Model

The moisture absorption data shown in Table 5.8 were fitted to equations A.1 (Fickian Diffusion Model) and A.2 (Langmuir Diffusion Model) using Mathcad tools. Fitting the data to the equations results in the estimation of the Maximum moisture content, M_m and Diffusion Coefficient, D. The results of the analysis using the equations A.1 and A.2 are presented in the Figures A.16 and A.25.

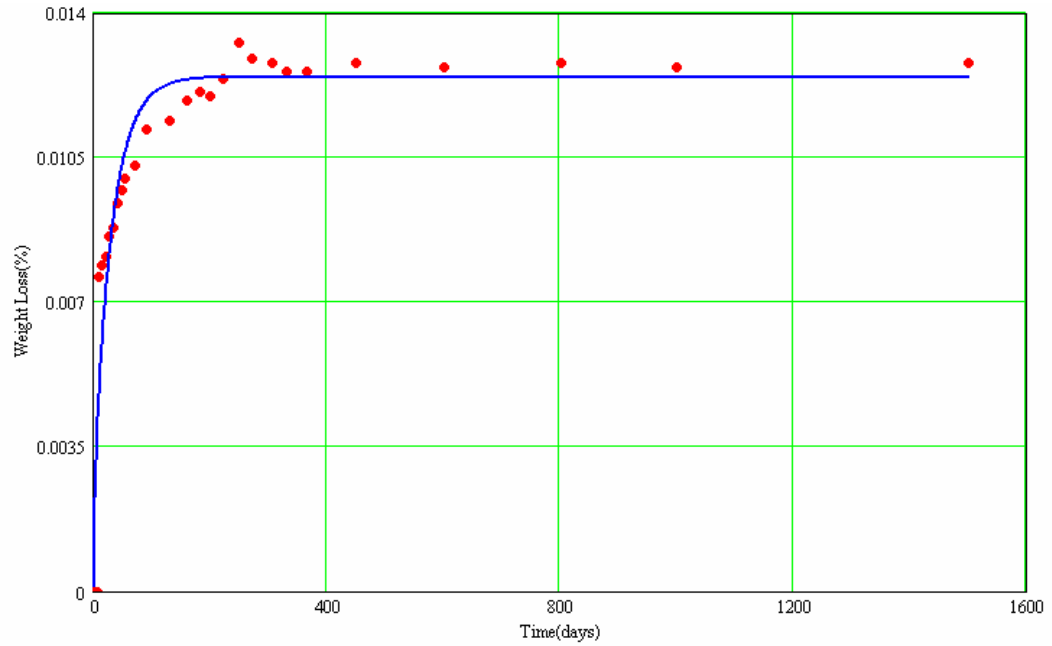

Fig. A.16 Comparison of experimental and predicted moisture absorption profile of E-glass vinylester composite specimen exposed to a relative humidity of 0-5 % at 23 ^{o}C using Fickian Full Model

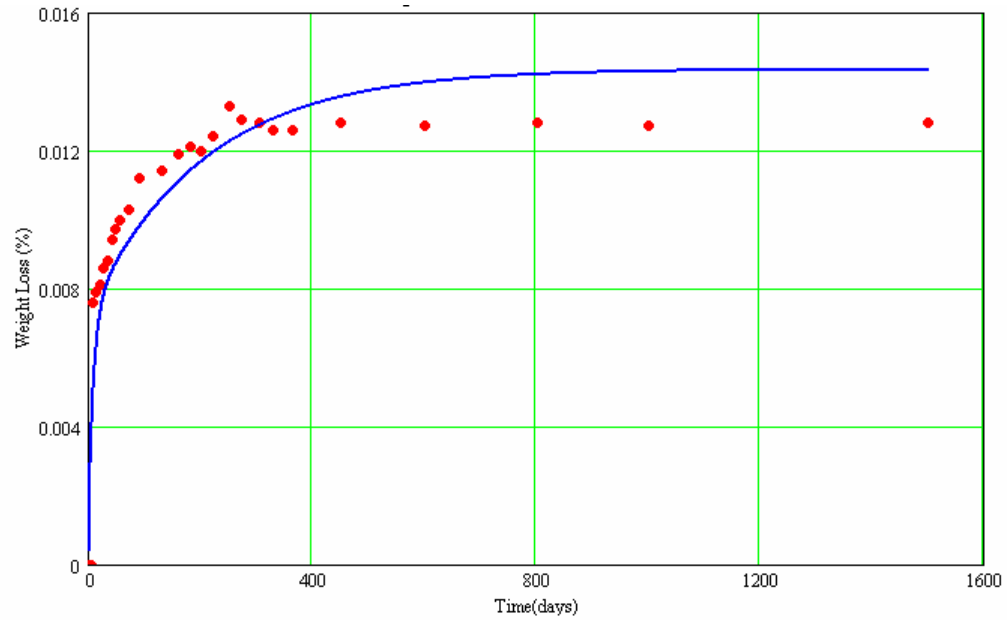

Fig. A.17 Comparison of experimental and predicted moisture absorption profile of E-glass vinylester composite specimen exposed to a relative humidity of 0-5 % at 23 ^{o}C using Langmuir Full Model

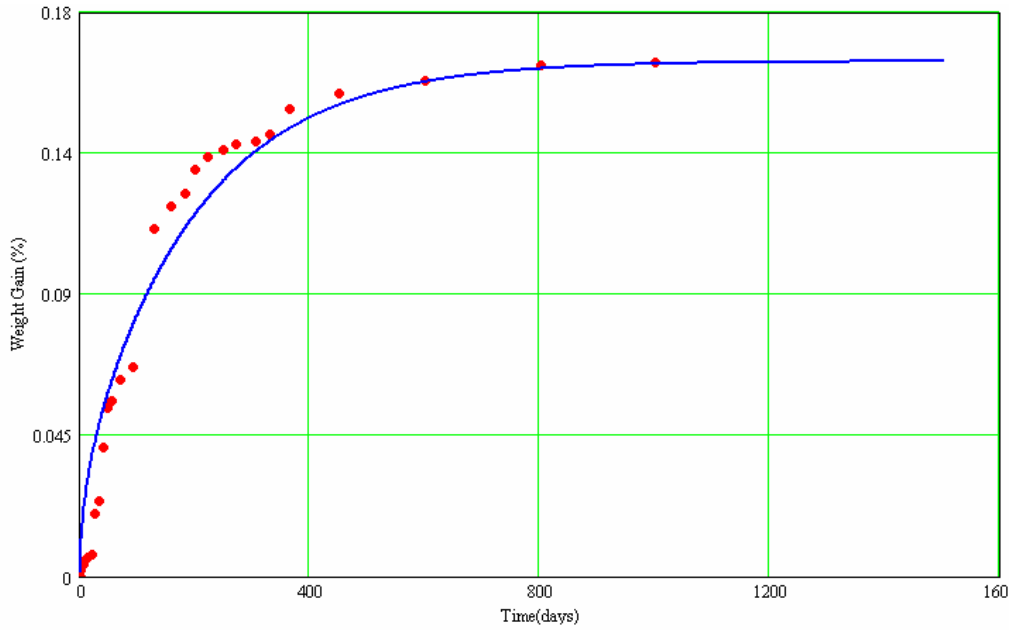

Fig. A.18 Comparison of experimental and predicted moisture absorption profile of E-glass vinylester composite specimen exposed to a relative humidity of 45 % at 23 ^{o}C using Fickian Full Model

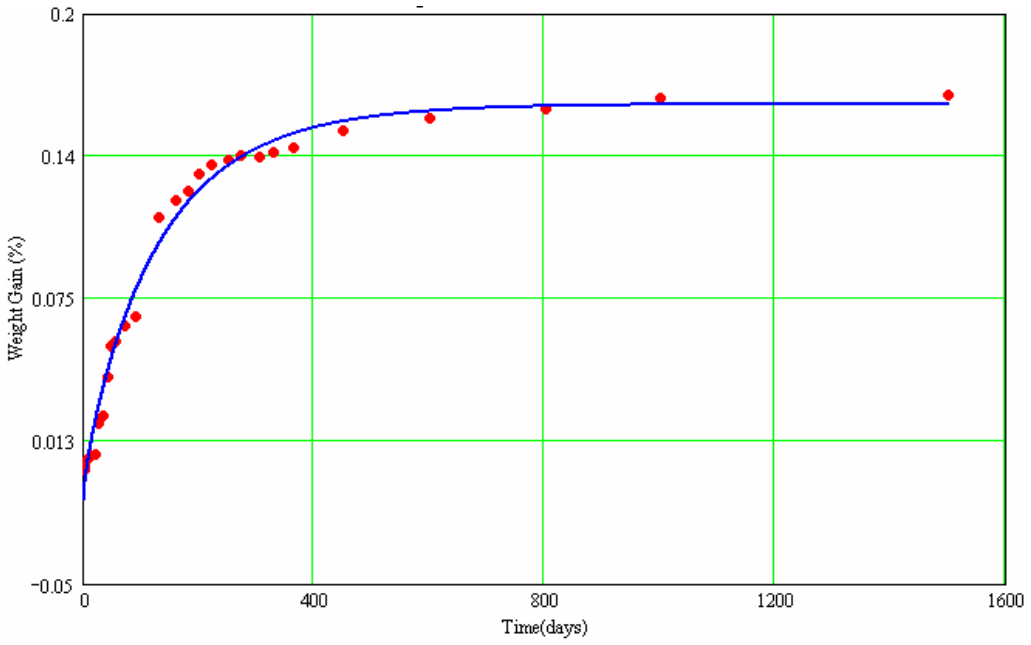

Fig. A.19 Comparison of experimental and predicted moisture absorption profile of E-glass vinylester composite specimen exposed to a relative humidity of 45 % at 23 ^{o}C using Langmuir Full Model

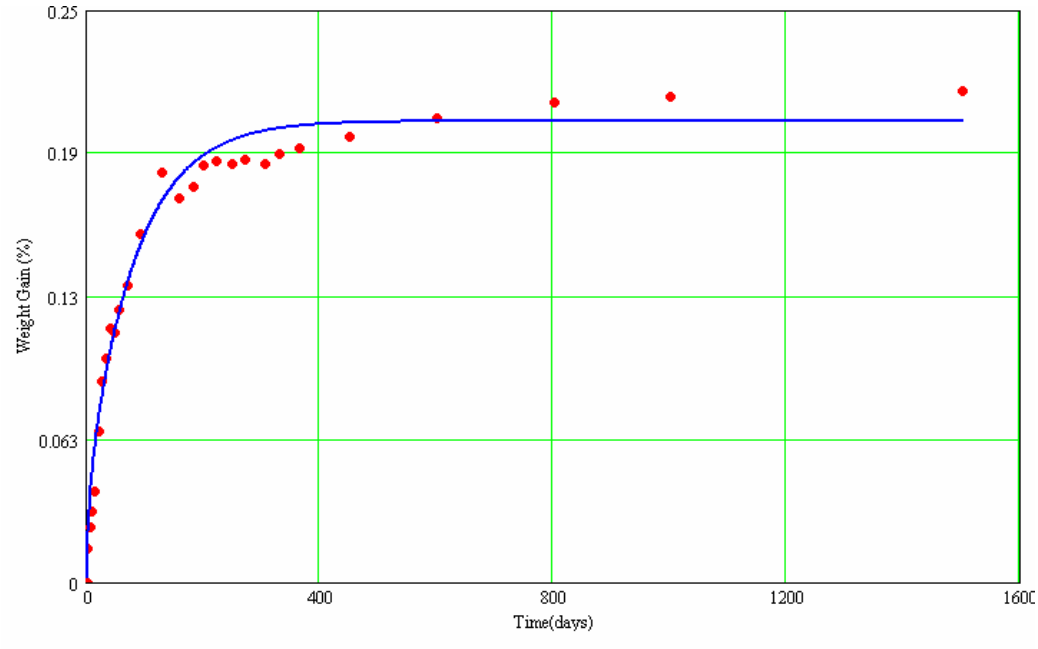

Fig. A.20 Comparison of experimental and predicted moisture absorption profile of E-glass vinylester composite specimen exposed to a relative humidity of 60 % at 23 ^{o}C using Fickian Full Model

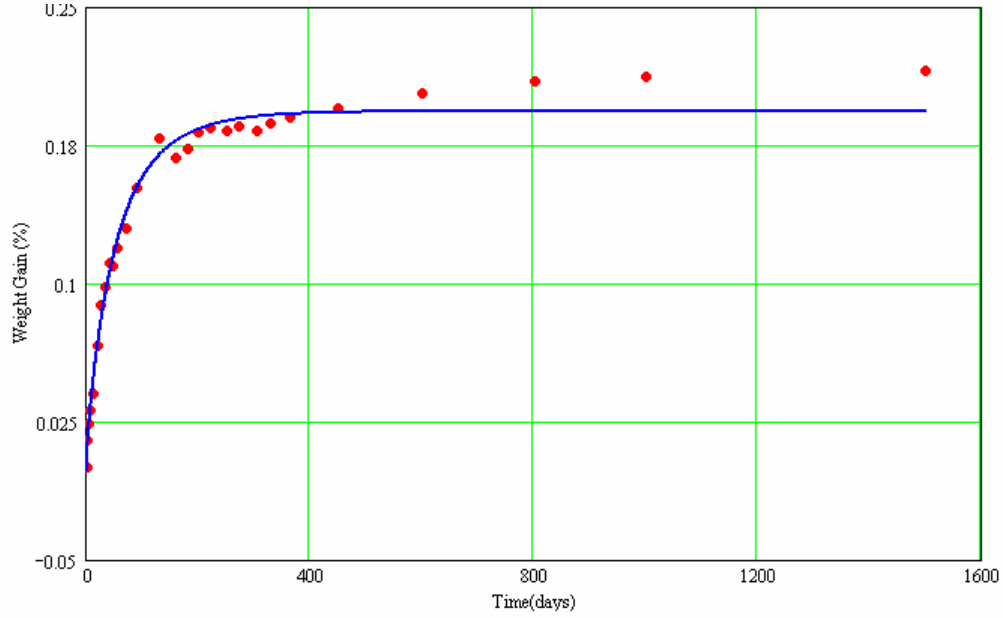

Fig. A.21 Comparison of experimental and predicted moisture absorption profile of E-glass vinylester composite specimen exposed to a relative humidity of 60 % at 23 ^{o}C using Langmuir Full Model

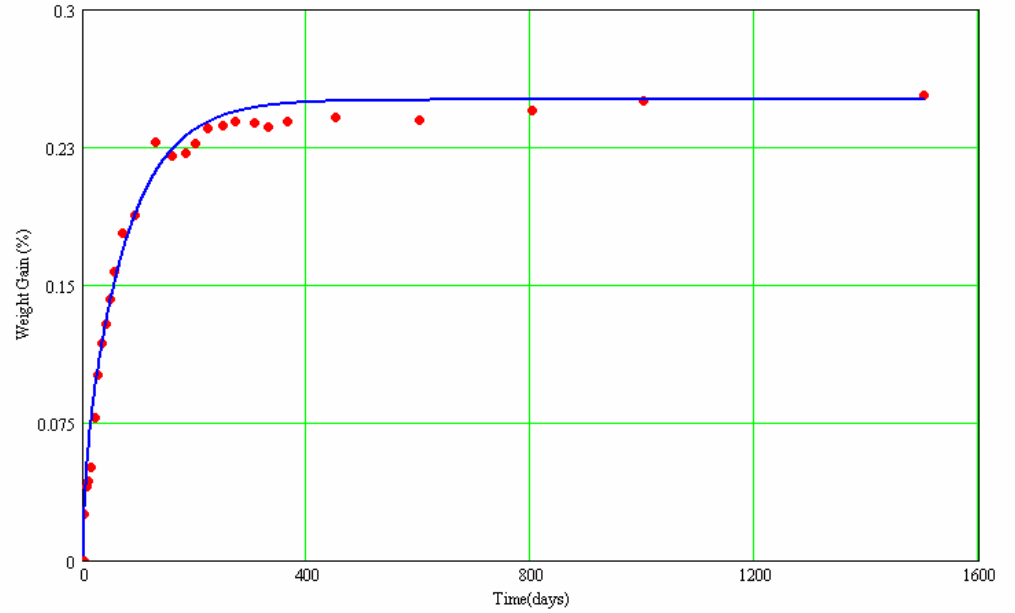

Fig. A.22 Comparison of experimental and predicted moisture absorption profile of E-glass vinylester composite specimen exposed to a relative humidity of 75 % at 23 ^{o}C using Langmuir Full Model

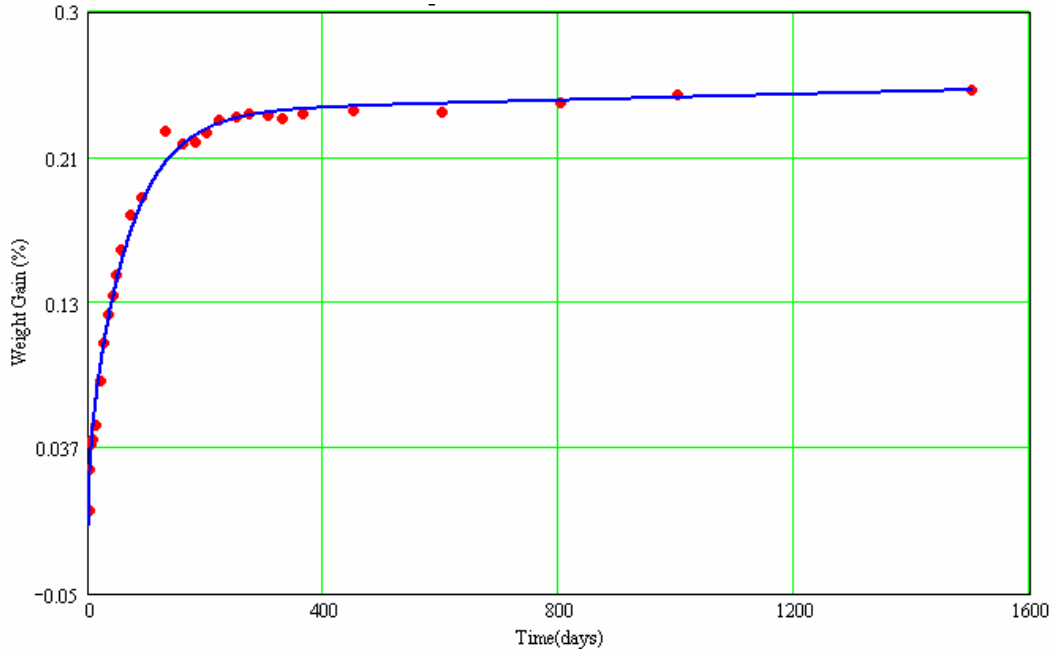

Fig. A.23 Comparison of experimental and predicted moistureabsorption profile of E-glass vinylester composite specimen exposed toa relative humidity of 75 % at 23 ^{o}C using Langmuir Full Model

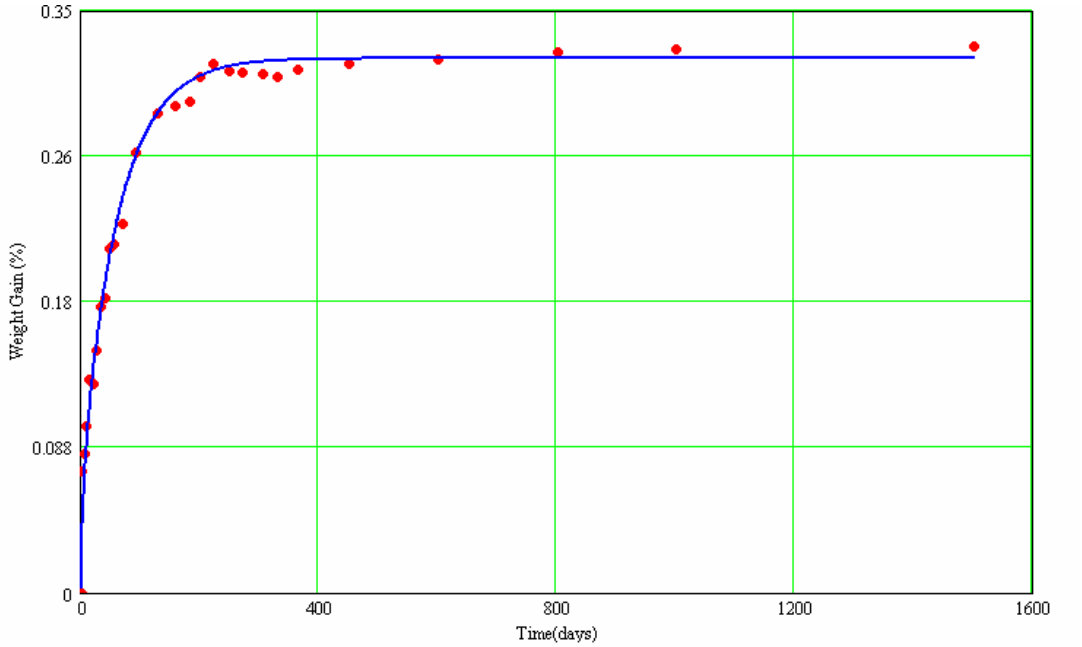

Fig. A.24 Comparison of experimental and predicted moisture absorption profile of E-glass vinylester composite specimen exposed to a relative humidity of 98 % at 23 ^{o}C using Fickian Full Model

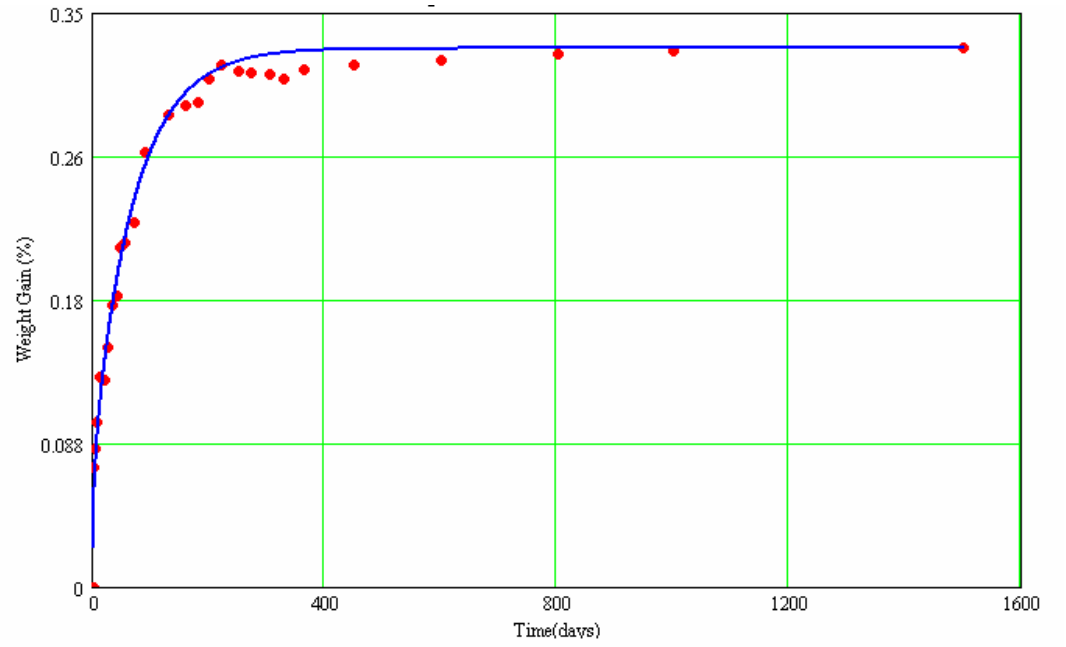

Fig. A.25 Comparison of experimental and predicted moisture absorption profile of E-glass vinylester composite specimen exposed to a relative humidity of 98 % at 23 ^{o}C using Langmuir Full Model

A.2.2 Long-term Approximation

The moisture absorption data in the table 5.8 is fitted to equations A.3 (Fickian Long-Term Approximation) and A.4 (Langmuir Long-term Approximation). The results are presented in figures A.26 through A.29.

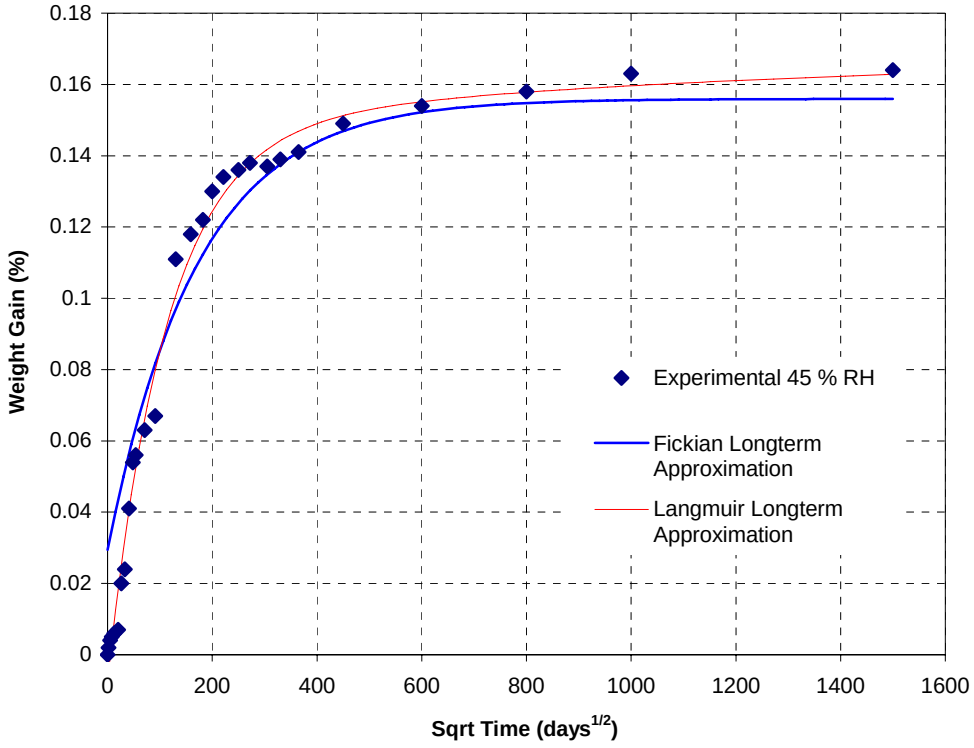

Fig. A.26 Comparison of experimental and predicted moisture absorption profile of E-glass vinylester composite specimen exposed to a relative humidity of 45 % at 23 ^{o}C using long-term approximation terms

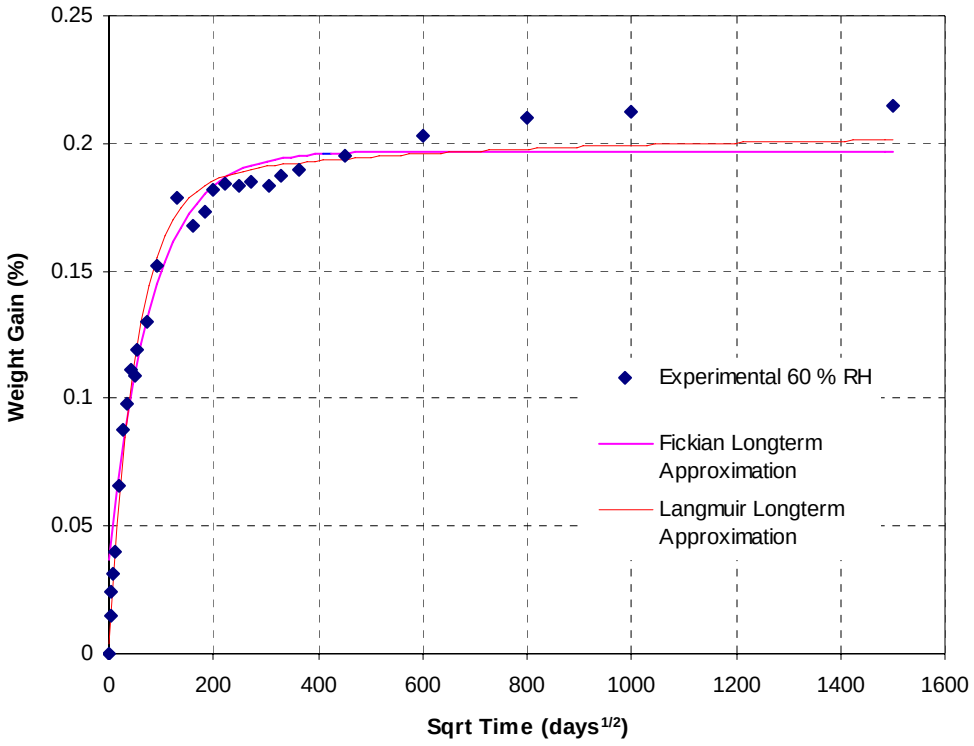

Fig. A.27 Comparison of experimental and predicted moistureabsorption profile of E-glass vinylester composite specimen exposed to arelative humidity of 60 % at 23 ^{o}C using long-term approximation terms

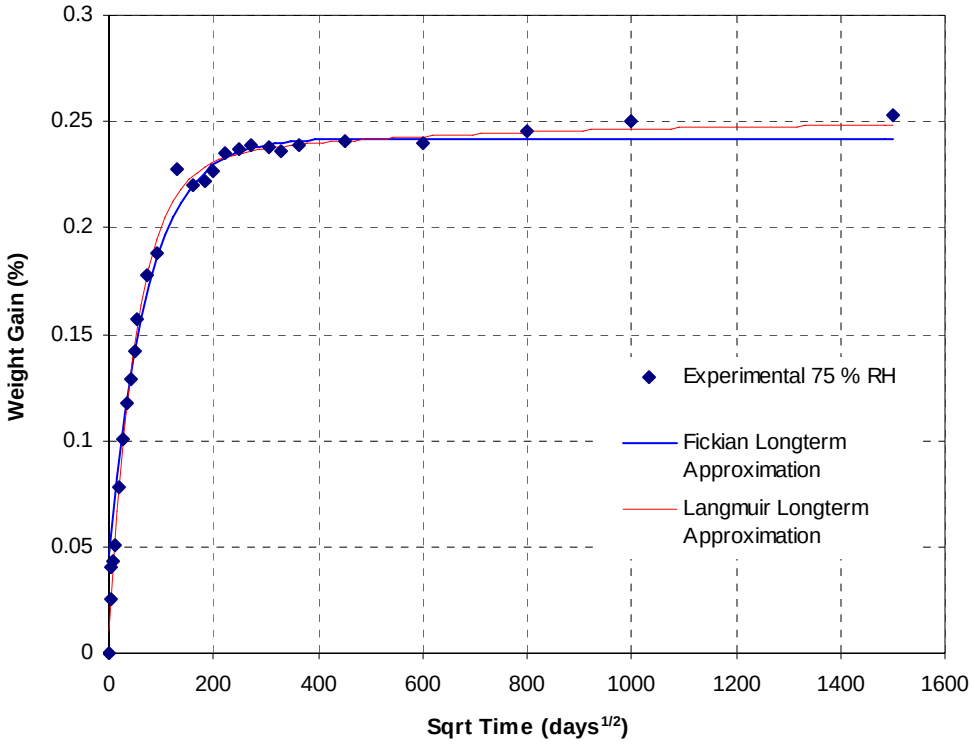

Fig. A.28 Comparison of experimental and predicted moistureabsorption profile of E-glass vinylester composite specimen exposed to arelative humidity of 75 % at 23 ^{o}C using long-term approximation terms

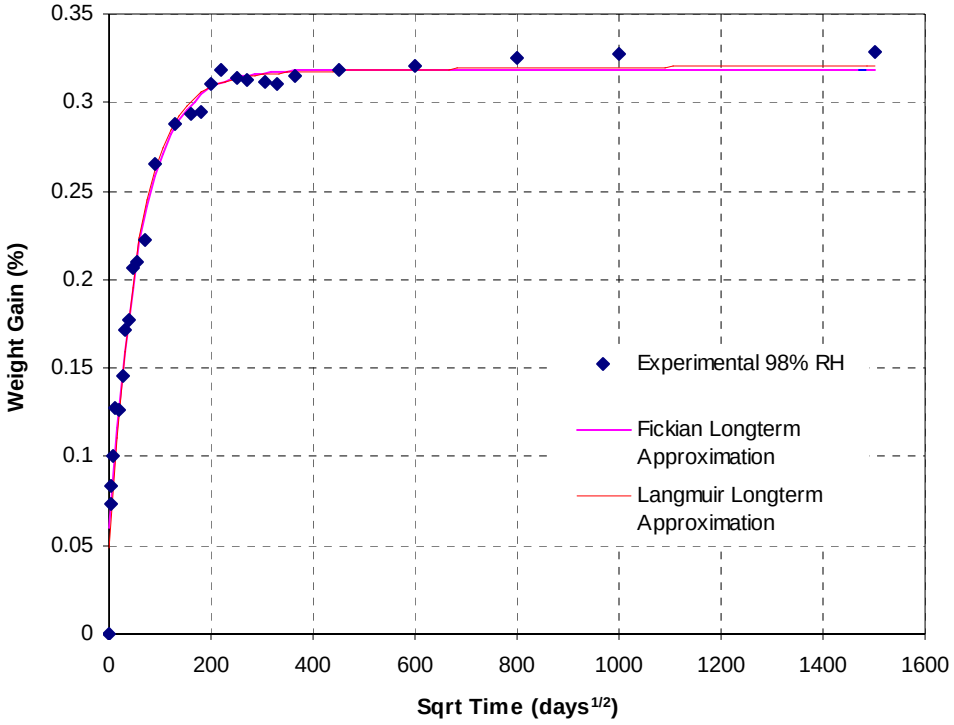

Fig. A.29 Comparison of experimental and predicted moistureabsorption profile of E-glass vinylester composite specimen exposed to arelative humidity of 98 % at 23 ^{o}C using long-term approximation terms

A.3 Exposure to Relative Humidity at 95 C

A.3.1 Full Model

The moisture absorption data shown in Table 5.15 were fitted to equations A.1 (Fickian Diffusion Model) and A.2 (Langmuir Diffusion Model) using Mathcad. Fitting the data to the equations, using the least squares method, results in the estimation of the Maximum moisture content, M_m and Diffusion Coefficient, D. The results of the analysis using the equations A.1 and A.2 are presented in the Figures A.30 and A.39.

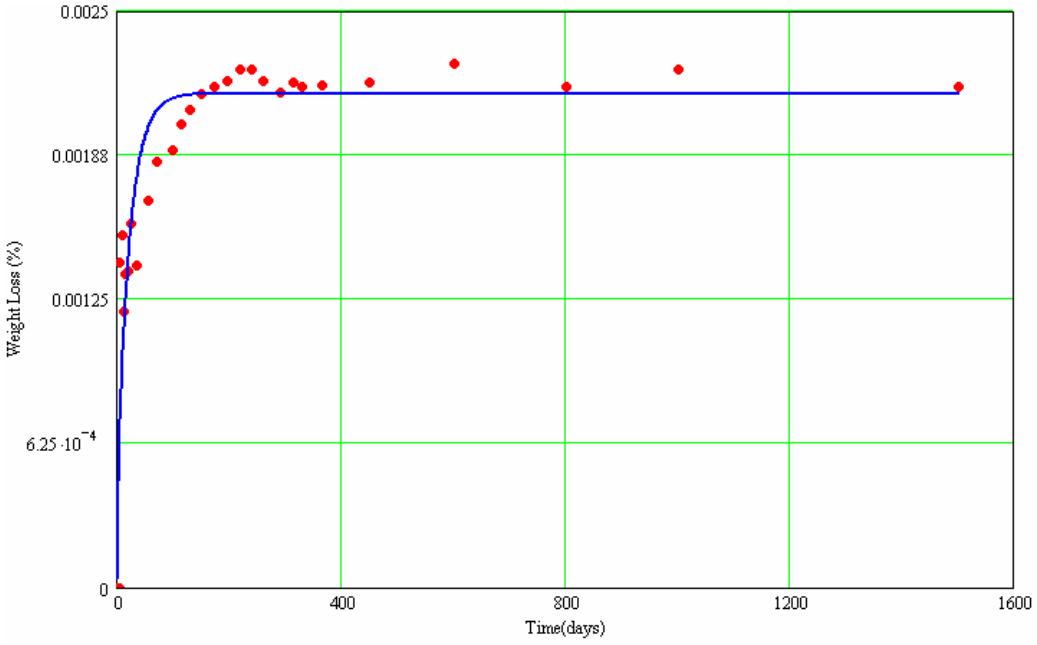

Fig. A.30 Comparison of experimental and predicted moisture absorption profile of E-glass vinylester composite specimen exposed to a relative humidity of 0-5 % at 95 ^{o}C using Fickian Full Model

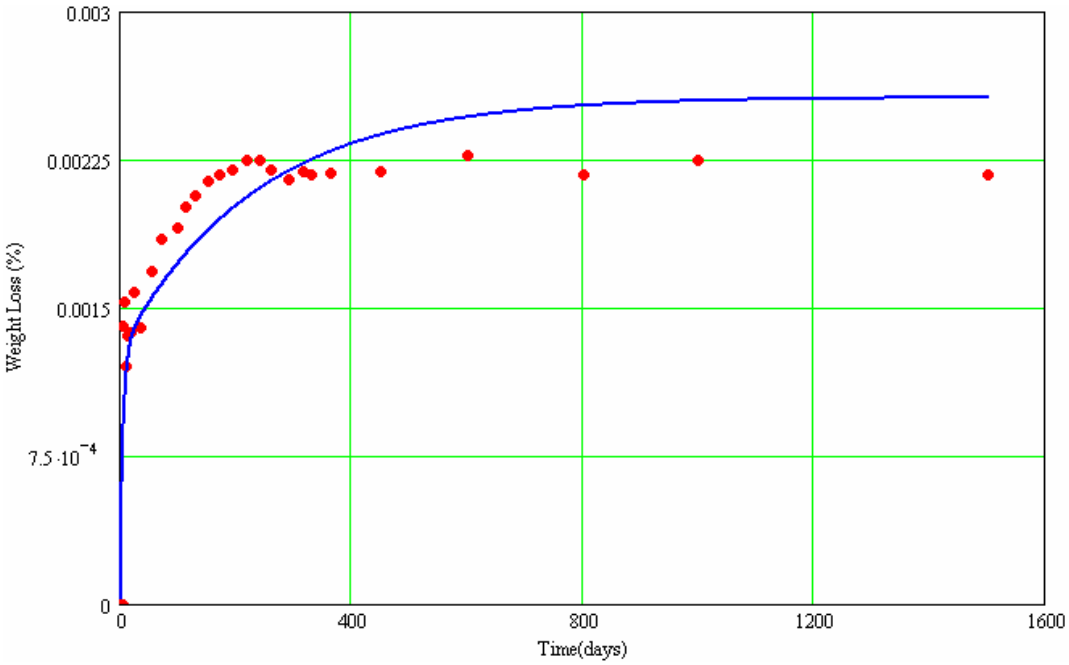

Fig. A.31 Comparison of experimental and predicted moisture absorption profile of E-glass vinylester composite specimen exposed to a relative humidity of 0-5 % at 95 ^{o}C using Langmuir Full Model

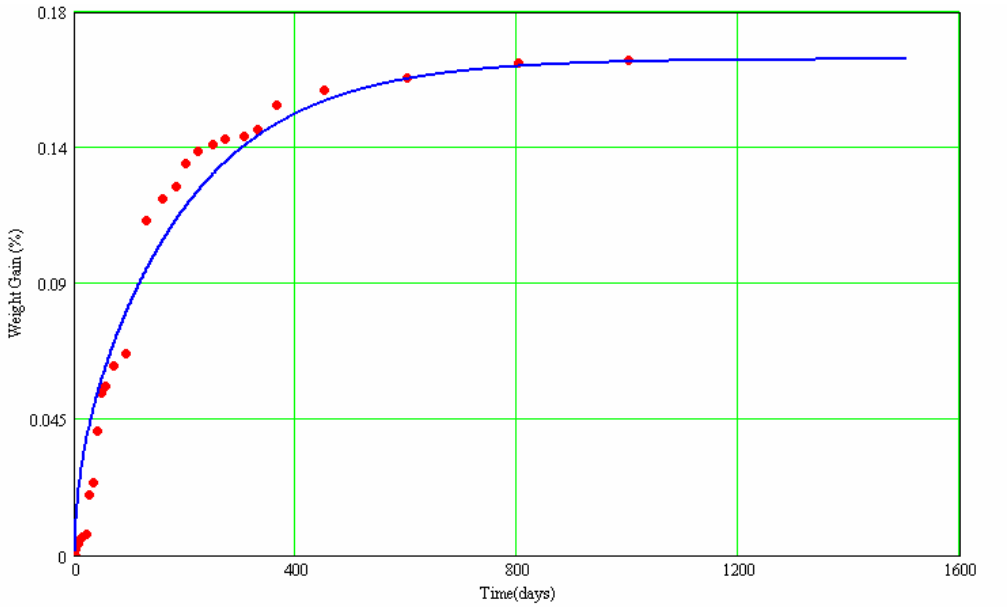

Fig. A.32 Comparison of experimental and predicted moisture absorption profile of E-glass vinylester composite specimen exposed to a relative humidity of 45 % at 95 ^{o}C using Fickian Full Model

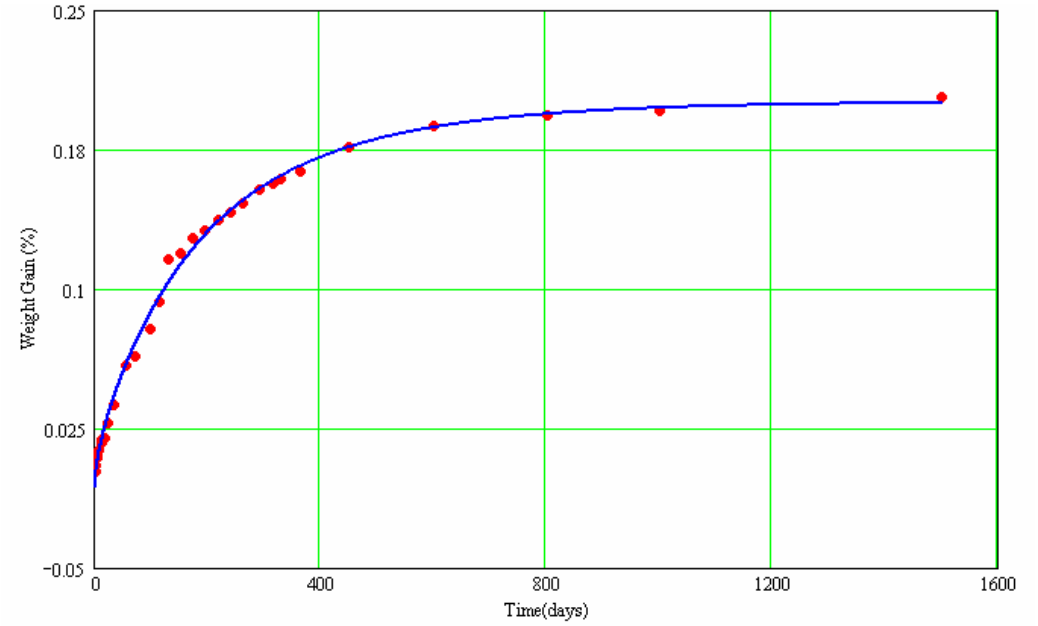

Fig. A.33 Comparison of experimental and predicted moisture absorption profile of E-glass vinylester composite specimen exposed to a relative humidity of 45 % at 95 ^{o}C using Langmuir Full Model

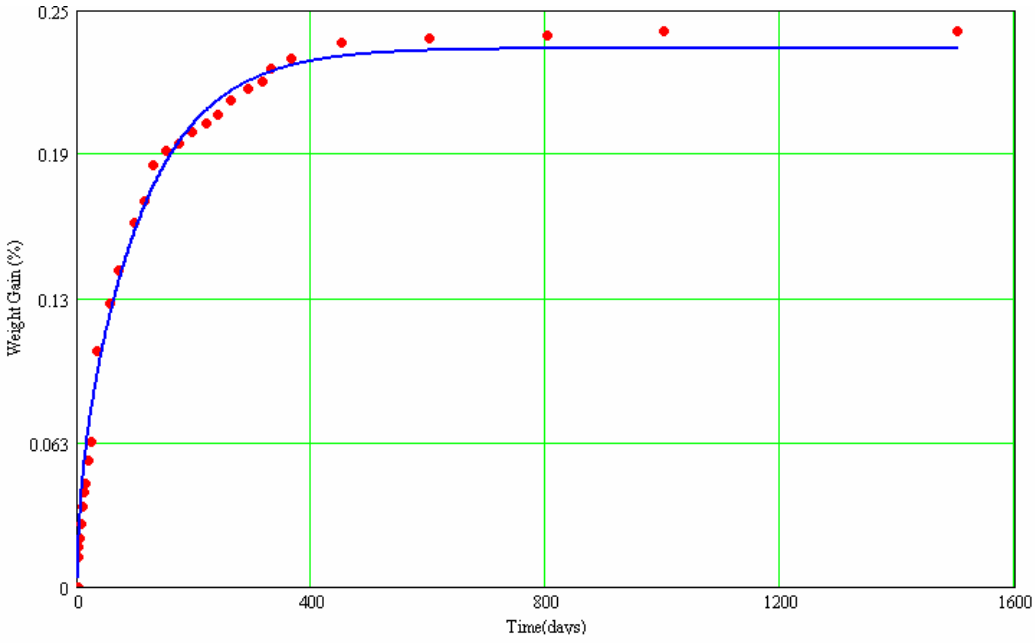

Fig. A.34 Comparison of experimental and predicted moisture absorption profile of E-glass vinylester composite specimen exposed to a relative humidity of 60 % at 95 ^{o}C using Fickian Full Model

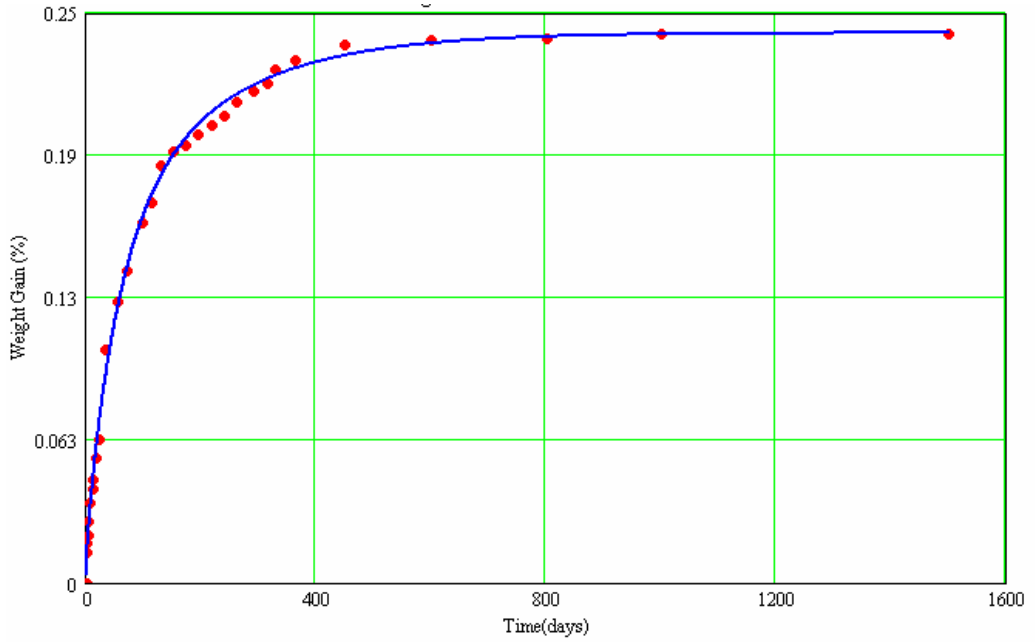

Fig. A.35 Comparison of experimental and predicted moisture absorption profile of E-glass vinylester composite specimen exposed to a relative humidity of 60 % at 95 ^{o}C using Langmuir Full Model

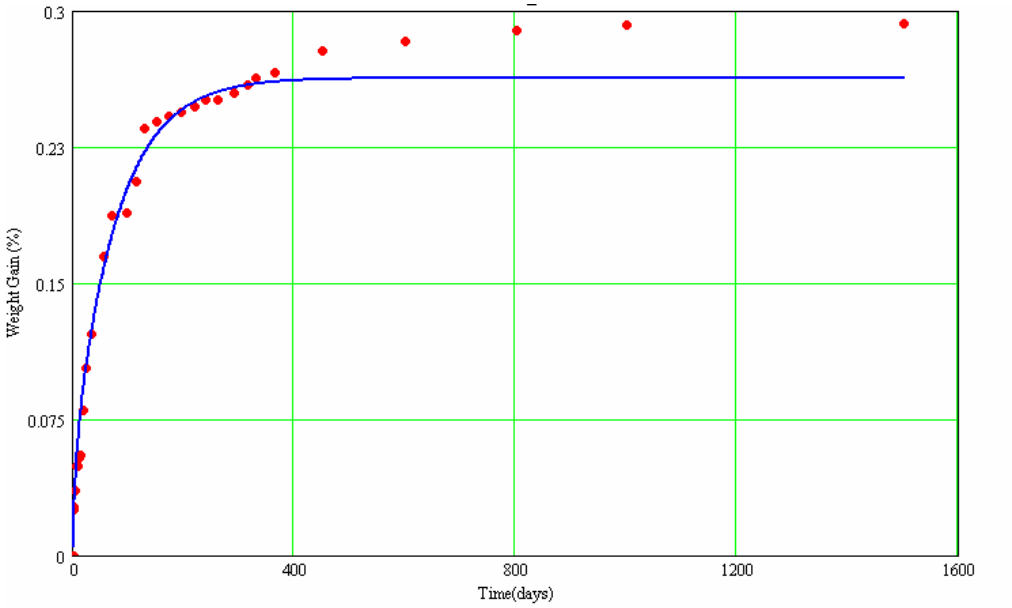

Fig. A.36 Comparison of experimental and predicted moisture absorption profile of E-glass vinylester composite specimen exposed to a relative humidity of 75 % at 95 ^{o}C using Fickian Full Model

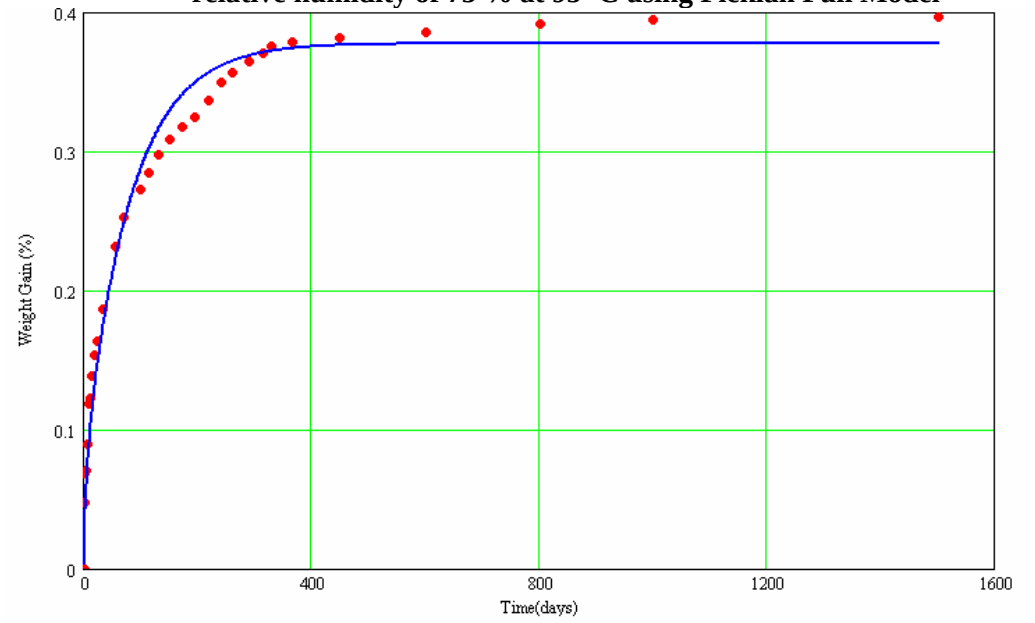

Fig. A.37 Comparison of experimental and predicted moisture absorption profile of E-glass vinylester composite specimen exposed to a relative humidity of 75 % at 95 ^{o}C using Langmuir Full Model

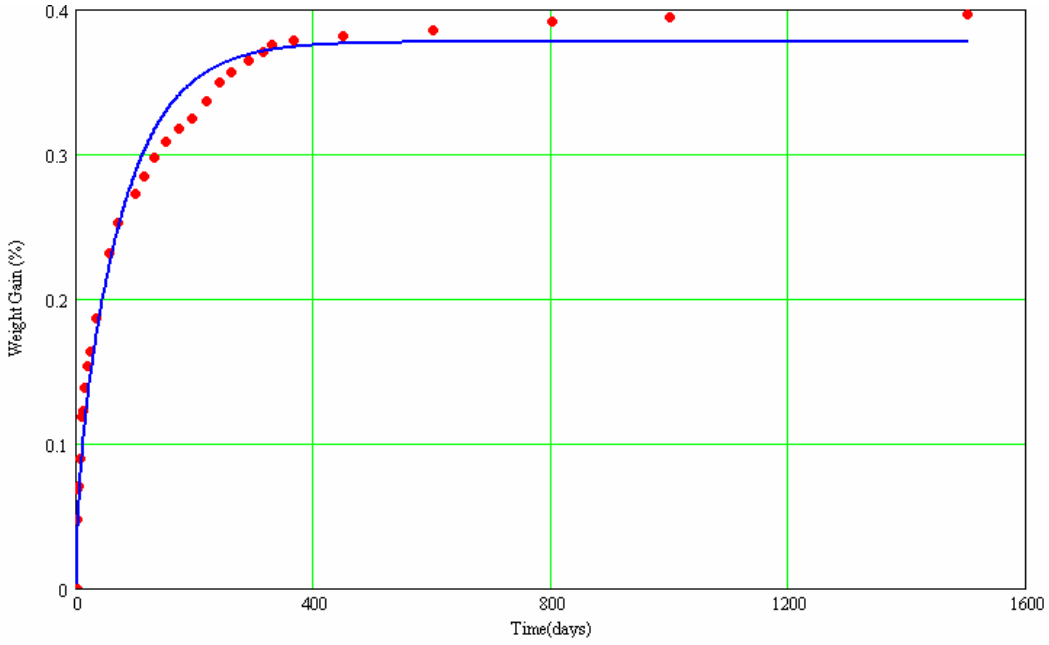

Fig. A.38 Comparison of experimental and predicted moisture absorption profile of E-glass vinylester composite specimen exposed to a relative humidity of 98 % at 95 ^{o}C using Fickian Full Model

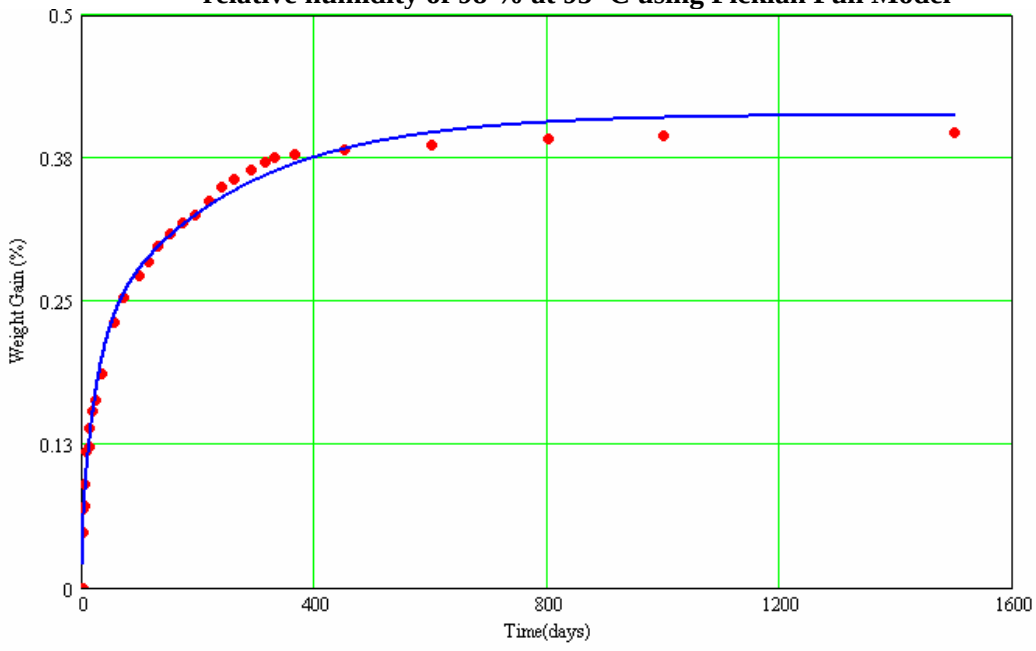

Fig. A.39 Comparison of experimental and predicted moisture absorption profile of E-glass vinylester composite specimen exposed to a relative humidity of 98 % at 95 ^{o}C using Langmuir Full Model

A.3.2 Long-term Approximation

The moisture absorption data in the table 5.8 is fitted to equations A.3 (Fickian Long-Term Approximation) and A.4 (Langmuir Long-term Approximation). The results are presented in figures A.40 through A.43.

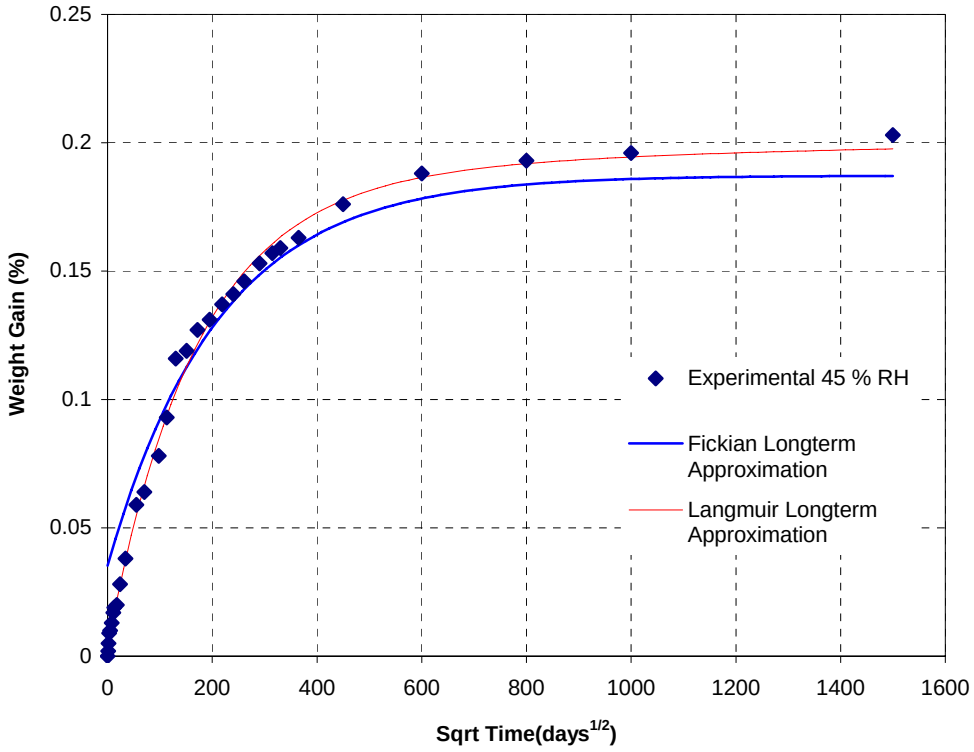

Fig. A.40 Comparison of experimental and predicted moisture absorption profile of E-glass vinylester composite specimen exposed to a relative humidity of 45 % at 95 ^{o}C using long-term approximation terms

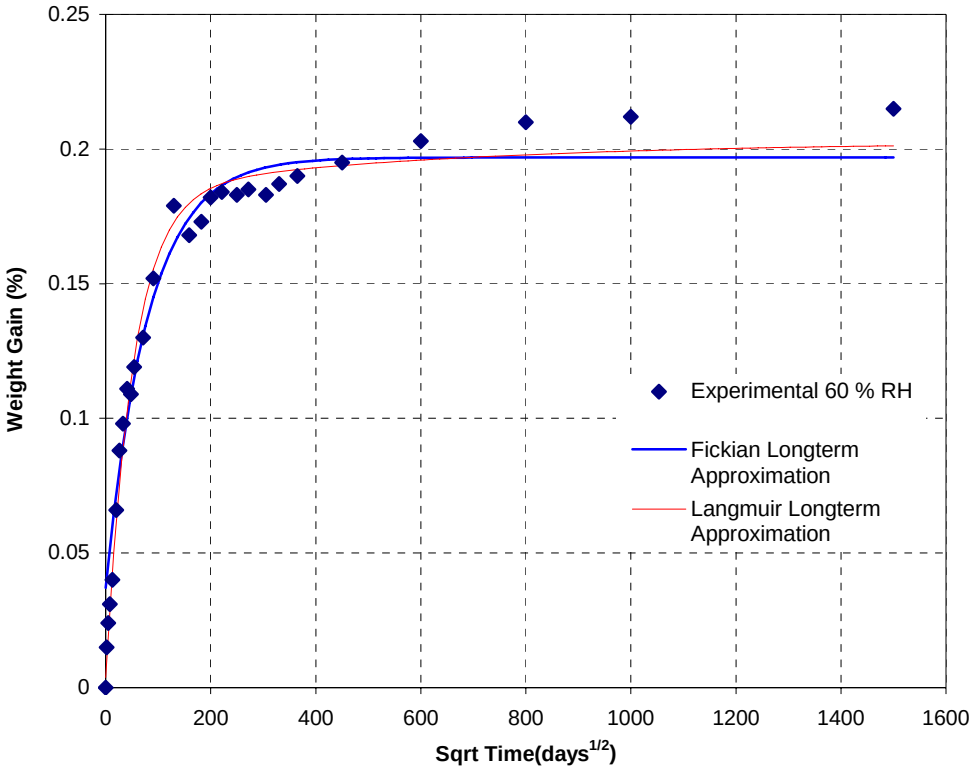

Fig. A.41 Comparison of experimental and predicted moisture absorption profile of E-glass vinylester composite specimen exposed to a relative humidity of 60 % at 95 ^{o}C using long-term approximation terms

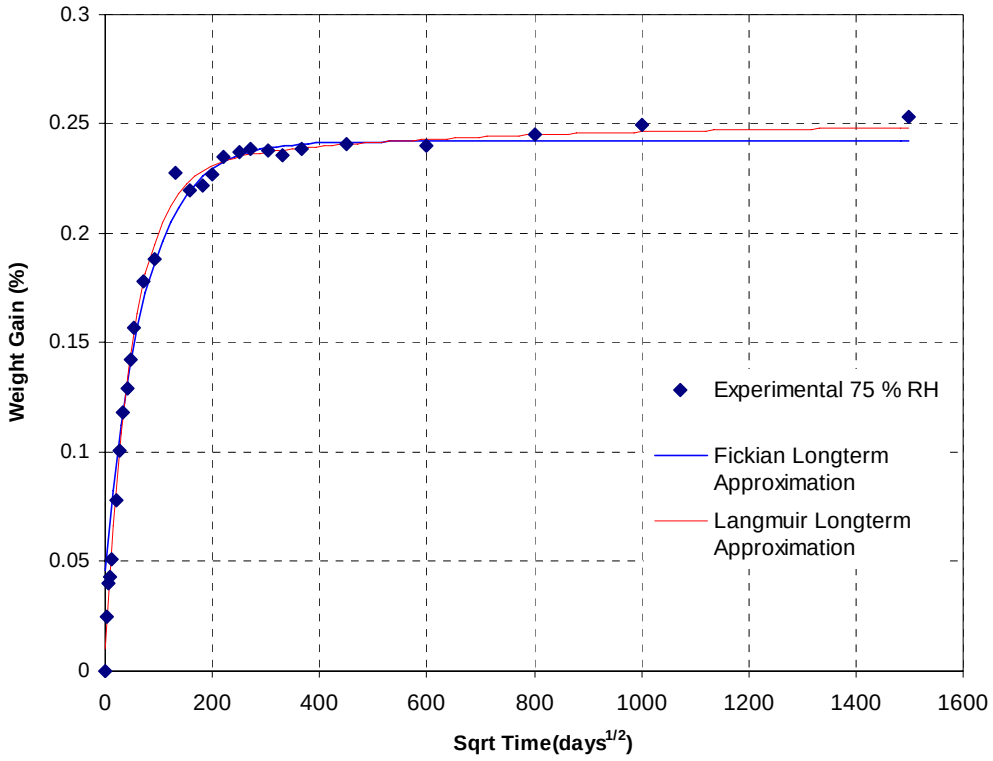

Fig. A.42 Comparison of experimental and predicted moisture absorption profile of E-glass vinylester composite specimen exposed to a relative humidity of 75 % at 95 ^{o}C using long-term approximation terms

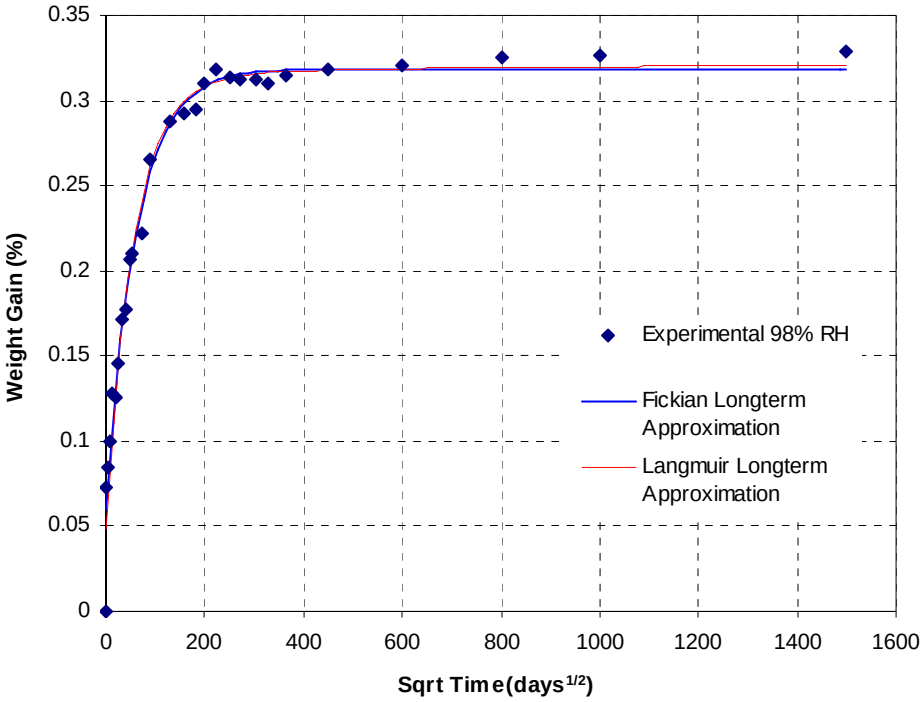

Fig. A.43 Comparison of experimental and predicted moisture absorption profile of E-glass vinylester composite specimen exposed to a relative humidity of 98 % at 95 ^{o}C using long-term approximation terms

APPENDIX B

In this section, the details of the MathCAD programs used for the determination of diffusion coefficients have been discussed. With the tools available in the MathCAD software, models were devised to analyse the moisture gain data using Fickian diffusion model, Long-term approximation Fickian model, Langmuir Fickian diffusion model and Long-term approximation Langmuir model. The programs for each of the above models are given in the following sections.

B.1 FICKIAN DIFFUSION – Full Model

The function genfit (vx,vy,vg,f) represents the vector containing the parameters that make a function of x and parameters u_o and u_1(maximum moisture content and diffusion coefficients respectively) which best approximate the data in vx and vy.

vx = time(days)(Input)
vy = percentage weight gain immersed in water at any temperature
vg = vector of guess values for M_m and D_c (Input)
l = thickness of the specimen in m
nmax = maximum number of iterations
$g(r, p)_0$ = function which gives the values of the percentage moisture gain fitted to the data in vx and vy (Output)
r = is the vector of time increments for which genfit calclautes the percentage moisture gain

vx :=

	0
0	0.00
1	1.00
2	2.00
3	7.00
4	12.00
5	14.00
6	16.00
7	20.00
8	27.00
9	33.00
10	40.00

vy :=

	0
0	0.0000
1	0.0900
2	0.1033
3	0.1380
4	0.1540
5	0.1640
6	0.1700
7	0.1730
8	0.1800
9	0.1920
10	0.2100

$$f(z,u) := \begin{bmatrix} u_0 \cdot \left[1 - \frac{8}{\pi^2} \cdot \sum_{n=0}^{nmax} \left[\frac{1}{(2\cdot n+1)^2} \cdot e^{\left[\frac{-u_1}{l^2} \cdot z \cdot \pi^2 \cdot (2\cdot n+1)^2 \right]} \right] \right] \\ 1 - \frac{8}{\pi^2} \cdot \sum_{n=0}^{nmax} \left[\frac{1}{(2\cdot n+1)^2} \cdot e^{\left[\frac{-u_1}{l^2} \cdot z \cdot \pi^2 \cdot (2\cdot n+1)^2 \right]} \right] \\ \frac{-8}{\pi^2} \cdot u_0 \cdot \sum_{n=0}^{nmax} \left[\frac{-z\cdot\pi^2}{l^2} \cdot e^{\left[\frac{-u_1}{l^2} \cdot z \cdot \pi^2 \cdot (2\cdot n+1)^2 \right]} \right] \end{bmatrix}$$

$p := genfit(vx, vy, vg, f)$

$vg := \begin{pmatrix} 0.7 \\ 0.00000005 \end{pmatrix}$

$r := 0, 1 .. 1500$

$g(r) := f(r, p)_0$

$nmax := 10$

B.2 FICKIAN DIFFUSION- Long-term Approximation

The function genfit (vx,vy,vg,f) represents the vector containing the parameters that make a function of x and parameters u_o and u_1(maximum moisture content and diffusion coefficients respectively) which best approximate the data in vx and vy.

vx = time(days) (Input)
vy = percentage weight gain immersed in water at any temperature
vg = vector of guess values for M_m and D_c(Input)
l = thickness of the specimen in m
$g(r, p)_0$ = function which gives the values of the percentage moisture gain fitted to the data in vx and vy (Output)
r = is the vector of time increments for which genfit calclautes the percentage moisture gain

vx :=

	0
0	0.00
1	1.00
2	2.00
3	7.00
4	12.00
5	14.00
6	16.00
7	20.00
8	27.00
9	33.00
10	40.00

vy :=

	0
0	0.0000
1	0.0900
2	0.1033
3	0.1380
4	0.1540
5	0.1640
6	0.1700
7	0.1730
8	0.1800
9	0.1920
10	0.2100

$$f(z,u) := \begin{bmatrix} u_0 \cdot \left[1 - \frac{8}{\pi^2} \cdot \left(e^{\frac{-u_1 \cdot z \cdot \pi^2}{l^2}}\right)\right] \\ 1 - \frac{8}{\pi^2} \cdot \left(e^{\frac{-u_1 \cdot z \cdot \pi^2}{l^2}}\right) \\ \frac{8 \cdot u_0 \cdot z}{l^2} \cdot \left(e^{\frac{-u_1 \cdot z \cdot \pi^2}{l^2}}\right) \end{bmatrix}$$

p := genfit(vx, vy, vg, f)

$$vg := \begin{pmatrix} 0.7 \\ 0.00000005 \end{pmatrix}$$

r := 0, 1 .. 1500

g(r) := f(r, p)$_0$

B.3 LANGMUIR DIFFUSION – Full Model

The function genfit (vx,vy,vg,f) represents the vector containing the parameters that make a function of x and parameters u_o and u_l(maximum moisture content and diffusion coefficients respectively) which best approximate the data in vx and vy.

vx = time(days) (Input)
vy = percentage weight gain immersed in water at any temperature
vg = vector of guess values for M_m and D_c (Input)
l = thickness of the specimen in m
nmax = maximum number of iterations
$g(r, p)_0$ = function which gives the values of the percentage moisture gain fitted to the data in vx and vy (Output)
r = is the vector of time increments for which genfit calclautes the percentage moisture gain

vx :=

	0
0	0.00
1	1.00
2	2.00
3	7.00
4	12.00
5	14.00
6	16.00
7	20.00
8	27.00
9	33.00
10	40.00

vy :=

	0
0	0.0000
1	0.0900
2	0.1033
3	0.1380
4	0.1540
5	0.1640
6	0.1700
7	0.1730
8	0.1800
9	0.1920
10	0.2100

$p := genfit(vx, vy, vg, f)$

$g(r) := f(r, p)_0$

$$vg := \begin{pmatrix} 0.7 \\ 0.00000005 \end{pmatrix}$$

$r := 0, 1 .. 1500$

$nmax := 10$

$$
f(z,u) := \begin{bmatrix}
u_0 \cdot \left[1 - \frac{u_2}{u_2+u_3} \cdot e^{\left(-u_2 \cdot z\right)} - \frac{u_2}{u_2+u_3} \cdot \frac{8}{\pi^2} \cdot \sum_{n=0}^{nmax} \left[\frac{1}{(2 \cdot n+1)^2} \cdot e^{\left[-u_1 \cdot z \cdot \frac{\pi^2}{l^2} \cdot (2 \cdot n+1)^2\right]} \right] \right] \\
1 - \frac{u_2}{u_2+u_3} \cdot e^{\left(-u_2 \cdot z\right)} - \frac{u_2}{u_2+u_3} \cdot \frac{8}{\pi^2} \cdot \sum_{n=0}^{nmax} \left[\frac{1}{(2 \cdot n+1)^2} \cdot e^{\left[-u_1 \cdot z \cdot \frac{\pi^2}{l^2} \cdot (2 \cdot n+1)^2\right]} \right] \\
\frac{-u_0 \cdot u_2}{u_2+u_3} \cdot \frac{8}{\pi^2} \cdot \sum_{n=0}^{nmax} \left[\frac{-z \cdot \pi^2}{l^2} \cdot e^{\left[-u_1 \cdot z \cdot \frac{\pi^2}{l^2} \cdot (2 \cdot n+1)^2\right]} \right] \\
\frac{u_0 \cdot e^{\left(-u_2 \cdot z\right)}}{\left(u_2+u_3\right)} \cdot \left(u_2 \cdot z + \frac{u_2}{u_2+u_3} - 1 \right) - \left[\frac{8 \cdot u_0}{\pi^2} \cdot \sum_{n=0}^{nmax} \left[\frac{1}{(2 \cdot n+1)^2} \cdot e^{\left[-u_1 \cdot z \cdot \frac{\pi^2}{l^2} \cdot (2 \cdot n+1)^2\right]} \right] \right] \cdot \left[\frac{1}{u_2+u_3} - \frac{u_2}{\left(u_2+u_3\right)^2} \right] \\
\frac{u_0 \cdot u_2}{\left(u_2+u_3\right)^2} \cdot \left[e^{\left(-u_2 \cdot z\right)} + \frac{8}{\pi^2} \cdot \sum_{n=0}^{nmax} \left[\frac{1}{(2 \cdot n+1)^2} \cdot e^{\left[-u_1 \cdot z \cdot \frac{\pi^2}{l^2} \cdot (2 \cdot n+1)^2\right]} \right] \right]
\end{bmatrix}
$$

B.4 LANGMUIR DIFFUSION – Long-term Approximation

The function genfit (vx,vy,vg,f) represents the vector containing the parameters that make a function of x and parameters u_o and u_1(maximum moisture content and diffusion coefficients respectively) which best approximate the data in vx and vy.

vx = time(days) (Input)
vy = percentage weight gain immersed in water at any temperature
vg = vector of guess values for M_m and D_c (Input)
l = thickness of the specimen in m
nmax = maximum number of iterations
$g(r, p)_0$ = function which gives the values of the percentage moisture gain fitted to the data in vx and vy (Output)
r = is the vector of time increments for which genfit calclautes the percentage moisture gain

vx :=

	0
0	0.00
1	1.00
2	2.00
3	7.00
4	12.00
5	14.00
6	16.00
7	20.00
8	27.00
9	33.00
10	40.00

vy :=

	0
0	0.0000
1	0.0900
2	0.1033
3	0.1380
4	0.1540
5	0.1640
6	0.1700
7	0.1730
8	0.1800
9	0.1920
10	0.2100

$$p := genfit(vx, vy, vg, f)$$

$$g(r) := f(r, p)_0$$

$$vg := \begin{pmatrix} 0.7 \\ 0.00000005 \end{pmatrix}$$

$$r := 0, 1 .. 1500$$

$$f(z,u) := \begin{bmatrix} u_0 \cdot \left[1 - \frac{u_2}{u_2 + u_3} \cdot e^{(-u_2 \cdot z)} - \frac{u_2}{u_2 + u_3} - \frac{8}{\pi^2} \cdot e^{\left(\frac{-u_1 \cdot z}{l^2} \cdot \pi^2 \right)} \right] \\ 1 - \frac{u_2}{u_2 + u_3} \cdot e^{(-u_2 \cdot z)} - \frac{u_2}{u_2 + u_3} - \frac{8}{\pi^2} \cdot e^{\left(\frac{-u_1 \cdot z}{l^2} \cdot \pi^2 \right)} \\ \frac{8 \cdot u_0 \cdot z}{l^2} \cdot e^{\left(\frac{-u_1 \cdot z}{l^2} \cdot \pi^2 \right)} \\ u_0 \cdot \left[\frac{-1}{u_2 + u_3} \cdot \exp(-u_2 \cdot z) + \frac{u_2}{(u_2 + u_3)^2} \cdot \exp(-u_2 \cdot z) + \frac{u_2}{u_2 + u_3} \cdot z \cdot \exp(-u_2 \cdot z) - \frac{1}{u_2 + u_3} + \frac{u_2}{(u_2 + u_3)^2} \right] \\ u_0 \cdot \left[\frac{u_2}{(u_2 + u_3)^2} \cdot \exp(-u_2 \cdot z) + \frac{u_2}{(u_2 + u_3)^2} \right] \end{bmatrix}$$